NASA/TM–2005-213896

Principal Investigator Microgravity Services (PIMS)

International Space Station

Increment-6/8 Microgravity Environment Summary Report

November 2002 to April 2004

Microgravity Environment Program

Glenn Research Center

Kenol Jules
NASA Glenn Research Center

Kenneth Hrovat, Vibratory Analyst
ZIN Technologies, Inc.

Eric Kelly
ZIN Technologies, Inc.

Timothy Reckart
ZIN Technologies, Inc.

National Aeronautics and Space Administration
Glenn Research Center
Cleveland, Ohio

Table of Contents

List of Tables

List of Figures

Acknowledgements

The authors would like to acknowledge a number of people who contributed significantly to this report. Without their contribution, this report would have not been possible. Nissim Lugasy, Ted Wright, and Gene Liberman made significant contributions in the area of software development. The software enabled PIMS to process, analyze, troubleshoot and display both MAMS and SAMS acceleration data acquired aboard the ISS. We would like also to acknowledge the hardware development contribution of the SAMS-II team and the MAMS project team/Canopus Inc. The authors appreciate the work of Richard DeLombard for his tenacious pursuit of information and contacts that ultimately led to identification of the formerly unknown “swoosh” signature. Thanks to Kevin McPherson and Bradley T. Humphreys for some fabulous ideas and suggestions that also helped with the "swoosh" characterization and identification effort. Yvon Laliberte from Hamilton Sundstrand and Gregory Gentry and Roger Von Jouanne from the Boeing Company provided detailed and much appreciated explanation of the Common Cabin Air Assembly operating characteristics. Thanks to Frederick Cerkan, Kevin Ferguson, Richard Burt, John Bendle, Michael Begley, Nathan Harris and others from the Boeing Company for guidance navigation and control information related to control moment gyroscope operations.

**PIMS ISS Increment-6/8 Microgravity Environment Summary Report:
November 2002 to April 2004**

Abstract

This summary report presents the analysis results of some of the processed acceleration data measured aboard the International Space Station during the period of November 2002 to April 2004. Two accelerometer systems were used to measure the acceleration levels for the activities that took place during Increment-6/8. However, not all of the activities during that period were analyzed in order to keep the size of the report manageable.

The National Aeronautics and Space Administration sponsors the Microgravity Acceleration Measurement System and the Space Acceleration Measurement System to support microgravity science experiments that require microgravity acceleration measurements. On April 19, 2001, both the Microgravity Acceleration Measurement System and the Space Acceleration Measurement System units were launched on STS-100 from the Kennedy Space Center for installation on the International Space Station. The Microgravity Acceleration Measurement System unit was flown to the station in support of science experiments requiring quasi-steady acceleration measurements, while the Space Acceleration Measurement System unit was flown to support experiments requiring vibratory acceleration measurement. Both acceleration systems are also used in support of the vehicle microgravity requirements verification as well as in support of the International Space Station support cadre.

The International Space Station Increment-6/8 reduced gravity environment analysis presented in this report uses acceleration data collected by both sets of accelerometer systems:

1. The Microgravity Acceleration Measurement System, which consists of two sensors: the Orbital Acceleration Research Experiment Sensor Subsystem, a low frequency range sensor (up to 1 Hz), is used to characterize the quasi-steady environment for payloads and vehicle, and the High Resolution Accelerometer Package, which is used to characterize the vibratory environment up to 100 Hz.

2. The Space Acceleration Measurement System measures vibratory acceleration data in the range of 0.01 to 400 Hz.

This summary report presents analysis of some selected quasi-steady and vibratory activities measured by these accelerometers during Increment-6/8 from November 2002 to April 2004.

PIMS ISS Increment-6/8 Microgravity Environment Summary Report: November 2002 to April 2004

1 Introduction

The NASA Exploration Systems Mission Directorate (ESMD) sponsors science experiments on various reduced-gravity carriers/platforms and facilities such as the Space Transportation System (STS), parabolic flight-path aircraft, sounding rockets, drop towers and the International Space Station (ISS). To provide support for the science experiments, which require acceleration data measurement on the ISS, the Human System Research and Technology (HSRT) sponsors two microgravity accelerometer systems, the Space Acceleration Measurement System (SAMS) and the Microgravity Acceleration Measurement System (MAMS). SAMS measures vibratory acceleration data in the range of 0.01 to 400 Hz for payloads requiring such measurement. MAMS consists of two sensors, the Orbital Acceleration Research Experiment (OARE) Sensor Subsystem (OSS) and the High Resolution Accelerometer Package (HiRAP). The OSS is a low frequency range sensor (up to 1 Hz) used to characterize the quasi-steady environment for payloads and the ISS vehicle. The HiRAP is used to characterize the ISS vibratory environment from 0.01 Hz to 100 Hz. Both MAMS and SAMS were flown to the ISS on STS-100, which was launched April 19, 2001, from the Kennedy Space Center (KSC).

The residual acceleration environment of an orbiting spacecraft in a low earth orbit is a complex phenomenon [1]. Many factors, such as experiment operation, life-support systems, crew activities, aerodynamic drag, gravity gradient, rotational effects and the vehicle structural resonance frequencies (structural modes) contribute to form the overall reduced gravity environment. Weightlessness is an ideal state, which cannot be achieved in practice because of the various sources of acceleration present in an orbiting spacecraft. As a result, the environment in which experiments are conducted is *not zero* gravity, and most experiments can be affected by the residual acceleration because of their dependency on acceleration magnitude, frequency, orientation and duration. Therefore, experimenters must know what the environment was when their experiments were performed in order to analyze and correctly interpret the result of their experimental data. In a terrestrial laboratory, researchers are expected to know and record certain parameters such as pressure, temperature, and humidity level in their laboratory prior to and possibly throughout their experiment runs. The same holds true in space, except that acceleration effects emerge as an important consideration.

The NASA Glenn Research Center (GRC) Principal Investigator Microgravity Services (PIMS) project has the responsibility for processing and archiving acceleration measurements, analyzing these measurements, characterizing the reduced gravity environment in which the measurements were taken, and providing expertise in reduced gravity environment assessment for a variety of carriers/platforms and facilities, such as the Space Shuttle, parabolic flight-path aircraft, sounding rockets, drop towers and the ISS in support of the NASA's HSRT Principal Investigators (PIs). The PIMS project supports PIs from the microgravity science disciplines of biotechnology, combustion science, fluid physics, material science and fundamental physics. The PIMS project is funded by the NASA Headquarters and is part of the NASA GRC's Human Health and Performance Systems (HHPS) office, which integrates the analysis and interpretation component of PIMS with the various NASA sponsored acceleration measurement systems. For the ISS, these acceleration measurement systems include SAMS and MAMS. The PIMS project is responsible for receiving, processing, analyzing, displaying, distributing, and archiving the acceleration data for SAMS and MAMS during ISS operations. This report presents to the microgravity scientific community the results of some of the analyses performed by PIMS using the acceleration data measured by the two-accelerometer systems during the period of November 2002 to April 2004 aboard the ISS.

2 International Space Station

2.1 Configuration at Assembly Complete

The ISS represents a global partnership of many nations. This project is an engineering, scientific and technological marvel ushering in a new era of human space exploration. Assembly of the ISS began in late 1998 [2] and will continue until completion sometime around the year 2010. During its assembly and over its nominal 10-year lifetime, the ISS will serve as an orbital platform for the United States and its International Partners to make advances in microgravity, space, life, and earth sciences, as well as in engineering research and technology development. The completed space station will have a number of fully equipped laboratories, a significant number of payload racks [3] or experiment storage facilities, and several external payload locations for conducting experiments in the vacuum of space. The main laboratories, which will house research facilities, are: Destiny (US), the Centrifuge Accommodations Module (CAM-US), Columbus (European Space Agency (ESA)), Kibo (Japan Aerospace Exploration Agency (JAXA)) and two possible Russian Research Modules (yet to be named). The pressurized living and working space aboard the completed ISS will be about 43,000 ft^3 [4] (Table 2-1). Its giant solar arrays will generate the electricity needed. An initial crew of three (after the Columbia accident on February 1, 2003, the crew was reduced to two), increasing to seven when assembly is complete (Figure 2-1), is living aboard the ISS. The space station represents a quantum leap in our ability to conduct research on orbit and explore basic questions in a variety of disciplines [4] such as biomedical, fundamental biology, biotechnology, fluid physics, advanced human support technology, materials science, combustion science, fundamental physics, earth science and space science.

TABLE 2-1 ISS SPECIFICATION AT ASSEMBLY COMPLETE

Wingspan Width	356 feet (108.5 m)
Length	290 feet (88.4 m)
Mass (weight)	About 1 million pounds (453,592 kg)
Operating Altitude	220 nautical miles average (407 km)
Inclination	51.6 degrees to the Equator
Atmosphere inside	14.7 psi (101.36 kilopascals)
Pressurized Volume	43,000 ft^3 (1,218 m^3) in 6 laboratories
Crew Size	3, increasing to 7

2.2 ISS Coordinate Systems

For ISS operations, PIMS reports acceleration data to the microgravity scientific community using the ISS analysis coordinate system unless a specific sensor's local coordinate system is specified.

2.2.1 Space Station Analysis Coordinate System

The ISS analysis system [5] is derived using the Local Vertical Local Horizontal (LVLH) flight orientation. When defining the relationship between this coordinate system and another, the Euler angle sequence to be used is a yaw, pitch, roll sequence around the Z_A, Y_A, and X_A axes, respectively (Figure 2-2). The ISS Analysis frame is aligned with the Starboard Truss Segment 0 (S0) Coordinate frame, and the origin (Figure 2-3) is located at the geometric center of the Integrated Truss Segment (ITS) S0. The X_A axis is parallel to the longitudinal axis of the module cluster. The positive X_A axis is in the forward (flight) direction. The Y_A axis is identical to the S0 axis. The nominal alpha solar array joint rotational axis is parallel with the Y_A axis. The positive Y_A axis is in the starboard direction. The positive Z_A axis is in the direction of Nadir (toward earth) and completes the right-handed Cartesian system (RHCS). This analysis coordinate system is used by PIMS in its analysis and reporting of the acceleration data measured on ISS unless a sensor coordinate system is specified. A more detailed description of the ISS coordinate systems can be found in [5].

2.2.2 Integrated Truss Segment S0 Coordinate System

This coordinate system defines the origin, orientation, and sense of the ISS analysis coordinate system. The YZ plane nominally contains the centerline of all four trunnion pins. The origin is defined as the intersection of two diagonal lines connecting the centers of the bases of opposite trunnion pins, running T1 to T3 and from T2 to T4 (Figure 2-3). The X-axis (X_{S0}) is parallel to the vector cross product of the Y-axis with the line from the center of the base trunnion pin T2 to the center of the base trunnion pin T3, and is positive forward. The Y-axis (Y_{S0}) is parallel with the line from the center of the base of trunnion pin T2 to the center of the base of trunnion pin T1. The positive Y-axis is toward starboard. The Z-axis (Z_{S0}) completes the RHCS.

2.3 ISS Flight Attitude at Assembly Complete

The basic flight attitude [6] for ISS is called X body axis toward the Velocity Vector (XVV) Z Nadir Torque Equilibrium Attitude (TEA), or XVV TEA for short. XVV Z Nadir (XVV for short) stands for X body axis toward the velocity vector, Z body axis toward Nadir (earth), and TEA is for torque equilibrium attitude. The ISS vehicle design is optimized for the XVV attitude (Figure 2-4). The XVV attitude places the most modules in the microgravity volume; supports altitude re-boosts, services vehicle dockings, and minimizes aerodynamic drag. The ISS is designed to tolerate deviations from perfect XVV Z Nadir of +/- 15 degrees in each axis. This envelope was expanded to -20 degrees in pitch.

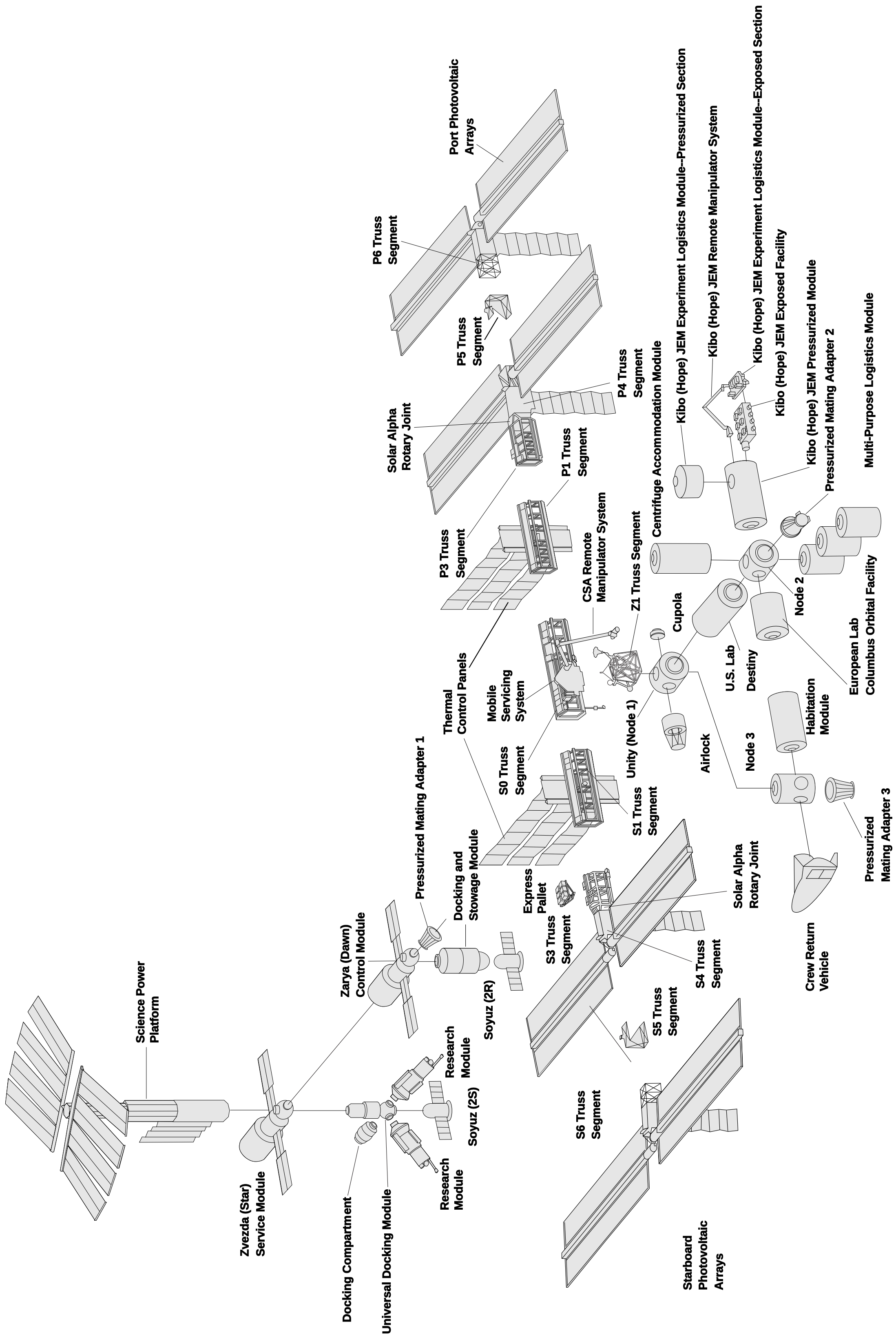

Figure 2-1 International Space Station at Assembly Complete

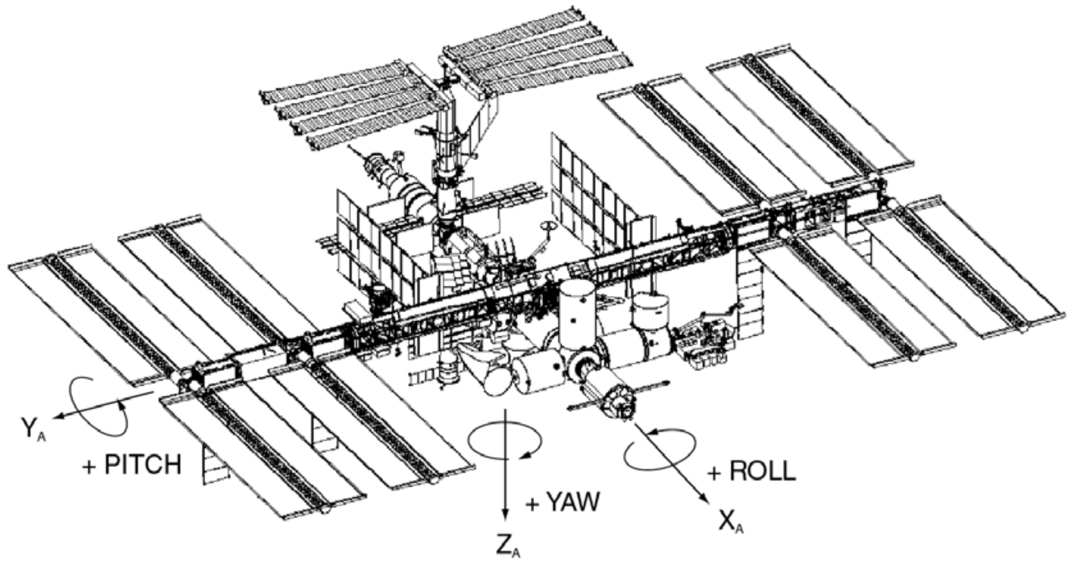

Figure 2-2 Space Station Analysis Coordinate System

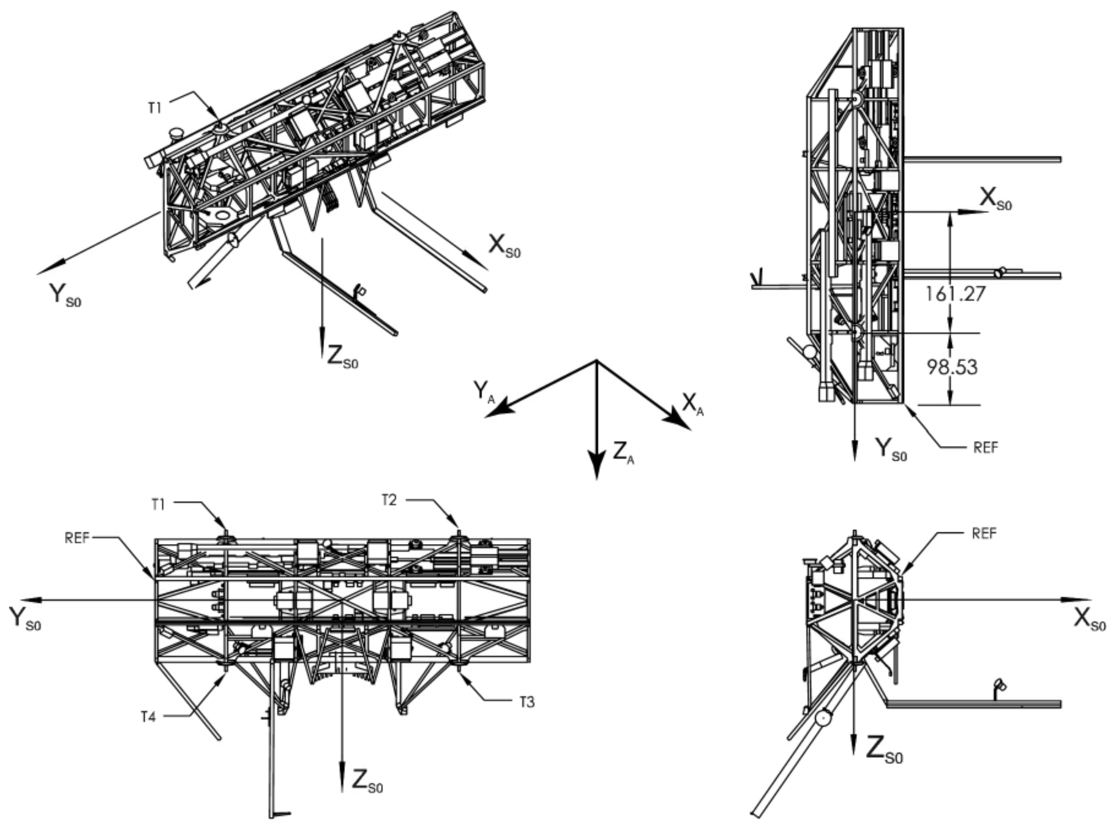

Figure 2-3 Integrated Truss Segment S0 Coordinate System

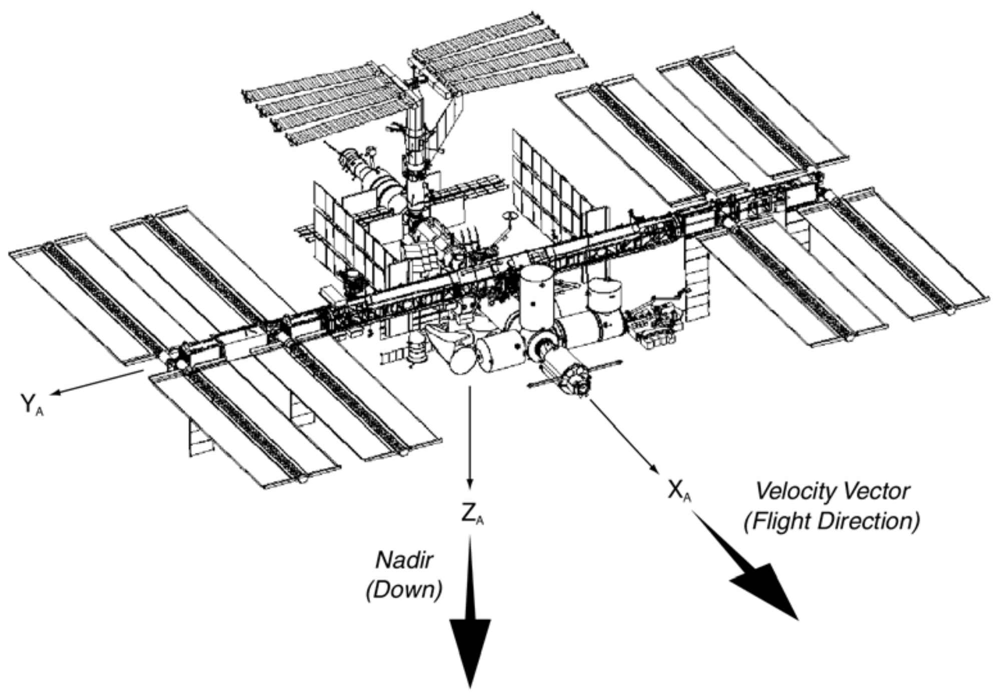

Figure 2-4 ISS XVV Flight Attitude

3 ISS Increment-6/8

An increment should average about 4 months (sometimes more---e.g., Increment-6 lasted over 5 months) and is determined by crew rotations and flights to/from ISS. Each increment has a theme that focuses on the primary science or activities to be performed.

3.1 Increment-6 Configuration

This increment is called Increment-6 or Expedition Six. The 3-member crew for Increment-6 mission was launched to ISS on November 23, 2002 on STS-113 from KSC and returned to earth on the Russian Soyuz TMA-1 on May 3, 2003 after a 161 days stay in space. During Increment-6, the Port 1 (P-1) Truss Structure, 13.7 meter-long (45-foot-long), 4.6 meter-wide (15-foot-wide), 4 meter-high (13-foot-high) and weighs 12,477 kg. (27,506-pound), was delivered by STS-113 and attached onto ISS on November 26, 2002. Two crewmembers of STS-113 performed three spacewalks and used the Shuttle and station robotic arms to install and outfit the P1 Truss to the station. The P1 Truss is the third of 11 such truss structures that will make up the station's external framework and will expand the ISS to 109 meters (357 feet) wide [7]. The P1 Truss was attached to the port side of the centerpiece truss, the Starboard 0 (S0), which is home to the Mobile Transporter (MT), Mobile Base System (MBS) and the Canadarm2 robotic arm. Like the S1 Truss, the P1 includes a Thermal Radiator Rotary Joint (TRRJ), which will provide the mechanical and electrical energy for rotating the station's heat-rejecting radiators [7]. Also, mounted to the P1 is the second Crew and Equipment Translation Aid (CETA) cart. The carts are manually operated by a spacewalker and can also be used as a work platform. The following modules are now on-orbit [8]: Unity (Node), Zarya (Functional Cargo Block), Zvezda (Service Module), Destiny, the Russian DC-1 (Pirs) and the Joint Airlock (Quest) (Figure 3-1).

3.2 Increment-6 Science and Crew Members

During Increment-6 (Expedition 6), the crew worked with several experiments. The experiments during Expedition Six were intended to lead to new insights in the fields of medicine, materials, plants science, commercial biotechnology, and manufacturing. Several experiments begun on earlier expeditions were returned to earth, while several others continued operating during the Expedition Six's stay aboard the ISS [9]. The research complement included 20 new or continuing investigations. The three Expedition Six crewmembers devoted nearly 260 hours to scientific investigations, bringing the total of crew research hours to about 1,270 since continuous ISS human presence began in November 2000. Far more research time has been accumulated by experiments controlled by investigators on the ground—total hours should be well over 100,000 by the end of Expedition Six [9]. Increment-6 had two astronauts and one cosmonaut. The commander was astronaut Kenneth Bowersox; flight engineers were astronaut Donald Pettit and cosmonaut Nikolai Budarin. The crew was launched to the ISS on November 23, 2002 aboard the Space Shuttle Discovery STS-113 and landed on the flat steppes of north central Kazakhstan (in central Asia) on May 3, 2003 aboard the Russian Soyuz TMA-1. That landing marked the first time American astronauts were returned to earth using a Russian Soyuz capsule. The grounding of the space shuttle fleet following the Columbia accident on February 1, 2003 initiated that change.

The Soyuz TMA spacecraft was designed to serve as the International Space Station's crew return vehicle in the unlikely event an emergency would require the crew to leave the station. The Soyuz spacecraft is launched to the space station from the Baikonur Cosmodrome in Kazakhstan using a Soyuz rocket. It consists of an Orbital Module, a Descent Module and an Instrumentation/Propulsion Module. The Descent Module is the only portion of the Soyuz that survives the return to Earth. A new Soyuz is delivered to the station by a Soyuz crew every six months, replacing the Soyuz capsule already docked to the ISS. The current Soyuz version (TMA) can spend up to one year in space [10].

3.3 Increment-7 Configuration

This Increment is called Increment-7/Soyuz 6 or Expedition Seven. The 2-member crew for Increment-7 mission was launched to ISS on April 25, 2003 on Soyuz TMA-2 from the Baikonur Cosmodrome, Kazakhstan, in central Asia and returned to earth on the Russian Soyuz TMA-2 on October 27, 2003 after a 184 days stay in space. Due to the grounding of the space shuttle fleet after the Columbia accident, crew rotation to and from the ISS is being performed by the Soyuz-TMA vehicles. And because of the up-mass/down-mass constraint of the Soyuz vehicle two changes took place until the shuttle returns to flight status: 1. starting with Increment-7, the number of crew was decreased to two (from the previous 3-member crew to 2-member crew); 2. no science facilities or new experiments are being sent to the ISS, unless they take up minimum space and weigh very little. Consequently, Increment-7 had a 2-member crew and no new facility and/or new experiments were sent to the ISS with the crew. There were no station assembly tasks performed during Increment-7 tour of duty to the ISS, thus, the ISS Increment-7's configuration was identical to the Increment-6's.

3.4 Increment-7 Science and Crew Members

Due to the up-mass and down-mass constraints of the Soyuz vehicle, most of the research complement for Increment-7 was carried out with scientific research facilities and samples already on board the space station from previous increments. The experiments during Expedition Seven were focused on life sciences, physics and chemistry, and their applications in materials and manufacturing processes. The crew performed studies as well in Earth observation—its environment, climate, geology and oceanography [10]. Expedition Seven crewmembers devoted nearly 200 hours to scientific investigations while continuing to maintain the orbiting research complex. Far more research time has been accumulated by experiments controlled by investigators on the ground, adding to the more than 100,000 hours of experiment operation time already accumulated aboard the station [10]. Increment-7 had one astronaut and one cosmonaut. The commander was cosmonaut Yuri Malenchenko and the flight engineer was astronaut Edward (Ed) Tsang Lu. The crew was launched to the ISS on April 25, 2003 aboard the Soyuz TMA-2 from the Baikonur Cosmodrome, Kazakhstan, and landed on the flat steppes of north central Kazakhstan (in central Asia) on October 27, 2003 aboard the Russian Soyuz TMA-2.

3.5 Increment-8 Configuration

This Increment is called Increment-8/Soyuz 7 or Expedition Eight. The 2-member crew for Increment-8 mission was launched to ISS on October 18, 2003 on Soyuz TMA-3 from the Baikonur Cosmodrome, Kazakhstan, in central Asia and returned to earth on the Russian Soyuz TMA-3 on April 29, 2004 after a 194 days stay in space. There were no station assembly tasks performed during Increment-8 tour of duty to the ISS for the reasons mentioned earlier. Consequently, the ISS Increment-8's configuration was identical to the previous increment.

3.6 Increment-8 Science and Crew Members

Due to the up-mass and down-mass constraints of the Soyuz vehicle, most of the research complement for Increment-8 was carried out with scientific research facilities and samples already on board the space station from previous increments. Additional studies in the life and physical sciences and space technology development were added. Also several Russian experiments were sent to the station on the Progress 12 resupply vehicle [11]. The two-member crew worked on more than four dozen U.S and Russian experiments. The experiments during Expedition Eight were focused on life sciences, physics and chemistry, and their applications in materials and manufacturing processes. The crew performed studies as well in Earth observation—its environment, climate, geology and oceanography. Expedition Eight crewmembers devoted nearly 300 hours to scientific investigations while continuing to maintain the orbiting research complex [12]. Far more research time has been accumulated by experiments controlled by investigators on the ground, adding to the more than 100,000 hours of experiment operation time already accumulated aboard the station [12]. Increment-8 had one astronaut and one cosmonaut. The commander was astronaut Michael Foale and the flight engineer was cosmonaut Alexander Kaleri. The crew was launched to the ISS on October 20, 2003 aboard the Soyuz TMA-3 from the Baikonur Cosmodrome, Kazakhstan, and landed on the flat steppes of north central Kazakhstan (in central Asia) on April 29, 2004 aboard the Russian Soyuz TMA-3.

3.7 Increment-6/8 Coordinate Systems

The coordinate systems [13] shown in Figure 3-2 were used in performing the data analysis presented in this report. Figure 3-2 shows MAMS OSS and MAMS HiRAP positive acceleration axes alignment relative to the ISS analysis coordinate system (for SAMS, see section 4.4). However, the origin of the coordinate systems shown is not exactly at the location shown (except for the ISS analysis coordinate system). They are shown here for relative alignment only, not their origin. For their location relative to the ISS analysis coordinate system, the reader should refer to section 4.2. In Figure 3-2, XYZ_A refers to the ISS analysis coordinate system, XYZ_H refers to the MAMS HiRAP coordinate system and XYZ_{OSS} refers to the MAMS OSS coordinate system. Figure 3-2 is provided only to illustrate the coordinate system relationships during Increment-6/8.

3.8 Increment-6/8 Overall Attitude

During the assembly stages (stages 2A through 12A.1), the ISS will not be capable of generating enough power to sustain the required electrical loads in the XVV flight attitude at mid-to-high solar beta angles because these vehicle configurations have only a single solar array gimbal axis, which is aligned so that it only perfectly tracks the Sun when the solar beta angle is near zero. Therefore, the ISS is designed to accommodate a second basic flight orientation for these increments. This attitude is referred to as X Principal Axis Perpendicular to the Orbit Plane (XPOP) (see Figure 3-3), which stands for X principal axis perpendicular to the orbit plane, Z Nadir at orbital noon. The XPOP flight attitude [6] sets up geometry between the ISS and the Sun so that the Sun aligns with the ISS/XZ body axis plane. This allows all the solar arrays to track the Sun regardless of the solar beta angle. XPOP also places the dominant inertia axis in the local horizontal to minimize gravity gradient torques and allow Control Moment Gyro (CMG) non-propulsive attitude control.

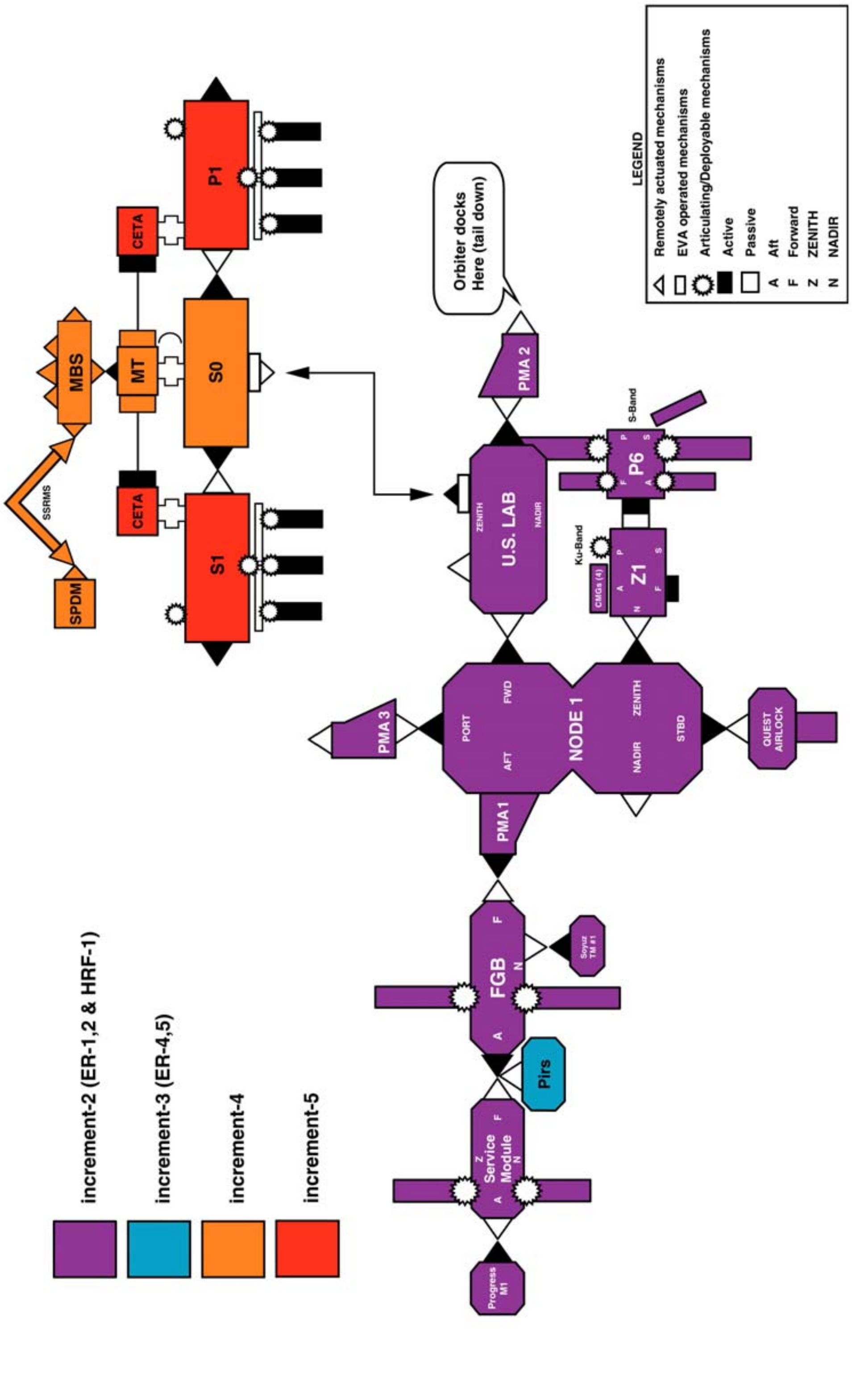

Figure 3-1 ISS Increment-6/8 Configuration

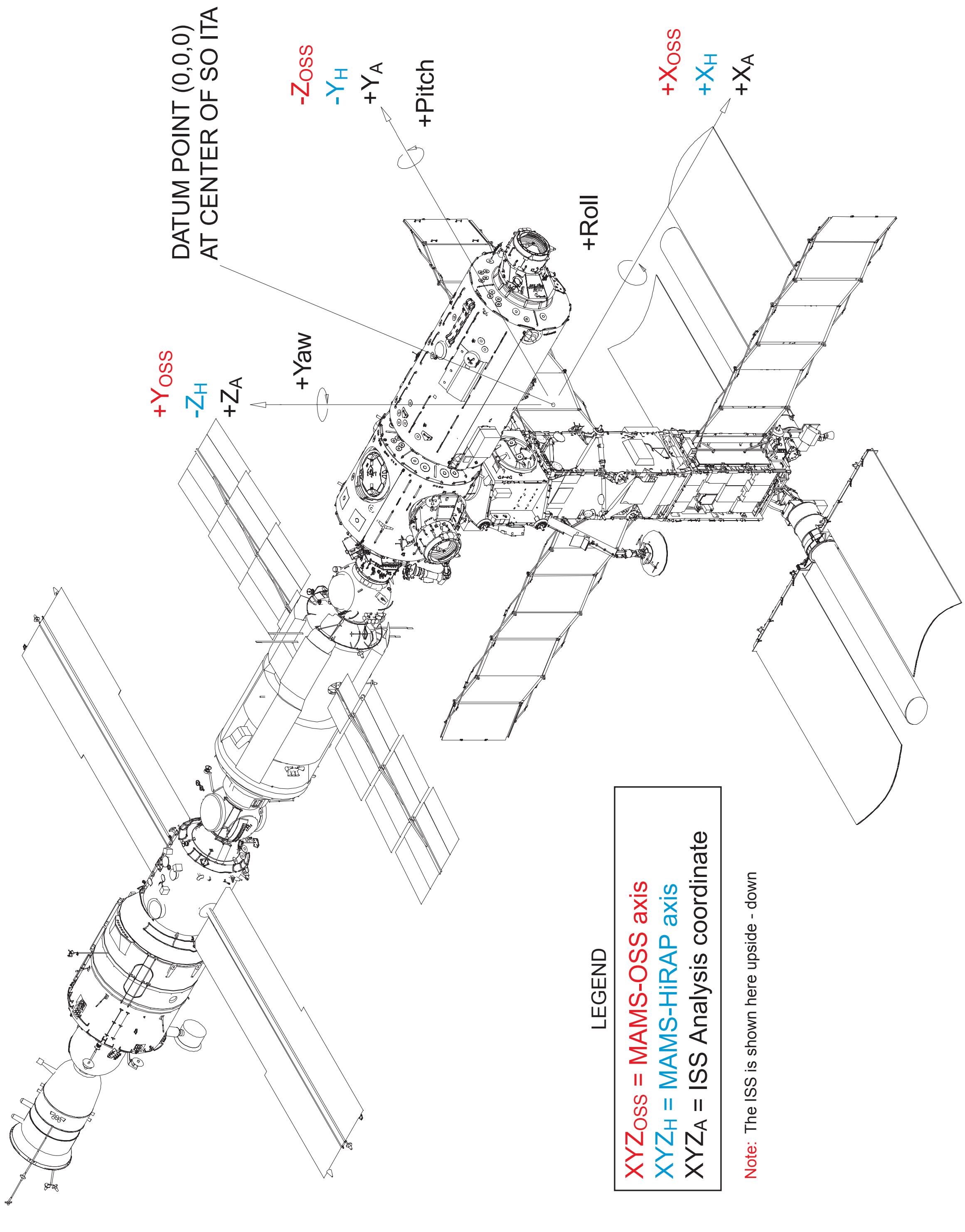

Figure 3-2 Increment-6/8 Coordinate Systems

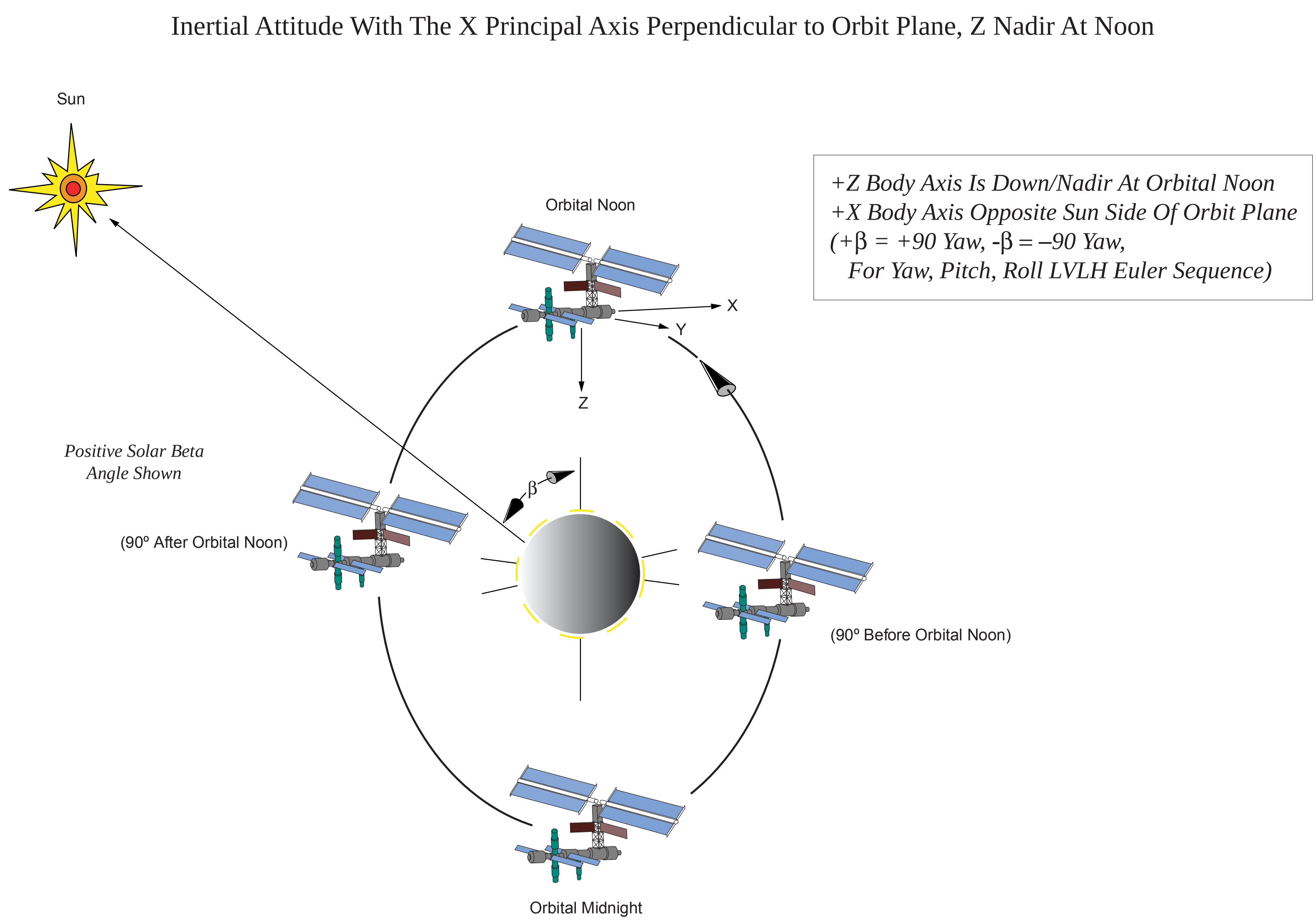

Figure 3-3 ISS in the XPOP Inertial Flight Attitude

4 Acceleration Measurement System Descriptions: Increment-6/8

One of the major goals of the ISS is to provide a quiescent low-gravity environment to perform fundamental scientific research. However, small disturbances aboard the Space Station impact the overall environment in which experiments are being performed. Such small disturbances need to be measured in order to assess their potential impact on the experiments. Two accelerometer systems developed by NASA's GRC in Cleveland, Ohio, are being used aboard the station to acquire such measurements. These two systems were flown to the ISS on April 19, 2001 aboard the space shuttle flight STS-100.

4.1 Microgravity Acceleration Measurement System (MAMS)

MAMS measures acceleration caused by aerodynamic drag, vehicle rotations, and vents of air and water. MAMS consists of two sensors. MAMS OSS, a low frequency sensor (up to 1 Hz), is used to characterize the quasi-steady environment for payloads and the vehicle. The raw MAMS OSS data are typically trimmean filtered to extract the quasi-steady acceleration data content. Details of the trimmean filter process and the exact implementation of it relative to MAMS OSS data are described in Appendix B.2. MAMS HiRAP [14] is used to characterize the ISS vibratory environment up to 100 Hz. For Increment-6/8, MAMS was located in a double middeck locker, in the US Laboratory Module (Destiny) in the EXpedite the PRocessing of Experiments to the Space Station (EXPRESS) Rack 1.

4.2 MAMS Coordinate Systems

MAMS was located in middeck lockers 3 and 4 of EXPRESS Rack 1, in overhead bay 2 of the US Laboratory Module (LAB1O2). The origin of the OSS coordinate system is located at the center of gravity of the OSS proof mass. Table 4-1 gives the orientation and location of the OSS and HiRAP coordinate systems with respect to the Space Station Analysis coordinate system.

TABLE 4-1 MAMS SENSOR COORDINATE SYSTEM

<table>
<tr><th rowspan="2">MAMS Sensor</th><th colspan="3">Location (inches)</th><th colspan="3">Orientation (degrees)</th><th colspan="4">Unit Vector in Analysis Coordinates</th></tr>
<tr><th>X_A</th><th>Y_A</th><th>Z_A</th><th>Roll</th><th>Pitch</th><th>Yaw</th><th>Axes</th><th>X_A</th><th>Y_A</th><th>Z_A</th></tr>
<tr><td rowspan="3">OSS</td><td rowspan="3">135.28</td><td rowspan="3">-10.68</td><td rowspan="3">132.12</td><td rowspan="3">90</td><td rowspan="3">0</td><td rowspan="3">0</td><td>X_{OSS}</td><td>1</td><td>0</td><td>0</td></tr>
<tr><td>Y_{OSS}</td><td>0</td><td>0</td><td>1</td></tr>
<tr><td>Z_{OSS}</td><td>0</td><td>-1</td><td>0</td></tr>
<tr><td rowspan="3">HiRAP</td><td rowspan="3">138.68</td><td rowspan="3">-16.18</td><td rowspan="3">142.35</td><td rowspan="3">180</td><td rowspan="3">0</td><td rowspan="3">0</td><td>X_H</td><td>1</td><td>0</td><td>0</td></tr>
<tr><td>Y_H</td><td>0</td><td>-1</td><td>0</td></tr>
<tr><td>Z_H</td><td>0</td><td>0</td><td>-1</td></tr>
</table>

4.3 Space Acceleration Measurement System (SAMS)

SAMS measures accelerations caused by vehicle, crew, and experiment disturbances. SAMS measures the vibratory/transient accelerations, which occur in the frequency range of 0.01 to 400 Hz. For Increment-6/8, there were four SAMS sensor heads located in the EXPRESS Racks 1 and 2. During Increments 7 and 8, a fifth SAMS sensor head, 121f08, located in the Microgravity Science Glovebox (MSG) rack, was sporadically activated in support of scientific experiments performed in that rack and to perform the low-gravity environment characterization of that facility. The sensors measure the accelerations electronically and transmit the data to the Interim Control Unit (ICU) located in the EXPRESS Rack drawer. Data are collected from all the sensors and downlinked to the Telescience Support Center (TSC) at GRC. Additional SAMS data flow details are provided in appendix C. The PIMS project processes and displays the acceleration data on the PIMS Web site for easy access by the microgravity scientific community at:

http://pims.grc.nasa.gov.

4.4 SAMS Coordinate Systems

During Increment-6/8, four SAMS Sensor Enclosure (SE) heads 121f02 through121f05 were active and 121f08 was, at time (sporadically during Increment-7/8), active as well. Each sensor head has a defined coordinate system whose location and orientation are with respect to the Space Station Analysis Coordinate System. The origin is defined as the triaxial center point of the three accelerometers that comprise the head.

SAMS SE 121f02 was mounted in the SAMS ISIS drawer 1 in EXPRESS Rack 1. Head 121f03 was mounted on the lower Z Panel assembly below EXPRESS Rack 2, head 121f04 was mounted on the lower Z Panel assembly below EXPRESS Rack 1, and head 121f05 was mounted on a bracket around the upper Z Panel light assembly of EXPRESS Rack 2. SAMS SE 121f08 was mounted inside the MSG rack on the left back side (or the back right side—see footnote in Table 4-2) of the ceiling plate. Table 4-2 summarizes the SAMS SE coordinate systems.

TABLE 4-2 SAMS SE COORDINATE SYSTEMS

Sensor	Location (inches)			Orientation (degrees)			Unit Vector in Analysis Coordinates			
	X_A	Y_A	Z_A	Roll	Pitch	Yaw	Axes	X_A	Y_A	Z_A
121f02	128.73	-23.53	144.15	-90	0	-90	X_{F02}	0	-1	0
							Y_{F02}	0	0	-1
							Z_{F02}	1	0	0
121f03	191.54	-40.54	135.25	0	30	-90	X_{F03}	0	-.866	-.500
							Y_{F03}	1	0	0
							Z_{F03}	0	-.5	.866
121f04	149.54	-40.54	135.25	0	30	-90	X_{F04}	0	-.866	-.500
							Y_{F04}	1	0	0
							Z_{F04}	0	-.5	.866
121f05	185.17	38.55	149.93	90	0	90	X_{F05}	0	1	0
							Y_{F05}	0	0	1
							Z_{F05}	1	0	0
121f08 [1]	118.14	53.52	160.52	-90	90	0	X_{F08}	0	0	-1
							Y_{F08}	-1	0	0
							Z_{F08}	0	1	0
121f08 [2]	87.99	55.19	160.98	90	90	0	X_{F08}	0	0	-1
							Y_{F08}	1	0	0
							Z_{F08}	0	-1	0

[1] Valid from August 26, 2003 to July 16, 2003—The head was located on the ceiling plate (back left side)
[2] Valid from July 17, 2003 to April 29, 2004—The head was located on the ceiling plate (back right side)

5 Increment-6/8 Facilities and Experiments Descriptions

5.1 Increment-6/8 Facilities Description

Due to the grounding of the space shuttle fleet following the Columbia Orbiter accident on February 1, 2003, all crew rotations, delivery and access to and from the ISS are being assured by the Russian Soyuz and Progress vehicles until the return to flight status of the space shuttle fleet. The Russian Soyuz and Progress vehicles are very limited in their upmass and downmass capability. Due to that constraint no new facility was delivered to the ISS during the period covered by Increment-7/8 (no facility was delivered by the shuttle space either during Increment-5/6 rotation because that flight was used for the ISS assembly component delivery—P-1 Truss). However, several research facilities were already in place, during previous Increments, to support science investigations. Therefore, only the facilities that were delivered to the ISS prior to Increment-6 were used by the crew to perform their scientific research.

During Increment-6/8, the following facilities were onboard the ISS: the Advanced Thermoelectric Refrigerator/Freezer (ARCTIC) 1 and 2, the EXpedite the PRocessing of Experiments to the Space Station (EXPRESS) racks 1 through 5, The Microgravity Science Glovebox (MSG) and the Human Research Facility (HRF) rack. Table 5-1 shows the locations, mission information, research areas and the expected duration of each of these facilities on the ISS. ARTIC 1 and 2 are the main cold storage (refrigerator/freezer) facilities on ISS until larger, more complex facilities are sent to the station. These two facilities provide cold storage for a range of perishable biomaterials and reagents [15]. ARCTIC-1 is installed in EXPRESS Rack 4 while ARCTIC-2 is installed in EXPRESS Rack 3. These two units provide a total of 38 liters of minus 20-degree cold stowage onboard the ISS [16]. The EXPRESS Rack [17] is a standardized payload rack system that transports, stores and supports experiments aboard ISS. The EXPRESS Rack system supports science payloads in several disciplines, including biology, chemistry, physics, ecology and medicine. The EXPRESS Rack with its standardized interfaces enables quick, simple integration of multiple payloads aboard the station. Each EXPRESS Rack is housed in an International Standard Payload Rack – a refrigerator-size container that acts as the EXPRESS Rack's exterior shell--and can be divided into segments. The EXPRESS Racks [18] have eight middeck locker locations and two drawer locations each (Figure 5-1 and Figure 5-2). Figure 5-3 illustrates the relative locations of each EXPRESS rack within the US laboratory volume. Utilities provided to experiments by the four EXPRESS racks currently on ISS include power, fluids, gasses, cooling, and data management support. Over the life of the Space Station, these facilities will support a wide range of experiments [19]. There are currently five EXPRESS Racks (Rack 1 through 5) onboard the ISS. Amongst the five EXPRESS Racks onboard the ISS, EXPRESS Racks 2 and 3 are equipped with the Active Rack Isolation System (ARIS)--a system that isolates the entire rack (and all the experiments being performed inside that specific rack) within a certain frequency band from vibrational disturbances present within the ISS environment. The empty weight of each EXPRESS rack is about 785 pounds [20]. The MSG—a sealed container with built-in gloves—provides an enclosed work space for investigations conducted in the unique, low-gravity environment created as ISS orbits earth [21]. MSG is designed to accommodate small and medium-sized investigations from many disciplines including biotechnology, combustion science, fluid physics, fundamental physics and materials science. The part of the unit that holds experiment equipment is called the work volume and has a usable volume of about 67 gallons (255 liters) [21]. An airlock under the work volume can be accessed to bring objects safely into the work volume, while other activities are going on inside the glovebox. The glovebox has side ports, 16 inches (40 centimeters) in diameter, for setting up and manipulating equipment inside the box. The ports are equipped with rugged gloves that can be sealed tightly to prevent leaks. The glovebox provides vacuum, venting and gaseous nitrogen, power and data interfaces to investigations. The HRF rack provides an on-orbit laboratory that allows life science researchers to study and evaluate the physiological, behavioral and chemical changes in human beings induced by space flight. The results of the research will provide data relevant to longer term adaptation to the space flight environment. The HRF rack provides to experiments electrical power, command and data handling, cooling air and water, pressurized gases and vacuum [22]. The HRF rack houses a computer workstation and portable computer laptop for crew to command, test, collect, store and send data to and from scientists on Earth.

TABLE 5-1 ISS INCREMENT-6/8 FACILITIES

Facility	Mission Information	Duration	Location on ISS	Research Area
EXPRESS Racks 1 and 2	Up on 6A	Permanent	Destiny lab module	Multi-disciplinary
EXPRESS Racks 4 and 5	Up on 7A.1	Permanent	Destiny lab module	Multi-disciplinary
Human Research Facility Rack 1	Up on 5A.1	Permanent	Destiny lab module	Human life sciences
EXPRESS Rack 3	Up on UF-2	Permanent	Destiny lab module	Multi-disciplinary
Microgravity Science Glovebox	Up on UF-2	Permanent	Destiny lab module	Multi-disciplinary
ARCTIC 1 and 2	1- Up on 8A 2- Up on UF-2	Permanent	EXPRESS Rack 4	Multi-disciplinary

5.2 Increment-6/8 Experiments Description

During Increment-6/8, some new experiments (mainly during Increment-6) were ferried to the ISS. The research complement for Increment-6 included 20 new or continuing investigations. The research complement included four experiments that were either new or making a repeat flight: Coarsening in Solid Liquid Mixture (CSLM), Investigating the Structure of Paramagnetic Aggregates from Colloidal Emulsions (InSPACE), Foot/Ground Reaction Forces During Spaceflight and Protein Crystal Growth Single-locker Thermal Enclosure System (PCG-STES). The first two investigations were conducted in the MSG and studied materials processing. The third investigation was a microgravity physiology study investigating lower body muscles and the fourth one, a Protein Crystal Growth, was a returning study from previous expedition. Sixteen experiments were continued from the previous Increment [9]. Table 5-2 and Table 5-3 show the U.S and the Russian research complements for Increment-6 [9]. For Increment-6, the PIMS project actively supported the following experiments, that required acceleration data measurements to assess the impact of the ISS low-gravity environment: CSLM and InSPACE.

Most of the research complement for Increment-7 was carried out with the scientific research facilities and samples already onboard the ISS. Many experiments from earlier Increments remained aboard the station, thus continued to benefit from the long-term research platform. A total of fourteen U.S experiments from previous Increments benefited from a longer stay on the ISS. Many of the Increment-7 Russian science experiments were delivered on the Russian Progress 10 vehicle. Table 5-4 and Table 5-5 show the U.S and the Russian experiments conducted during Increment-7 [10]. Besides the experiments listed in Table 5-4 and Table 5-5, U.S conducted four Pre and Post flight experiments in human physiology dealing with changes in the body due to exposure to the microgravity environment, while the Russian conducted 11 Pre and Post flight experiments in the areas of motor control, muscular characteristics, sensor adaptation, kinematics and dynamic locomotion, anti-g force countermeasures development and human peripherical thermo-regulation during readaptation to earth gravity [10].

As was the case for Increment-7, the research complement for Increment-8 was made up mainly of the scientific research facilities and samples left onboard the station from previous Increments. A total of thirteen U.S investigations benefited from the longer stay on the station. Several Russian science experiments were delivered to the ISS by the Russian Progress 12 vehicle. Table 5-6 and Table 5-7 show the U.S and the Russian experiments conducted during Increment-8 [12]. Besides the experiments listed in Table 5-6 and Table 5-7, U.S conducted five Pre and Post flight experiments in human physiology dealing with changes in the body due to exposure to the microgravity environment, while the Russian conducted 11 Pre and Post flight experiments in the areas of motor control, locomotion, sensor adaptation, radiation dosage level and human tolerance to space flight condition [12]. Also, during the crew rotation period, the third European Space Agency (ESA) astronaut, Pedro Duque, performed a series of experiments in the fields of life and physical sciences, Earth observation, education and technology. Most of the experiments were performed in the Russian segment of the Station. The MSG was used for the ESA's physical science experiments. Table 5-8 shows some of the experiments performed during the crew rotation by the ESA astronaut [12].

In addition to the experiments supported by PIMS during Increment-6/8, the PIMS project continues to characterize the reduced gravity environment of the ISS in an uninterrupted manner from increment to increment so that both current and future investigators can access the impact of the ISS reduced gravity environment on their experiments based on the analyses performed and distributed by PIMS using the two set of accelerometers aboard the ISS. It is hoped that future investigators will take such potential impact into account during the design phase and preliminary analysis of their experiment scheduled to be performed aboard the ISS.

TABLE 5-2 USOS ISS INCREMENT-6 PAYLOADS COMPLEMENT

Experiment	Mission information	Duration	Location on ISS	Research Area
Coarsening in Solid Liquid Mixture (CSLM)	Up on 11-A Down on ULF1	4 months	Glovebox	Microgravity Materials
Investigating the Structure of Paramagnetic Aggregates from Colloidal Emulsion (InSPACE)	Up on 11-A & Samples down on ULF-1	4 months	Glovebox	Microgravity Materials
Crew Earth Observation (CEO)	Increments 1-7	34 months	Destiny and Zvezda modules	Earth observation
Earth Knowledge Acquired by Middle School students (EarthKAM)	Up on 5-A	On-going	ISS windows	Education
Effect of Prolonged Spaceflight on Human Skeletal Muscle (Biopsy)	Increments 5-8	N/A	Pre- and post-flight	Human Life Sciences
Pore Formation and Mobility Investigation (PFMI)	Up on UF-2 Down on ULF-1	9 months	Glovebox	Microgravity sciences
Microgravity Acceleration Measurement System (MAMS)	Up on 6-A	Permanent	EXPRESS Rack 1	Microgravity
Space Acceleration Measurement System II (SAMS-II)	Up on 6-A	Permanent	EXPRESS Racks 1 & 4	Microgravity
Sub-regional Assessment of Bone Loss in Axial Skeleton in Long term Spaceflight (Sub-regional Bone)	Increments 2-9	39 months	Pre- and post-flight	Human Life Sciences
Promoting Sensorimotor Response Generalizability (Mobility)	Increments 5-10	N/A	Pre- and post-flight	Human life sciences
Space Flight Induced Reactivation of Epstein-Bar Virus (Epstein-Barr)	Increments 5-8 and 10	N/A	Pre- and post-flight	Human life sciences
Materials International Space Station Experiment (MISSE)	Up on 7-A.1 Down on ULF-1	19 months	External attachement on Quest airlock	Materials exposure
Pulmonary Function in Flight (PuFF)	Increments 3-6	19 months	Human Research Facility	Human Life Sciences
EVA Radiation Monitoring (EVARM)	Increments 4-6	15 months	Human Research Facility	Human life sciences
Protein Crystal Growth-single- locker Thermal Enclosure System (PCG-STES) housing the Diffusion-controlled Crystallization Apparatus for Microgravity (DCAM)	Up on 11-A Down on ULF-1	4 months	EXPRESS Rack 4	Biotechnology
Foot/Ground Reaction Forces During Space Flight	Up on 11-A Down on ULF-1	4 months	Human Research Facility	Human life sciences
Renal Stone Risk During Spaceflight (Renal Stone)	Increments 3-12	49 months	Human Research Facility	Human life sciences
Zeolite Crystal Growth Furnace (ZCG)	Furnace unit up on UF-1; samples up and down on most Shuttle flights	Increments 4-8	EXPRESS Rack 2	Space product development

TABLE 5-3 ROS-ISS INCREMENT-6 PAYLOADS COMPLEMENT

Experiment Name	Research Objective	Hardware Used	Up/Down Flight or Vehicle	Research Area
КНТ-1 "GTS"—Global Timing System	Global timing System test development	Electronic unit; Antenna unit with attachment mechanism	Existing on orbit	Commercial
КНТ-2-- MPAC & SEED	Study of meteoroid and man-made particle and the outer space impact on exposed materials	Micro particles collection device and material exposure array MPAC & SEED	Existing on orbit	Commercial
ГФИ-1 "Relaksatsiya" (Relaxation)	Study of the chemiluminescent chemical reactions and atmospheric light phenomena	"Fialka-MV Kosmos" spectral-zonal ultraviolet system	Existing on orbit	Geophysical
ГФИ-8 "Uragan"	Experimental testing and verification of the ground-space system for eliminating the impact of man-made catastrophes	Binocular telescopic device Rubinar; Photo camera Hasselblad; Video complex LIV	Existing on orbit	Geophysical
ГФИ-10 "Molnia-SM	Study of atmosphere, ionosphere and magnetosphere electromagnetic interaction related to storms & seismic activities	BFS-3M video-photometric system	Existing on-orbit; Progress	Geophysical
МБИ-3 "Parodont"	Study of periodontal tissue condition under space flight conditions	Kriogem-03/1 refrigerator	Progress	Biomedical
МБИ-4 "Farma"	Study of specific pharmacological effects under long duration space flight	Saliva-F kit	Progress	Biomedical
МБИ-5 "Kardio-ODNT"	Comprehensive study of the cardiac activity and blood circulation primary parameter dynamics	"Gamma-1M" equipment, "Chibis" LBNP device	Existing on-orbit	Biomedical
МБИ-8 Profilaktika (Countermeasure)	Study of mechanisms and efficiency of various countermeasures aimed at preventing locomotor system disorders in weightlessness	Reflotron-4 complex; TVIS treadmill; VB-3 bicycle ergometer; Bungee cords set; Gamma-1M equipment; Laptop; Kardiokasseta; power unit Tsentr	Existing on-orbit	Biomedical
РБО-1 "Prognoz"	Development of a method for real-time prediction of radiation dose loads on the crews of manned space stations	P-16 radiometer; ДБ-8 dosimeters (4 units)	Existing on-orbit Progress	Biomedical
РБО-2 "Bradoz".	Bioradiation dosimetry during spaceflight	"Bradoz" kit	Progress	Biomedical
МБи-9 "Pulls"	Study of the autonomic regulation of the human cardio-respiratory system in weightlessness	Pulse set, Pulse kit And computer	On-orbit	Biomedical
Био-2 "Biorisk"	Study of space flight impact on micro-organism substrates systems state related to space technique ecological safety and planetary quarantine problem	Biorisk-KM set (4 units); Biorisk-MSV containers (6 units); Biorisk-MSN set	Progress	Biomedical
Био-5 "Rasteniya-2"	Study of the space flight effect on the growth and development of higher plants	Lada greenhouse; Water container; BVP-70P video camera from the LIV video system; Computer	On-orbit	Biomedical
TEX-20 "Plazmennyi Kristall"	Study of the plasma dust crystals and fluids under microgravity	Plazmennyi kristal equipment; telescience flight equipment		Technical studies
БТХ-11 "Biodegradatsiya"	Assessment of the initial stages of biodegradation and biodeterioration of the surfaces of structural materials	Biodegradatsiya-G01 kit; GO2 kit	Progress	Biotechnology
TEX-3 "Akustika-M"	Acoustic study of ISS crew voice communication optimization	Akustika-M kit	Progress	Technical studies
TEX-5 "Meteoroid" (SDT 16002-R)	Recording meteoroid and man-made particle impacts on the exterior of ISS RS SM	MMK-2 electronic unit; stationary capacitor sensors	Existing on-orbit	Technical studies
TEX-13 "Tenzor" (SDTO 12001-R)	Determination of ISS dynamic characteristics	ISS RS motion control system; sensors; star tracker; GPS GLONAS satellite system	Existing on-orbit	Technical studies
TEX-14 "Vektor-T" (SDTO 12002-R)	Study of high-precision system for ISS motion prediction	ISS RS sensors; ISS RS orbit radio tracking system; GPS	Existing on-orbit	Technical studies

Table 5-3, Continued from previous page

Experiment Name	Research Objective	Hardware Used	Up/Down Flight or Vehicle	Research Area
TEX-15 “izgib” (Bending-SDTO 13002-R)	Study of the relationship between the onboard operating modes and ISS flight conditions	ISS RS accelerometers and rotational speed sensors	Existing on-orbit	Technical studies
TEX-16 “Privyazka” (Alignment-SDTO 12003-R)	High-precision orientation of science instruments in space with consideration given of ISS hull deformation	ISS RS sensors (SM-8M) and magnetometer	Existing on-orbit	Technical studies
TEX-17 “Iskazheniye” (Distorsion-SDTO 16001-R)	Determination and analysis of magnetic disturbances on the ISS	ISS RS SM attitude control sensors and control loop magnetometers	Existing on-orbit	Technical studies
TEX-22 “Identifikatsiya” (Identification) (SDTO 13001-R)	Identification of disturbance sources when the microgravity conditions on the ISS are disrupted	Linear optical accelerometer with cables; micro acceleration measurement device with cables.	Existing on-orbit	Technical Studies
TEX-3 “Skorpion”	Development, testing, and verification of a multi-functional instrument to monitor the science experiment conditions inside the ISS pressurized compartments	Skorpion equipment (CKP-1)	TBD	Technical studies
ИКЛ-1В “Platan”	Search for low energy heavy nuclei of solar and galactic origin	Platan-M equipment	Existing on-orbit	Study of cosmic rays
ПКЕ-1В “Kromba”	Study of the dynamics of contamination from liquid-fuel thruster jets during buns, and verification of the efficacy of devices designed to protect the ISS exterior surfaces from contamination	Tray with materials to be exposed	Existing on-orbit	Space energy systems
Д33-2 “Diatomea”	Study of stability of the geography position and form of the boundaries of the world ocean biologically active water areas observed by space station crews	Nikon F5 camera; Video camera; Dictaphone; Laptop # 3; “Diatomea” kit	Existing on-orbit	Study of Earth natural resources and ecological monitoring

TABLE 5-4 USOS ISS INCREMENT-7 PAYLODS COMPLEMENT

Experiment	Mission information	Duration	Location on ISS	Research Area
Coarsening in Solid Liquid Mixture (CSLM)	Up on 11-A Down on ULF1	4 months	Glovebox	Microgravity Materials
Investigating the Structure of Paramagnetic Aggregates from Colloidal Emulsion (InSPACE)	Up on 11-A & Samples down on ULF-1	4 months	Glovebox	Microgravity Materials
Crew Earth Observation (CEO)	Increments 1-7	34 months	Destiny and Zvezda modules	Earth observation
Earth Knowledge Acquired by Middle School students (EarthKAM)	Up on 5-A	On-going	ISS windows	Education
Pore Formation and Mobility Investigation (PFMI)	Up on UF-2 Down on ULF-1	9 months	Glovebox	Microgravity sciences
Microgravity Acceleration Measurement System (MAMS)	Up on 6-A	Permanent	EXPRESS Rack 1	Microgravity
Space Acceleration Measurement System II (SAMS-II)	Up on 6-A	Permanent	EXPRESS Racks 1 & 4	Microgravity
Sub-regional Assessment of Bone Loss in Axial Skeleton in Long term Spaceflight (Sub-regional Bone)	Increments 2-9	39 months	Pre- and post-flight	Human Life Sciences
Promoting Sensorimotor Response Generalizability (Mobility)	Increments 5-10	N/A	Pre- and post-flight	Human life sciences
Space Flight Induced Reactivation of Epstein-Bar Virus (Epstein-Barr)	Increments 5-8 and 10	N/A	Pre- and post-flight	Human life sciences
Materials International Space Station Experiment (MISSE)	Up on 7-A.1 Down on ULF-1	19 months	External attachement on Quest airlock	Materials exposure
EVA Radiation Monitoring (EVARM)	Increments 4-6	15 months	Human Research Facility	Human life sciences

Table 5-4, Continued from previous page

Experiment	Mission information	Duration	Location on ISS	Research Area
Protein Crystal Growth-single- locker Thermal Enclosure System (PCG-STES) housing the Diffusion-controlled Crystallization Apparatus for Microgravity (DCAM)	Up on 11-A Down on ULF-1	4 months	EXPRESS Rack 4	Biotechnology
Renal Stone Risk During Spaceflight (Renal Stone)	Increments 3-12	49 months	Human Research Facility	Human life sciences
Zeolite Crystal Growth Furnace (ZCG)	Furnace unit up on UF-1; samples up and down on most Shuttle flights	Increments 4-8	EXPRESS Rack 2	Space product development
Cell Biotechnology Operations Support System (CBOSS)	Increments 3-4 & 7-10	Increment-10	Destiny Module	Human life science
Crewmember and crew-ground interaction during ISS missions	Increments 2 and 6; 5A-1	Increments 7-10	Human research Facility	Phycho-social
Education Payload Operation (EPO)	Increment-7	Increments 7-10	Destiny Module	Education
Earth Science Toward Exploration Research (ESTER)	Increment-7	Increments 7-8	ISS windows	Earth observation

TABLE 5-5 ROS-ISS INCREMENT-7 PAYLOADS COMPLEMENT

Experiment Name	Research Objective	Hardware Used	Up/Down Flight or Vehicle	Research Area
КНТ-1 “GTS”—Global Timing System	Global timing System test development	Electronic unit; Antenna unit with attachment mechanism	Existing on orbit	Commercial
КНТ-2-- MPAC & SEED	Study of meteoroid and man-made particle and the outer space impact on exposed materials	Micro particles collection device and material exposure array MPAC & SEED	Existing on orbit	Commercial
КНТ-21 “STARMAIL”	Downlink of messages with images and text records from ISS RS	Nikon D1; Sony PD 150P; Laptop TP1; CD-disk	Existing on orbit	Commercial
ГФИ-1 “Relaksatsiya” (Relaxation)	Study of the chemiluminescent chemical reactions and atmospheric light phenomena	“Fialka-MV Kosmos” spectral-zonal ultraviolet system	Existing on orbit	Geophysical
ГФИ-8 “Uragan”	Experimental testing and verification of the ground-space system for eliminating the impact of man-made catastrophes	Binocular telescopic device Rubinar; Photo camera Hasselblad; Video complex LIV	Existing on orbit	Geophysical
МБИ-1 “Sprut-MB1”	Study of human bodily fluids during long duration space flight	Sprut-K kit; Tsentr power supply; central Laptop computer	On orbit	Biomedical
МБИ-2 “Diurez”	Study of fluid electrolyte metabolism and hormonal regulation of blood volume in microgravity	Urine receptacle kit; Kriogem-freezer; plazma kit; Hematocrit kit	On orbit	Biomedical
ГФИ-10 “Molnia-SM	Study of atmosphere, ionosphere and magnetosphere electromagnetic interaction related to storms & seismic activities	BFS-3M video-photometric system	Existing on-orbit; Progress	Geophysical
МБИ-3 “Parodont”	Study of periodontal tissue condition under space flight conditions	Kriogem-03/1 refrigerator	Progress	Biomedical
МБИ-4 “Farma”	Study of specific pharmacological effects under long duration space flight	Saliva-F kit	Progress	Biomedical
МБИ-5 “Kardio-ODNT”	Comprehensive study of the cardiac activity and blood circulation primary parameter dynamics	“Gamma-1M” equipment, “Chibis” LBNP device	Existing on-orbit	Biomedical
МБИ-7 “Biotest”	Biochemical mechanism of metabolic adaptation to space flight environment	Gamma-1 M equipment; Hematocrit kit	Existing on-orbit	Biomedical
МБИ-8 Profilaktika (Countermeasure)	Study of mechanisms and efficiency of various countermeasures aimed at preventing locomotor system disorders in weightlessness	Reflotron-4 complex; TVIS treadmill; VB-3 bicycle ergometer; Bungee cords set; Gamma-1M equipment; Laptop; Kardiokasseta; power unit Tsentr	Existing on-orbit	Biomedical

Table 5-5, Continued from previous page

Experiment Name	Research Objective	Hardware Used	Up/Down Flight or Vehicle	Research Area
РБО-1 "Prognoz"	Development of a method for real-time prediction of radiation dose loads on the crews of manned space stations	P-16 radiometer; ДБ-8 dosimeters (4 units)	Existing on-orbit Progress	Biomedical
РБО-2 "Bradoz".	Bioradiation dosimetry during spaceflight	"Bradoz" kit	Progress	Biomedical
МБи-9 "Pulse"	Study of the autonomic regulation of the human cardio-respiratory system in weightlessness	Pulse set, Pulse kit And computer	On-orbit	Biomedical
МБИ-11 "Gematologia"	New data obtaining of the outer space factor effects on human blood system in order to extend its diagnostic and prognostic capabilities, studying the mechanism of appearance of changes in hematological values (space anemia)	Erythrocyte kit; Kriogem-freezer; Plazma kit; Hematocrit kit	Existing on orbit	Biomedical
МБИ-15 "Pilot"	Researching for individual features of psychophysiological regulation of cosmonauts' state and crewmembers professional activities during long space flight	Right Control Handle Left Control Handle Synchronizer unit ULTRABIY-2000 unit; Laptop No 3	Existing on orbit	Biomedical
Био-2 "Biorisk"	Study of space flight impact on micro-organism substrates systems state related to space technique ecological safety and planetary quarantine problem	Biorisk-KM set (4 units); Biorisk-MSV containers (6 units); Biorisk-MSN set	Progress	Biomedical
Био-5 "Rasteniya-2"	Study of the space flight effect on the growth and development of higher plants	Lada greenhouse; Water container; BVP-70P video camera from the LIV video system; Computer	On-orbit	Biomedical
Био-10 "Mezhkletochnoe vzaimodeistvie—intercellular interaction"	Study of the microgravity influence on cells surface behavior and intercellular interaction	Fibroblast-1 kit; Aquarius hardware; Glovebox; KB-03 container	On orbit	Biomedical
ТЕХ-20 "Plazmennyi Kristall"	Study of the plasma dust crystals and fluids under microgravity	Plazmennyi kristal equipment; telescience flight equipment		Technical studies
БТХ-10 "Kon'yugatsiya—Conjugation"	Working through the process of genetic material transmission using bacteria conjugation method	Rekomb-K hardware; Biocont-T hardware; Aquarius hardware	On orbit	Biotechnology
БТХ-11 "Biodegradatsiya"	Assessment of the initial stages of biodegradation and biodeterioration of the surfaces of structural materials	Biodegradatsiya-G01 kit; GO2 kit	Progress	Biotechnology
БТХ-32 "MSC—Mesenchymal stem cells)	Study of behavior of mesenchymal stem cells from bone marrow under space flight conditions	Embrion kit; Aquarius hardware	On orbit	Biotechnology
ТЕХ-3 "Akustika-M"	Acoustic study of ISS crew voice communication optimization	Akustika-M kit	Progress	Technical studies
ТЕХ-5 "Meteoroid" (SDT 16002-R)	Recording meteoroid and man-made particle impacts on the exterior of ISS RS SM	MMK-2 electronic unit; stationary capacitor sensors	Existing on-orbit	Technical studies
ТЕХ-13 "Tenzor" (SDTO 12001-R)	Determination of ISS dynamic characteristics	ISS RS motion control system; sensors; star tracker; GPS GLONAS satellite system	Existing on-orbit	Technical studies
ТЕХ-14 "Vektor-T" (SDTO 12002-R)	Study of high-precision system for ISS motion prediction	ISS RS sensors; ISS RS orbit radio tracking system; GPS	Existing on-orbit	Technical studies
ТЕХ-15 "izgib" (Bending-SDTO 13002-R)	Study of the relationship between the onboard operating modes and ISS flight conditions	ISS RS accelerometers and rotational speed sensors	Existing on-orbit	Technical studies
ТЕХ-16 "Privyazka" (Alignment-SDTO 12003-R)	High-precision orientation of science instruments in space with consideration given of ISS hull deformation	ISS RS sensors (SM-8M) and magnetometer	Existing on-orbit	Technical studies
ТЕХ-17 "Iskazheniye" (Distorsion-SDTO 16001-R)	Determination and analysis of magnetic disturbances on the ISS	ISS RS SM attitude control sensors and control loop magnetometers	Existing on-orbit	Technical studies
ТЕХ-22 "Identifikatsiya" (Identification) (SDTO 13001-R)	Identification of disturbance sources when the microgravity conditions on the ISS are disrupted	Linear optical accelerometer with cables; micro acceleration measurement device with cables.	Existing on-orbit	Technical Studies

Table 5-5, Continued from previous page

Experiment Name	Research Objective	Hardware Used	Up/Down Flight or Vehicle	Research Area
TEX-3 “Skorpion”	Development, testing, and verification of a multi-functional instrument to monitor the science experiment conditions inside the ISS pressurized compartments	Skorpion equipment (CKP-1)	TBD	Technical studies
ИКЛ-1В “Platan”	Search for low energy heavy nuclei of solar and galactic origin	Platan-M equipment	Existing on-orbit	Study of cosmic rays
ПКЕ-1В “Kromba”	Study of the dynamics of contamination from liquid-fuel thruster jets during buns, and verification of the efficacy of devices designed to protect the ISS exterior surfaces from contamination	Tray with materials to be exposed	Existing on-orbit	Space energy systems
Д33-2 “Diatomea”	Study of stability of the geography position and form of the boundaries of the world ocean biologically active water areas observed by space station crews	Nikon F5 camera; Video camera; Dictaphone; Laptop # 3; “Diatomea” kit	Existing on-orbit	Study of Earth natural resources and ecological monitoring

TABLE 5-6 USOS ISS INCREMENT-8 PAYLOADS COMPLEMENT

Experiment	Mission information	Duration	Location on ISS	Research Area
Crew Earth Observation (CEO)	Increments 1-7	34 months	Destiny and Zvezda modules	Earth observation
Earth Knowledge Acquired by Middle School students (EarthKAM)	Up on 5-A	On-going	ISS windows	Education
Pore Formation and Mobility Investigation (PFMI)	Up on UF-2 Down on ULF-1	9 months	Glovebox	Microgravity sciences
Microgravity Acceleration Measurement System (MAMS)	Up on 6-A	Permanent	EXPRESS Rack 1	Microgravity
Space Acceleration Measurement System II (SAMS-II)	Up on 6-A	Permanent	EXPRESS Racks 1 & 4	Microgravity
Sub-regional Assessment of Bone Loss in Axial Skeleton in Long term Spaceflight (Sub-regional Bone)	Increments 2-9	39 months	Pre- and post-flight	Human Life Sciences
Promoting Sensorimotor Response Generalizability (Mobility)	Increments 5-10	N/A	Pre- and post-flight	Human life sciences
Space Flight Induced Reactivation of Epstein-Bar Virus (Epstein-Barr)	Increments 5-8 and 10	N/A	Pre- and post-flight	Human life sciences
Materials International Space Station Experiment (MISSE)	Up on 7-A.1 Down on ULF-1	19 months	External attachement on Quest airlock	Materials exposure
Protein Crystal Growth-single- locker Thermal Enclosure System (PCG-STES) housing the Diffusion-controlled Crystallization Apparatus for Microgravity (DCAM)	Up on 11-A Down on ULF-1	4 months	EXPRESS Rack 4	Biotechnology
Renal Stone Risk During Spaceflight (Renal Stone)	Increments 3-12	49 months	Human Research Facility	Human life sciences
Zeolite Crystal Growth Furnace (ZCG)	Furnace unit up on UF-1; samples up and down on most Shuttle flights	Increments 4-8	EXPRESS Rack 2	Space product development
Cell Biotechnology Operations Support System (CBOSS)	Increments 3-4 & 7-10	Increment 10	Destiny Module	Human life science
Crewmember and crew-ground interaction during ISS missions	Increments 2 and 6; 5A-1	Increment 7-10	Human research Facility	Phycho-social
Education Payload Operation (EPO)	Increment-7	Increments 7-10	Destiny Module	Education
Earth Science Toward Exploration Research (ESTER)	Increment-7	Increments 7-8	ISS windows	Earth observation
Effect of Prolonged Space Flight on Human Skeletal Muscle (Biopsy)	Increment-7	Increment 7		Human life sciences
Fluid Merging Viscosity Measurement (FMVM)	Increments 8/9	Increments 8 and 9	Destiny Module	Materials science
Viscous Liquid Foam—Bulk Metallic Glass (Foam)	Increments 8/9	Increments 8 and 9	Destiny Module	Materials science

Table 5-6, Continued from previous page

Experiment	Mission information	Duration	Location on ISS	Research Area
Foot/Ground Reaction Forces During Spaceflight (FOOT)	Up on 11-A; Down on ULF-1; Up on Increment-8	Increment 8	Human Research Facility	Human life science
Group Activation Packs YEAST (GAP)	Increment-8	Increment 8	Destiny Module	Biotechnology
In Space Soldering Investigation (ISSI)	Increment-8	Increment 8	Destiny Module	Materials science

TABLE 5-7 ROS-ISS INCREMENT-8 PAYLOADS COMPLEMENT

Experiment Name	Research Objective	Hardware Used	Up/Down Flight or Vehicle	Research Area
КНТ-1 “Global Timing System”	Global timing System test development	Electronic unit; Antenna unit with attachment mechanism	Existing on orbit	Commercial
КНТ-2-- MPAC & SEED	Study of meteoroid and man-made particle and the outer space impact on exposed materials	Micro particles collection device and material exposure array MPAC & SEED	Existing on orbit	Commercial
КНТ-20—GCF-NASDA	Cristaligeishen protein	Kit GCF-02	On orbit	Commercial
ГФИ-1 “Relaksatsiya” (Relaxation)	Study of the chemiluminescent chemical reactions and atmospheric light phenomena	“Fialka-MV Kosmos” spectral-zonal ultraviolet system	Existing on orbit	Geophysical
ГФИ-8 “Uragan”	Experimental testing and verification of the ground-space system for eliminating the impact of man-made catastrophes	Binocular telescopic device Rubinar; Photo camera Hasselblad; Video complex LIV	Existing on orbit	Geophysical
МБИ-1 “Sprut-MB1”	Study of human bodily fluids during long duration space flight	Sprut-K kit; Tsentr power supply; central Laptop computer	On orbit	Biomedical
МБИ-2 “Diurez”	Study of fluid electrolyte metabolism and hormonal regulation of blood volume in microgravity	Urine receptacle kit; Kriogem-freezer; plazma kit; Hematocrit kit	On orbit	Biomedical
ГФИ-10 “Molnia-SM	Study of atmosphere, ionosphere and magnetosphere electromagnetic interaction related to storms & seismic activities	BFS-3M video-photometric system	Progress	Geophysical
МБИ-3 “Parodont”	Study of periodontal tissue condition under space flight conditions	Kriogem-03/1 refrigerator	Progress	Biomedical
МБИ-4 “Farma”	Study of specific pharmacological effects under long duration space flight	Saliva-F kit	Progress	Biomedical
МБИ-5 “Kardio-ODNT”	Comprehensive study of the cardiac activity and blood circulation primary parameter dynamics	“Gamma-1M” equipment, “Chibis” LBNP device	Existing on-orbit	Biomedical
МБИ-7 “Biotest”	Biochemical mechanism of metabolic adaptation to space flight environment	Gamma-1 M equipment; Hematocrit kit	Existing on-orbit	Biomedical
МБИ-8 Profilaktika (Countermeasure)	Study of mechanisms and efficiency of various countermeasures aimed at preventing locomotor system disorders in weightlessness	Reflotron-4 complex; TVIS treadmill; VB-3 bicycle ergometer; Bungee cords set; Gamma-1M equipment; Laptop; Kardiokasseta; power unit Tsentr	Existing on-orbit	Biomedical
РБО-1 “Prognoz”	Development of a method for real-time prediction of radiation dose loads on the crews of manned space stations	P-16 radiometer; ДБ-8 dosimeters (4 units)	Progress	Biomedical
РБО-2 “Bradoz”.	Bioradiation dosimetry during spaceflight	“Bradoz” kit	Progress	Biomedical
РБО-3 “Matryeshka-R”	Study of radiation environment dynamics along the ISS RS flight path and in ISS compartments, and dose accumulation in antroph-amorphous phantom, located inside and outside ISS	Passive detectors unit Phantom set; Matryeshka equipment (monoblock)	During EVA	Biomedical
МБи-9 “Pulse”	Study of the autonomic regulation of the human cardio-respiratory system in weightlessness	Pulse set, Pulse kit And computer	On-orbit	Biomedical

Table 5-7, Continued from previous page

Experiment Name	Research Objective	Hardware Used	Up/Down Flight or Vehicle	Research Area
МБИ-11 “Gematologia”	New data obtaining of the outer space factor effects on human blood system in order to extend its diagnostic and prognostic capabilities, studying the mechanism of appearance of changes in hematological values (space anemia)	Erythrocyte kit; Kriogem-freezer; Plazma kit; Hematocrit kit	Existing on orbit	Biomedical
МБИ-15 “Pilot”	Researching for individual features of psychophysiological regulation of cosmonauts’ state and crewmembers professional activities during long space flight	Right Control Handle Left Control Handle Synchronizer unit ULTRABIY-2000 unit; Laptop No 3	Existing on orbit	Biomedical
Био-2 “Biorisk”	Study of space flight impact on micro-organism substrates systems state related to space technique ecological safety and planetary quarantine problem	Biorisk-KM set (4 units); Biorisk-MSV containers (6 units); Biorisk-MSN set	Progress	Biomedical
Био-5 “Rasteniya-2”	Study of the space flight effect on the growth and development of higher plants	Lada greenhouse; Water container; BVP-70P video camera from the LIV video system; Computer	On-orbit	Biomedical
Био-10 “Mezhkletochnoe vzaimodeistvie—intercellular interaction”	Study of the microgravity influence on cells surface behavior and intercellular interaction	Fibroblast-1 kit; Aquarius hardware; Glovebox; KB-03 container	On orbit	Biomedical
ТЕХ-20 “Plazmennyi Kristall”	Study of the plasma dust crystals and fluids under microgravity	Plazmennyi kristal equipment; telescience flight equipment		Technical studies
БТХ-11 “Biodegradatsiya”	Assessment of the initial stages of biodegradation and biodeterioration of the surfaces of structural materials	Biodegradatsiya-G01 kit; GO2 kit	Progress	Biotechnology
БТХ-32 “MSC—Mesenchymal stem cells)	Study of behavior of mesenchymal stem cells from bone marrow under space flight conditions	Embrion kit; Aquarius hardware	On orbit	Biotechnology
ТЕХ-3 “Akustika-M”	Acoustic study of ISS crew voice communication optimization	Akustika-M kit	Progress	Technical studies
ТЕХ-5 “Meteoroid” (SDT 16002-R)	Recording meteoroid and man-made particle impacts on the exterior of ISS RS SM	MMK-2 electronic unit; stationary capacitor sensors	Existing on-orbit	Technical studies
ТЕХ-13 “Tenzor” (SDTO 12001-R)	Determination of ISS dynamic characteristics	ISS RS motion control system; sensors; star tracker; GPS GLONAS satellite system	Existing on-orbit	Technical studies
ТЕХ-14 “Vektor-T” (SDTO 12002-R)	Study of high-precision system for ISS motion prediction	ISS RS sensors; ISS RS orbit radio tracking system; GPS	Existing on-orbit	Technical studies
ТЕХ-15 “izgib” (Bending-SDTO 13002-R)	Study of the relationship between the onboard operating modes and ISS flight conditions	ISS RS accelerometers and rotational speed sensors	Existing on-orbit	Technical studies
ТЕХ-16 “Privyazka” (Alignment-SDTO 12003-R)	High-precision orientation of science instruments in space with consideration given of ISS hull deformation	ISS RS sensors (SM-8M) and magnetometer	Existing on-orbit	Technical studies
ТЕХ-17 “Iskazheniye” (Distorsion-SDTO 16001-R)	Determination and analysis of magnetic disturbances on the ISS	ISS RS SM attitude control sensors and control loop magnetometers	Existing on-orbit	Technical studies
ТЕХ-22 “Identifikatsiya” (Identification) (SDTO 13001-R)	Identification of disturbance sources when the microgravity conditions on the ISS are disrupted	Linear optical accelerometer with cables; micro acceleration measurement device with cables.	Existing on-orbit	Technical Studies
ТЕХ-3 “Skorpion”	Development, testing, and verification of a multi-functional instrument to monitor the science experiment conditions inside the ISS pressurized compartments	Skorpion equipment (CKP-1)	TBD	Technical studies
ИКЛ-1В “Platan”	Search for low energy heavy nuclei of solar and galactic origin	Platan-M equipment	Existing on-orbit	Study of cosmic rays
ПКЕ-1В “Kromba”	Study of the dynamics of contamination from liquid-fuel thruster jets during buns, and verification of the efficacy of devices designed to protect the ISS exterior surfaces from contamination	Tray with materials to be exposed	Existing on-orbit	Space energy systems

Table 5-7, Continued from previous page

Experiment Name	Research Objective	Hardware Used	Up/Down Flight or Vehicle	Research Area
Д33-2 "Diatomea"	Study of stability of the geography position and form of the boundaries of the world ocean biologically active water areas observed by space station crews	Nikon F5 camera; Video camera; Dictaphone; Laptop # 3; "Diatomea" kit	Existing on-orbit	Study of Earth natural resources and ecological monitoring
БТХ-2 "Mimetik-K"	Anti-idiotypic antibodies as adjuvant-active glycoproteid mimetic	Luch-2 biocrystallizer	On orbit	Biotechnology
БТХ-3 "KAF"	Crystallization of Caf1M protein and its complex with C-end peptide as a basis for formation of new generation of antimicrobial medicines and vaccine ingredients effective against yersiniosis	Luch-2 biocrystallizer	On orbit	Biotechnology
БТХ-4 "Vaktsina-K"	Structural analysis of proteins candidates for vaccine effective against AIDS	Luch-2 biocrystallizer	On orbit	Biotechnology
БТХ-20 "Interleukin-K"	Obtaining of high quality 1α, 1β interleukin receptor antagonist-1	Luch-2 biocrystallizer	On orbit	Biotechnology
БТХ-12 "Bioekologiya"	Generation of high efficiency strains of microorganisms to produce petroleum biodegradation compounds, organo-phosphorous substances, vegetation protection agents, and exopolysaccharides to be used in the petroleum industry	Bioekologiya kit; (Kits # 1 to 4)	On orbit	Biotechnology
ТЕХ-3 "Toksichnost"	Development of a system for express monitoring of water toxicity in spaceflight	Biotox-10K	On orbit	Technical Studies

TABLE 5-8 INCREMENT-7/8 ROTATION PERIOD PAYLOADS COMPLEMENT

Experiment Name	Research Objective	Duration	Location on ISS	Research Area
Ageing	Study of the increased activity of fruit flies in weightlessness	During Increment-7/8 rotation period	Russian Segment	Biology
Gene	Effects of space environment on gene expression of embryos of fruit flies	During Increment-7/8 rotation period		
Root	Effects of space environment on the nuclear structure and function of Arabidopses Thalina root cells	During Incrment-7/8 rotation period		
MESSAGE	Effects of weightlessness on bacterial gene expression with special attention to genes involved in the response to stress, in motility (flagella) and in genetic rearrangements	During Increment-7/8 rotation period	Russian Segment	Microbiology
WINOGRAD	Study of growth of winogradski columns in weightlessness	During Increment-7/8 rotation period		
NEUROCOG	Analysis of human spatial perception and the effect of gravity on it and the spatial memory	During Increment-7/8 rotation period	Russian Segment	Human Physiology
CARDIOCOG	Study of the effects of weightlessness on the cardiovascular system, the respiratory system and the physiological reactions	During Increment-7/8 rotation period	Russian Segment	
SYMPATHO	Study of adrenal activity in the sympathetic nervous system in humans	During Increment-7/8 rotation period	Russian Segment	
BMI	Study of cardiovascular assessment in weightlessness	During Increment-7/8 rotation period	Russian Segment	
RHYTHM	Evaluation of the change in cardiovascular control and adaptation mechanism in humans	During Increment-7/8 rotation period	Russian Segment	
Carbon Dioxide Survey	Investigation of Carbon Dioxide concentration onboard ISS	During Increment-7/8 rotation period	US/Russian Segmetns	
NANOSLAB	Analysis of the formation of a zeolite structure from two separate materials, e.g., ammonium hydroxide and aluminum silicate	During Increment-7/8 rotation period	US/Glovebox	Physical Science
PROMISS	Monitoring of protein crystal growth	During Increment-7/8 rotation period	US/Glovebox	
LSO	Study of optical radiation in the ionosphere of the Earth related to thunder activity and seismic processes	During Increment-7/8 rotation period	ISS windows	Earth Observation
Crew restraint	Testing of new crew restraint technologies	During Increment-7/8 rotation period	In different modules	Technology

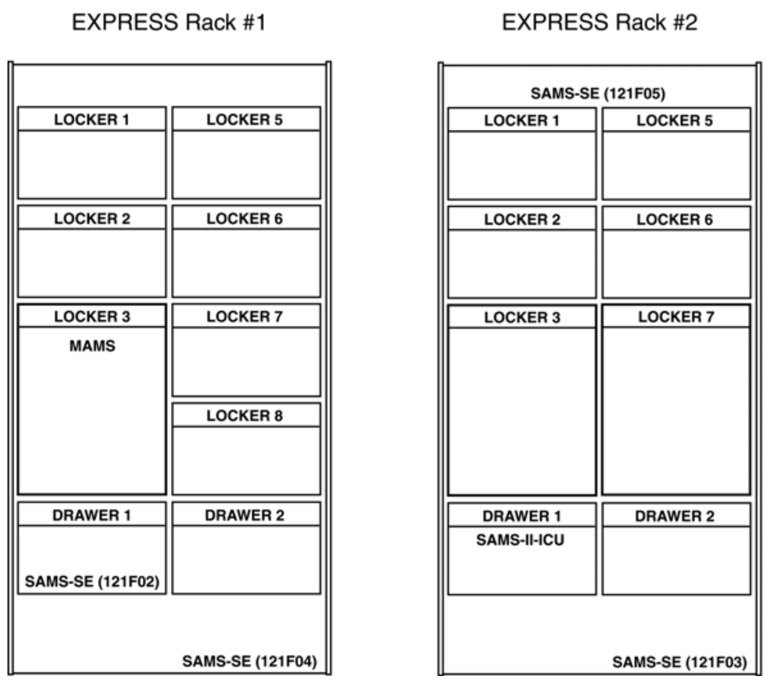

Figure 5-1 EXPRESS Racks 1 and 2 Generic Configuration with SAMS/MAMS On-orbit Locations

EXPRESS Rack / Flight	UF-1 (Inc 6)	8A (Inc 7)	UF-2 (Inc 8)
<EXP Rk #1>			
Locker1	BCSS-R	BCSS-R (SE)	BCSS-R (SE)
Locker2	BCSS-CS1 (support Equipt.)	BCSS-CS1 (SE)	BCSS-CS1 (SE)
Locker3	MAMS	MAMS	MAMS
Locker4	MAMS	MAMS	MAMS
Locker5		BCSS-FDI	BCSS-FDI
Locker6			
Locker7			
Locker8	MEPSII (inactive)	MEPSII (I)	MEPSII
Drawer1	SAMS-RTS1	SAMS-RTS1	SAMS-RTS1
Drawer2	SAMS-RTS2	SAMS-RTS2	SAMS-RTS2
<EXP Rk #2>			
Locker1	ARIS-ICE1 (inactive)	ARIS-POP	ARIS-POP
Locker2	ARIS-ICE2 (inactive)		
Locker3			
Locker4			
Locker5	ZCG-FU1	ZCG-FU1	ZCG-FU1
Locker6	ZCG-FU1	ZCG-FU1	ZCG-FU1
Locker7			
Locker8	ADVASC-SS2 (stowed)		
Drawer1			
Drawer2			
<EXP Rk #4>			
Locker1	BSTC1 (stowed)	BSTC1	BSTC1
Locker2	GSM1 (stowed)		
Locker3	PCG-STES 10	PCG-STES10	PCG-STES10
Locker4			
Locker5	ARTIC 2	GSM1	GSM1
Locker6	ARTIC 1	ARCTIC 1	ARCTIC 1
Locker7		CGBA2	CGBA2
Locker8		ADVASC-SS2 (S)	ADVASC-SS2 (S)
Drawer1	KU-REC	KU-REC	KU-REC
Drawer2	SAMS-II-ICU	SAMS-II-ICU	SAMS-II-ICU
Continuously powered payload			

Figure 5-2 EXPRESS Rack Topologies for Increments 6 through 8

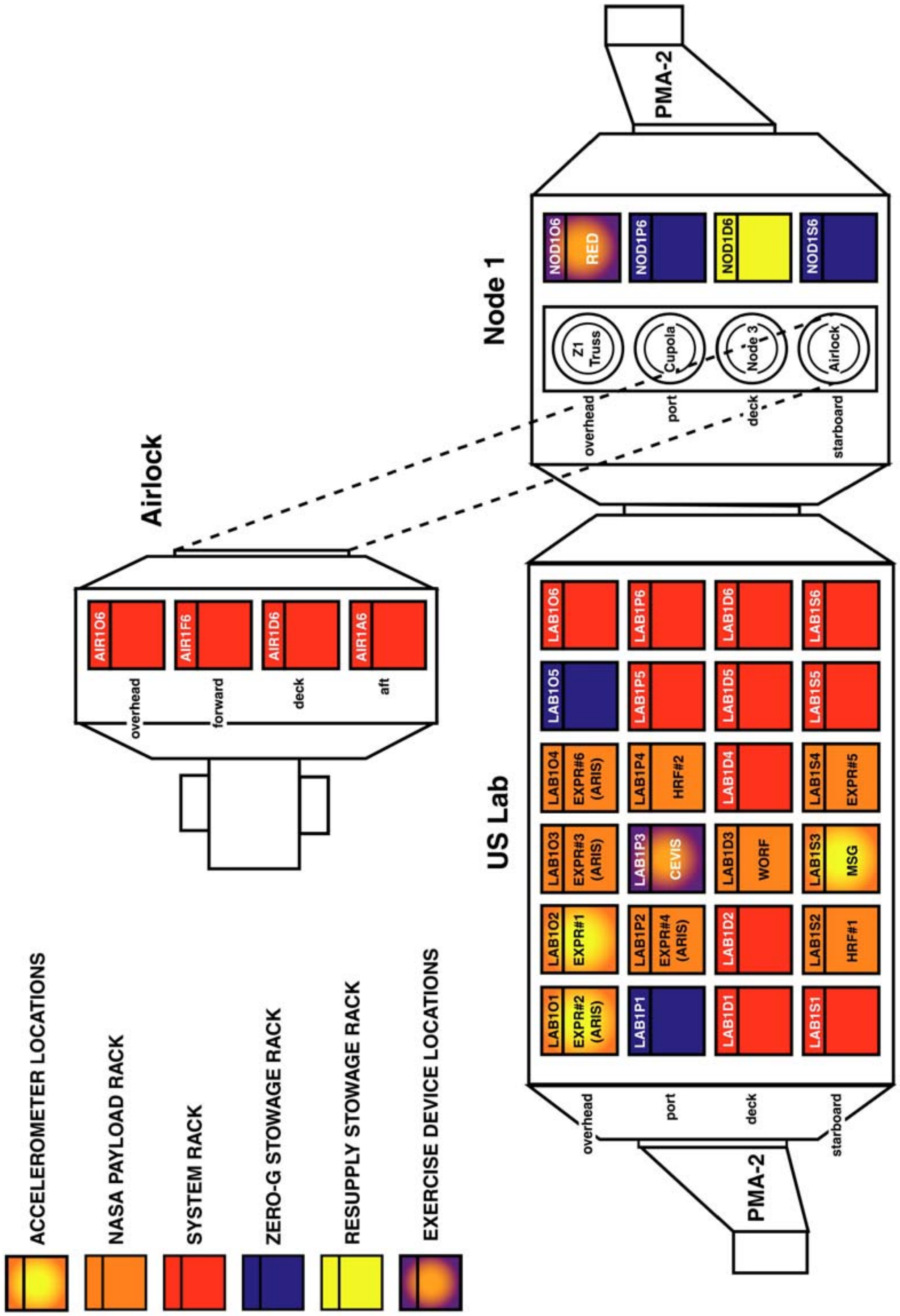

Figure 5.3 US Lab Rack Locations.

6 ISS Increment-6/8 Reduced Gravity Environment Description

The reduced gravity environment for Increment-6/8 was measured by the SAMS accelerometer, the MAMS HiRAP accelerometer, and the MAMS OSS accelerometer. In order to readily observe the availability of acceleration data for a particular sensor for a particular time period, Figure 6-1 through Figure 6-18 were created. These figures show the available acceleration data for the active SAMS SEs, the MAMS OSS sensor, and the MAMS HiRAP sensor for the Increment-6/8 time span analyzed in this report. They can also be accessed via the PIMS ftp site at:

http://pims.grc.nasa.gov/ftp/pad

6.1 Quasi-steady Microgravity Environment

The quasi-steady regime is comprised of accelerations with frequency content below 0.01 Hz and magnitudes expected to be on the order of 2 μg or less. These low-frequency accelerations are associated with phenomena related to the orbital rate, primarily aerodynamic drag. However, gravity gradient and rotational effects may dominate in this regime, depending on various conditions and an experiment's location relative to the vehicle's center of mass (CM). Other sources of acceleration to consider in this regime are venting of air or water from the spacecraft and appendage movement such as solar arrays, Space Station Remote Manipulator System (SSRMS) or communication antennas. The different quasi-steady environment characteristics seen on the ISS for Increments 6-8 are primarily related to altitude and attitude of the station. Variation in atmospheric density with time and altitude contribute to the differences in the aerodynamic drag component. Different attitudes will affect the drag component due to the variation of the frontal cross-sectional area of the station with respect to the velocity vector.

6.1.1 ISS Attitudes

ISS primarily used three different attitudes during Increments 6-8 as described in section 2.3 and section 3.8. The dynamics particular to each attitude have profound effects on the quasi-steady vector. The amount of time spent in each attitude during Increments 6-8 is summarized in Table 6-1. These values are rough estimates calculated from available MAMS OSSBTMF data and the ISS Attitude timelines. The category labeled "Others" includes special attitudes for maneuvers, Extra Vehicular Activities (EVA), thruster tests and other miscellaneous events.

TABLE 6-1 ATTITUDE DURATION CALCULATED FROM AVAILABLE MAMS OSSBTMF DATA

Attitude		Increments 6	7	8	All
XVV/ZLV	Hours	1200.5	1179.3	895.5	3275.3
	Percent	35.4	26.9	21.2	27.3
XPOP	Hours	1893.0	1979.5	2359.6	6232.1
	Percent	55.8	45.2	55.8	51.9
YVV/ZLV	Hours	107.6	826.5	788.1	1722.1
	Percent	3.2	18.9	18.6	14.3
Other*	Hours	193.4	395.3	184	772.8
	Percent	5.6	9.0	4.4	6.5
Total**	Hours	3394.5	4380.6	4227.2	12002.3
	Percent	100.0	100.0	100.0	100.0

* Calculated by subtracting time spent in each attitude from total.
** Calculated from ISS Attitude Timelines.

6.1.1.1 XVV/ZLV Torque Equilibrium Attitude

XVV/ZLV is a Torque Equilibrium Attitude (TEA), an attitude that balances the vehicle's gravity gradient and aerodynamic drag torques as the ISS completes an orbit. XVV/ZLV is an “airplane like” attitude maintained relative to the Local Vertical Local Horizontal (LVLH) reference frame, a rotating coordinate system. Except for docking purposes, when the ISS is in XVV/ZLV attitude, the positive X_A-axis is aligned with the velocity vector (+XVV/ZLV). For Increments 6-8, the ISS body axes were maintained centered on a yaw-pitch-roll sequence of YPR = [350.0 350.9 0.0] (degrees) relative to the LVLH coordinate axes. However, this attitude varies with configuration because of changing mass and aerodynamic properties. XVV/ZLV attitude is sometimes referred to as LVLH attitude or simply XVV attitude.

Figure 6-19 is a time series plot of MAMS OSSBTMF data that was measured at GMT 10-July-2003, 191/00:00:00, during a typical crew sleep period while the ISS was in +XVV/+ZLV attitude. The black line shows data at the MAMS location, which was [X_A, Y_A, Z_A] = [44.5, -0.96, 2.36] (feet) from the center of mass (CM) of the ISS. Even though MAMS is farthest in distance from the CM in the X_A-direction, the X_A quasi-steady component has a mean of only -0.09 μg. This is because in LVLH attitudes, in the axis aligned with the velocity vector, the gravity gradient and rotational components cancel each other out. This is demonstrated by the red line, which represents an estimate of the quasi-steady vector at the CM. ISS telemetry data was used to calculate the expected gravity gradient and rotational components at the MAMS location and subtracting them from the measured values. PIMS refers to this calculation as “mapping” the quasi-steady data from the measured location to a specified location. The closeness of the two curves nicely illustrates the cancellation effect of the two components for the X_A-axis. Since there is no cancellation in the Y_A and Z_A-axes, the difference between the data mapped to the CM (red lines) and the as-measured data is more pronounced than for the X_A-axis. The “dips” appearing in the Y_A and Z_A-axes at 1:09, 2:50 and 4:30 are caused by the Ku-band antenna (see 6.1.3).

The Quasi-steady Three Dimensional Histogram (QTH) is a useful in comparing time periods, attitudes or other conditions. Here, we apply the QTH to compare differences in increments for XVV/ZLV attitude. Figure 6-20, Figure 6-21, and Figure 6-22 are QTH plots of MAMS OSSBTMF data collected during Increments 6, 7 and 8 respectively. The data was carefully selected so that the ISS was in either +XVV/+ZLV or -XVV/-ZLV attitude, avoiding maneuvers or other attitudes. Figure 6-23 is a compilation QTH of the previous three, giving a summary of Increments 6-8 together. The mean accelerations on all three axes show close agreement amongst the Increments. This is expected due to the lack of large mass transfers and relatively static configuration of the ISS for these time periods. Table 6-2 summarizes the mean acceleration values from these plots.

TABLE 6-2 QUASI-STEADY ACCELERATION SUMMARY FOR XVV/ZLV ATTITUDE

Increment(s)	Mean Acceleration (μg)			
	X	Y	Z	Mag.
6	-0.16	-0.54	-1.16	1.29
7	-0.14	-0.48	-1.09	1.20
8	-0.19	-0.63	-1.21	1.38
6-8	-0.16	-0.54	-1.15	1.28

Two observations are worth noting. A quick glance at the QTH plot of Increment 6 (Figure 6-20) reveals a noticeably larger distribution of the quasi-steady vector than those of Increment 7 (Figure 6-21) or Increment 8 (Figure 6-22). This can be explained by the reduction in number of crew members aboard the ISS. There were 3 crew members for Increment 6 and only 2 crew members for Increments 7 and 8. It is reasonable to expect a corresponding reduction in disturbances to the quasi-steady environment due to crew activity and vehicle response to crew activity.

The XY and YZ planes in each of the four QTH plots for XVV/ZLV show that the Y_A-axis accelerations primarily dwell in two spots, at -0.39 μg and -0.69 μg. This is most evident in Figure 6-23, which also includes two red arrows for highlighting purposes. These two loci result from the phenomenon described in section 6.1.2.

6.1.1.2 XPH/ZNN XPOP Attitude

XPOP stands for X Principal Axis Perpendicular to the Orbital Plane. XPOP is an inertial flight attitude (maintained relative to inertial frame of reference) that allows for close Sun tracking for maximum power generation. XPOP inertial attitude places the Sun in the ISS X/Z plane so that the Y-axis gimbling solar arrays can point accurately at the Sun, and the $+X_A$-axis is always pointing to the side of the orbital plane opposite of the Sun. This condition allows for either the $+X_A$-axis or $-X_A$-axis to be aligned with the orbital angular momentum vector, and the $+Z_A$-axis pointing nadir when the ISS is at orbital noon (Figure 3-3). These two variations of XPOP attitude are called out in the ISS Attitude timeline as +XPH/+ZNN or +XPH/-ZNN. XPOP attitude will no longer be needed, when the ISS begins 2-axis Sun tracking after flight 12A.1.

When the ISS is in XPOP attitude, the quasi-steady vector at the MAMS location has very distinctive attributes. Y_A and Z_A-axes show cyclical variation as they are alternately subjected to varying drag and gravity gradient vectors. These two components vary due to the station's rotation with respect to the Local Vertical Local Horizontal (LVLH) frame of reference. The X_A-axis is perpendicular to the velocity vector, so there is no cancellation of the gravity gradient and rotational components. In fact, the rotational components for each of the three axes are on the order of a thousand times smaller than the gravity gradient components. These features are evident in time series of MAMS OSSBTMF data captured at 07−March−2004, 067/02:00:12 shown in Figure 6-24. The black line represents the as measured data at the MAMS location and the red line is data mapped to the CM. In this orientation, the MAMS location is 44.3 ft away from the CM in the horizontal plane, giving a gravity gradient estimate of 1.69 µg. The measured 1.65 µg X_A-axis component mean closely agrees with this estimate. The Y_A and Z_A-axes profiles are the results of the varying gravity gradient and drag components as the ISS completes an orbit. Visual inspection and rough spectral analysis has revealed frequency peaks at 1.83×10^{-4} Hz and 3.66×10^{-4} Hz, which correlate with the orbital period (91 minutes) and half the orbital period (45 minutes), respectively.

Longer looks at the quasi-steady vector in XPOP attitude using the QTH plots do not show a significant difference in the means or general profile between Increments. (Figure 6-25, Figure 6-26, Figure 6-27 and Figure 6-28). The drop in "noise" associated with the crew movements between Increments 6 and 7 is also evident in the QTH plots for XPOP attitude. Table 6-3 summarizes the mean acceleration values from these plots

TABLE 6-3 QUASI-STEADY ACCELERATION SUMMARY FOR XPOP ATTITUDE

Increment(s)	Mean Acceleration (µg)			
	X	Y	Z	Mag.
6	1.67	-0.13	-0.41	1.73
7	1.62	-0.03	-0.34	1.65
8	1.66	-0.09	-0.41	1.71
6-8	1.65	-0.09	-0.39	1.70

6.1.1.3 YVV/ZLV Attitude

During Increment 6, the ISS began to fly in a new attitude proposed by the Russians called YVV/ZLV. YVV/ZLV is a Torque equilibrium attitude in which the Y_A-axis is maintained in the velocity vector and the Z-axis is pointing nadir. The ISS flies with either the $+Y_A$-axis (+YVV/+ZLV) or $-Y_A$-axis (-YVV/+ZLV) in the forward direction. In this attitude the X-axis is perpendicular to the orbital plane. During high solar beta angles (>60 degrees) the ISS is flown in YVV attitude to avoid overheating of the Progress batteries. For this reason, YVV has been referred to as "barbeque" mode.

Figure 6-29 is a time series plot of MAMS OSSBTMF data from GMT 08−February−2004, 039/00:00:03, when the ISS was in +YVV/+ZLV attitude. Similar to that of XPOP, in YVV attitude, there is no rotational component to cancel the gravity gradient in the X_A-axis. The quasi-steady vector at the MAMS location (black line in the plot) reflects this with a mean of

1.45. The Y_A-axis component is near zero (-0.02 µg) due to the close proximity of MAMS to the ISS CM in that direction. Also, the Y_A-axis is in the direction of the velocity vector and the rotational and gravity gradient components cancel each other. The Z_A-axis component is similar in magnitude to that of XVV attitude. The large negative excursions from the baseline are effects of the Ku-band antenna operations (Section 6.1.3).

The QTH plots for Increments 6, 7 and 8 (Figure 6-30, Figure 6-31, Figure 6-32 and Figure 6-33) demonstrate a very consistent profile. The double loci phenomenon seen in the QTH plots for XVV attitude can also be seen in those for YVV attitude during Increments 7 and 8 of YVV attitude (Section 6.1.2). Table 6-4 summarizes the mean acceleration values from these plots

TABLE 6-4 QUASI-STEADY ACCELERATION SUMMARY FOR YVV/ZLV ATTITUDE

Increment(s)	Mean Acceleration (µg)			
	X	Y	Z	Mag.
6	1.70	-0.15	-1.35	2.17
7	1.55	-0.10	-1.33	2.04
8	1.49	-0.12	-1.40	2.05
6-8	1.53	-0.12	-1.37	2.05

6.1.2 Unknown Signal

An unidentified source is causing a disturbance in both the vibratory and quasi-steady regimes onboard the ISS. This signal of unknown origin was first reported in the PIMS Increment 4/5 report [23]. This disturbance is omnipresent in the vibratory regime, as seen by the SAMS instrument, ranging from 100 - 160 Hz. It is when the vibratory component of the disturbance is near 100 Hz that the quasi-steady component is manifested as approximately 0.3 µg offset in the MAMS OSS $+Z_{OSS}$-axis ($-Y_A$-axis). No other axis of the MAMS OSS tri-axial sensor exhibits this offset under this condition. It is uncertain as whether the quasi-steady component is a real, physical effect or an artifact of the instrumentation.

The vibratory component of this disturbance can be described as having five states. The signal cycles through these five states over a long duration. Any state in this cycle may last for hours, days or weeks. A cycle can be defined as beginning with a ~160 Hz (State 1). At some point in time the signal will ramp down to approximately 130Hz in a matter of minutes (State 2). Figure 6-34 is a spectrogram showing the signal transitioning from 158 Hz to 138 Hz over a few minutes. The signal will slowly decrease in frequency until it reaches a range from 120-125 Hz (State 3). The signal will often broaden in frequency giving it a "drying paint" look. The signal will appear to suddenly drop in frequency to 100-105 Hz range (State 4). Figure 6-35 contains a spectrogram with examples of States 3 and 4. Jumping from 100 Hz to 120 Hz will continue randomly (State 5) as seen in Figure 6-36. At some point the signal jumps back to 159 Hz and the cycle begins again (Figure 6-35). The vibratory disturbance has been seen on all SAMS heads. It is most strong on 121F02, the head located in Express Rack 2.

Whenever the vibratory component is in the 100-105 Hz range (States 4 and 5), an additional -0.3 to -0.5 micro-g components is added in the Y-axis (SSA) in the quasi-steady regime. Figure 6-37 and Figure 6-38 are, respectively, a time series plot of MAMS OSSBTMF data, and a spectrogram of SAMS 121f04 data recorded on GMT 02-July-2003, 183/00:00, when the signal was switching between 100 Hz and 120 Hz. These two plots show good correlation between the switchover from 100 Hz to 120 Hz in the vibratory regime and the shift in the quasi-steady accelerations as measured by MAMS in the Y_A-direction. Since the ISS was in XVV attitude, the Y_A-axis component of the quasi-steady vector is primarily gravity gradient and rotational effects. Using ISS telemetry data, the expected Y_A-axis component was calculated and plotted along side the MAMS measured values in Figure 6-39. The quasi-steady Y_A-axis component measured by MAMS and the calculated component agree when the unknown signal is at 120 Hz (mean of -0.36 µg), and diverge when the unknown signal is at 100 Hz (an additional -0.37 µg component is present in MAMS data). The slight dip in the MAMS data at 5.67 hours into the plot (dotted-box) is due to the Ku-band antenna effects (Section 6.1.3).

Figure 6-40 and Figure 6-41 show two hours of SAMS SE 121F02 and MAMS OSSBTMF data starting at GMT 06−December−2003, 340/00:00:00. From 00:00 to 00:59 in the spectrogram, the vibratory signal is loosely controlled, centered near 104.4 Hz. The quasi-steady Y_A-axis component mean is -0.83 µg for the same time period, as seen in the time-series plot. At 00:59 in the spectrogram, the signal jumps to 127.3 Hz, with a corresponding quasi-steady Y_A-axis change to -0.37 µg in the time-series plot. At 01:25, the signal drops down to 103.4, but as a more tightly controlled, narrow band signal, and the mean for the quasi-steady Y_A-axis data becomes -0.70 µg. This suggests correlations between the strength and frequency of the signal and the quasi-steady effects seen in MAMS. Figure 6-42 and Figure 6-43 present further evidence in the form of cumulative RMS plots of 121F02 data taken during each of the three states seen in the spectrogram of Figure 6-40. The trace for the loosely controlled signal (blue line) shows the 104.4 Hz contribution to be larger for the Y_A-axis than those of the X_A and Z_A-axes, as well as the 103.4 Hz contribution of the narrow-band signal (red line) in each of the three axes. Table 6-5 summarizes the contribution of the unknown signal as measured by 121F02 and Y_A-axis quasi-steady component as measured by MAMS. The quasi-steady Y_A-axis mean for the case when the signal in the vibratory regime is at 127.3 HZ is used as the baseline value in the offset calculation.

TABLE 6-5 CUMULATIVE RMS AND QUASI-STEADY CONTRIBUTIONS OF UNKNOWN SIGNAL (GMT 340)

Time	121F02 RMS Contribution (mg_{RMS})					Quasi-steady
GMT 340	Freq. (Hz)	X_A	Y_A	Z_A	Sum	Y_A Offset (µg)
00:00 - 00:59	104.4	0.41	1.17	0.39	1.25	-0.46
01:02 - 01:22	127.3	1.34	0.26	0.08	1.23	0
01:26 - 01:46	103.4	0.67	0.25	0.61	0.88	-0.33

A test was performed from GMT 19-September-2004, 263/09:24 to GMT 21-September-2004, 265/13:38 to determine if the Z_{OSS}-axis was the only axis sensitive to this disturbance, or if it was truly uniaxial. For this test, the inner gimbal of the MAMS Bias Calibration Table Assembly (BCTA) was rotated 90 degrees from the home position, aligning the Y_{OSS}-axis with the disturbance. In the home position, the Z_{OSS}-axis is aligned with the Y_A-axis, but in the rotated position, the Y_{OSS}-axis is aligned with the Y_A-axis. Therefore, when the BCTA is in the rotated position, a uniaxial disturbance in the Y_A-axis should show in the Z-axis of our plots. The signal switched from 103.1 Hz to 127.3 Hz at GMT 19-September-2004, 263/23:01 and back to 101.7 Hz at GMT 20-September-2004, 264/02:20. The quasi-steady effect of this event is highlighted with the red box in Z-axis of Figure 6-44. To verify the state of the signal, spectrograms covering the time period in which the BCTA was rotated can be viewed at:

http://pims.grc.nasa.gov/calendars/roadmap_index.php?year=2004&month=09&day=19
http://pims.grc.nasa.gov/calendars/roadmap_index.php?year=2004&month=09&day=20
http://pims.grc.nasa.gov/calendars/roadmap_index.php?year=2004&month=09&day=21

As before, cumulative RMS plots of 121F02 data were generated for the three states (Figure 6-45 and Figure 6-46) and the results are summarized in Table 6-6. The results with the BCTA inner gimbal rotated show similar trends to that of Table 6-5 for the RMS contribution of the unknown signal. This test showed that the quasi-steady effect of the unknown disturbance is not specific to a particular axis (Y_{OSS} or Z_{OSS}) of the MAMS OSS sensor, but is specific to the Y_A-axis. The X_{OSS}-axis was not tested in this way because it is not possible for the BCTA to rotate in such away as to align the X_{OSS} axis with the Y_A-axis.

TABLE 6-6 CUMULATIVE RMS AND QUASI-STEADY CONTRIBUTIONS OF UNKNOWN SIGNAL (GMT 263-264)

Time	12F02 RMS Contribution (mg_{RMS})					Quasi-steady
GMT 263	Freq. (Hz)	X_A	Y_A	Z_A	Sum	Z Offset (μg)
22:00 - 23:00	103.1	0.68	0.86	0.27	1.11	-0.48
23:30 - 02:20	127.3	1.28	0.49	0.44	1.41	0
04:00 - 06:00	101.7	0.47	0.24	0.37	0.62	-0.38

Although our knowledge concerning the unknown signal and its effect on the quasi-steady measurements recorded by MAMS has increased, we do not yet know the source of the disturbance. It is possible that the Y_A-axis offset seen is an adverse artifact in the MAMS OSS sensors ability to measure the quasi-steady environment. For this reason, it is suggested that MAMS OSS data be used in conjunction with SAMS (121F02 or 121F04) data to determine when the signal is near 100 Hz. When using MAMS OSS data during these periods, extra consideration should be taken for the Y_A-axis component.

6.1.3 Ku-Band Antenna

The Ku-band antenna system is used to transmit payload science data and television from the ISS. The ISS Ku-band system uses the Tracking and Data Relay Satellite (TDRS) constellation for uplink and downlink. The Ku-band antenna is located on the end of a boom arm attached to the Z1 truss. The antenna is positioned during satellite tracking using two gimbals, an elevation (EL) gimbal and a cross elevation gimbal (XEL). These gimbals are labeled in Figure 6-47, a picture taken during the STS-92 mission, when the Ku-band system was installed. Location information for the ISS center of mass, Ku-Band antenna, and MAMS OSS sensor are given as a reference in Table 6-7. The center of mass values are representative of typical values seen in Increments 6-8 and were recorded on GMT 350/16-December-2003, from down linked telemetry data

TABLE 6-7 ELEMENT LOCATIONS IN SPACE STATION ANALYSIS COORDINATES

Location	X (m)	Y (m)	Z (m)
Center of Mass	-10.08	0.02	2.38
Ku-Band Antenna (EL Gimbal)	4.76	-4.16	-4.04
MAMS OSS Sensor	3.44	-0.27	3.36

Movement of the antenna by these gimbals is seen in the quasi-steady data of MAMS. Figure 6-48 is eight hours of MAMS data recorded at GMT 30-November-2003, 334/00:00:12. The plot shows a pattern of 0.2-5.0 μg spikes in the negative Z-direction which are attributable to the Ku band antenna “open loop slew” mode. In this mode, the antenna is rapidly moved into position to begin tracking a satellite, typically lasting1-2 minutes in duration. Figure 6-49 demonstrates the correlation between the gimbal movements and the spikes in MAMS data by plotting the magnitude of the quasi-steady vector along side Ku-band operations data retrieved from the Operational Data Reduction Complex (ODRC). For nearly every spike in the MAMS vector magnitude plot, the Ku-band operations is in “open slew in progress” mode and is accompanied by rapid changes in one or both of the EL and XEL position. Mean gimbal slew rates calculated from the plot for these time periods vary from 1.5 - 3.0 degrees/sec. Some of the more prominent peaks are highlighted with green dotted boxes.

Broader disturbance in the quasi-steady profile can also be attributed to the Ku-band antenna movement. Figure 6-50 and Figure 6-51 show these broader disturbances in the negative Y and Z-directions, caused by the Ku-band antenna when it is in auto-track mode. Figure 6-50 is a plot of data recorded on GMT 10-May-2003, 130/00:00:10, when the ISS was in +XVV/+ZLV attitude. Figure 6-51 is a plot of data recorded on GMT 16-December-2003, 350/00:00:07, when the ISS was in +YVV/+ZLV attitude. In both these attitudes, the disturbance is manifested as 0.2-0.5 μg dips in the baseline in the negative Y and Z-directions (red dotted boxes). These disturbances tend to last 15-20 minutes for these attitudes. Although, in the case of the +XVV/+ZLV attitude, the disturbances are more regular in frequency. The vector magnitude composite plot of Figure 6-52 shows a correlation between the Ku-band auto-track mode and the broad disturbances. During auto-track, the gimbals slew at a much lower rate than in open-loop mode, on the order of 0.05 degrees/sec.

The appearance of the Ku-band effects in the quasi-steady vector depends on the acquisition and maintenance of communication links with the geosynchronous TDRS. Accordingly, Ku-band antenna effects will vary with different ISS attitudes. +XVV/+ZLV and +YVV/+ZLV are attitudes in which the ISS is maintained relative to the rotating LVLH reference frame. However, when the ISS is in XPOP attitude, it is maintained relative to an inertial frame. Less gimbal movement is required when the KU-band is tracking a TDRS while in XPOP attitude than when in XVV or YVV attitude. Figure 6-53 shows data taken during XPOP attitude at GMT 14-January-2004, 014/00:00:08. In this plot, none of the broad disturbances are evident during the periods of auto-track (red dotted boxes), unlike the cases for XVV (Figure 6-50) and YVV (Figure 6-52). However, the shorter spikes of open loop slew are present. More details of Ku-band operation can be found in the vibratory section, section 6.2.1.1.

6.1.4 Venting

6.1.4.1 Flash Evaporator Subsystem Water Dump

The Flash Evaporator Subsystem (FES) is part of the Active Thermal Control System of the Shuttle. During docked operations, the FES is periodically used to dump excess water. The FES is described on the Kennedy Space Center's Technology, Science and Engineering website,

http://science.ksc.nasa.gov/shuttle/technology/sts-newsref/sts-eclss-wcl.html

> The flash evaporators are located in the aft fuselage of the orbiter. There are two evaporators in one envelope. One is the high-load evaporator; the other is the topping evaporator. There are two major differences between the evaporators. The high-load evaporator has a higher cooling capacity than the topping evaporator, and it's overboard vent is only on the left side. The topping evaporator vents steam equally to the left and right sides of the orbiter, which is non-propulsive…The high-load evaporator would not normally be used on orbit because it has a propulsive vent and might pollute a payload.

Figure 6-54 shows MAMS data taken during an FES water from STS-113 Joint operations at 30-November-2002, 334/19:47 to GMT 335/02:28. No discernable effect can be seen in the quasi-steady data due to the FES water dump. The small spikes at 23:04 and 01:10 in the plot can not be directly attributable to the water dump. The lack of effect can be explained by the slow rate of the dump and the non-propulsive venting method.

6.1.4.2 Progress Fuel Line Purge

As part of a propellant resupply procedure, fuel and oxidizer are transferred from a newly arrived Progress to the FGB storage tanks. During this procedure the line is purged between steps. An example of a fuel line purge can be seen in Figure 6-55. This particular propellant purge occurred prior to Progress 10P undocking, at approximately GMT 22-Aug-2003 234/06:07, with a peak acceleration that approached 3 µg occurring in the Y_A-axis at 06:08. A momentum management event, which is used to desaturate the Control Moment Gyroscopes (CMG), occurs at GMT 06:22.

6.1.5 Reboosts

6.1.5.1 Progress Reboosts

Periodic reboosts of the ISS are necessary due to orbital decay. The primary method for conducting a reboost is using the aft facing attitude control thrusters of a docked cargo vehicle, typically a Progress. Station reboosts are open loop burns, where the firing is initiated at a prescribed time and place in orbit. The basic sequence of events requires that the station maneuver to the reboost attitude. Then, at the appropriate time, commands are issued for the jets to fire for a specific length of time. During Increments 6-8, PIMS was asked by various customers to provide MAMS OSS measurements during these reboost events. PIMS took the opportunity to compare expected increase in velocity with values calculated from the MAMS OSS data. Figure 6-56 shows MAMS data for a reboost event at GMT 10-Apr-2003, 100/10:55. Using the X -axis (axis in direction of the velocity vector) mean acceleration, a 1.46 (m/sec) increase in velocity is calculated. This closely agrees with the expected 1.48 (m/sec) value obtained from the Increment 6A Operations timeline from the web site of the Attitude Determination and Control Officer (ADCO). Similar results were obtained for the other reboost events during Increments 6-8 that MAMS was able to measure. The results are presented in Table 6-8.

TABLE 6-8 SUMMARY OF PROGRESS REBOOSTS DURING INCREMENTS 6-8

Reboost Information		Predictions/Expected Results		Calculations from MAMS OSS Data	
Ignition (GMT)	Comments	Duration (sec)	Δ V (m/sec)	Duration (sec)	ΔV (m/sec)
11-February-2003, 042/11:34:30	8 Progress +X Thrusters, Off-Pulsing	~1200	5.1	1168	4.01
12-March-2003, 071/22:58	Progress Manifold 1 4 Progress +X Thrusters	597	1.38	634	1.3
12-March-2003, 072/23:37	Progress Manifold 2 4 Progress +X Thrusters	198	0.37	219	0.3
04-April-2003, 094/12:59:18	8 Progress +X Thrusters Off-Pulsing	N/A	1.8	835	1.83
10-Apr-2003, 100/10:55	8 Progress +X Thrusters Off-Pulsing	661	1.48	672	1.46
30-May-2003, 150/16:50	8 Progress +X Thrusters Off-Pulsing	447	1.0	448	0.93
01-Oct-2003 274/13:11	8 Progress +X Thrusters Off-Pulsing	450	1.7	469	1.72
08-Jan-2004, 008/19:59	8 Progress +X Thrusters, Off-Pulsing	329	1.4	367	1.41
02-Mar-2004, 062/22:40	8 Progress +X Thrusters, Off-Pulsing	531	2.2	528	2.08

6.1.5.2 Orbiter Reboost

Orbiter reboosts of the ISS occur during joint operations, when the Space Shuttle is docked to the forward Pressurized Mating Adaptor (PMA2). During Increments 6-8, only three orbiter reboosts of the ISS were performed, all during STS-113 (11A) joint operations. Of these three, MAMS OSS data exists for only two of them. The first reboost (Figure 6-57) started at GMT 27−November−2002, 331/17:11 and lasted approximately 44 minutes. The 11A as-flown operations timeline obtained from the ADCO website records a change in velocity of 8.7 feet/s (2.65 m/s). The data points that fall within the reboost time period are highlighted with red circles and are used in the delta velocity calculation. The mean acceleration in the X -axis was -98.8 µg, resulting in a calculated change in velocity of -2.58 m/s. This shows close agreement with the as-flown timeline value. Note that the values for these calculations are negative, opposite of those for Progress reboosts. This is because, for this reboost, the ISS was in -XVV/+ZLV attitude, placing the $+X_A$-axis opposite of the velocity vector.

Figure 6-58 shows MAMS data captured during the second reboost two days later starting at GMT 29−November−2002, 333/16:55. The calculated mean during the reboost was -14.1 µg, much lower than the mean for the first reboost. The corresponding calculated change in velocity of -0.46 m/s does not agree with the value recorded in the 11A as-flown operations timeline of 2.4 ft/s (0.73 m/s). The as-flown timeline also includes a note for this reboost that reads “40m underburn”. The ISS attitude for this reboost was different than the first reboost, -XVV/-ZLV Bias.

6.1.6 Miscellaneous Events

6.1.6.1 Russian / US GNC Force Fight

On GMT 30-Aug-2003, 242/02:45 a Loss of Attitude Control (LOAC) recovery procedure was inadvertently invoked causing the Russian system to unconditionally take control of the ISS. This included ignoring the US Guidance, Navigation and Control (GN&C) control status. This resulted in a 106 second “force fight” between the Russian thrusters and US CMGs. The CMGs torqued against an RS thruster pitch adjustment until the force fight ended with CMGs saturated (could no longer provide torque) and their gimbals’ rates zeroed. Mission Control Center-Moscow later traced the problem to an early uplink of the post-Progress 12P docking cyclogram (timeline for automated control procedures).

Figure 6-59 and Figure 6-60 are a 3-panel time series plot and vector magnitude plot of MAMS data recorded during the force fight and the subsequent recovery. Figure 6-61 shows a zoom view of the force fight effects on the quasi-steady environment, a 9.50 µg peak in the +Z-axis, highlighted by the dotted red lines. Key events captured in the MAMS data are labeled in Figure 6-60, and detailed in Table 6-9 below.

TABLE 6-9 TIMELINE OF RUSSIAN / US GNC FORCE FIGHT AND RECOVERY

Event	Time (hh:mm)	Description	Peak (µg)
1	02:45 to 02:47	Force fight between US CMGs and RS Thrusters.	9.83
2	02:47:15	Loss of attitude control due to the saturation of the CMGs, SM thrusters not available for desaturation.	
3	05:00	US GN&C changed mode from CMGTA to Drift (Inertial)	6.20
4	05:30	Final steps for Attitude Control Handover from RS to US begun	5.2
5	05:30:49	Thrusters available for CMG	

6.1.6.2 Control Moment Gyroscope 2 Shutdown

At GMT 21-April-2004, 112/20:18 CMG-2 lost power and spun down when its controlling Remote Power Controller Module (RPCM) tripped and could not be reset. During troubleshooting steps, the ISS drifted away from nominal +XVV/+ZLV LVLH attitude. Effects on the quasi-steady vector at the MAMS location can be seen in Figure 6-62. The greatest effect due to the drift was on the Z_A-axis, but only approximately 0.5 µg from what the nominal baseline for LVLH attitude. However, momentum increased in the remaining CMGs, which required thruster firings for desaturation. These thruster firings appear as 2.5 µg to 7.5 µg spikes in the -Z_A-axis. The ISS was returned to nominal attitude by 22:23, under 2-CMG operations.

6.1.6.3 Inadvertent Torque

An unexpected attitude disturbance occurred while in XPOP attitude at GMT 27-October-2003, 300/18:59. This disturbance resulted in -29.9 µg spike on the Z_A-axis in the quasi-steady vector at the MAMS location, as seen in Figure 6-63. Also, thruster firings used for CMG desaturation and attitude restoration caused spikes as large as -51.7 µg in the Z_A-axis. One explanation for the torque is an accidental activation of the Translational Hand Controller, used for manual attitude control. A brief timeline included in an email to PIMS from the GN&C personnel details this theory:

> An unexpected attitude disturbance while in XPOP momentum management led to ADCO* transitioning to an Attitude Hold controller this afternoon, hours before the Soyuz 6S departure. A brief timeline and explanation is provided below:
>
> GMT 300/14:45 Manual desat for XPOP momentum management initiation
>
> - 14:50 - 18:59 XPOP MM continues to settle smoothly, momentum peaked around 5500 N-m-s, then decreased to <2500 N-m-s.
> - 18:59 Unexpected station torque disturbance causes CMG 110 N-m response torque, rapid increase in momentum, and build-up of attitude error.
> - 19:01 - 19:15 A series of 19 desats occurred as MM fought to suppress the attitude disturbance. Attitude errors peaked at (-6.0, -6.9, 17.8) deg YPR at about 19:06.
> - 19:16 ADCO modes GN&C to Attitude Hold. Seven more desats occur as the controller restores attitude to the XPOP TEA.
> - 20:00 Attitude control handover to the Russian segment in preparation for 6S separation.
>
> * ADCO is Attitude Determination and Control Office

The MAMS data collected during this event is consistent with the accidental thruster firing theory. To PIMS' knowledge, there has been no further investigation or confirmation of details regarding this event.

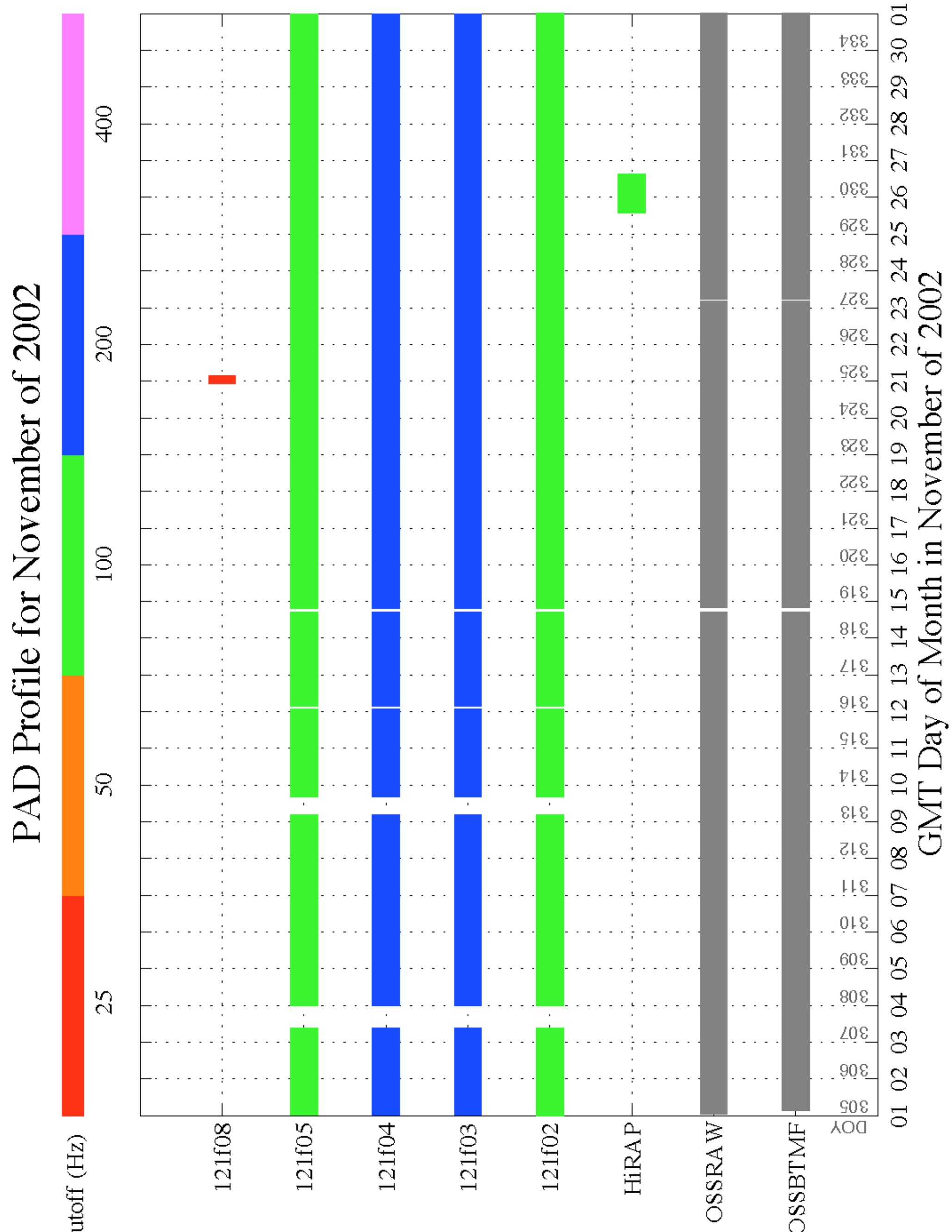

Figure 6-1 PAD Profile for November 2002

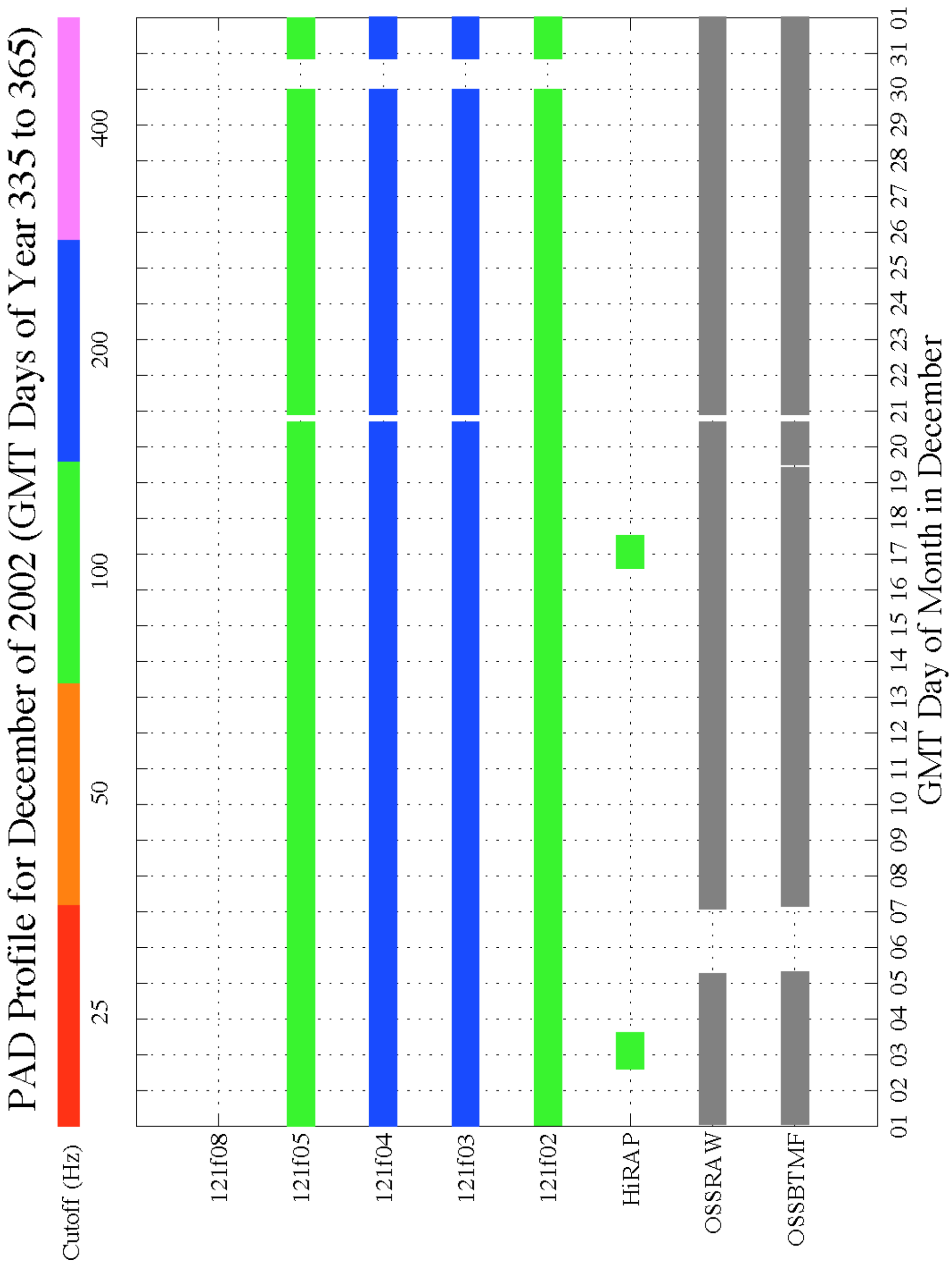

Figure 6-2 PAD Profile for December 2002

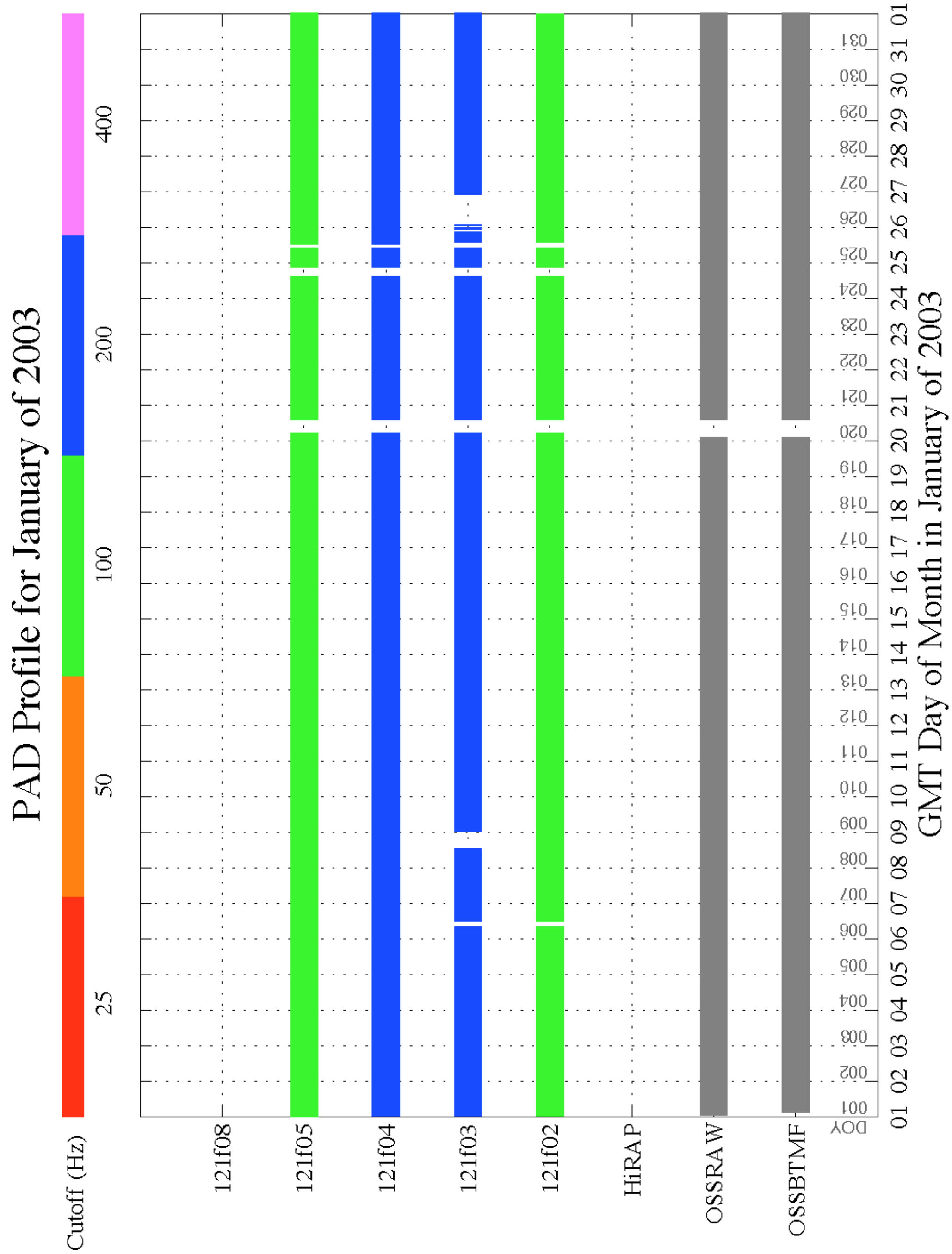

Figure 6-3 PAD Profile for January 2003

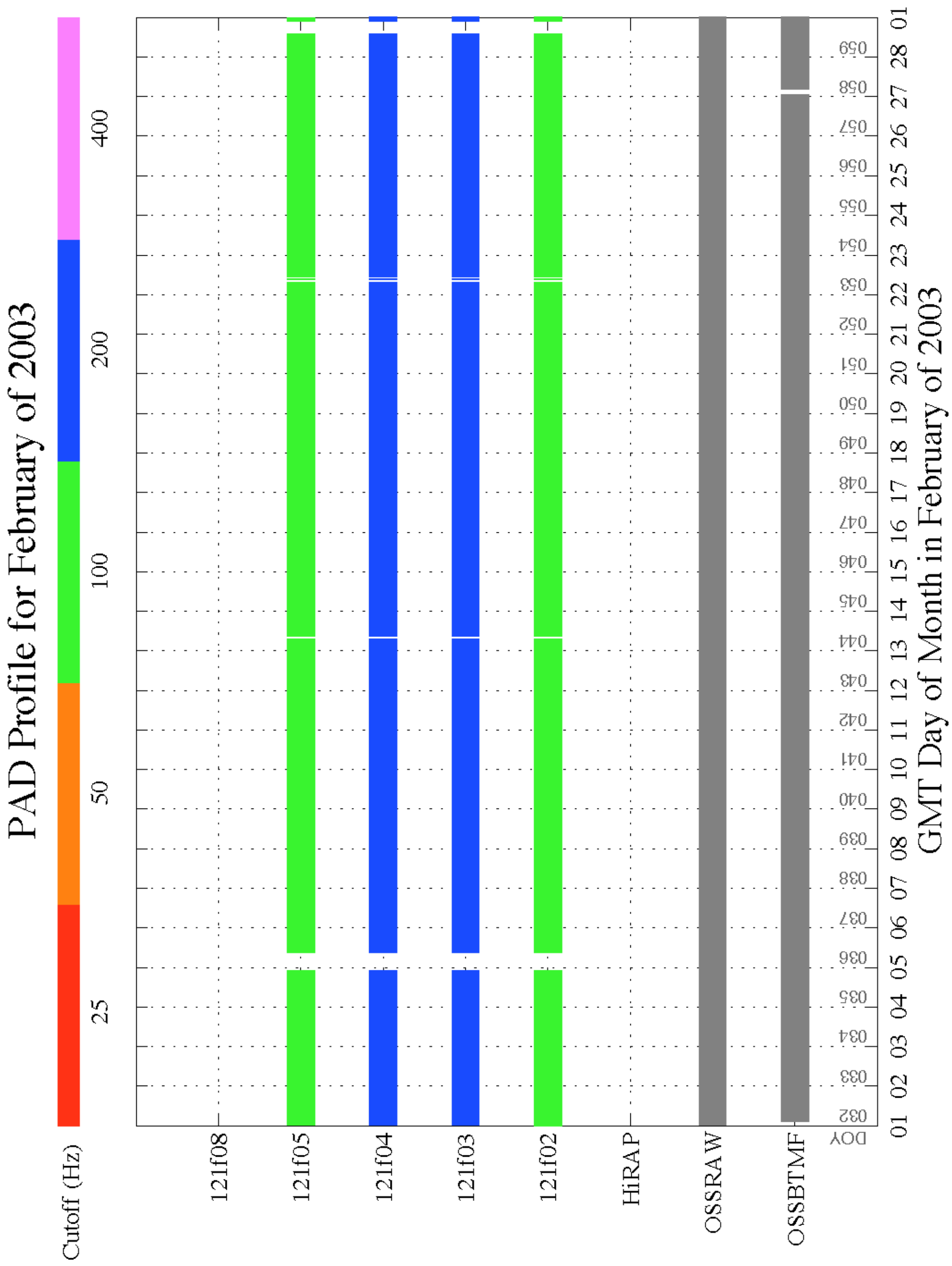

Figure 6-4 PAD Profile for February 2003

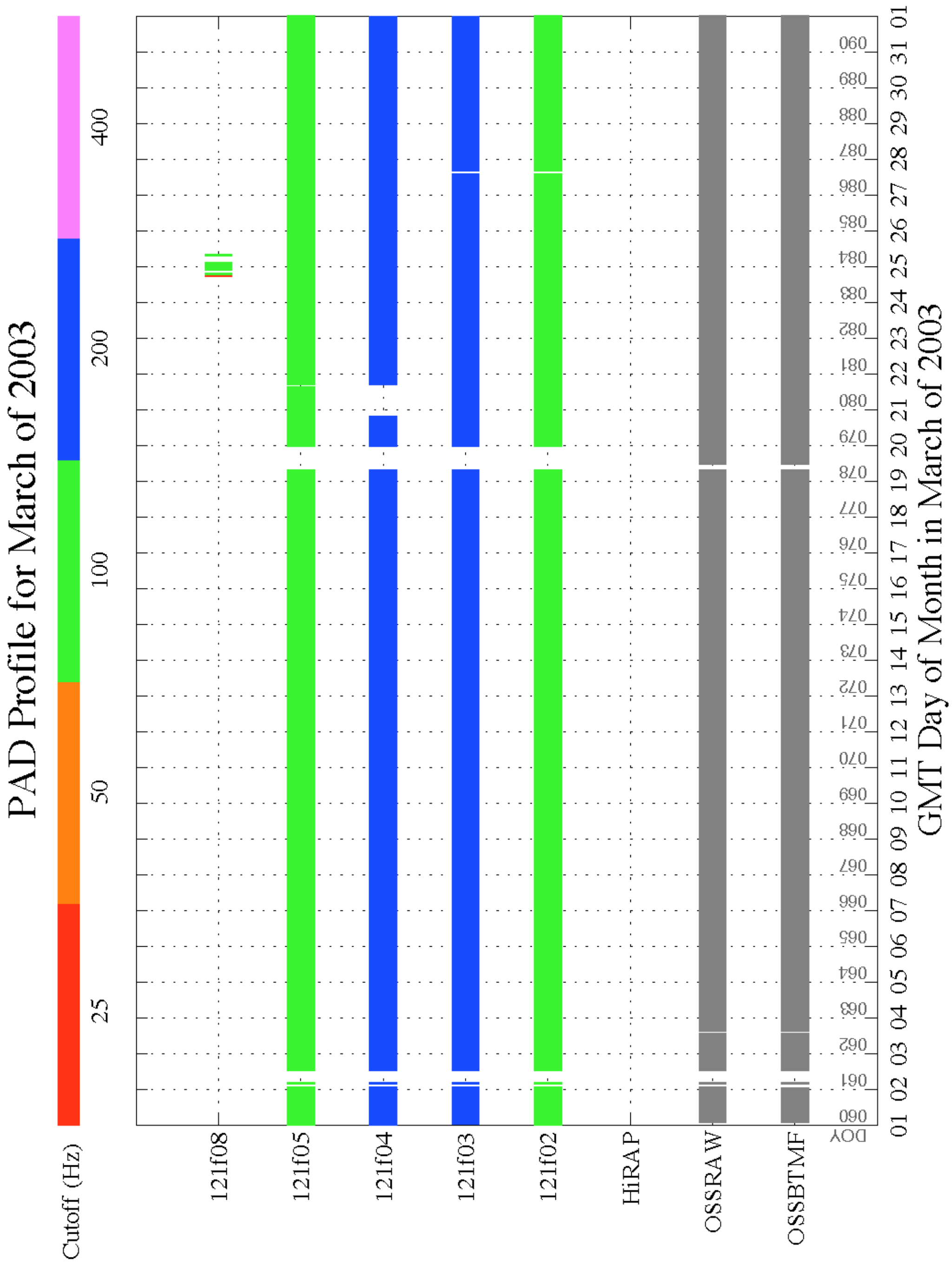

Figure 6-5 PAD Profile for March 2003

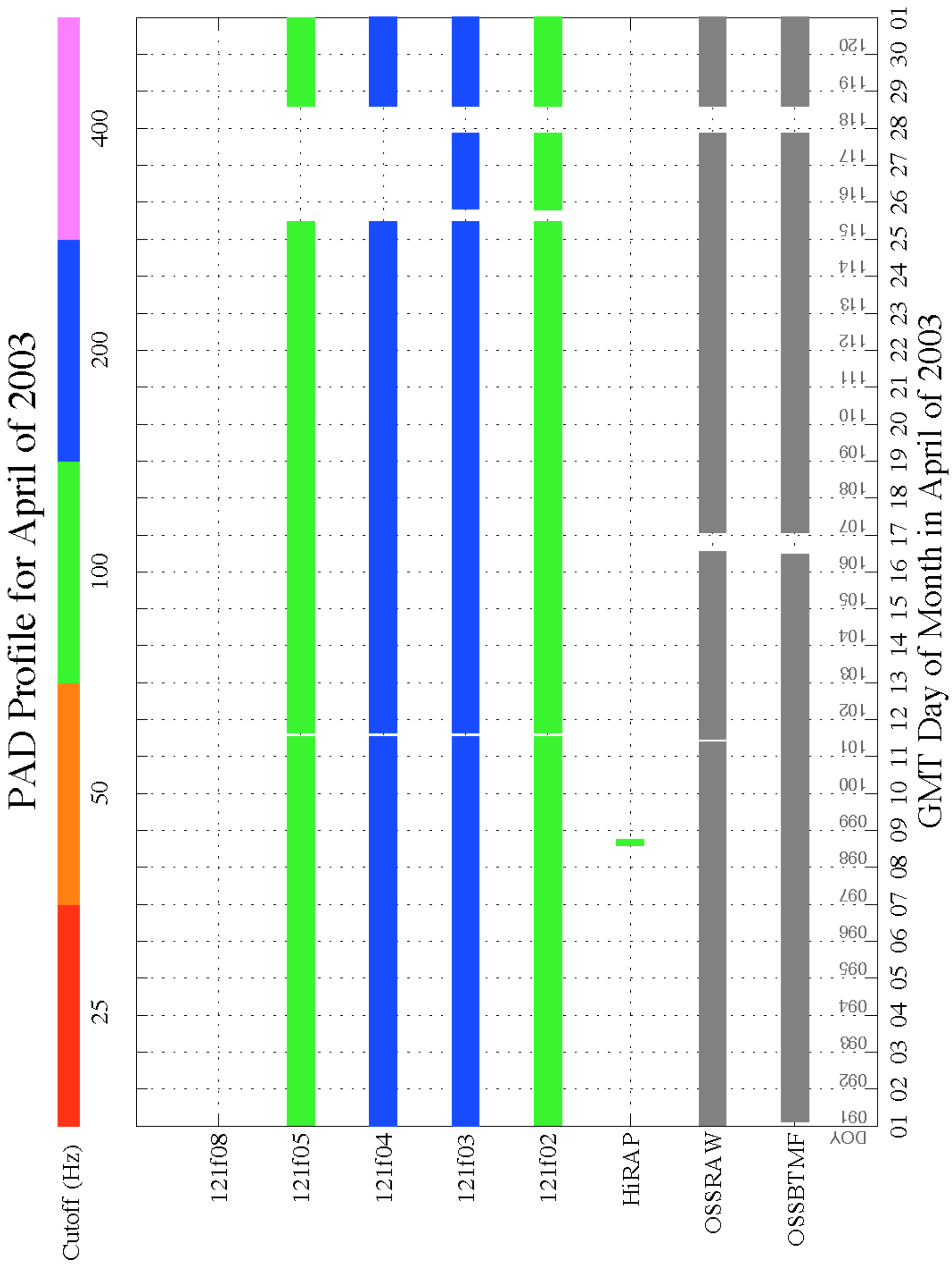

Figure 6-6 PAD Profile for April 2003

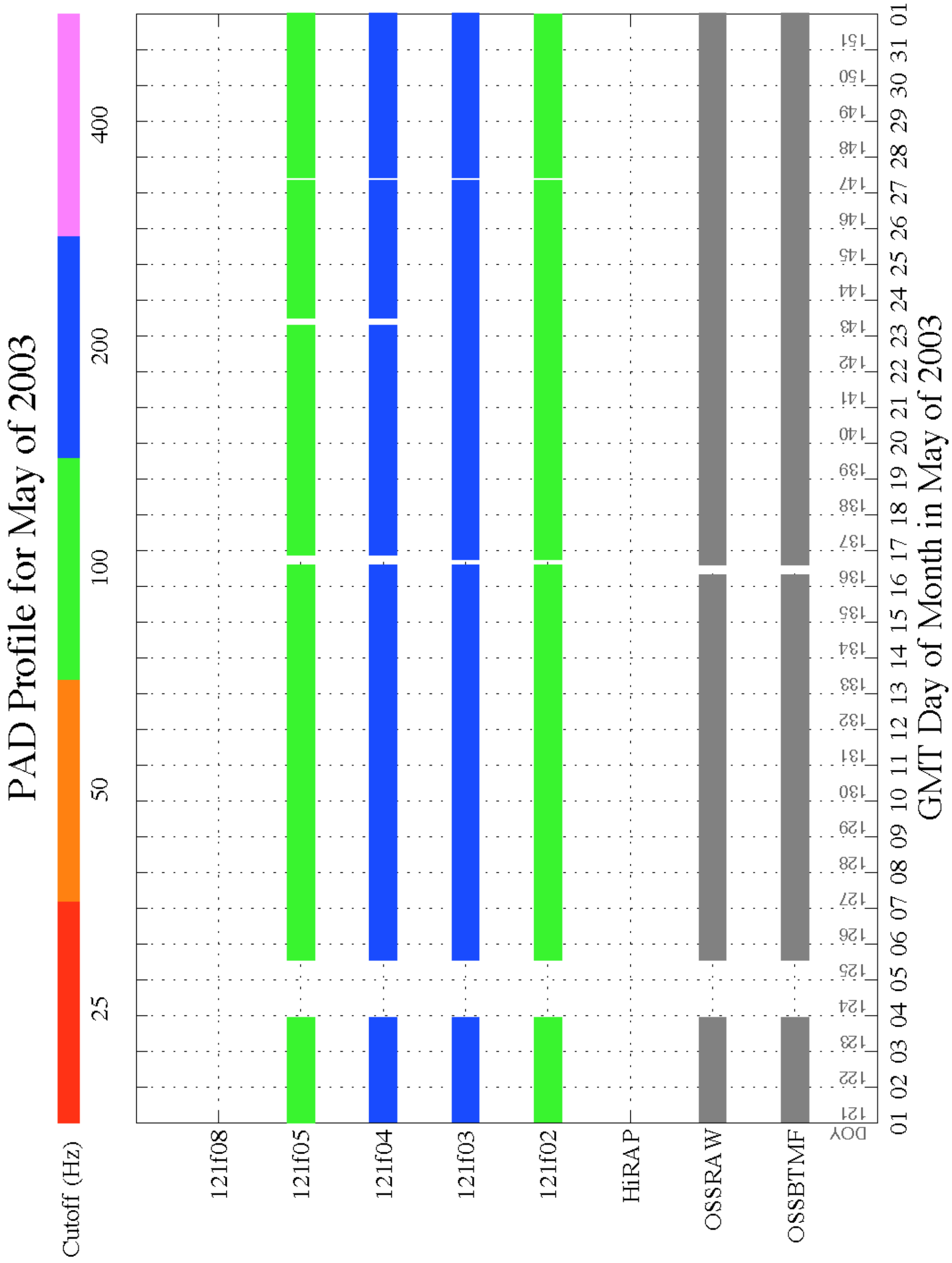

Figure 6-7 PAD Profile for May 2003

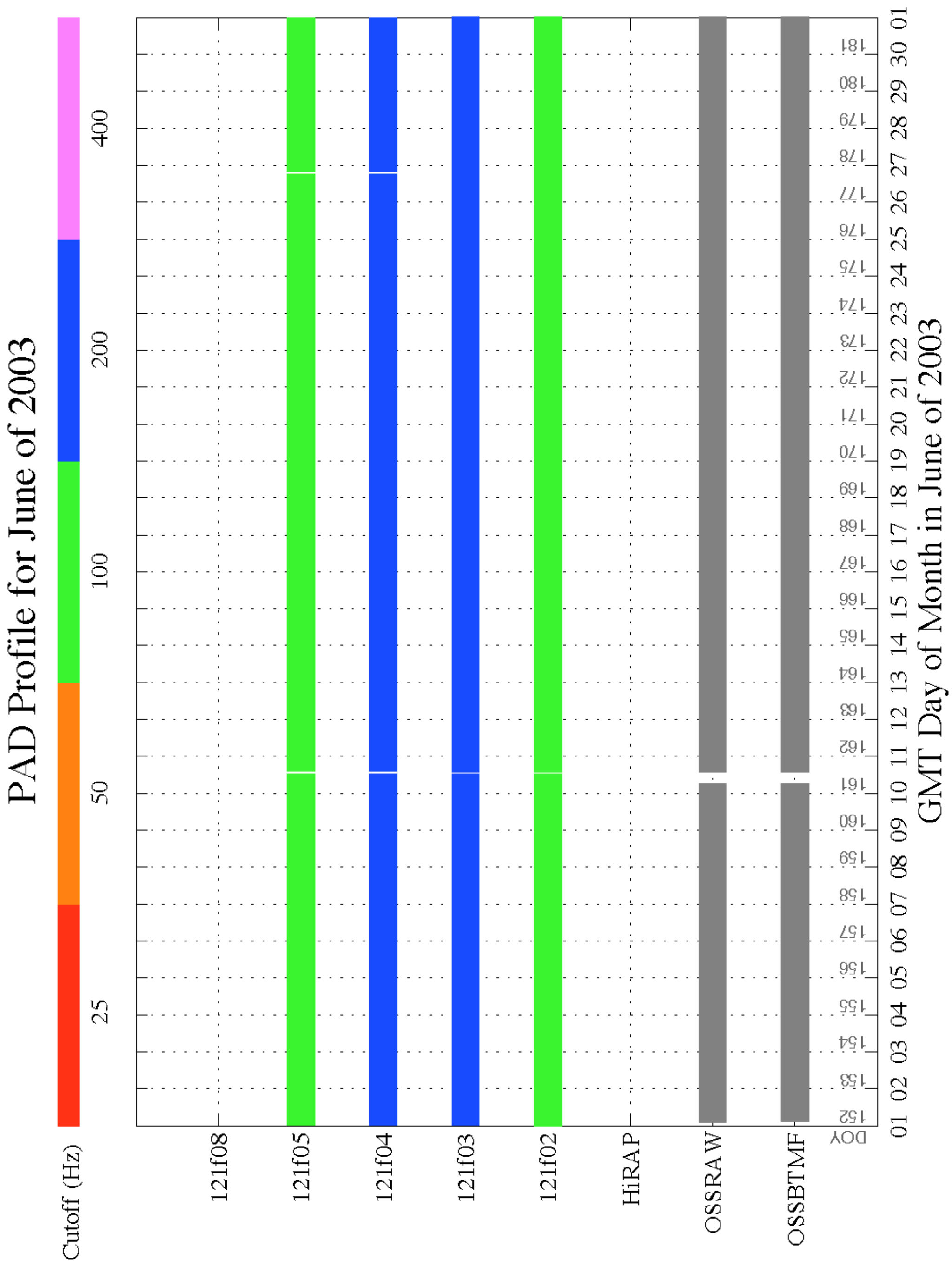

Figure 6-8 PAD Profile for June 2003

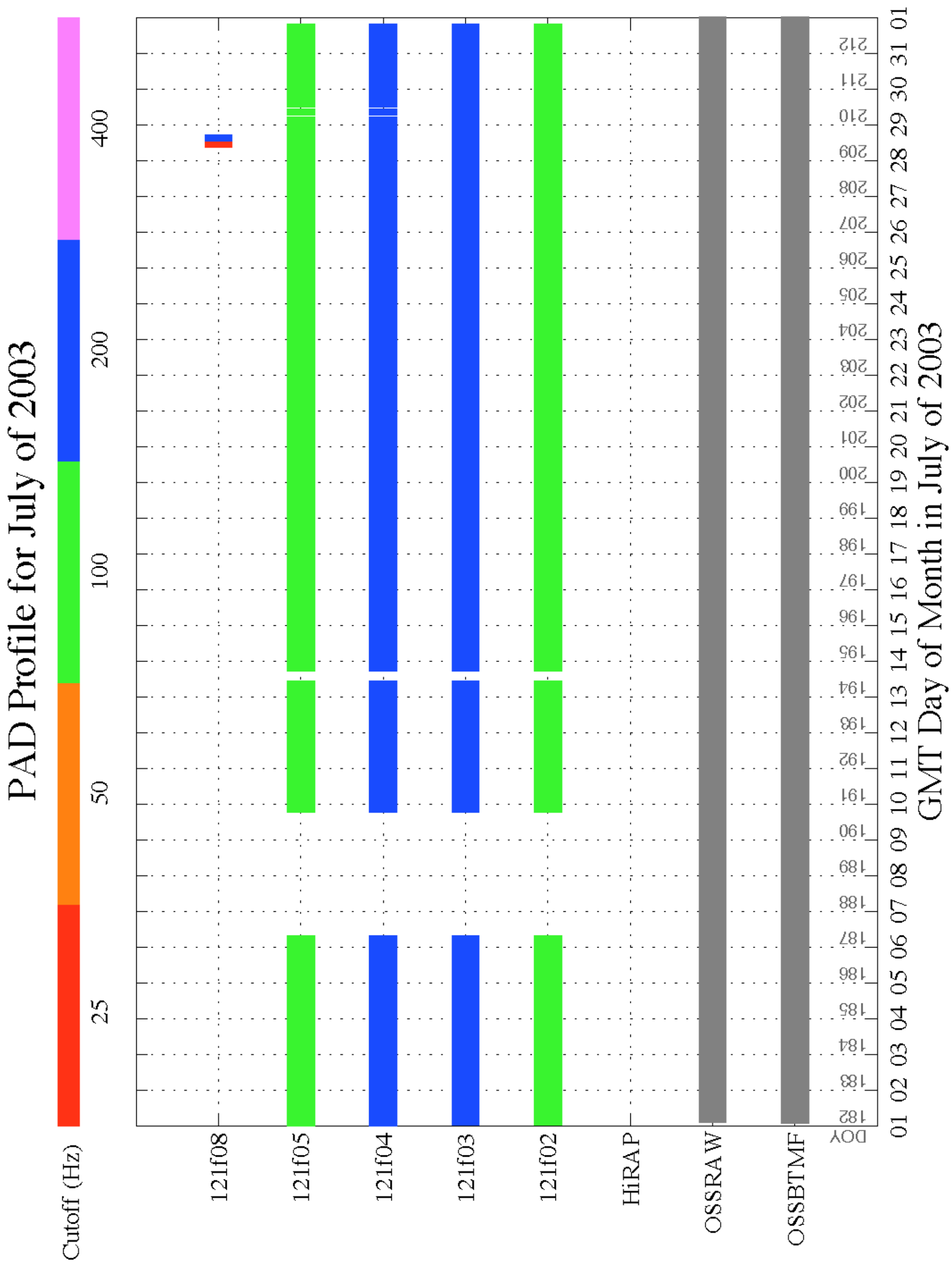

Figure 6-9 PAD Profile for July 2003

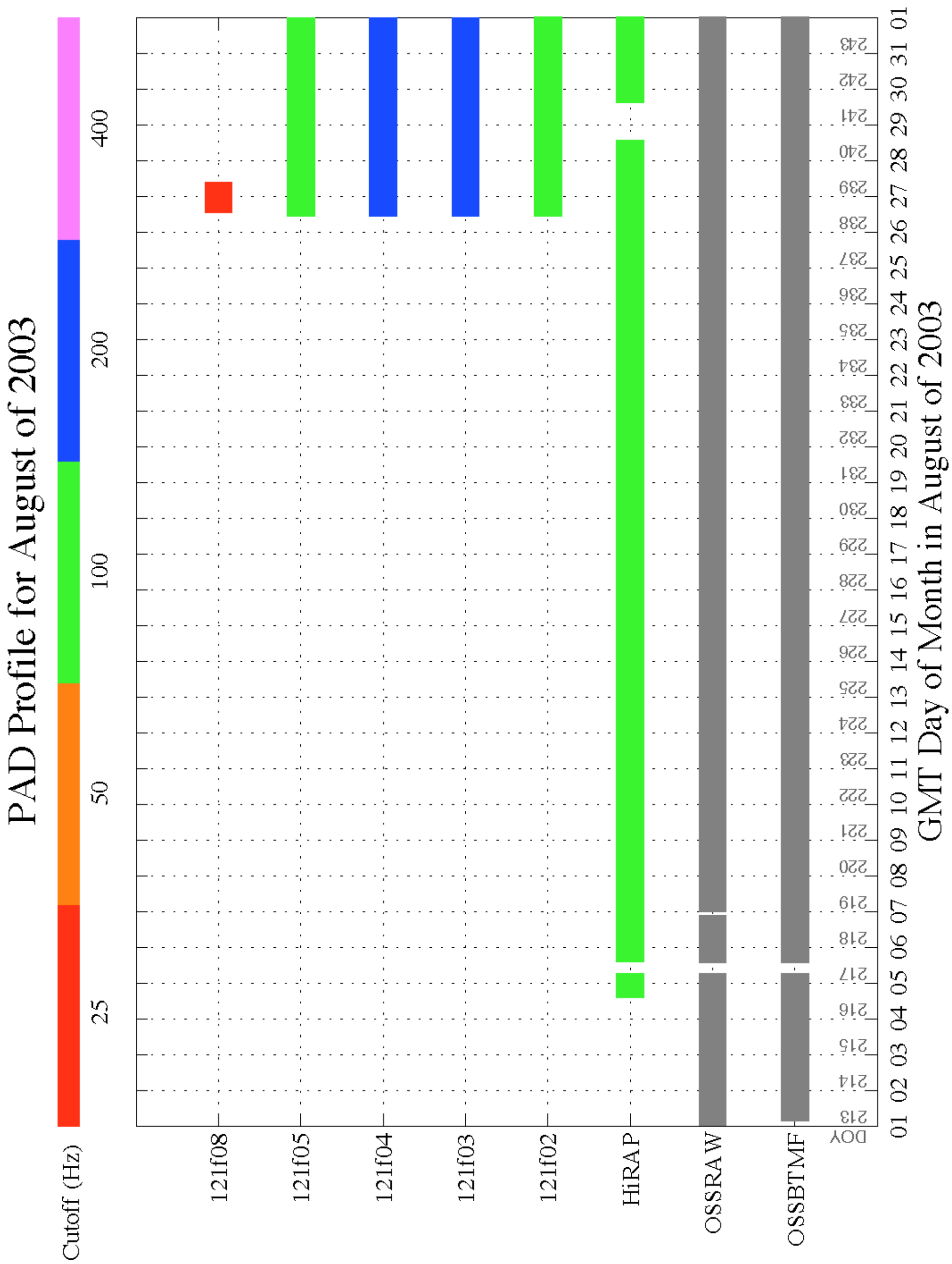

Figure 6-10 PAD Profile for August 2003

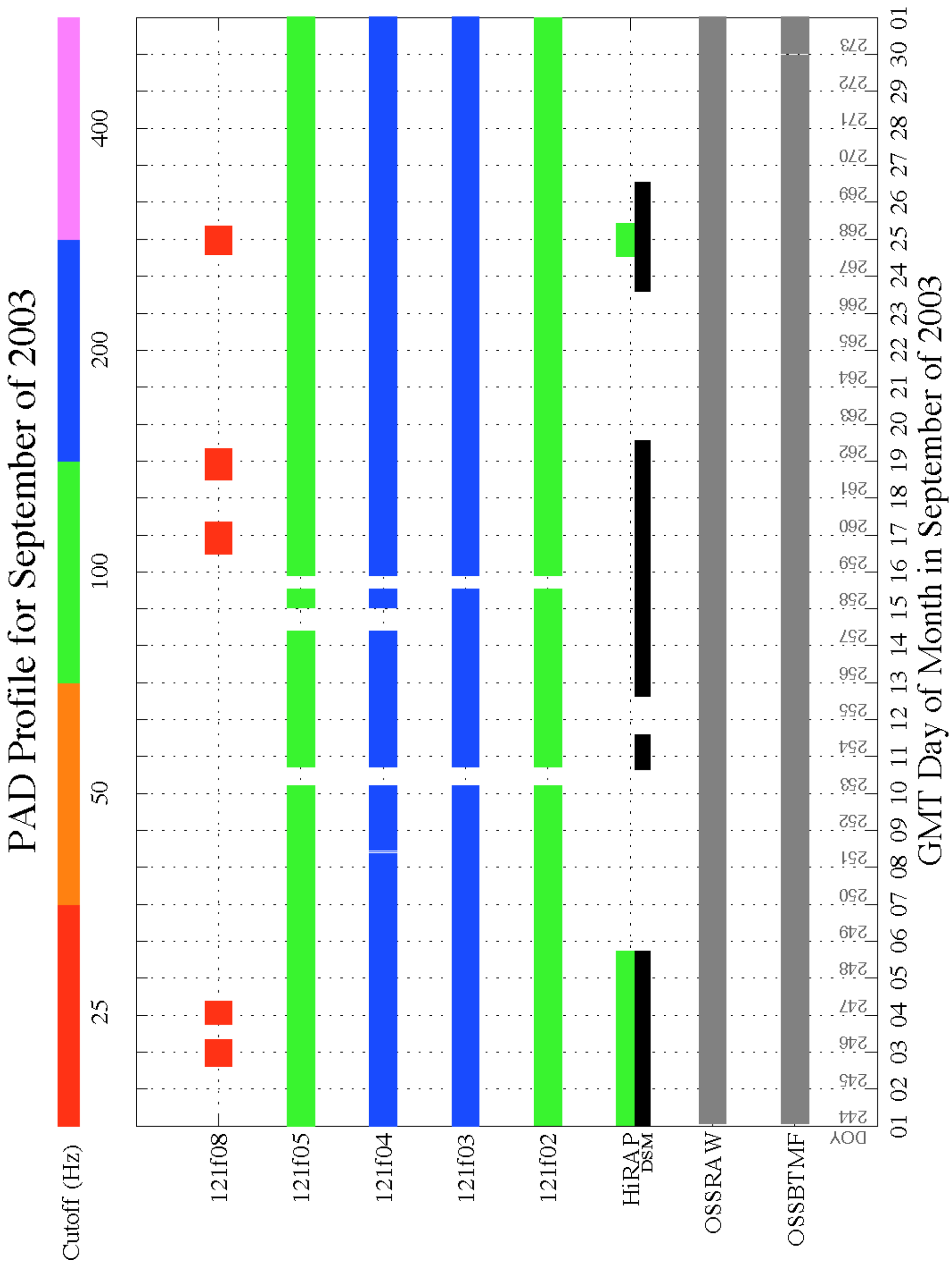

Figure 6-11 PAD Profile for September 2003

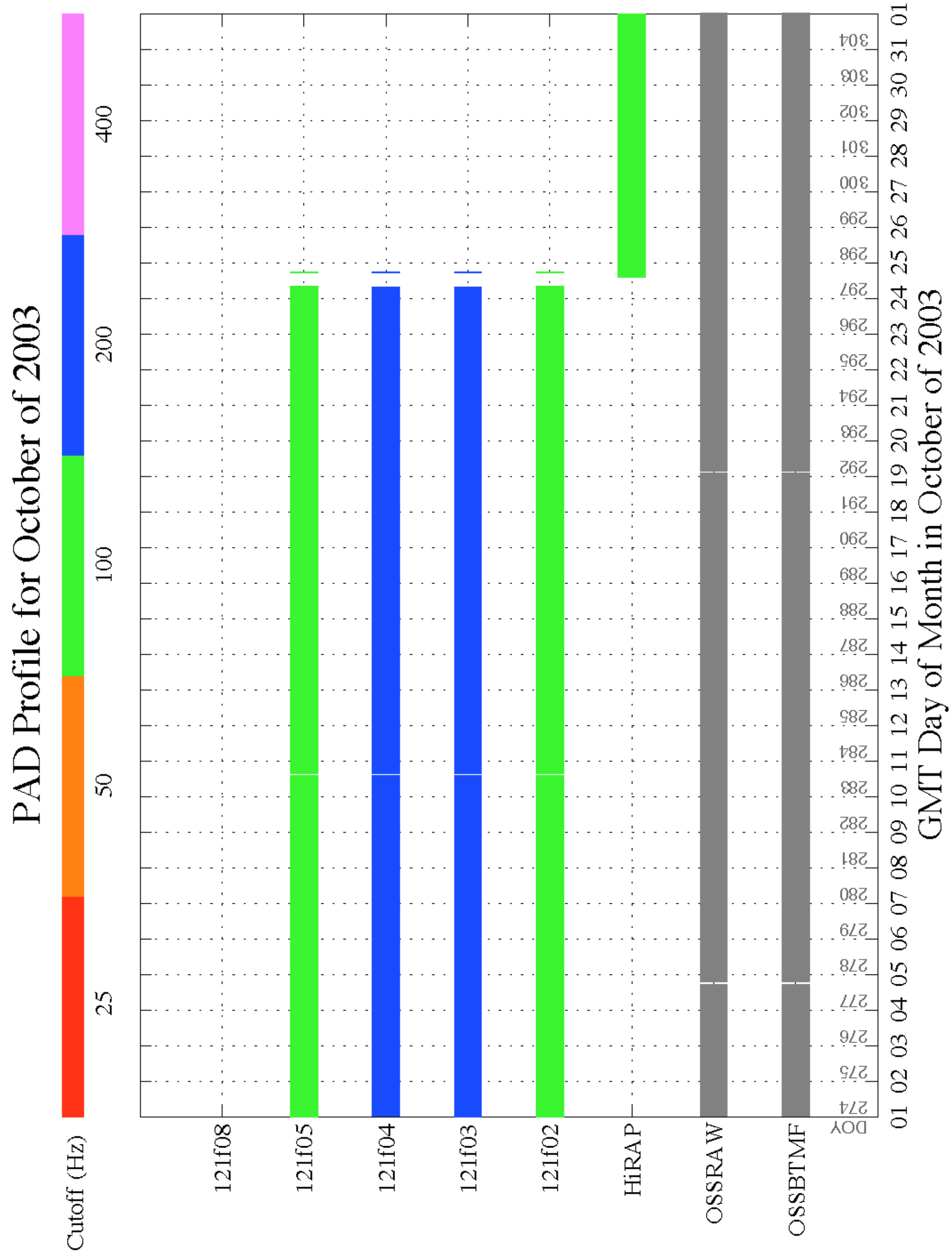

Figure 6-12 PAD Profile for October 2003

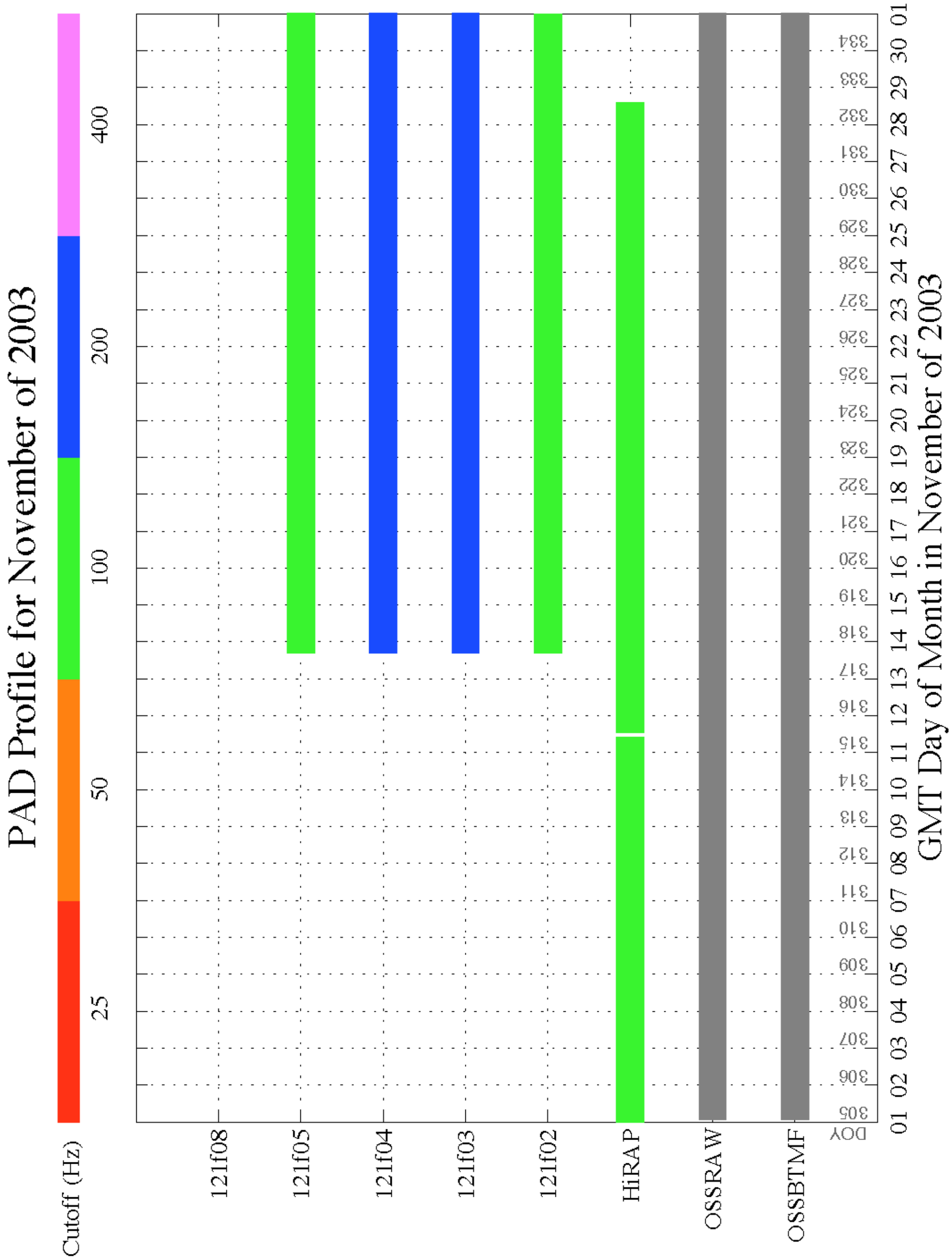

Figure 6-13 PAD Profile for November 2003

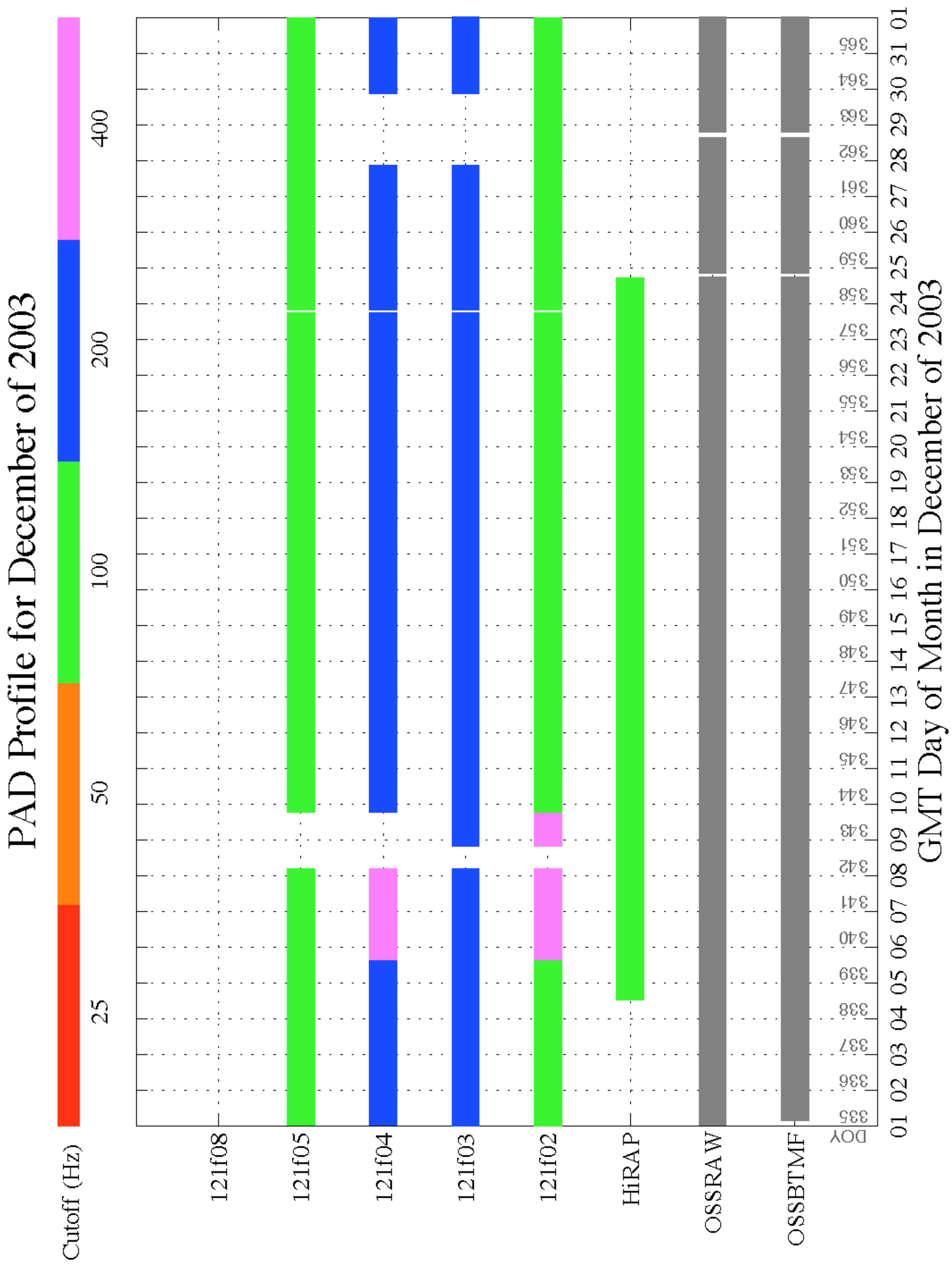

Figure 6-14 PAD Profile for December 2003

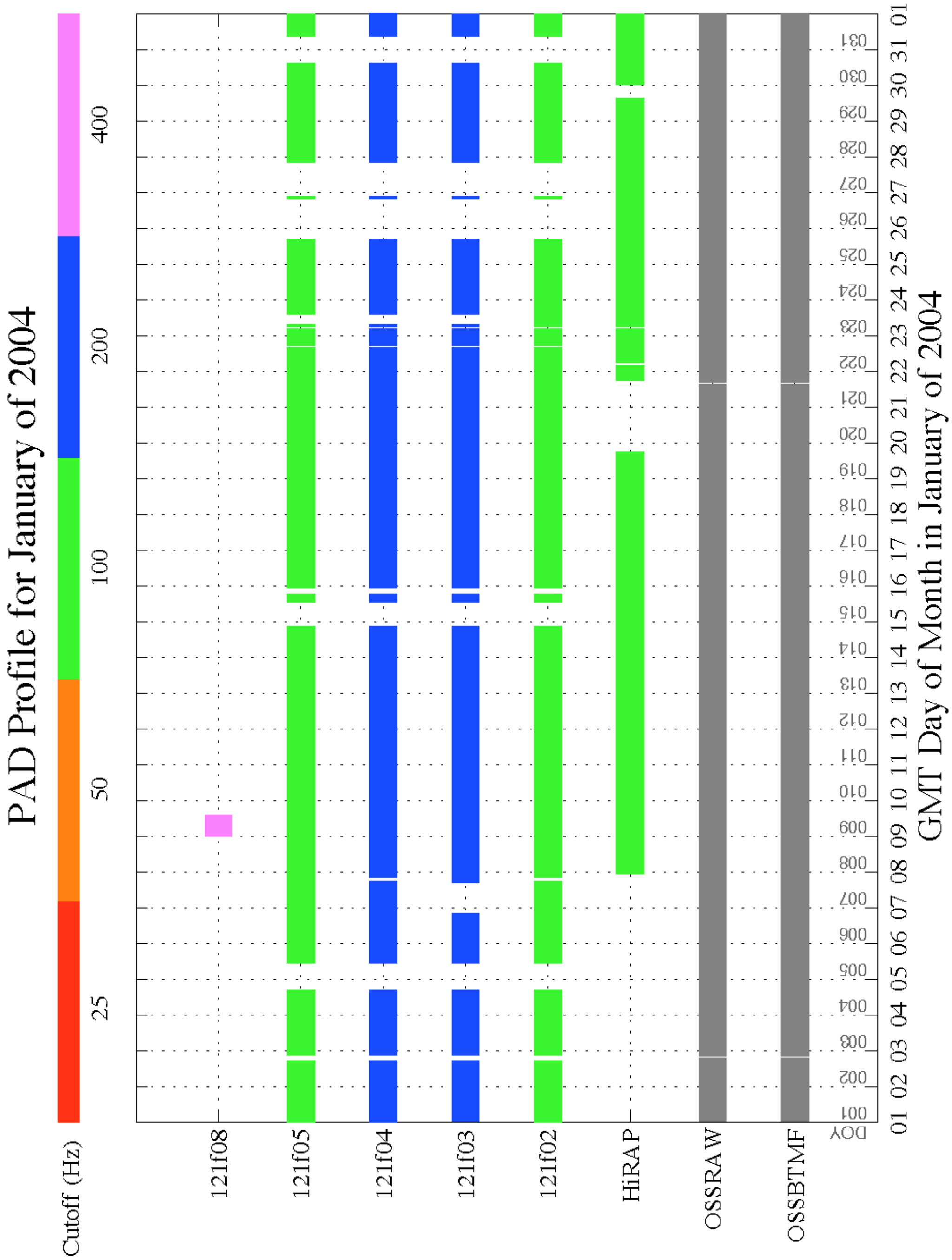

Figure 6-15 PAD Profile for January 2004

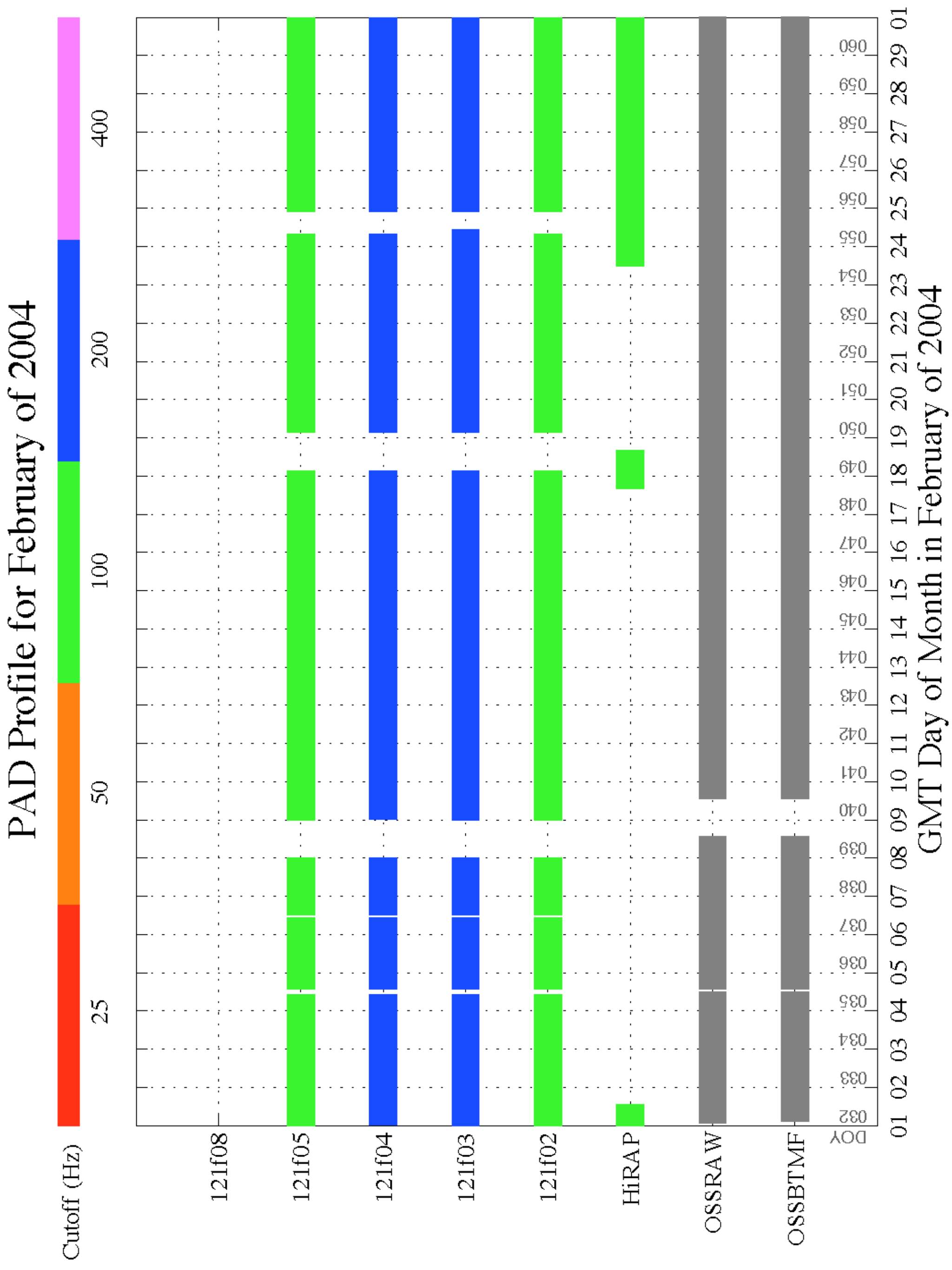

Figure 6-16 PAD Profile for February 2004

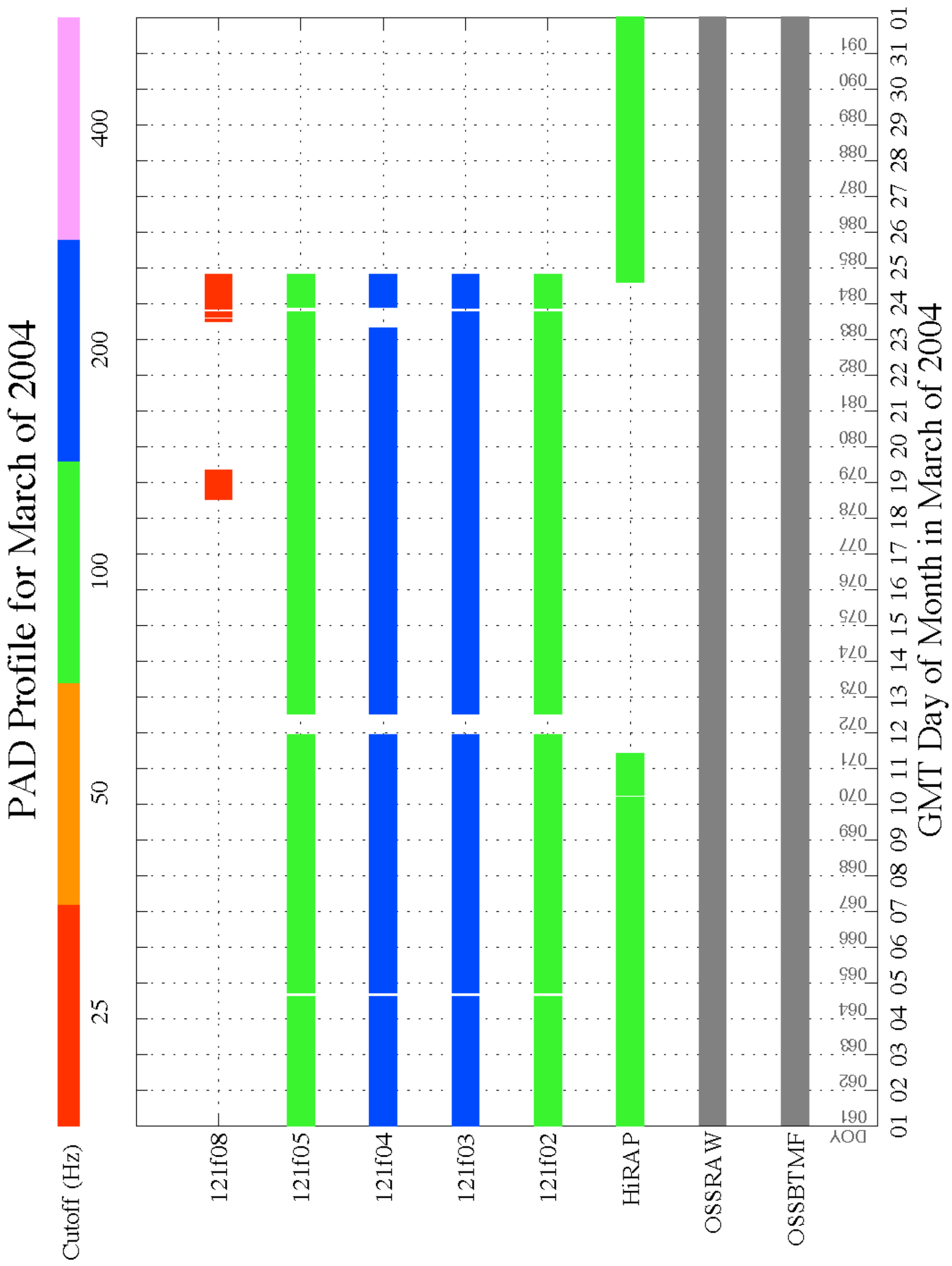

Figure 6-17 PAD Profile for March 2004

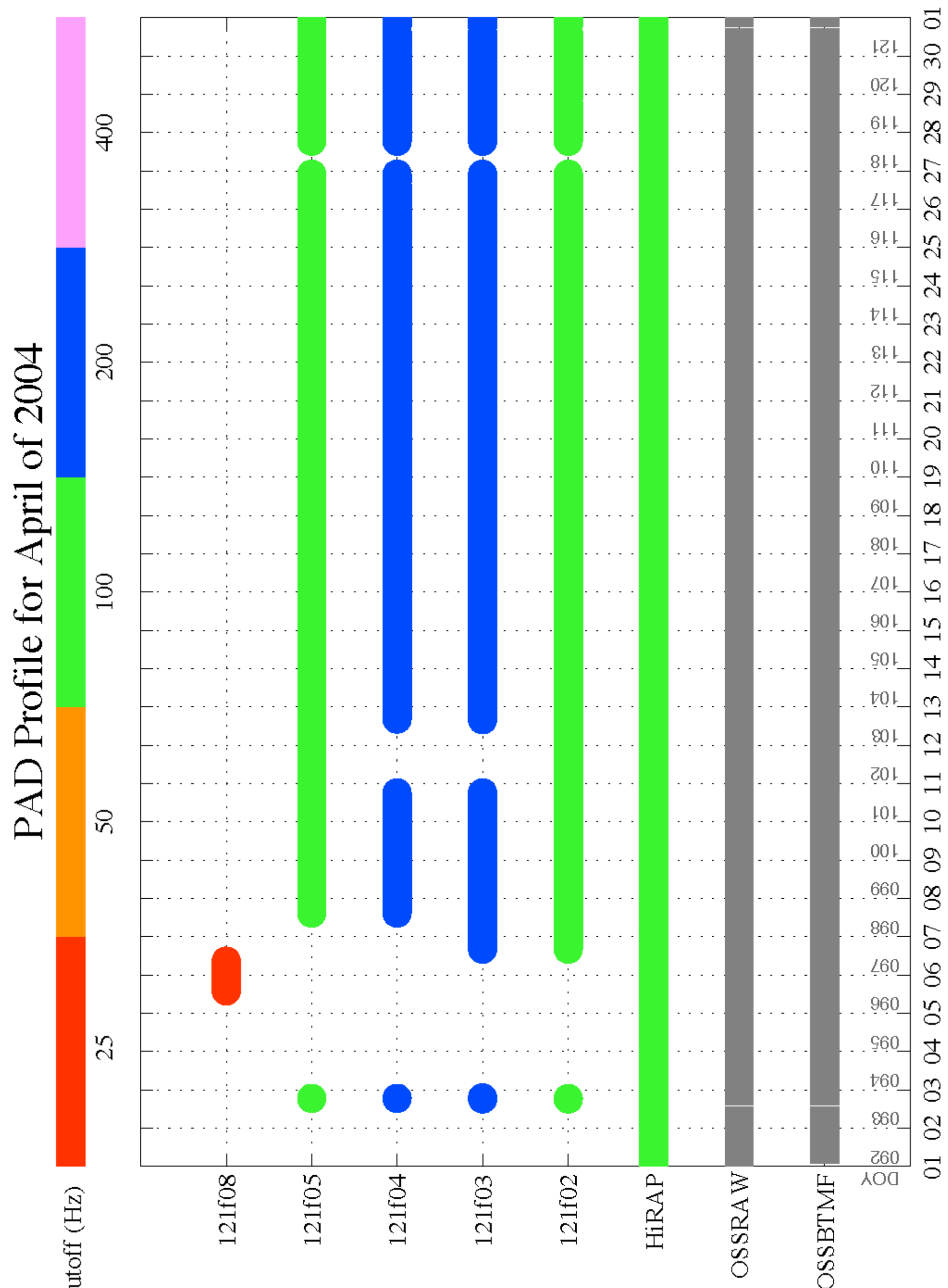

Figure 6-18 PAD Profile for April 2004

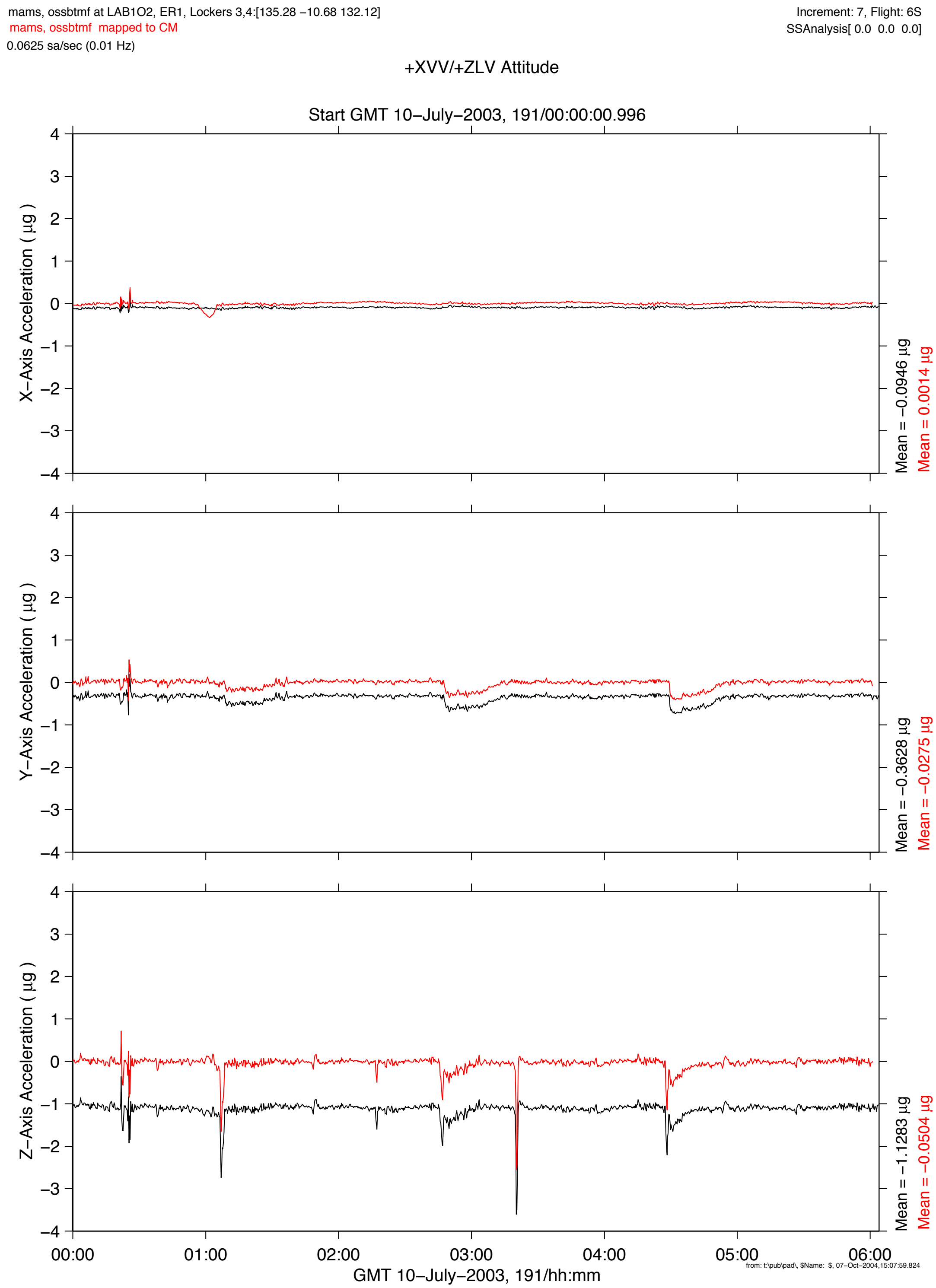

Figure 6-19 Time Series of +XVV/+ZLV Attitude (OSSBTMF)

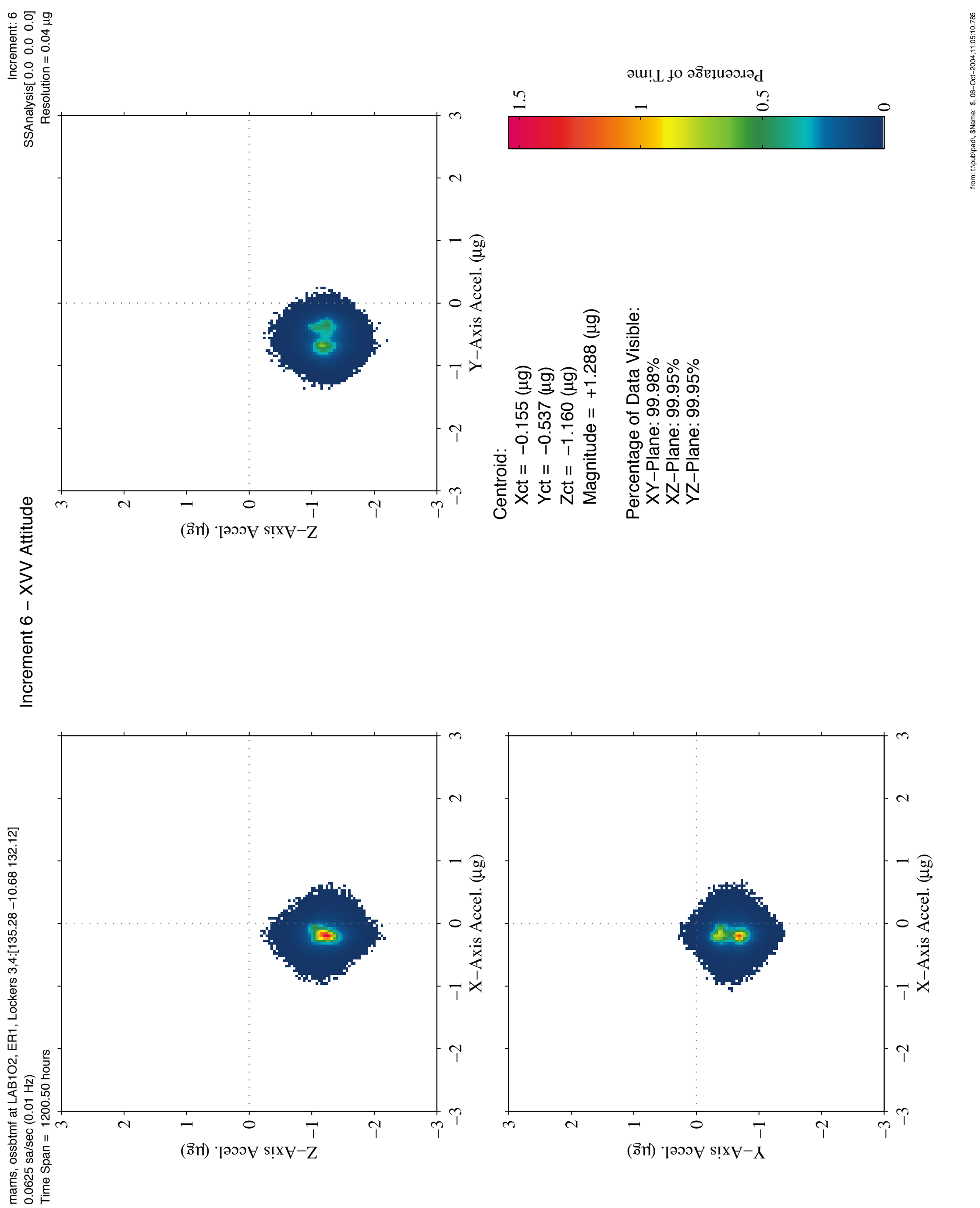

Figure 6-20 QTH Composite of XVV/ZLV Attitude for Increment 6 (OSSBTMF)

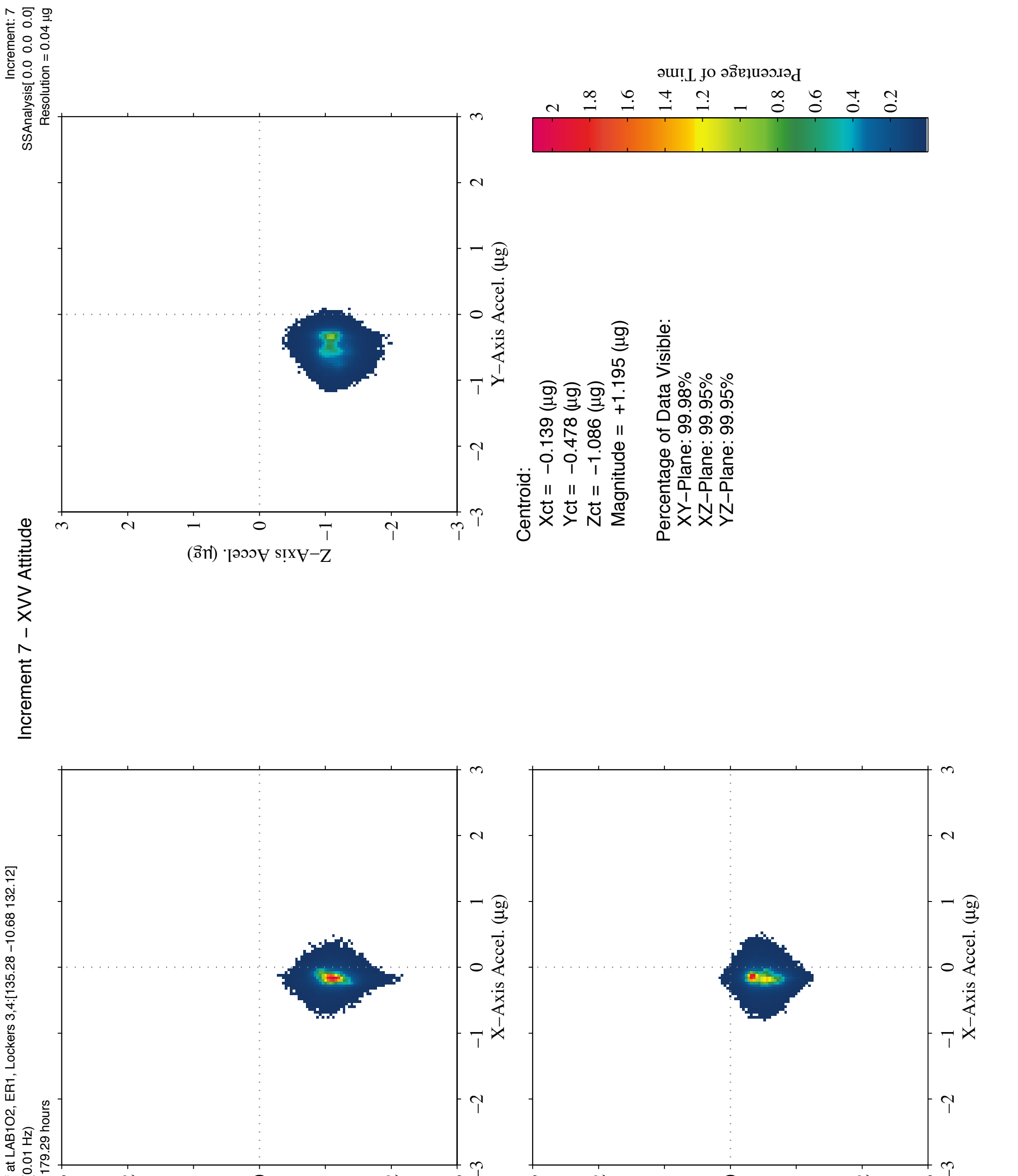

Figure 6-21 QTH Composite of XVV/ZLV Attitude for Increment 7 (OSSBTMF)

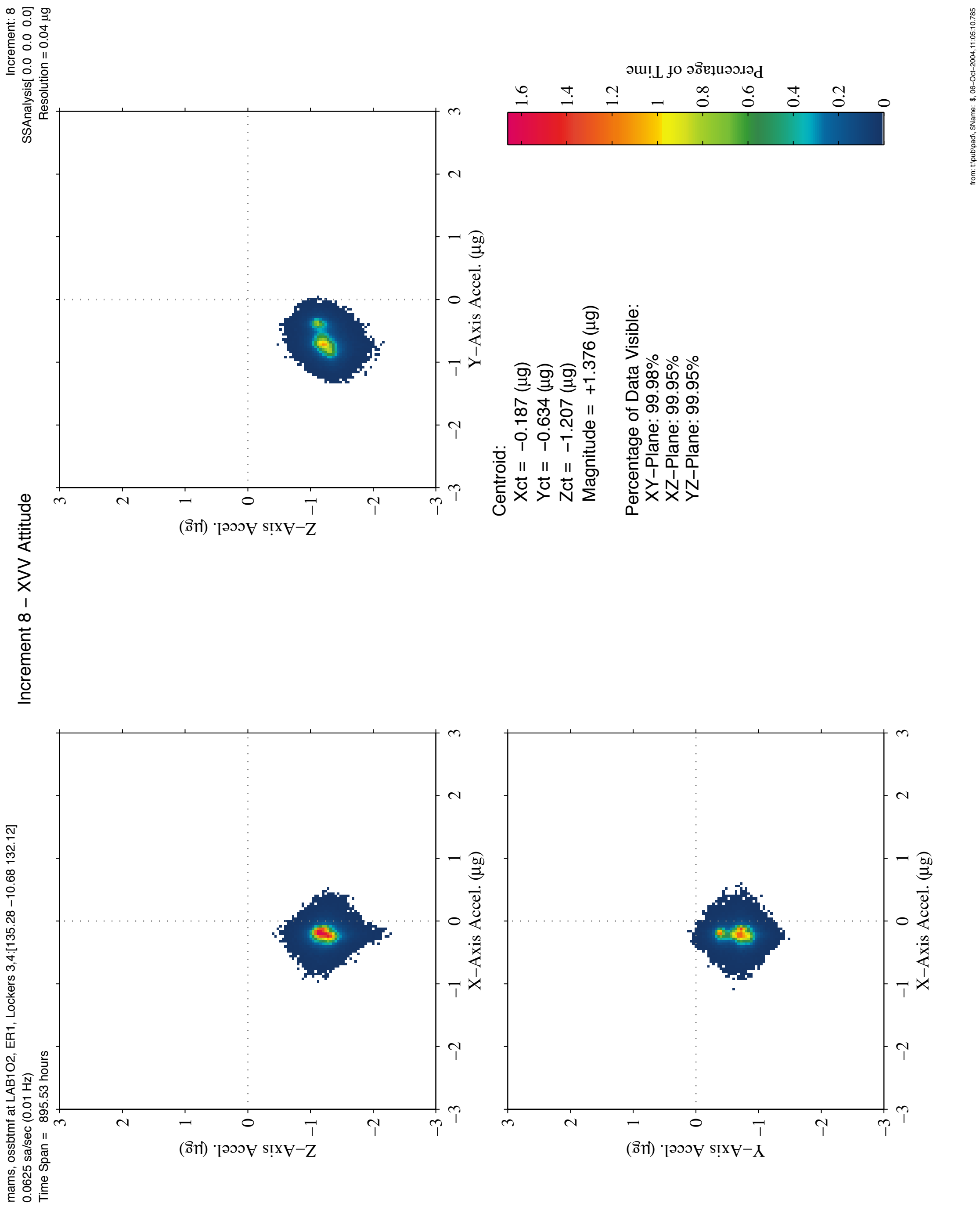

Figure 6-22 QTH Composite of XVV/ZLV Attitude for Increment 8 (OSSBTMF)

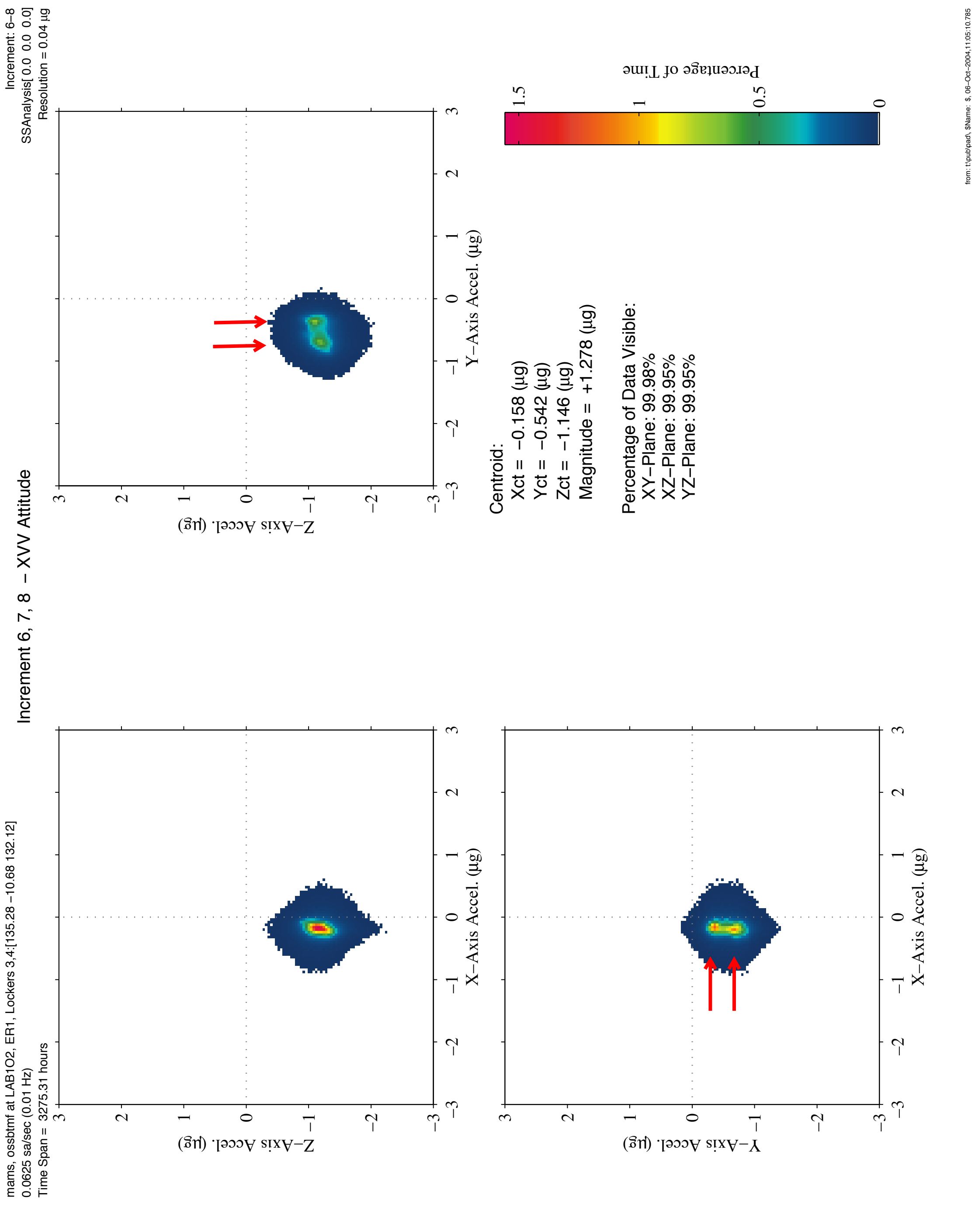

Figure 6-23 QTH Composite of XVV/ZLV Attitude for Increments 6-8 (OSSBTMF)

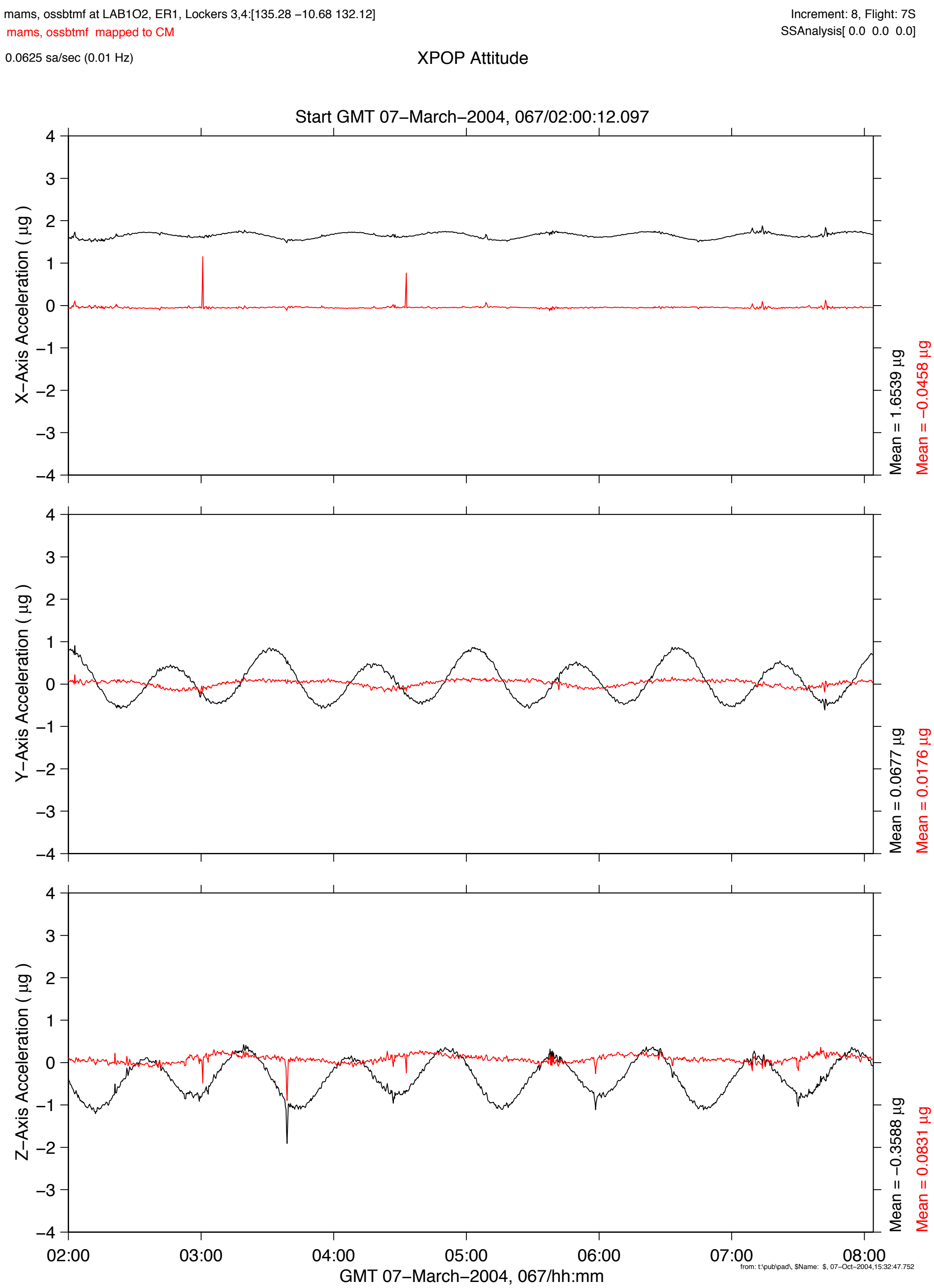

Figure 6-24 Time Series of XPOP Attitude (OSSBTMF)

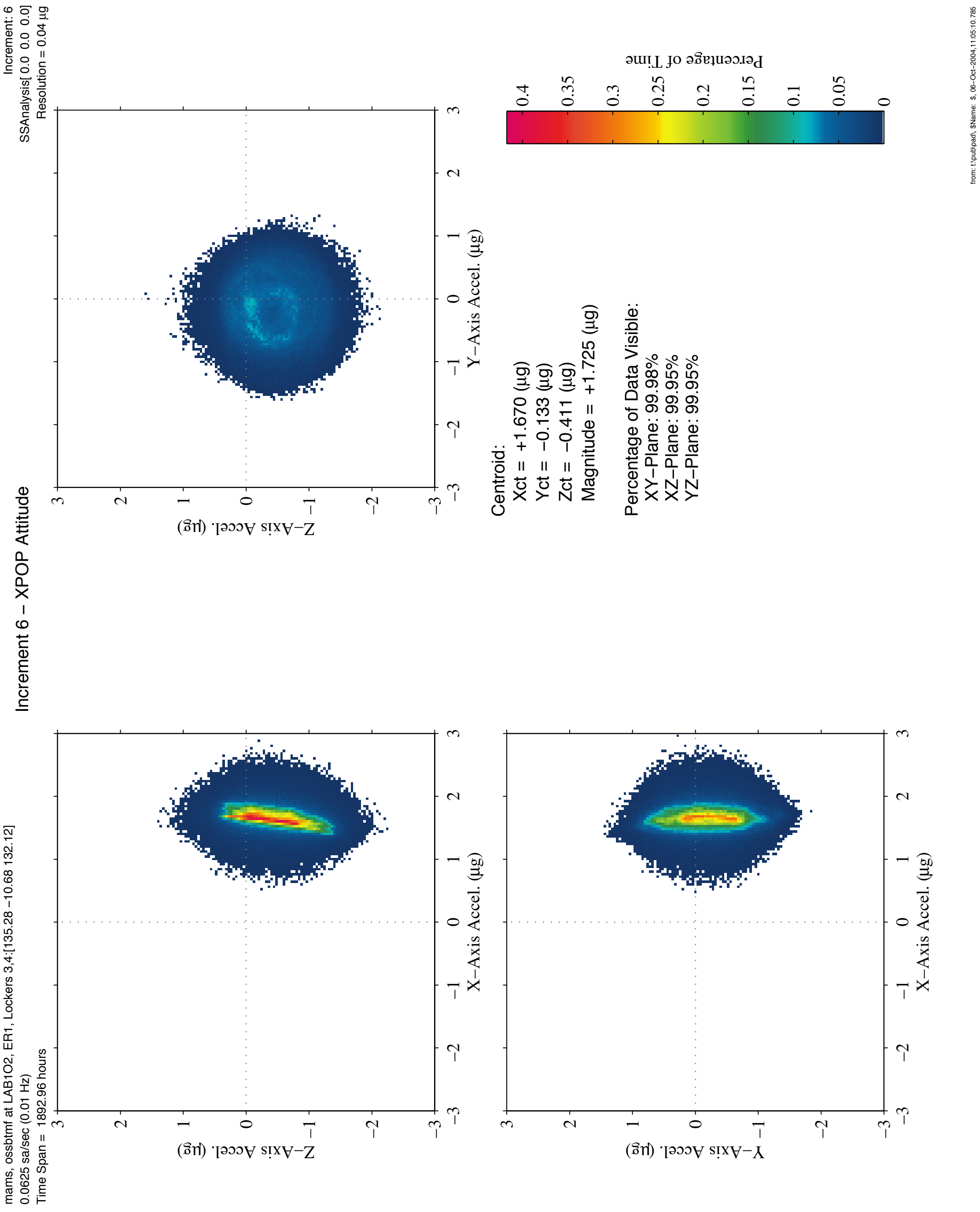

Figure 6-25 QTH Composite of XPOP Attitude for Increment 6 (OSSBTMF)

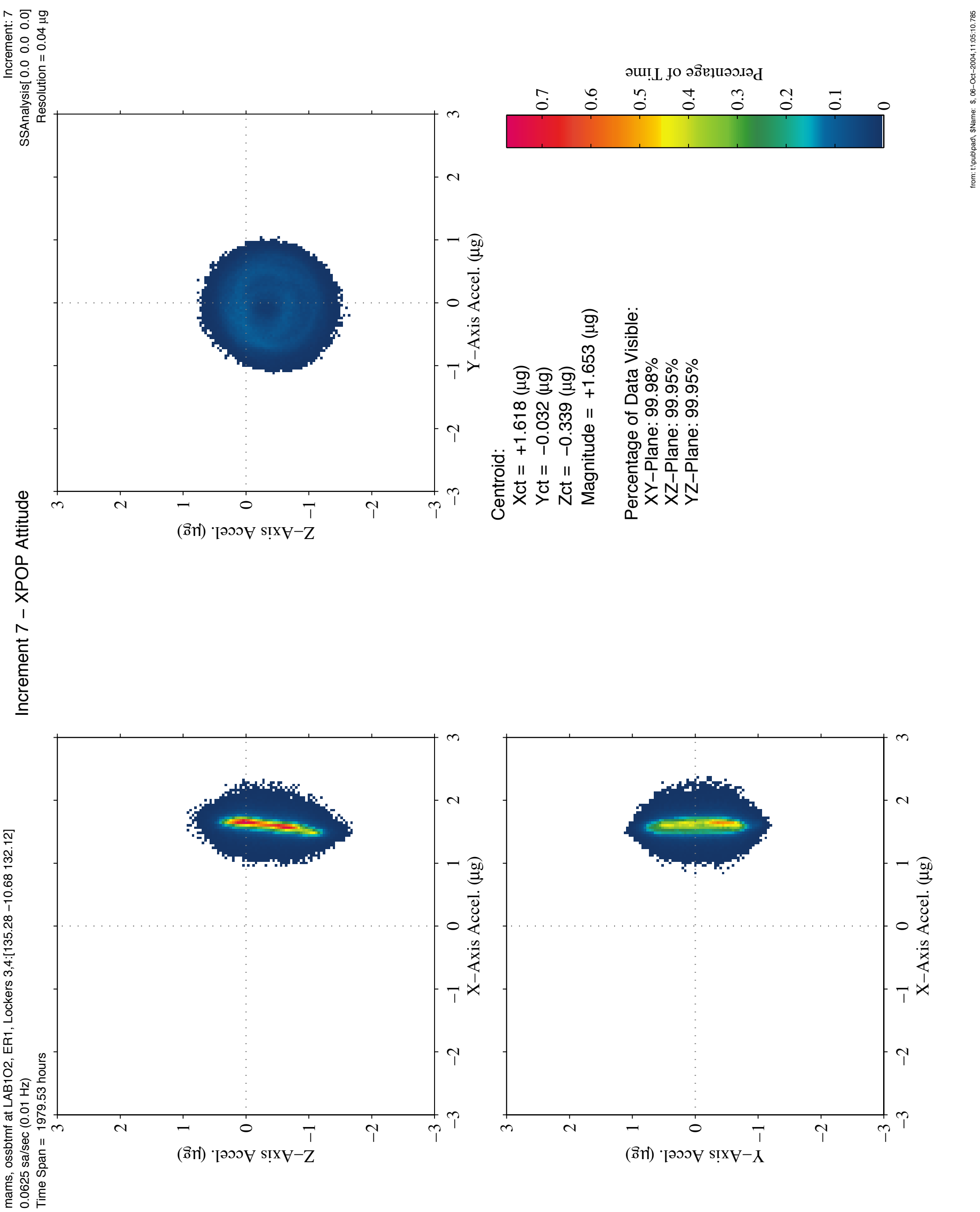

Figure 6-26 QTH Composite of XPOP Attitude for Increment 7 (OSSBTMF)

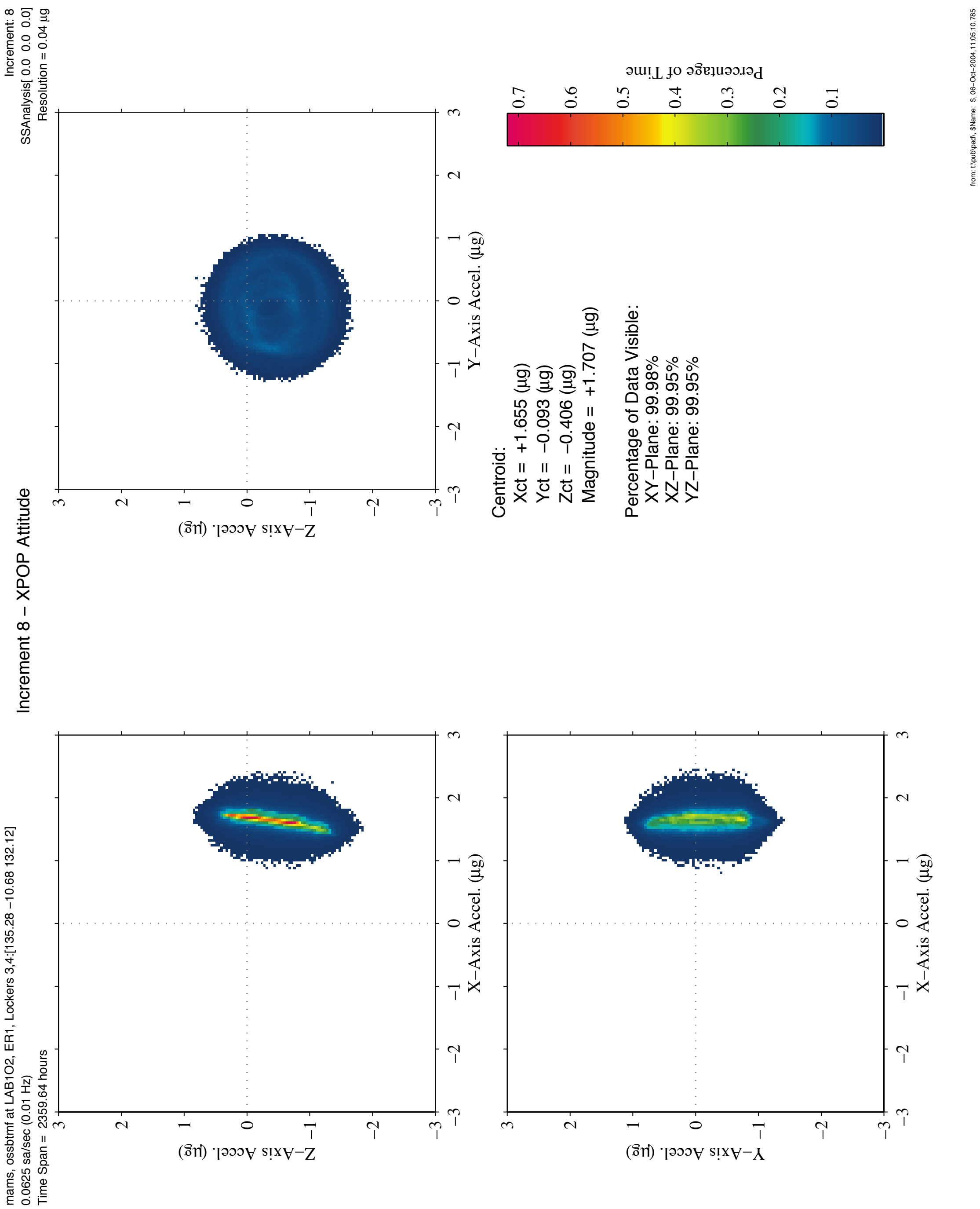

Figure 6-27 QTH Composite of XPOP Attitude for Increment 8 (OSSBTMF)

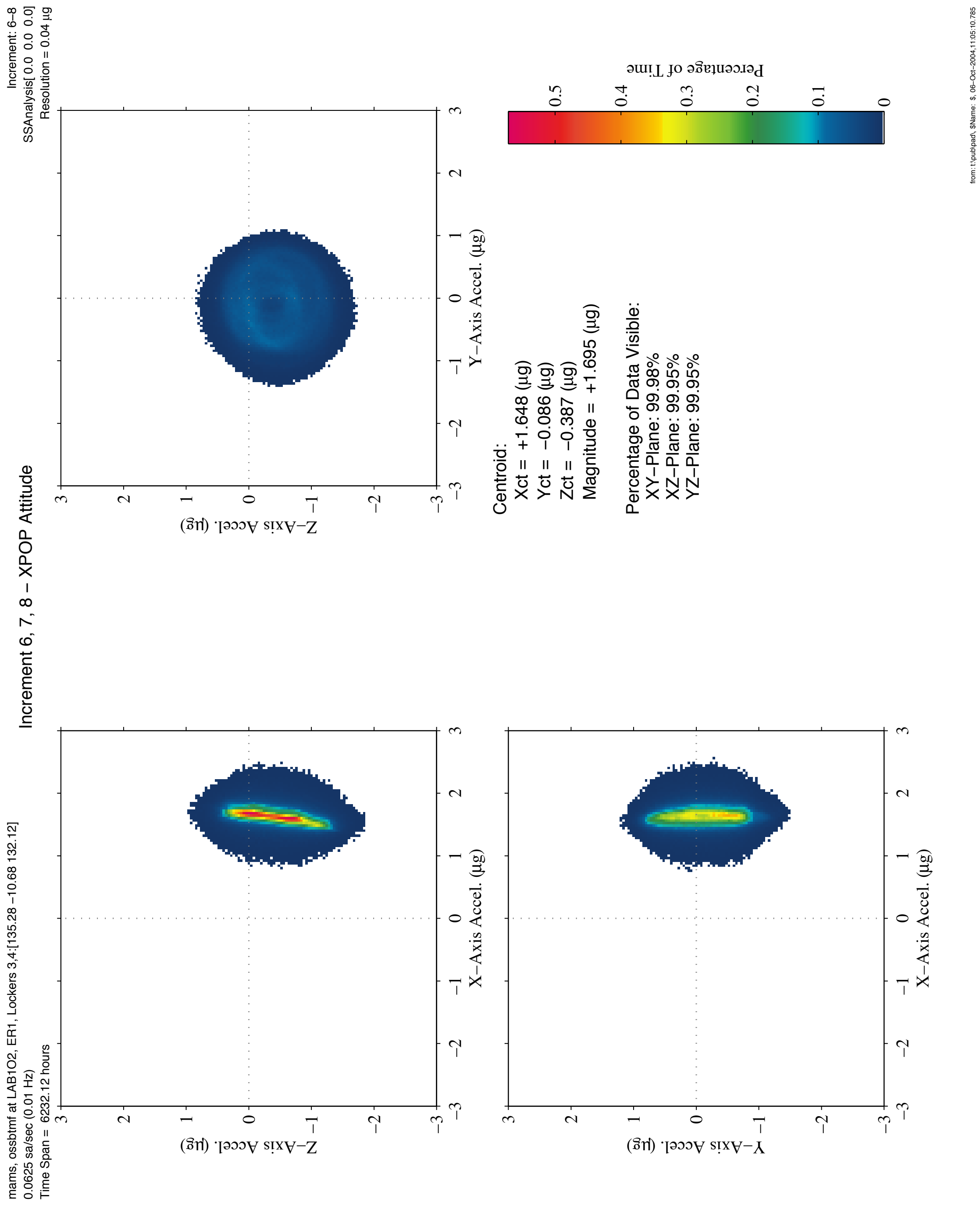

Figure 6-28 QTH Composite of XPOP Attitude for Increments 6-8 (OSSBTMF)

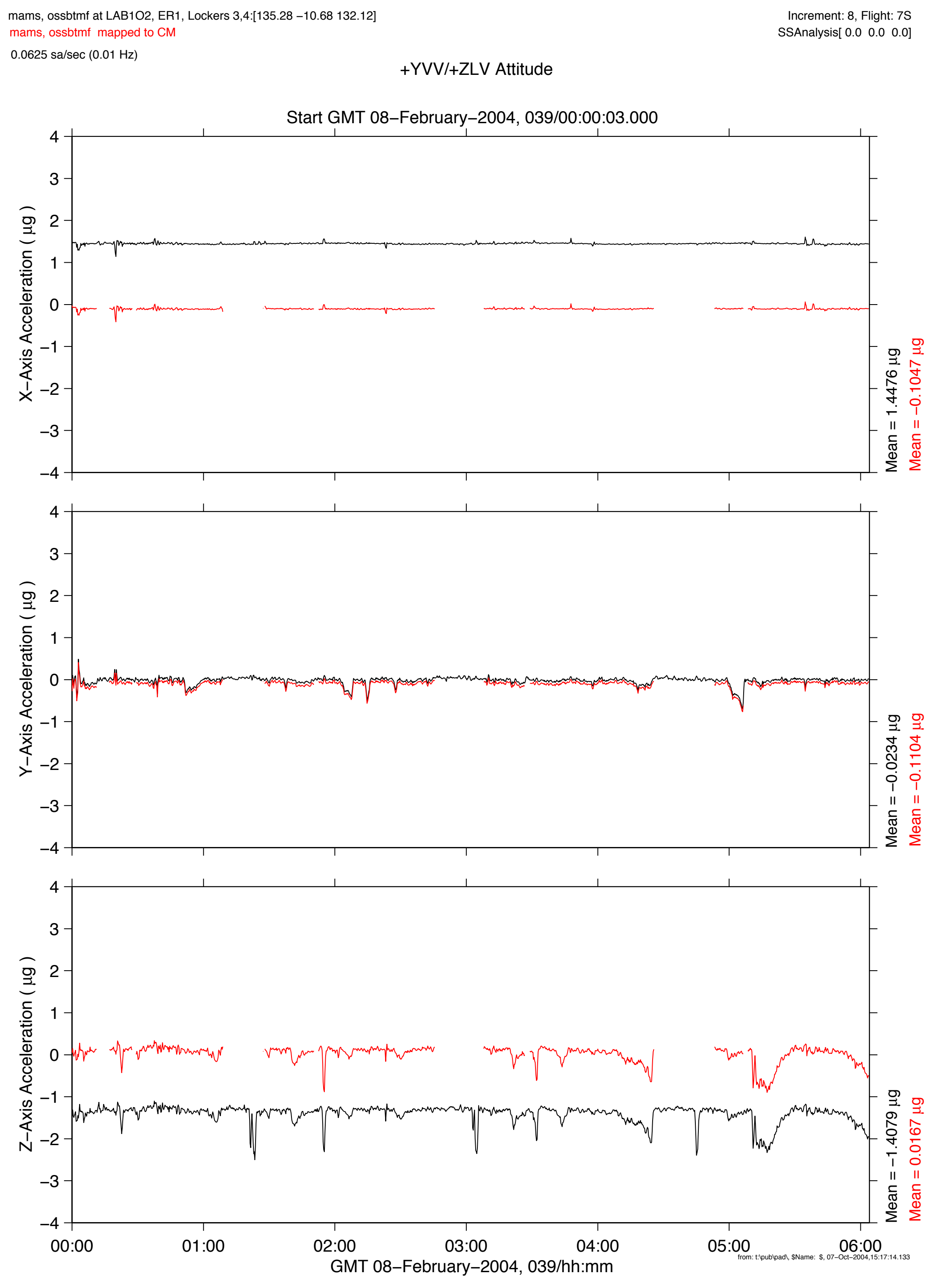

Figure 6-29 Time Series of +YVV/+ZLV Attitude (OSSBTMF)

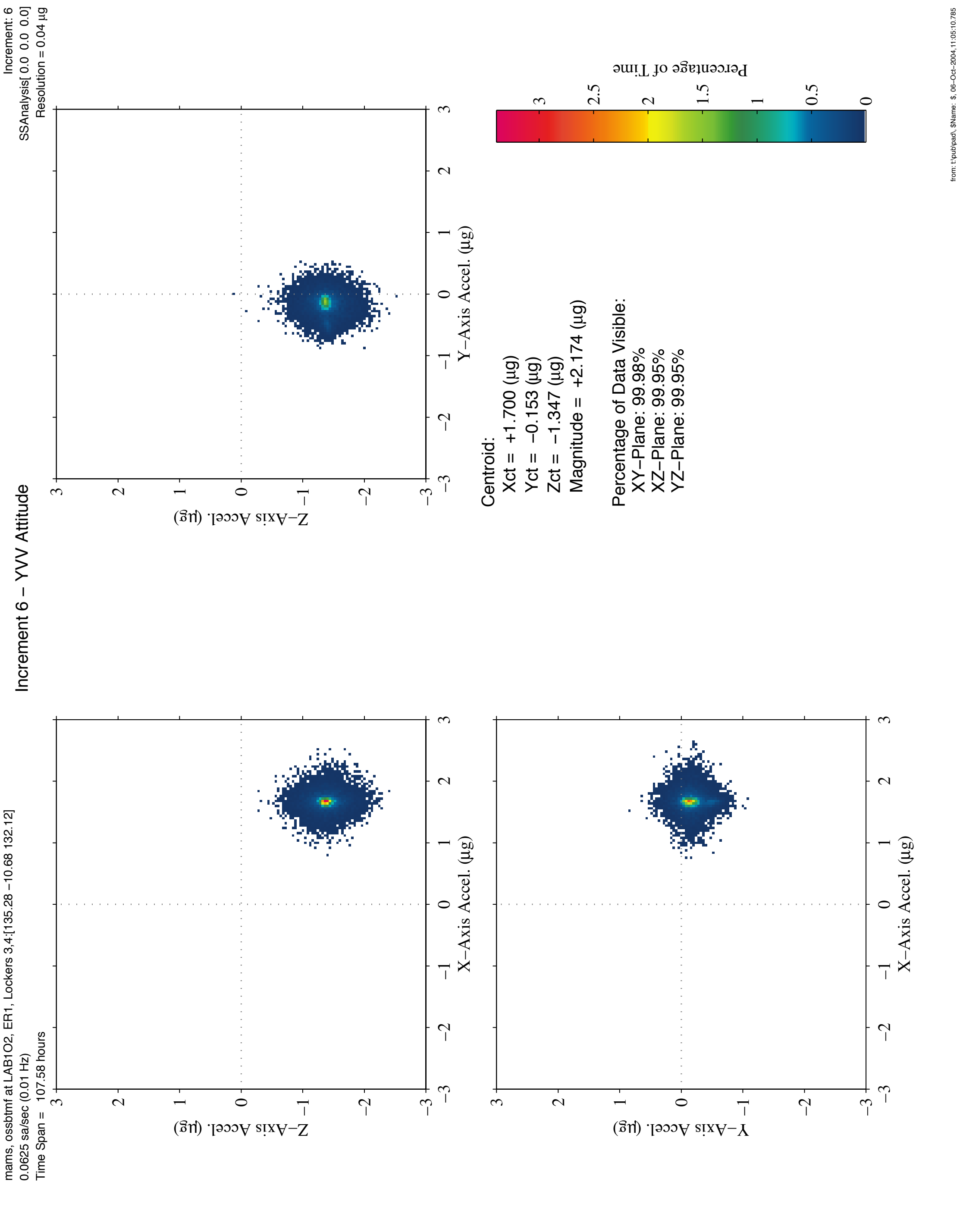

Figure 6-30 QTH Composite of YVV/ZLV Attitude for Increment 6 (OSSBTMF)

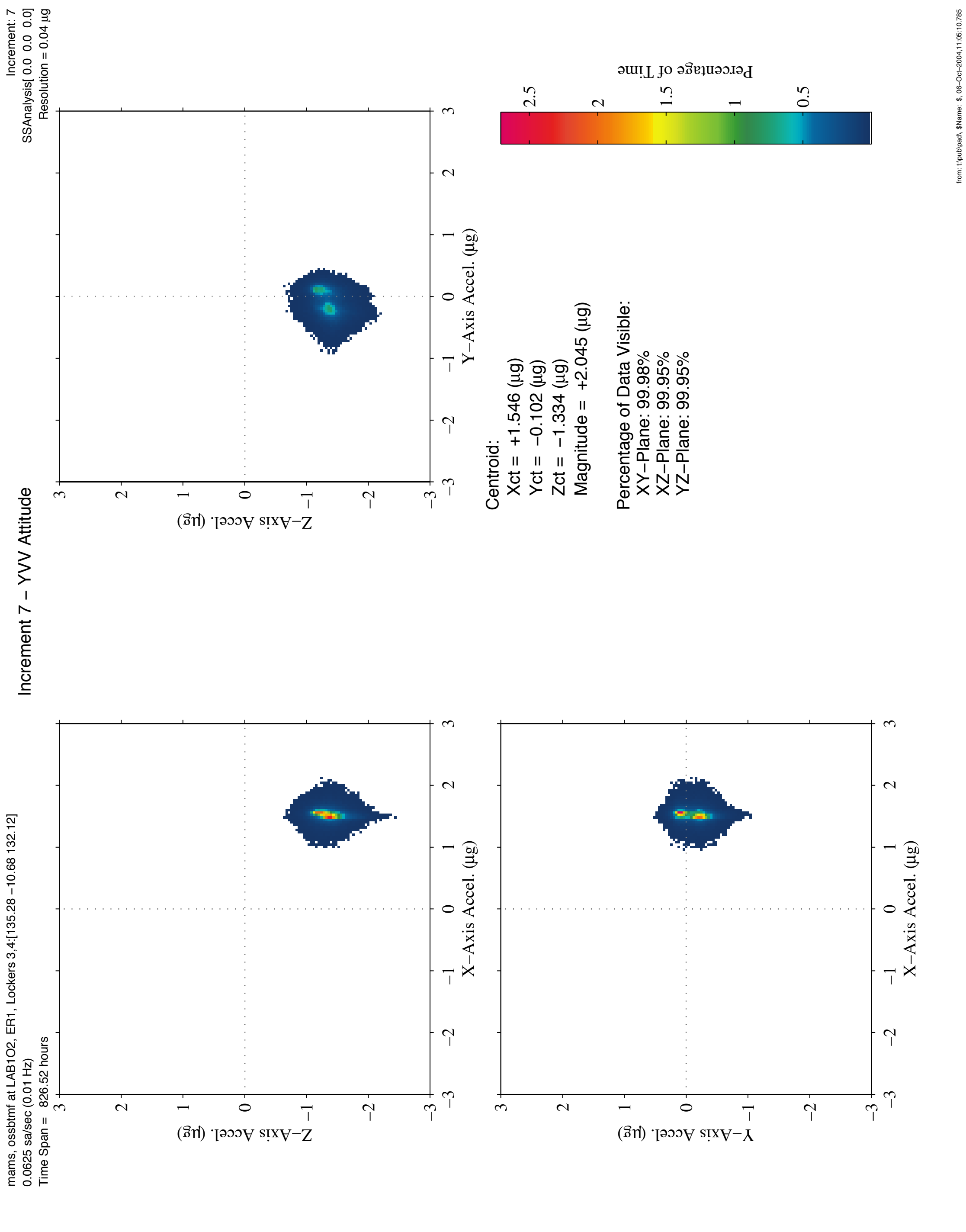

Figure 6-31 QTH Composite of YVV/ZLV Attitude for Increment 7 (OSSBTMF)

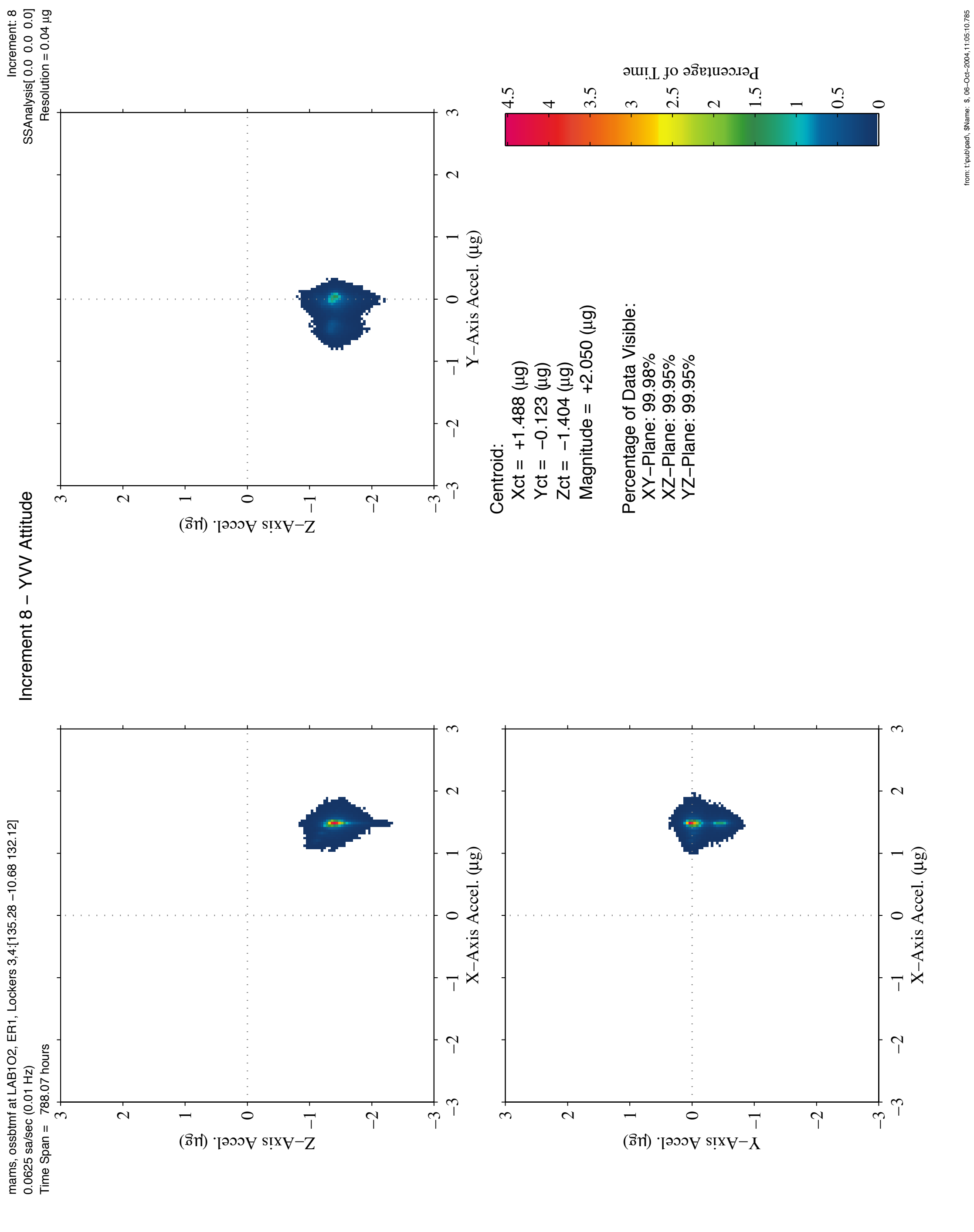

Figure 6-32 QTH Composite of YVV/ZLV Attitude for Increment 8 (OSSBTMF)

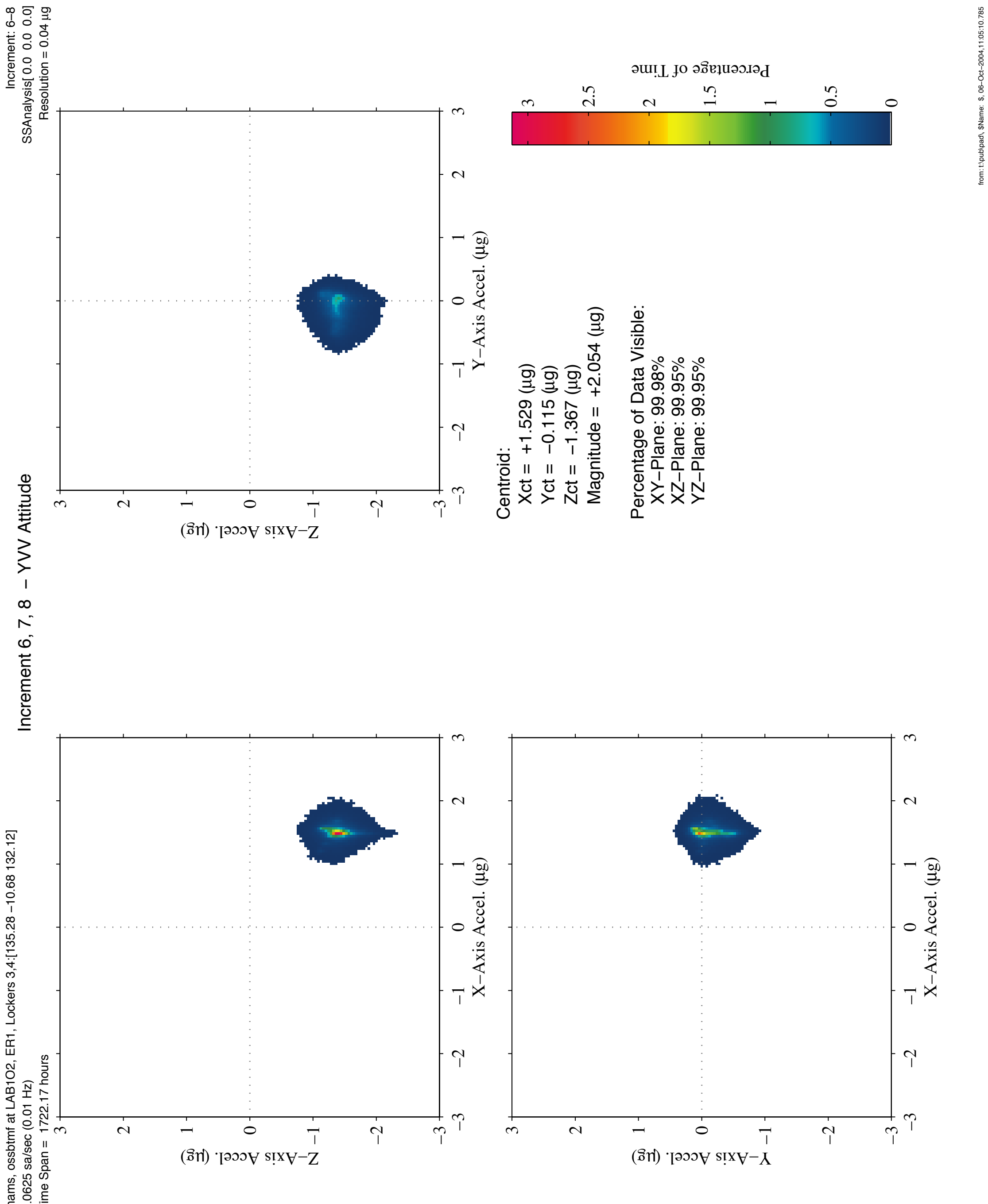

Figure 6-33 QTH Composite of YVV/ZLV Attitude for Increments 6-8 (OSSBTMF)

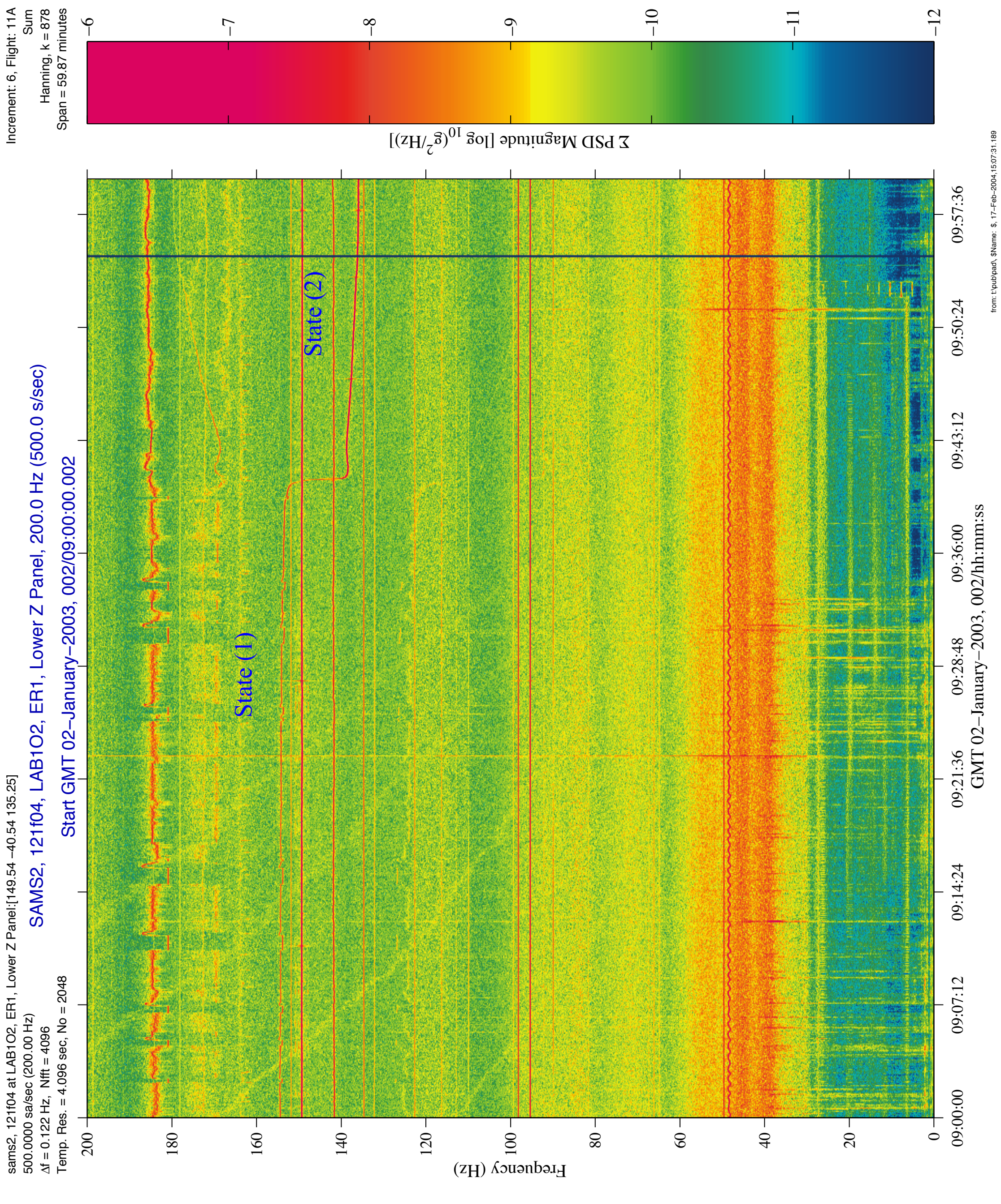

Figure 6-34 Spectrogram of Unknown Signal, States 1 and 2 (121F04)

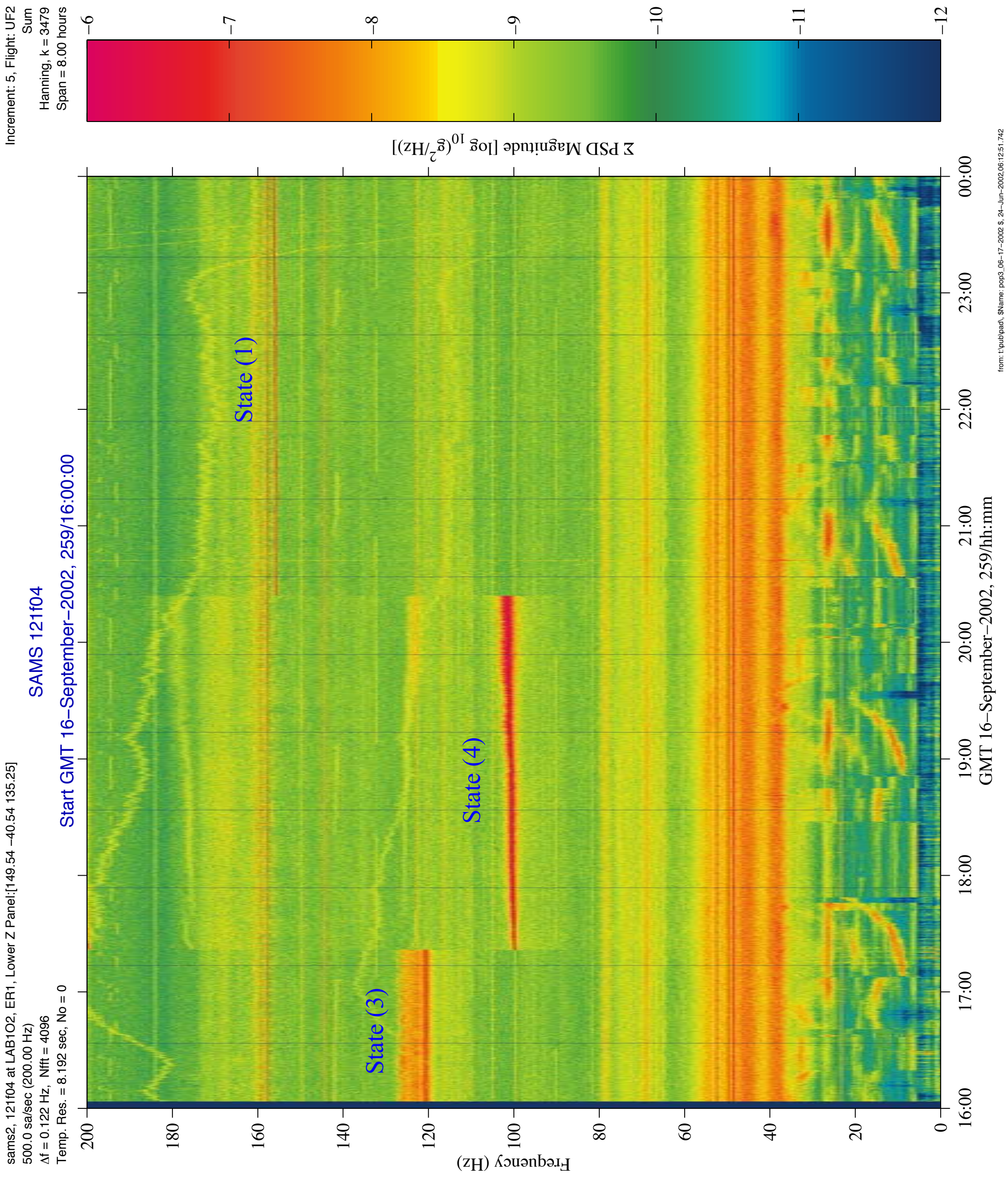

Figure 6-35 Spectrogram of Unknown Signal, States 3 and 4 (121F04)

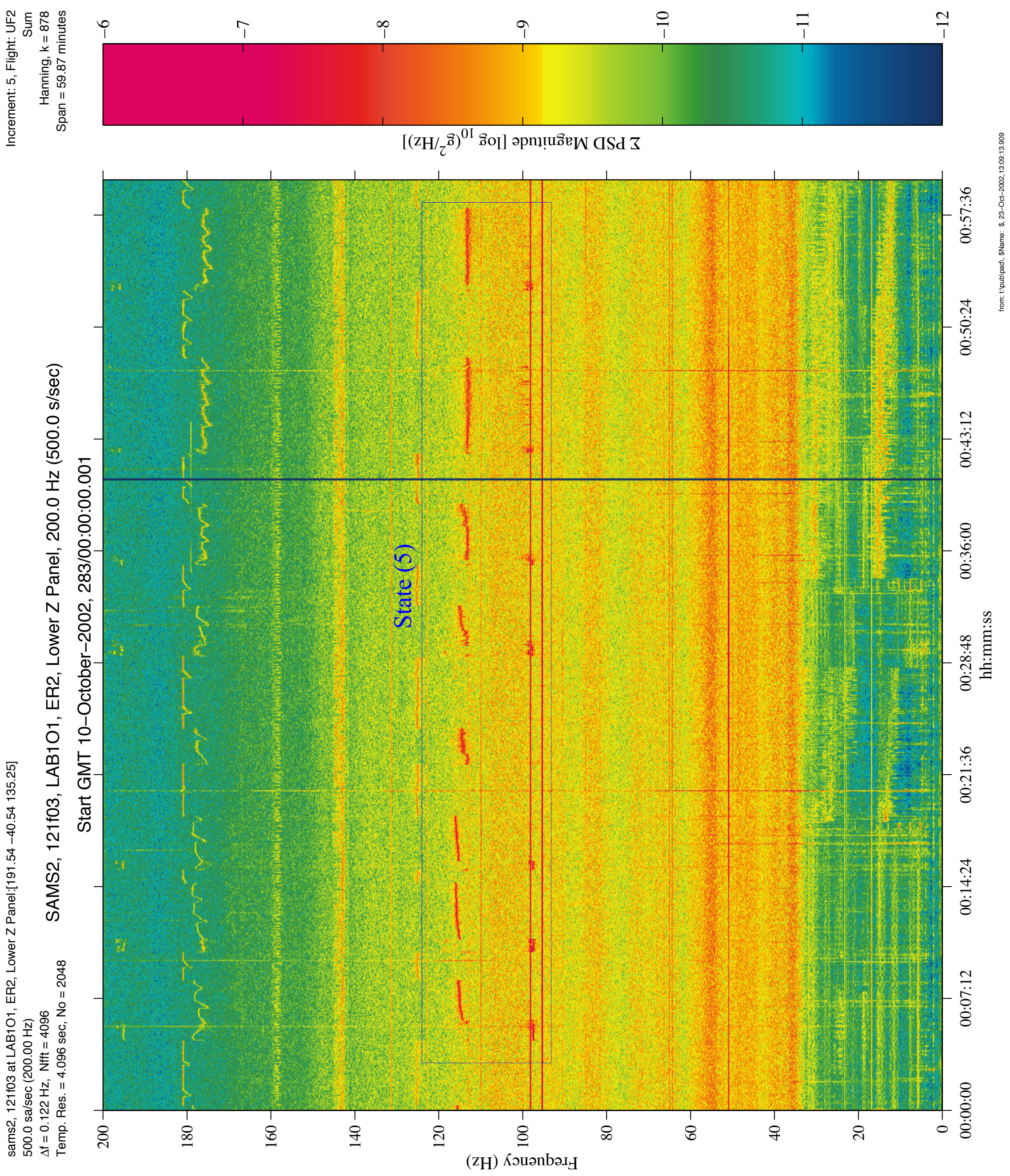

Figure 6-36 Spectrogram of Unknown Signal, State 5 (121F04)

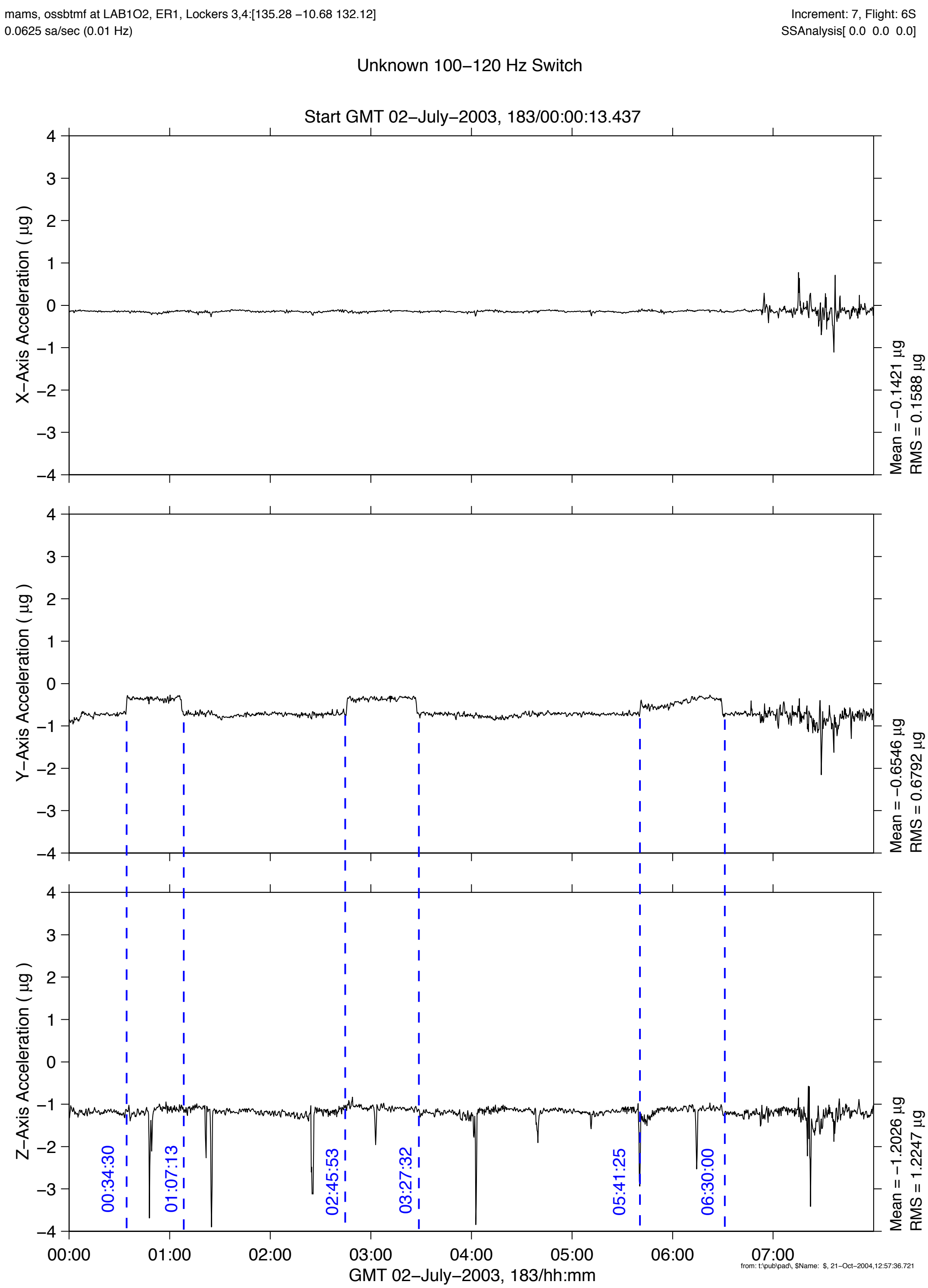

Figure 6-37 Time series of Unknown Signal Switch (OSSBTMF)

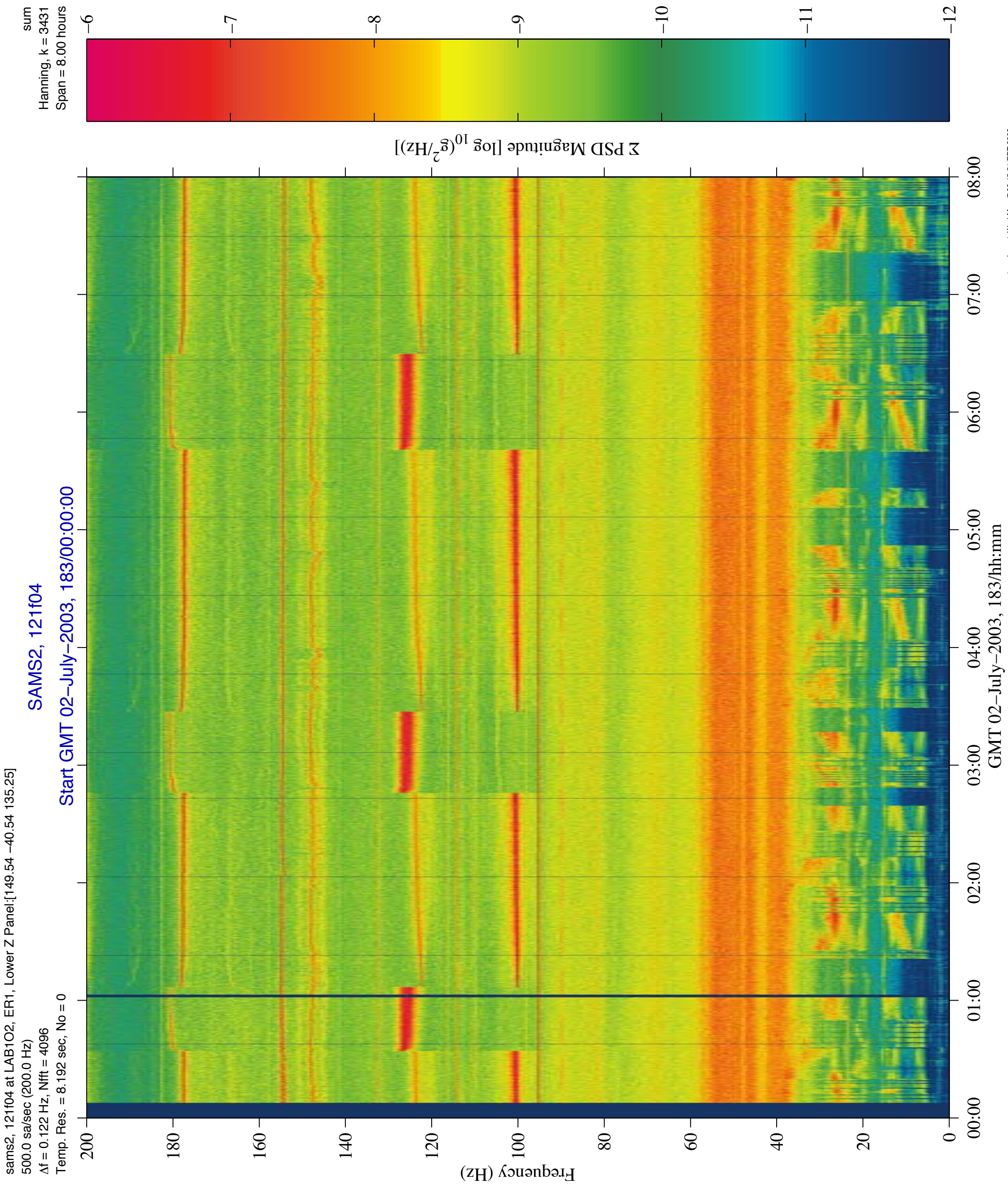

Figure 6-38 Spectrogram of Unknown Signal Switch (121F04)

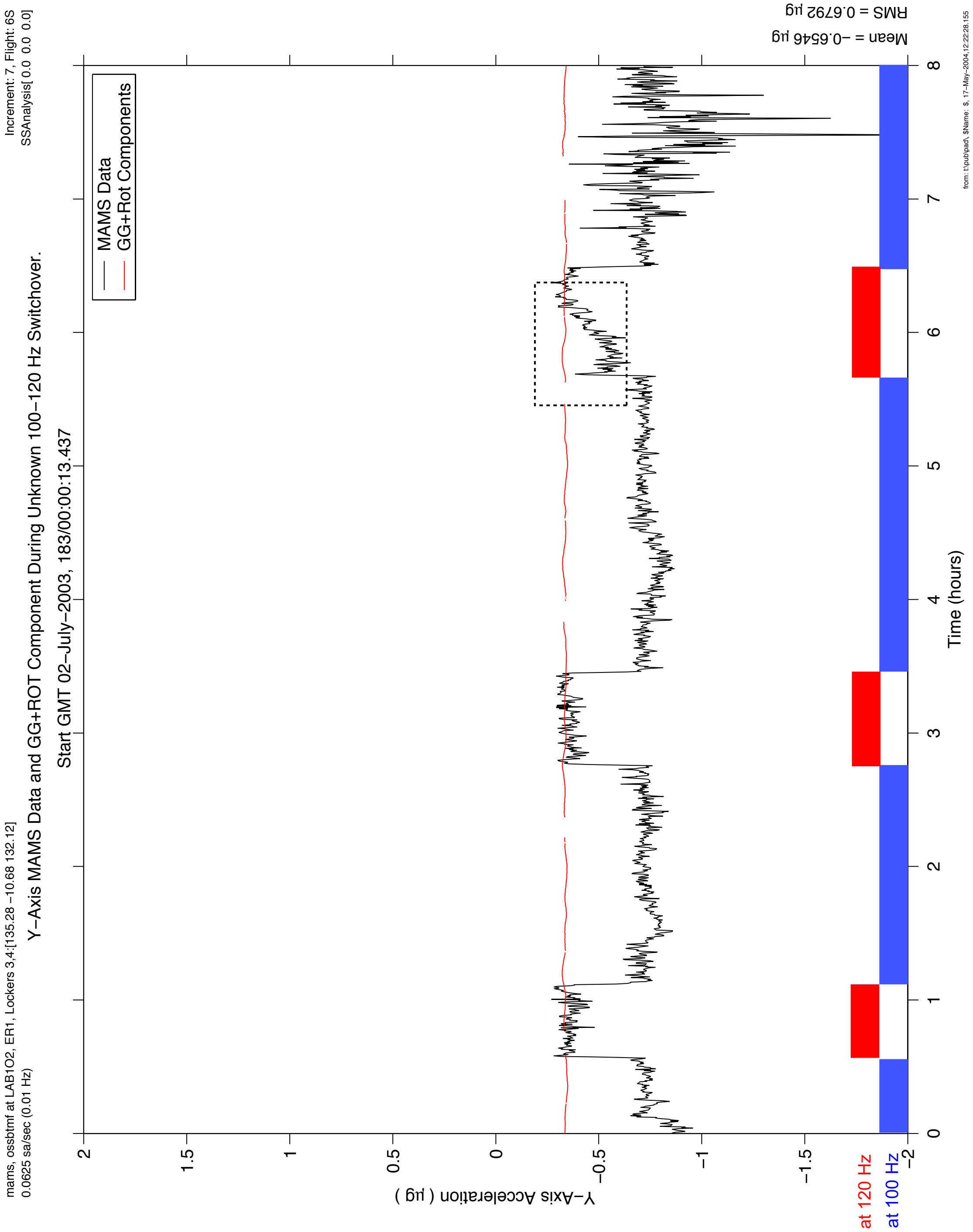

Figure 6-39 Time Series of Y_A-axis Overlaid with Calculated Components (OSSBTMF)

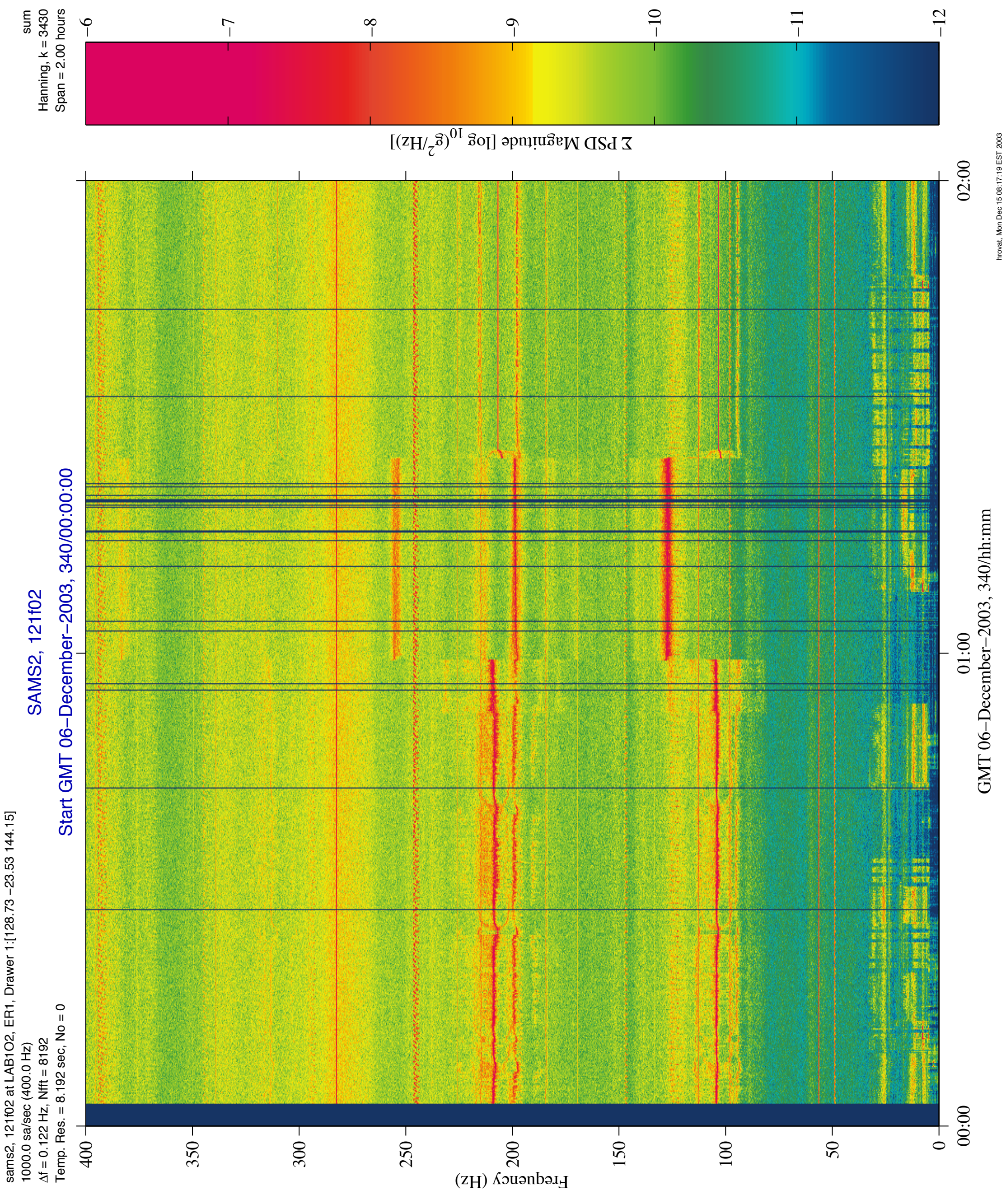

Figure 6-40 Spectrogram of Unknown Signal Switch on GMT 340 (121F02)

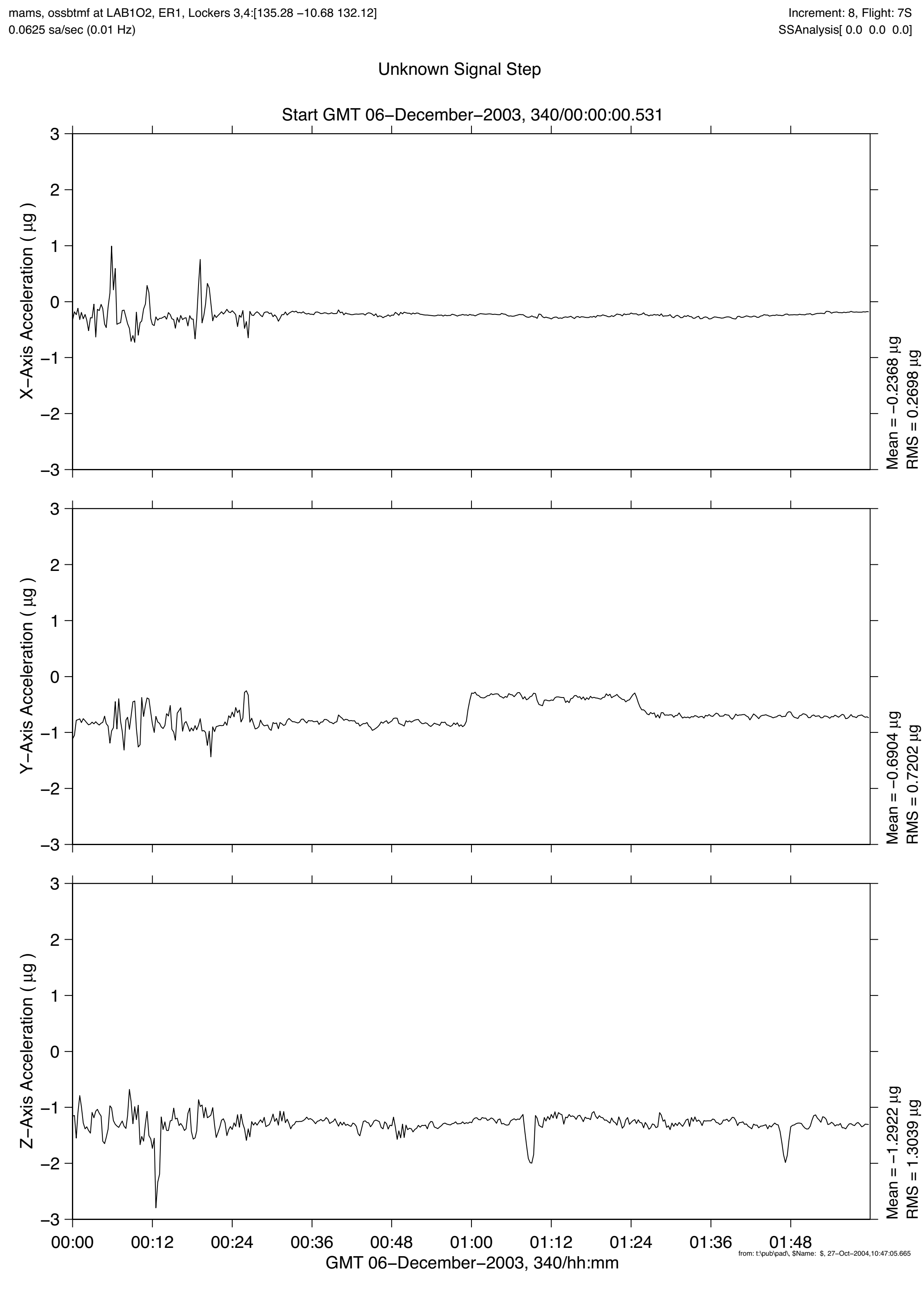

Figure 6-41 Time Series of Unknown Signal Switch on GMT 340 (OSSBTMF)

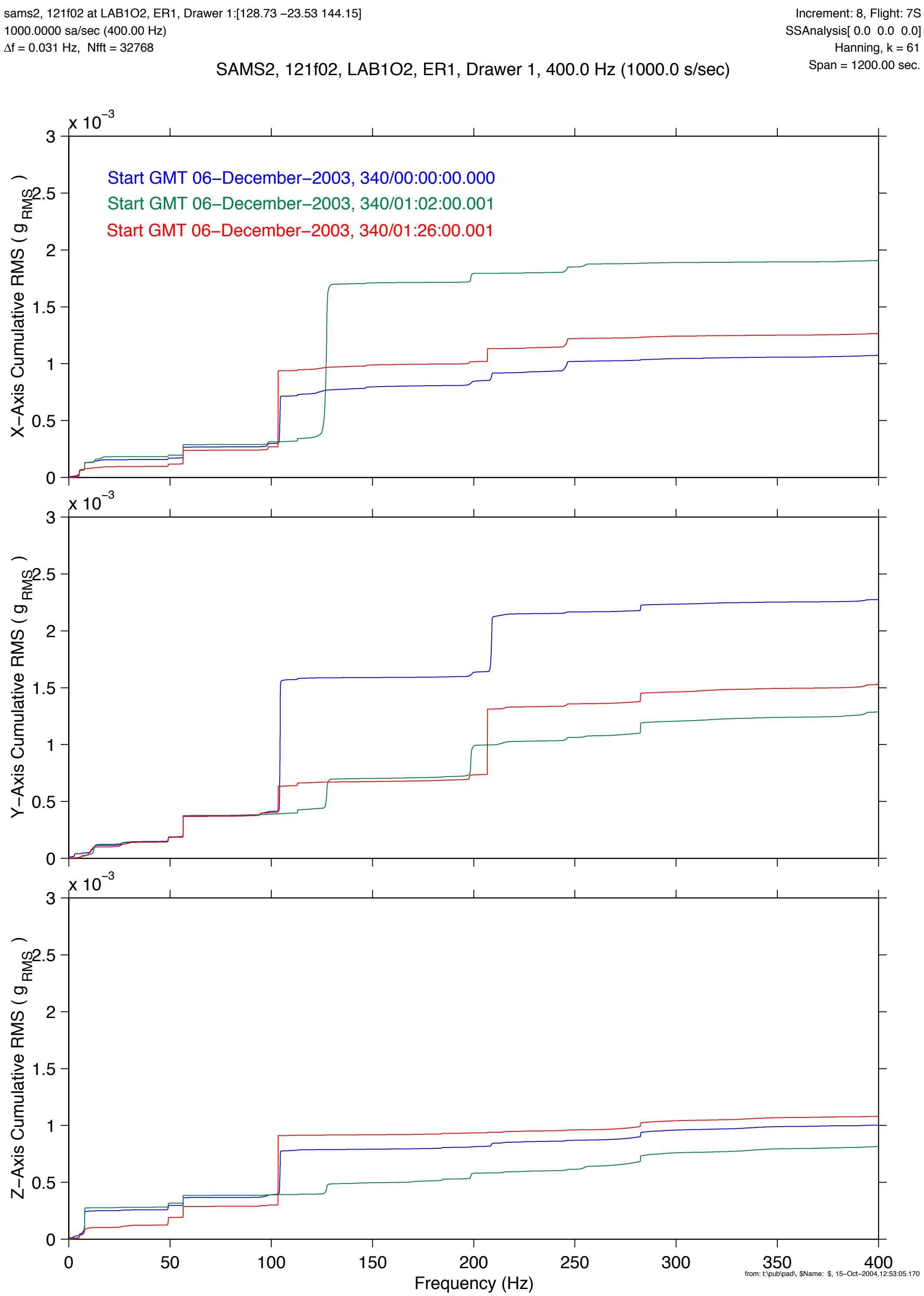

Figure 6-42 Cumulative RMS (XYZ) Composite for GMT 340 (121F02)

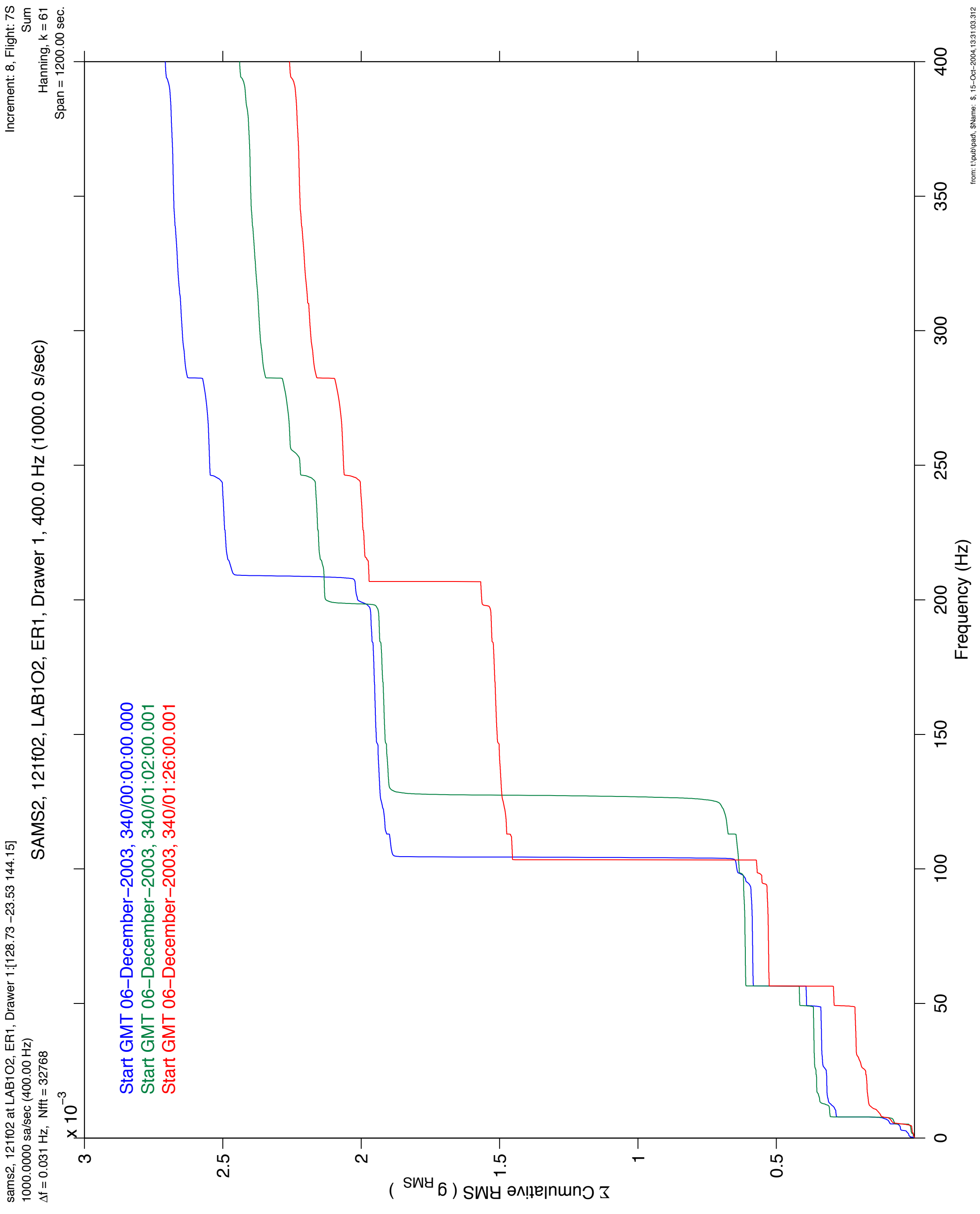

Figure 6-43 Cumulative RMS (SUM) Composite for GMT 340 (121F02)

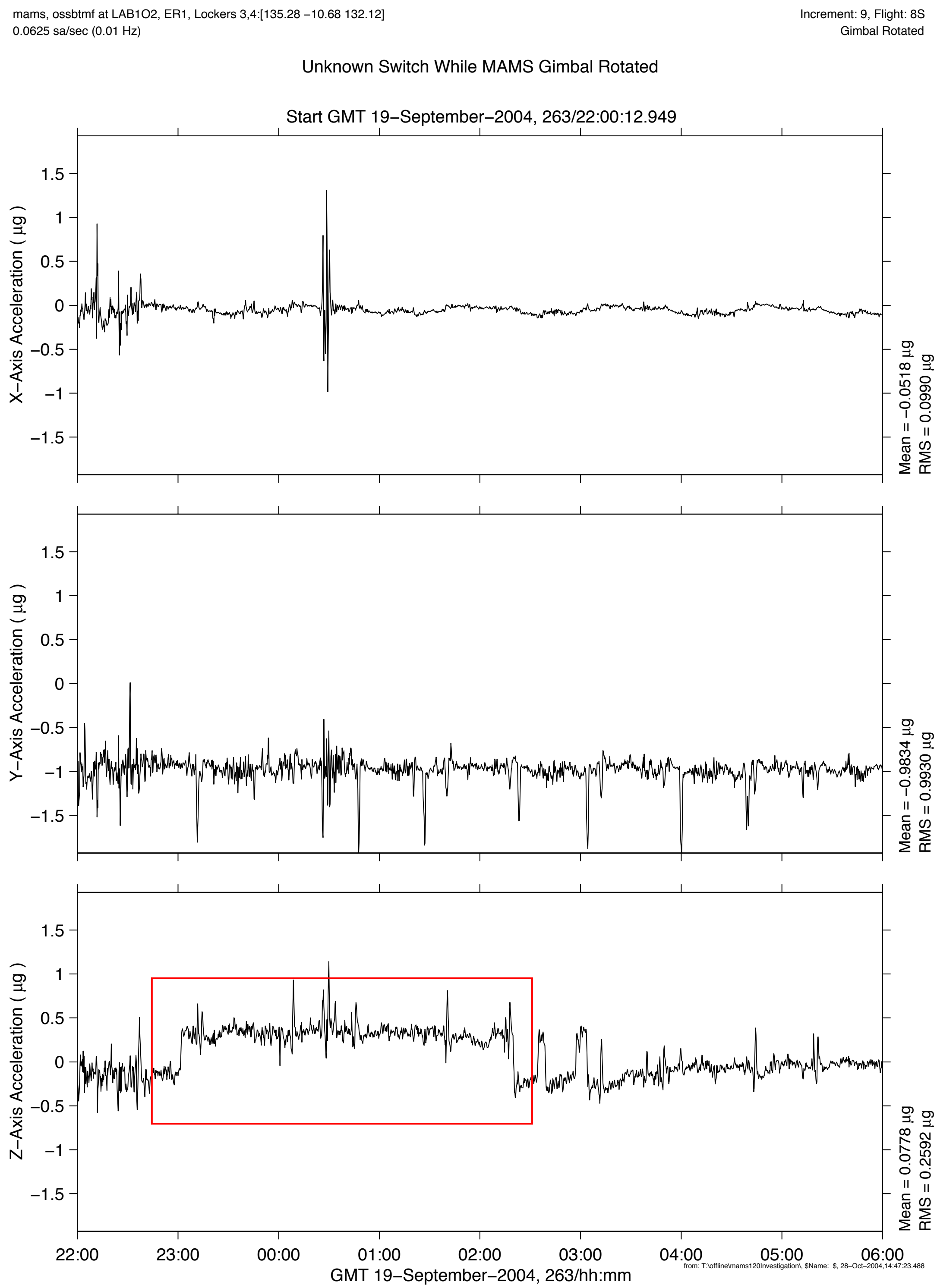

Figure 6-44 Time Series of Unknown Signal Switch on GMT 263 (OSSBTMF)

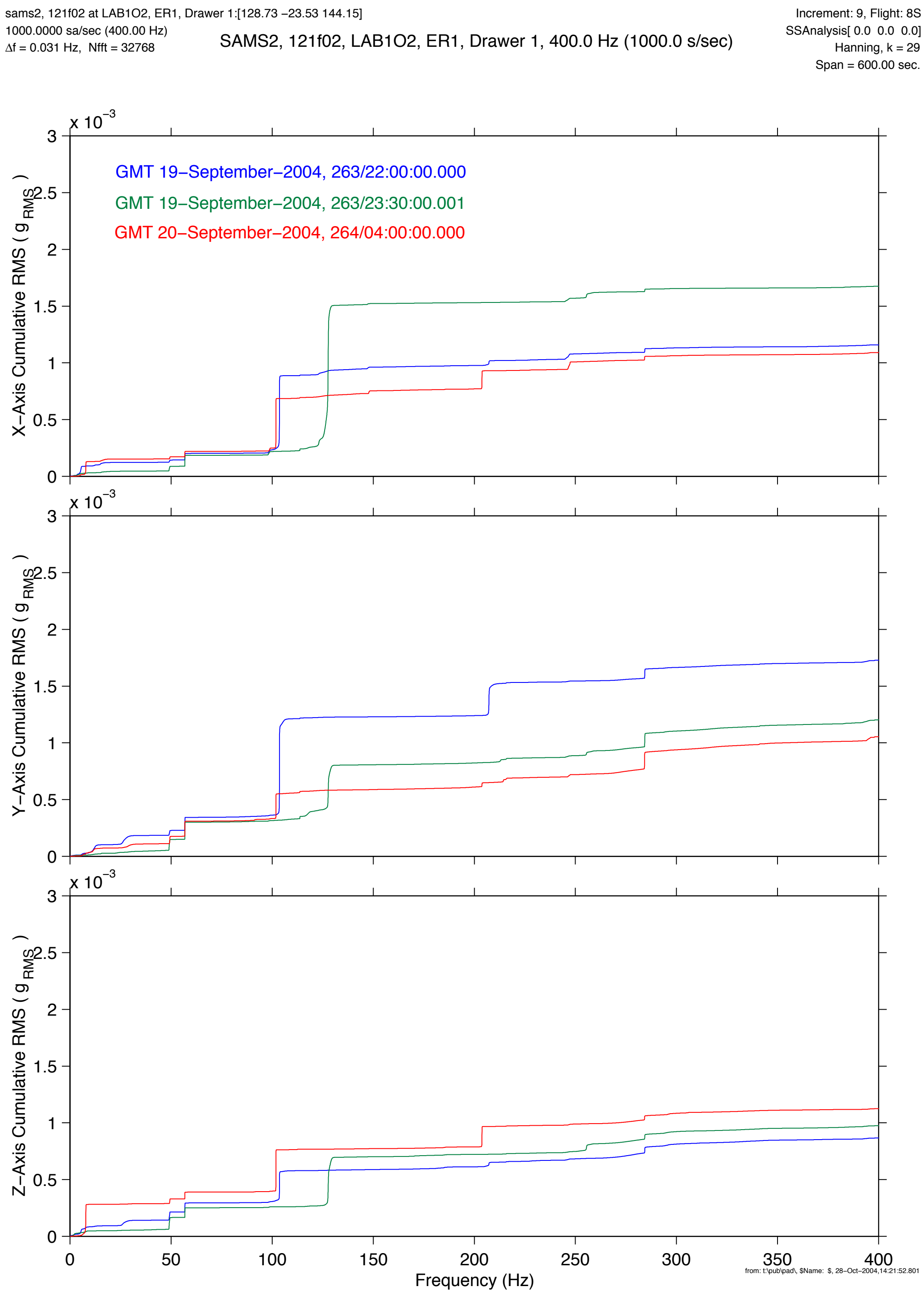

Figure 6-45 Cumulative RMS (XYZ) Composite for GMT 263 (121F02)

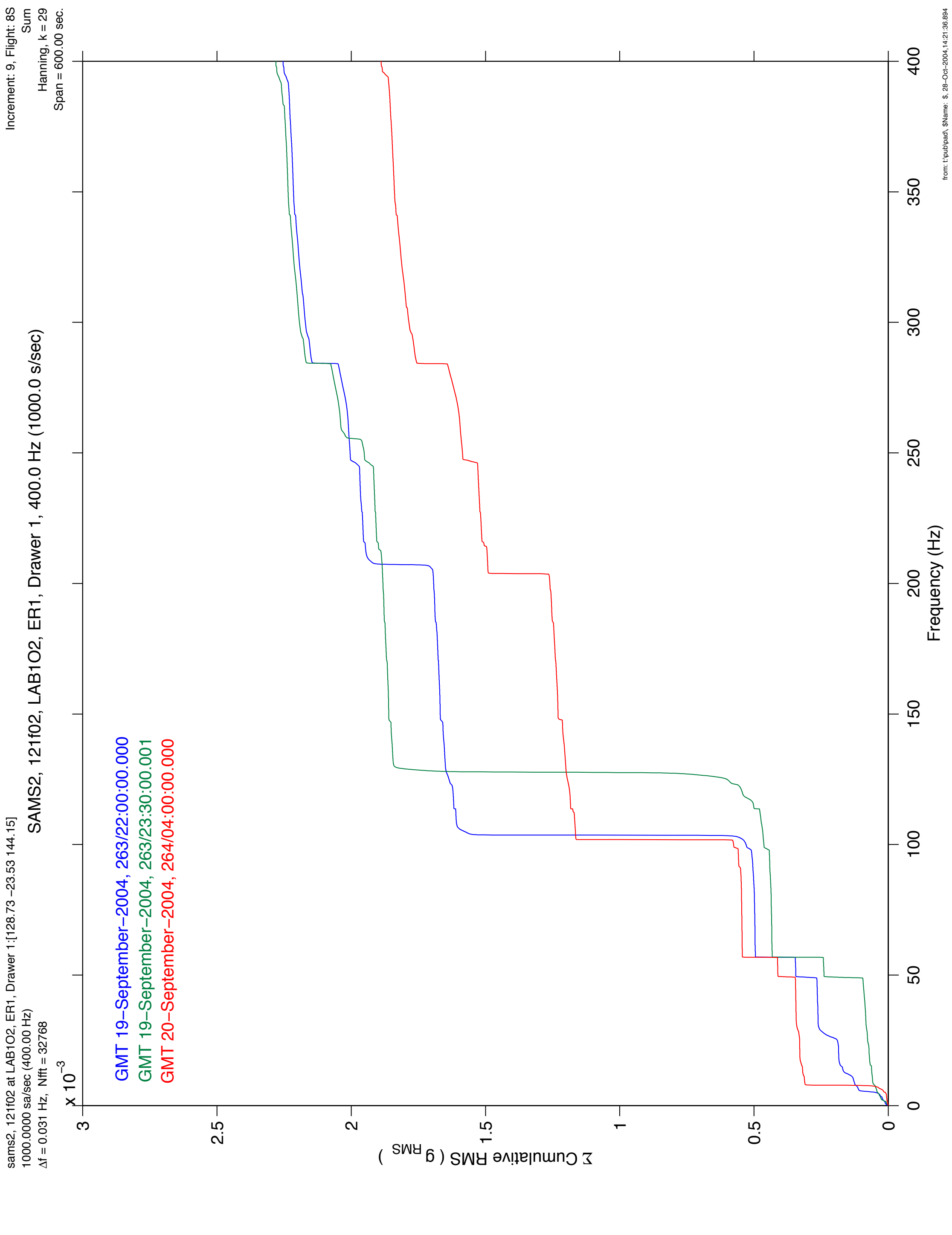

Figure 6-46 Cumulative RMS (SUM) Composite for GMT 263 (121F02)

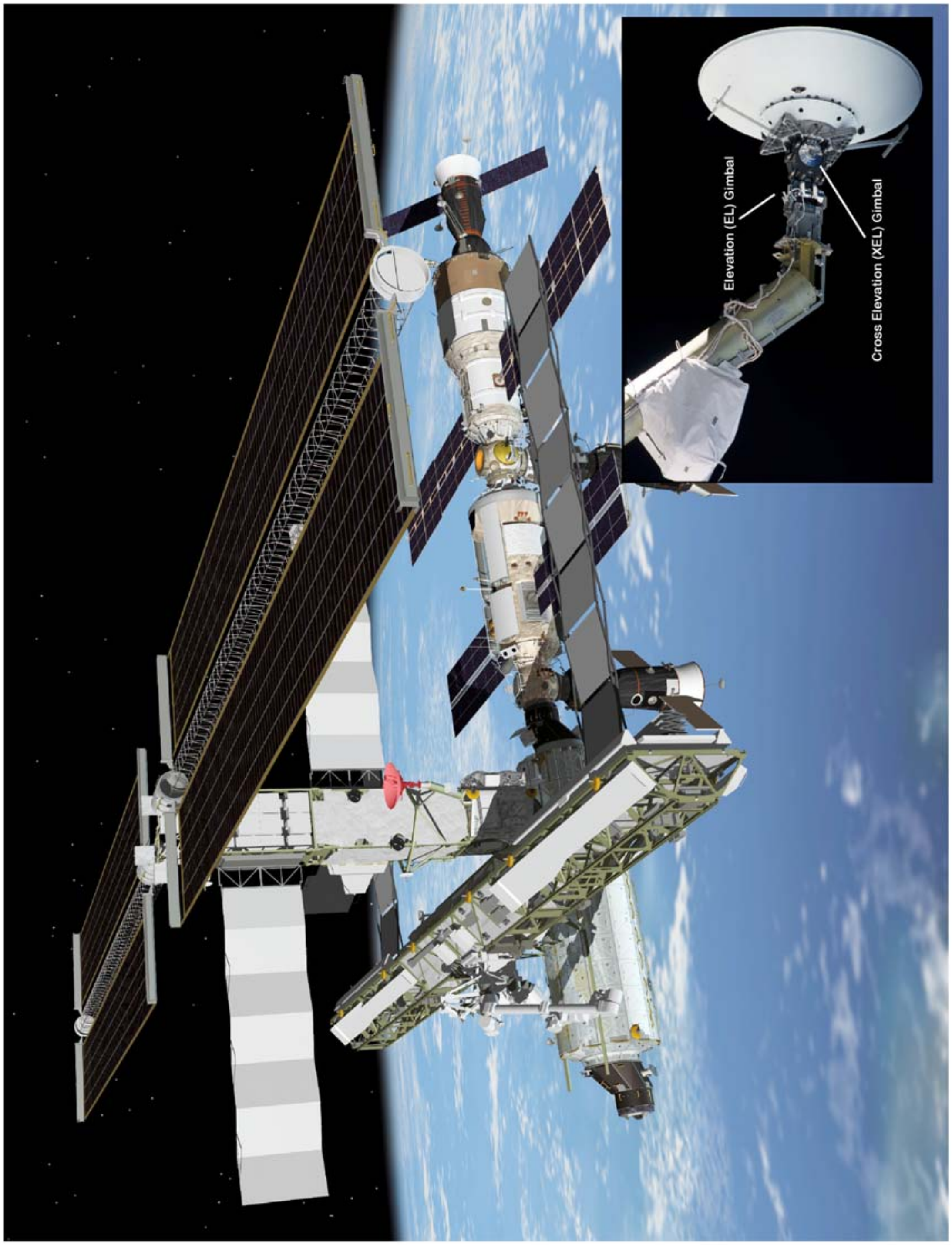

Figure 6-47 Ku-Band Antenna

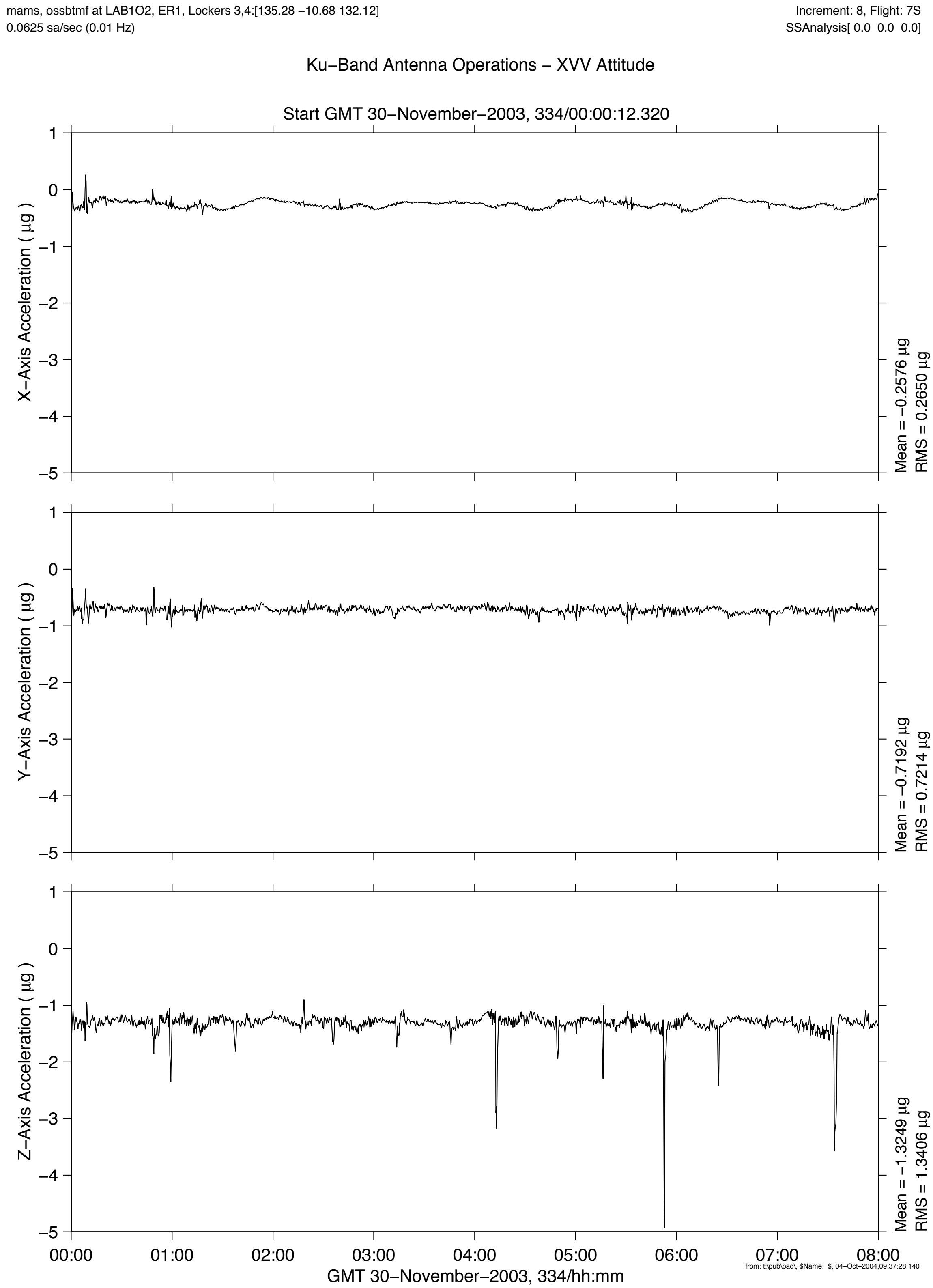

Figure 6-48 Time Series of Ku-Band Operations (OSSBTMF)

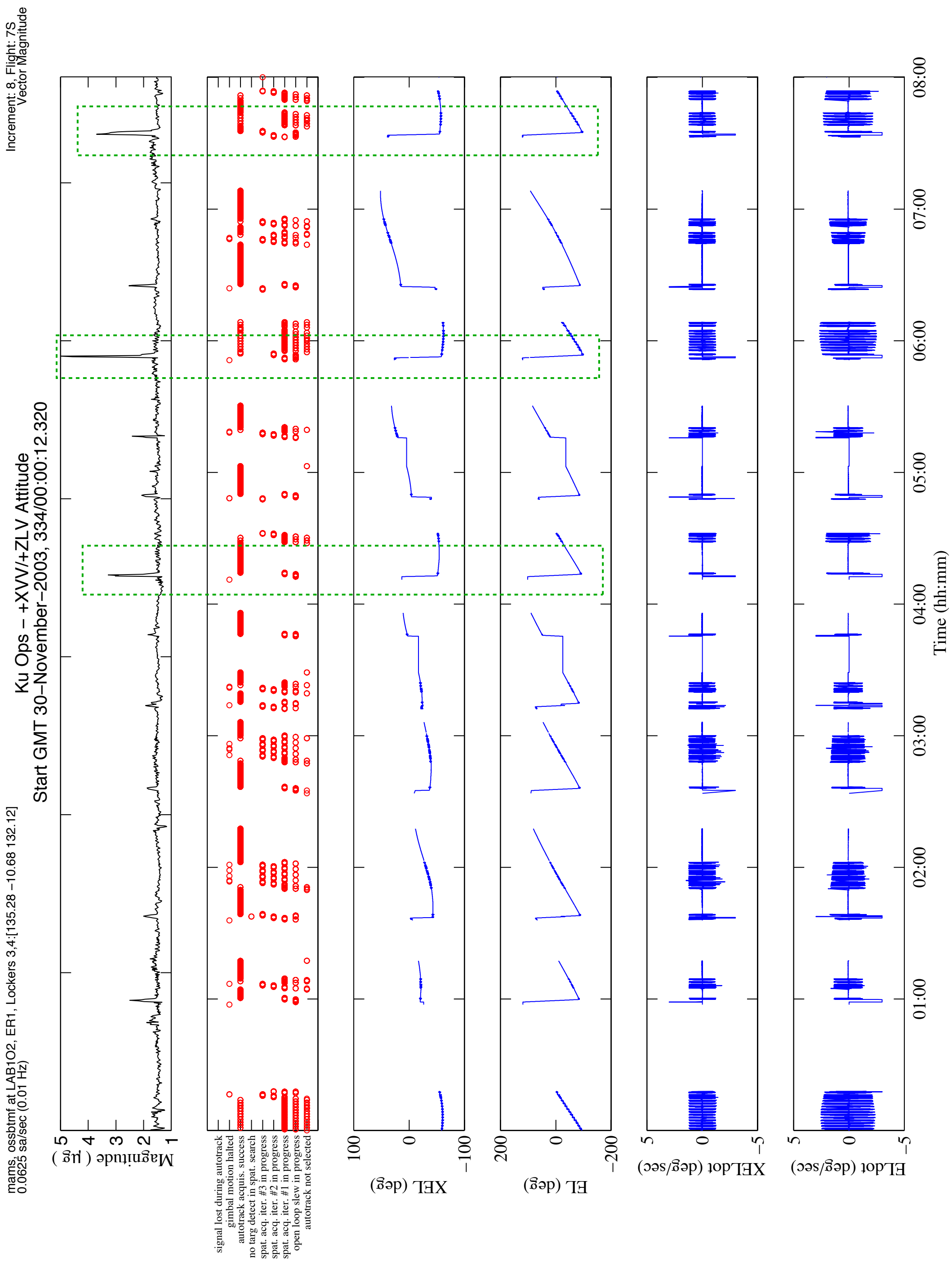

Figure 6-49 Vector Magnitude Correlation Composite of Ku-Band Open Slew (OSSBTMF)

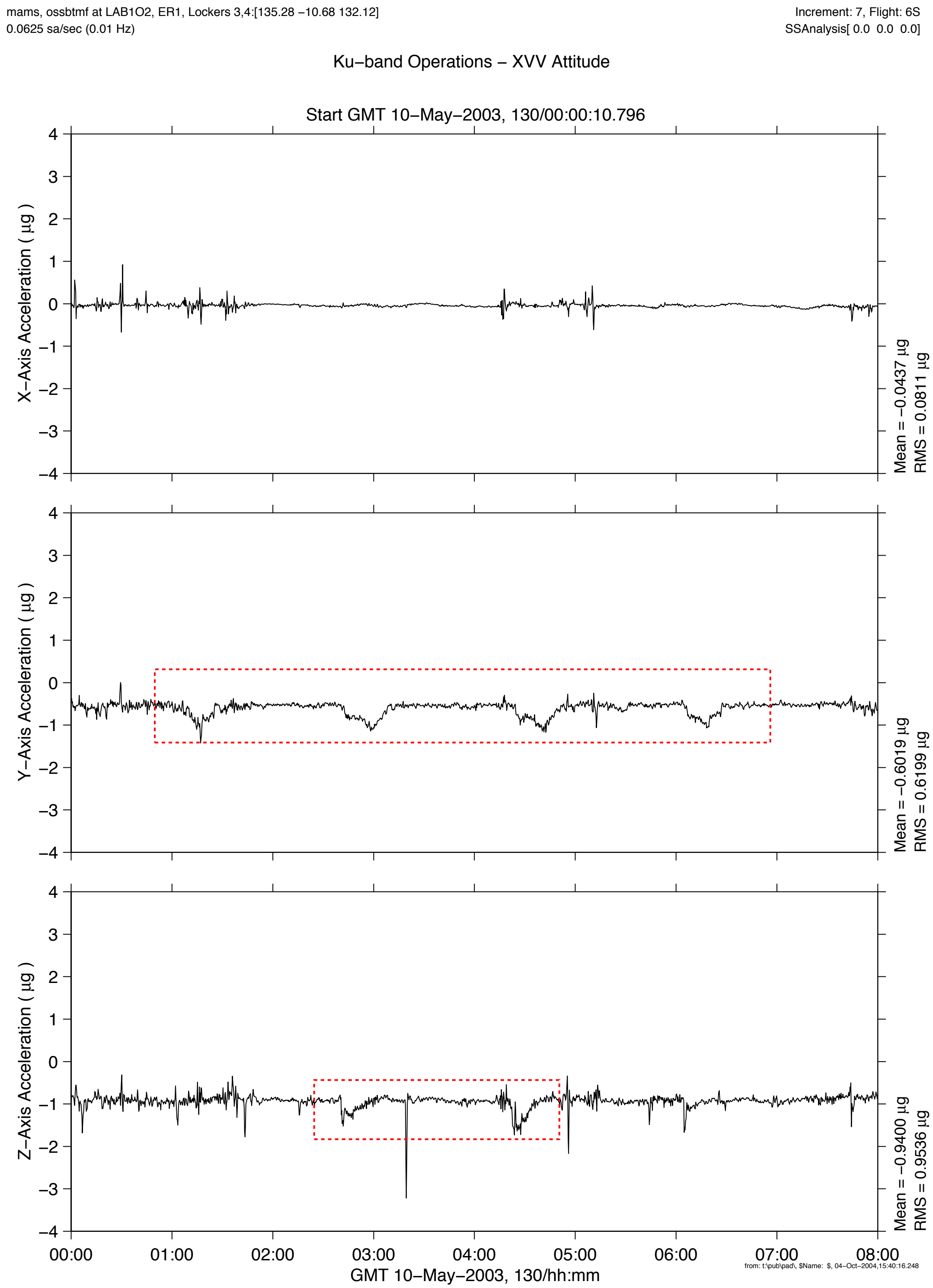

Figure 6-50 Time Series of Ku-Band Auto-Track during XVV Attitude (OSSBTMF)

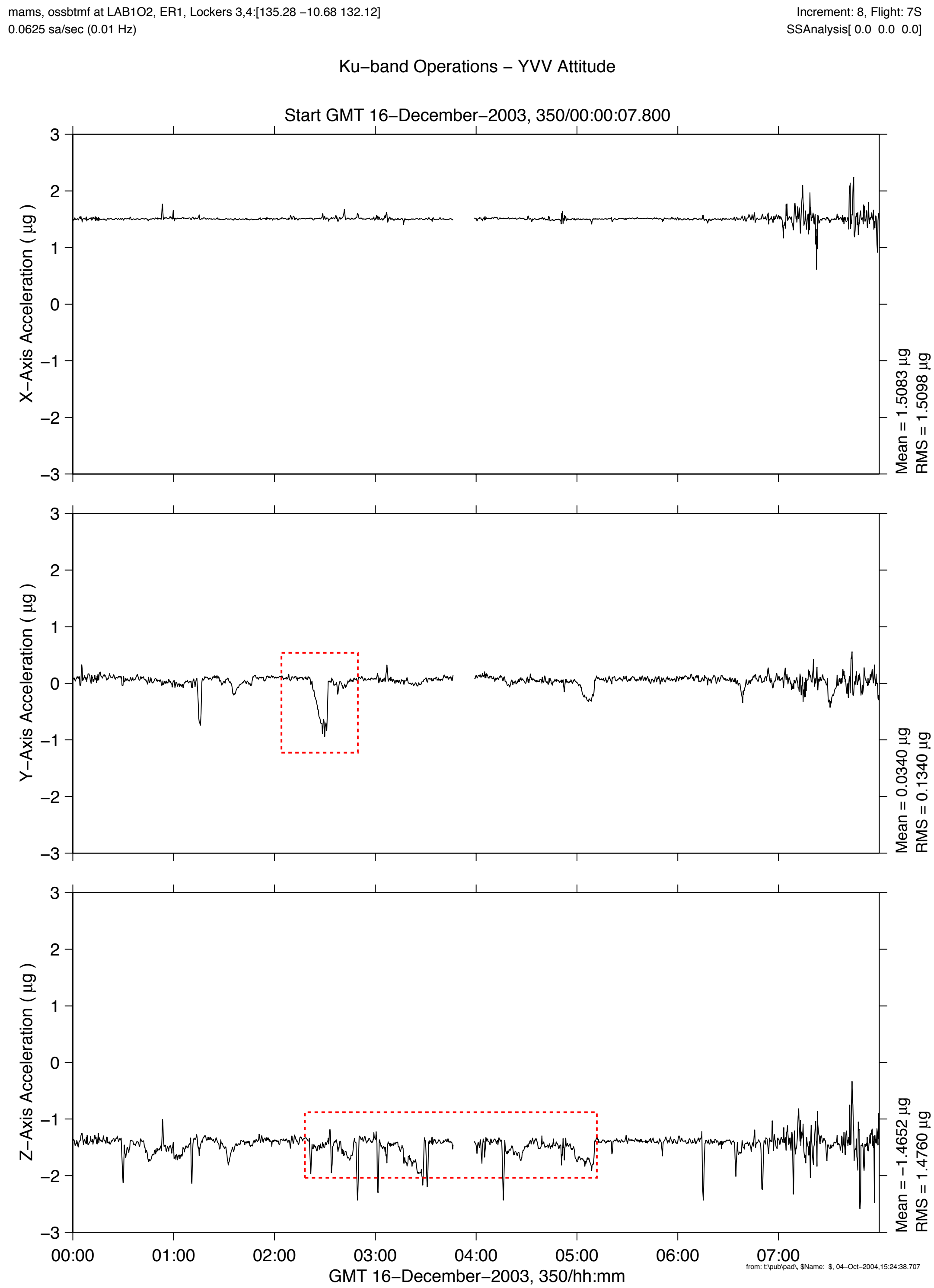

Figure 6-51 Time Series of Ku-Band Auto-Track during YVV Attitude (OSSBTMF)

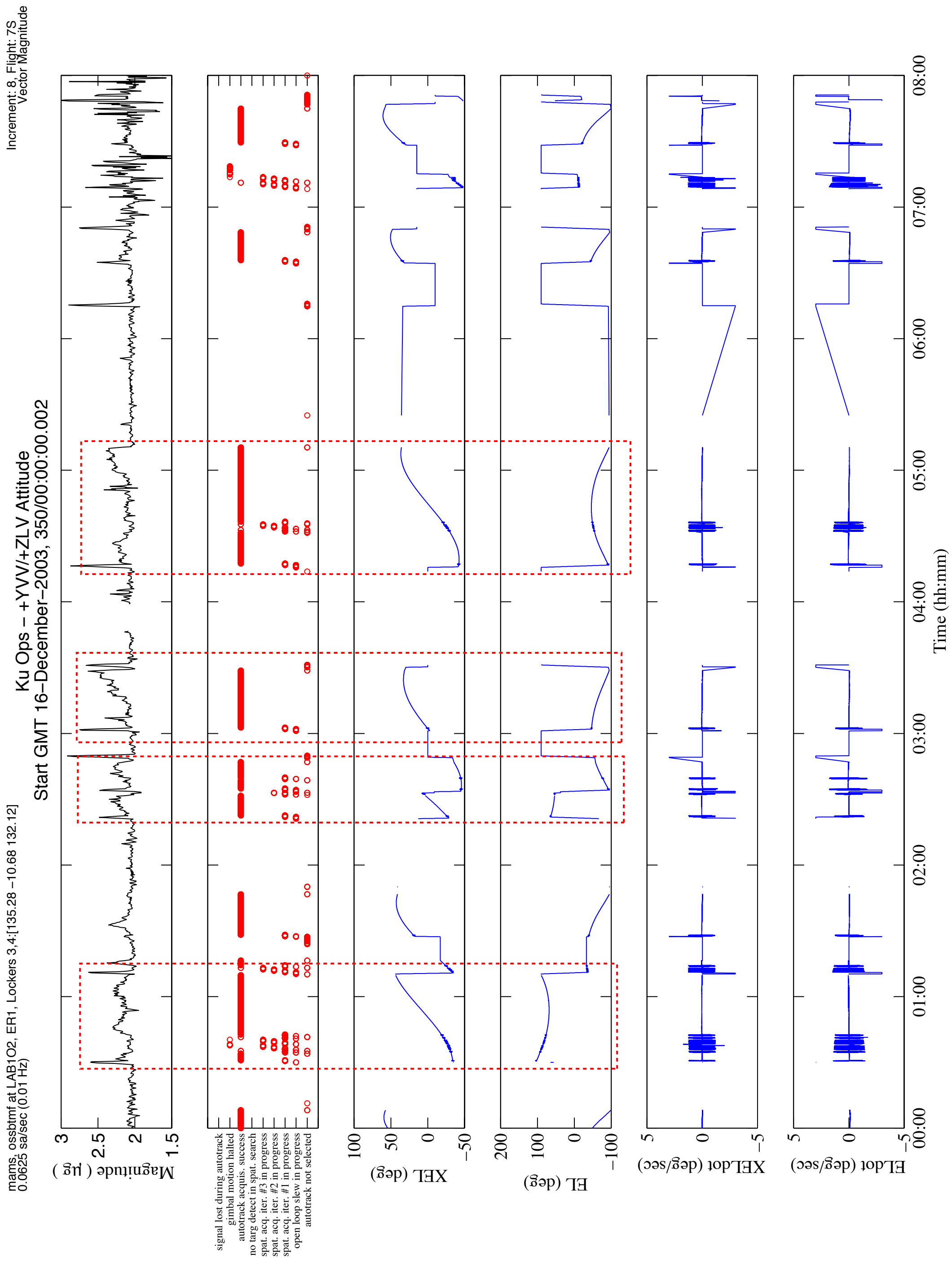

Figure 6-52 Vector Magnitude Correlation Composite of Ku-Band Auto-Track (OSSBTMF)

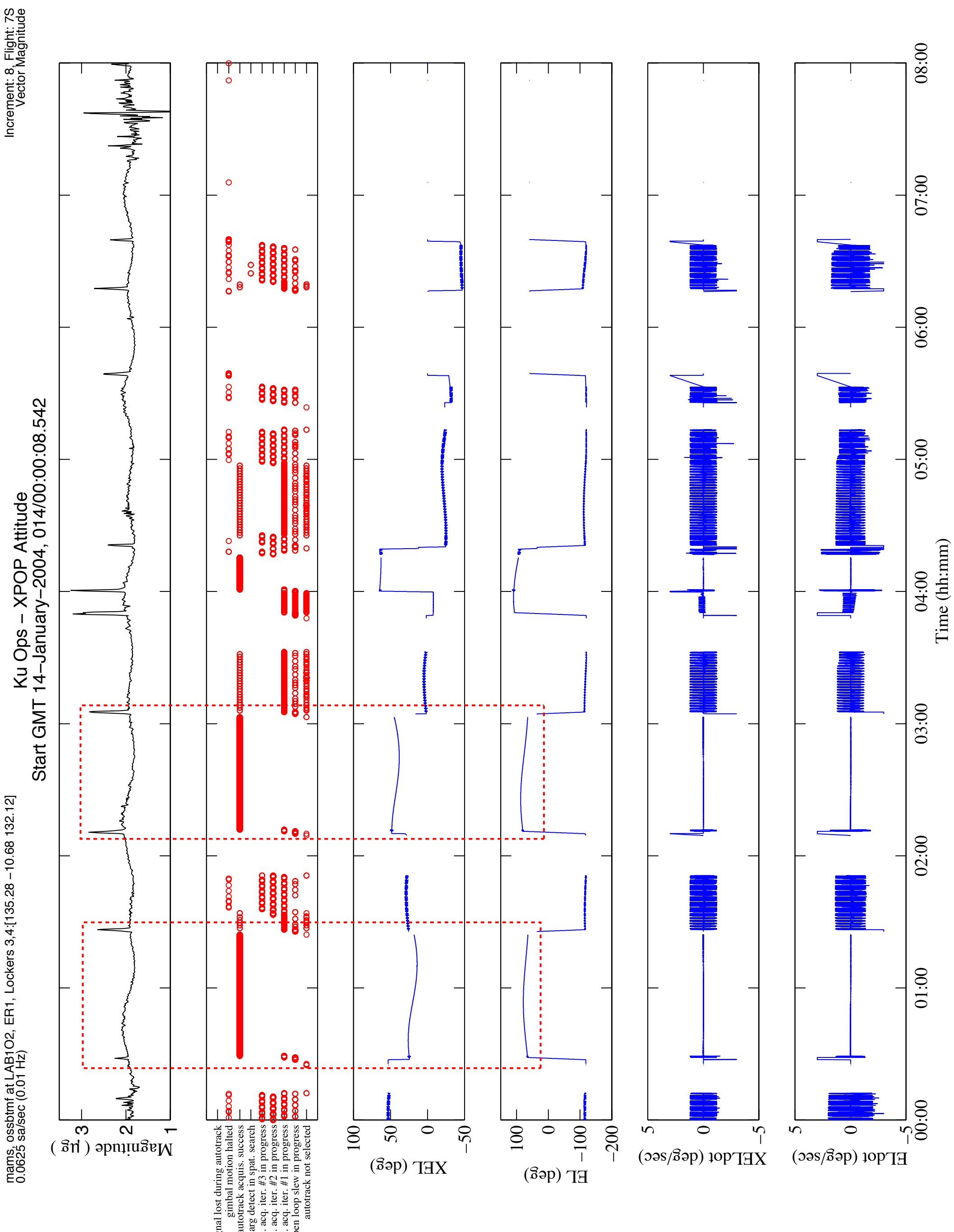

Figure 6-53 Vector Magnitude Correlation Composite of Ku-Band during XPOP Attitude (OSSBTMF)

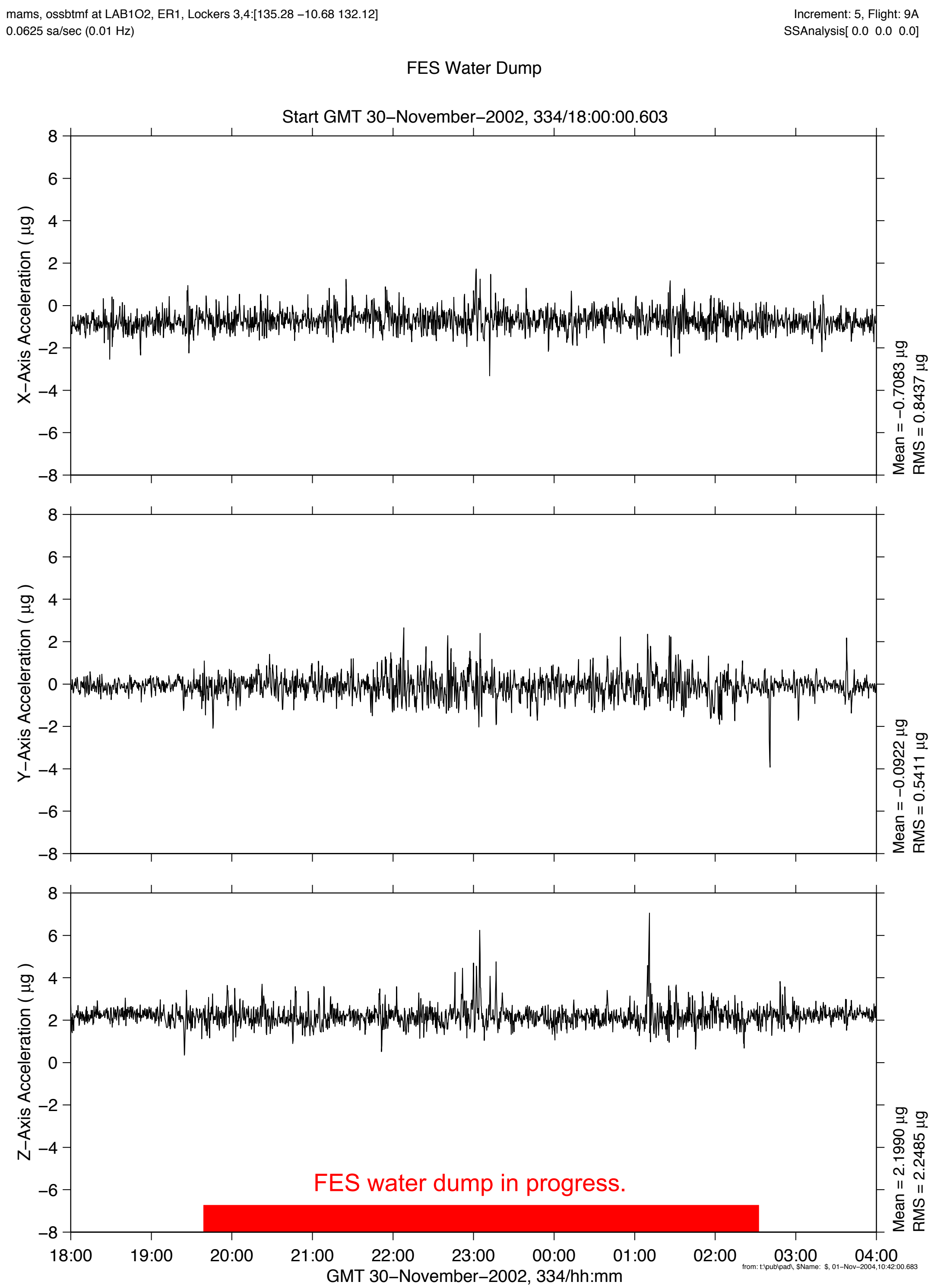

Figure 6-54 Time Series of FES Water Dump During STS-113 Joint Operations (OSSBTMF)

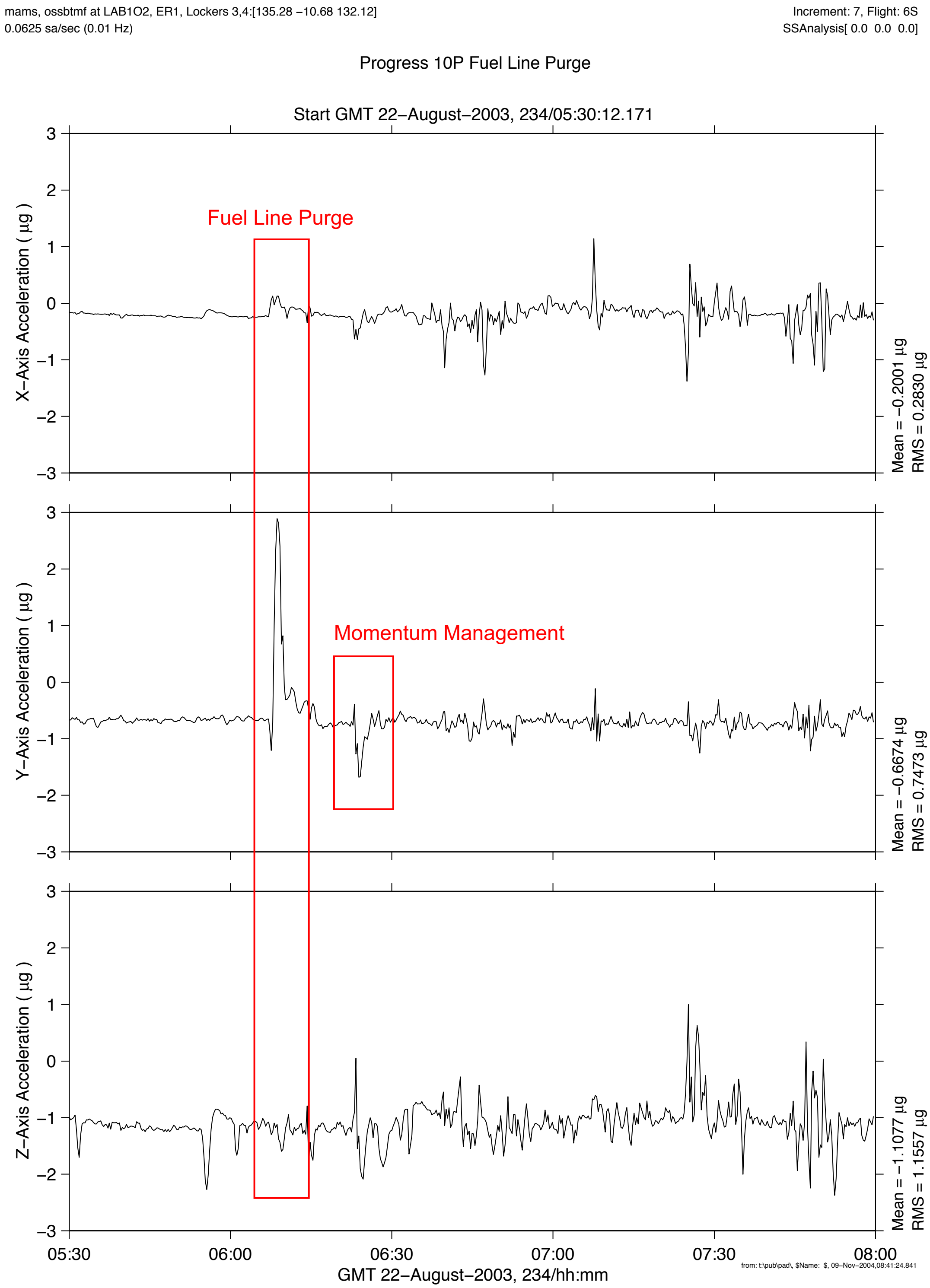

Figure 6-55 Time Series of Propellant Purge (OSSBTMF)

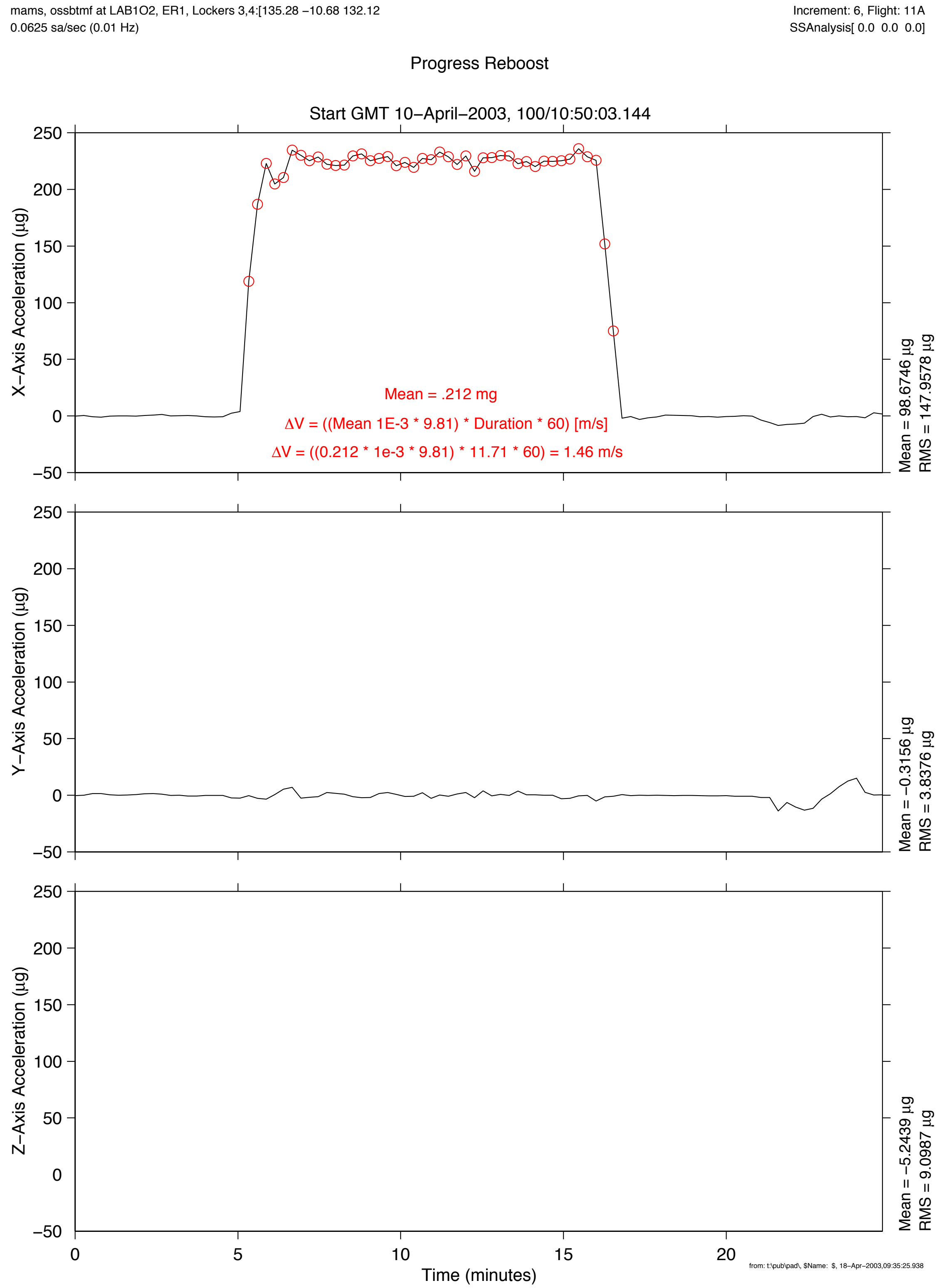

Figure 6-56 Time Series of Progress Reboost (OSSBTMF)

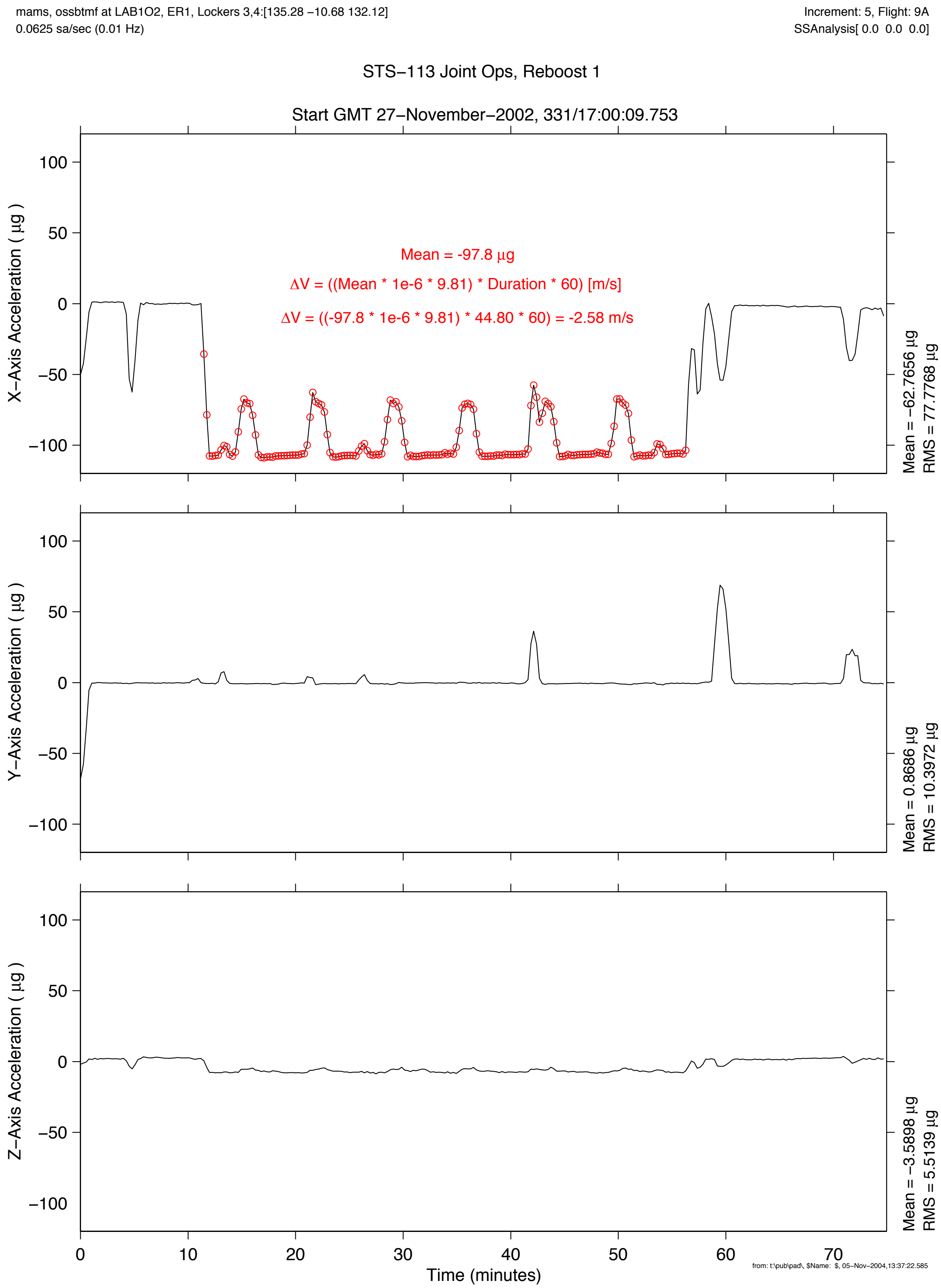

Figure 6-57 Time Series of Orbiter Reboost #1, STS-113 (OSSBTMF)

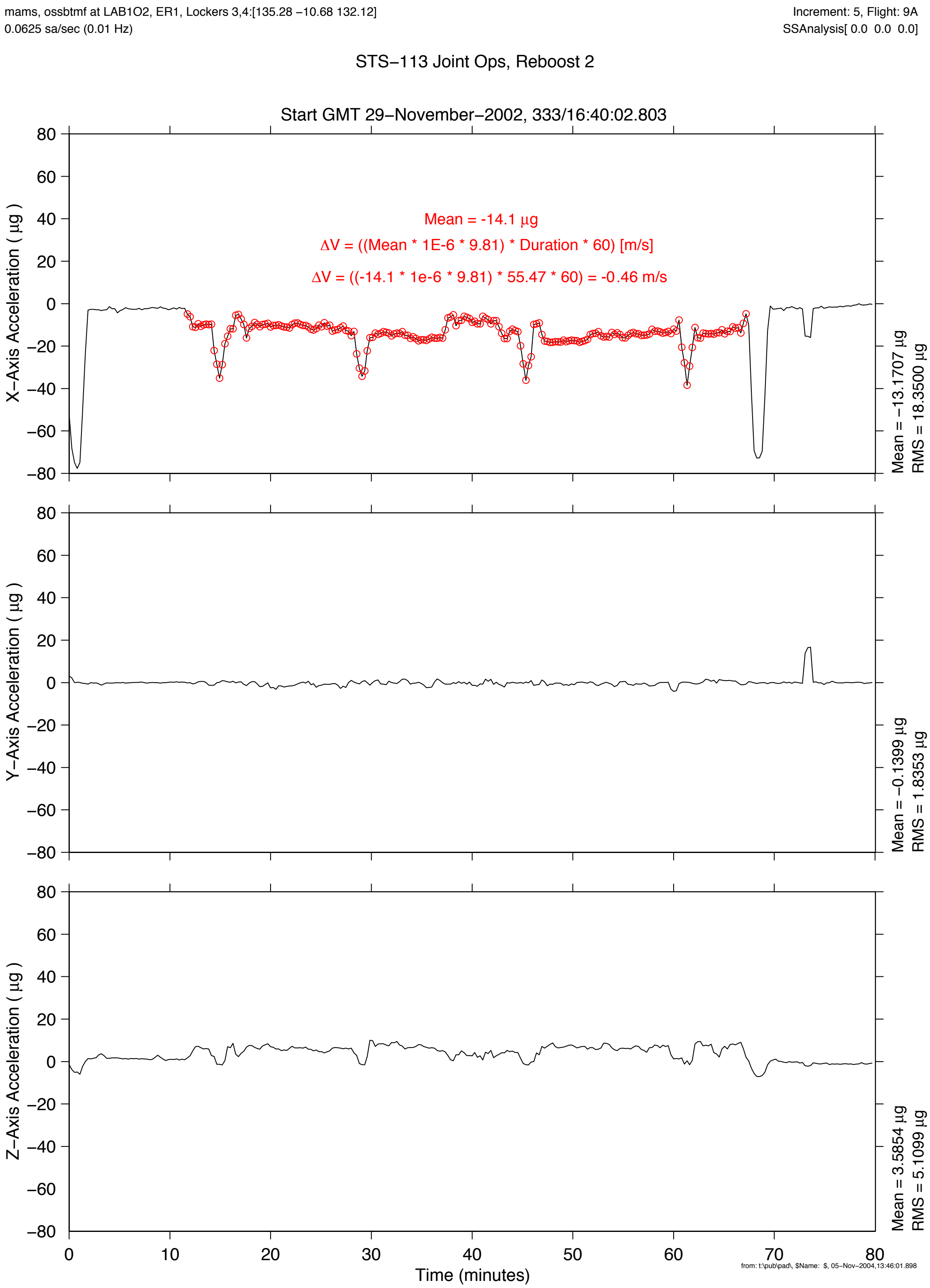

Figure 6-58 Time Series of Orbiter Reboost #2, STS-113 (OSSBTMF)

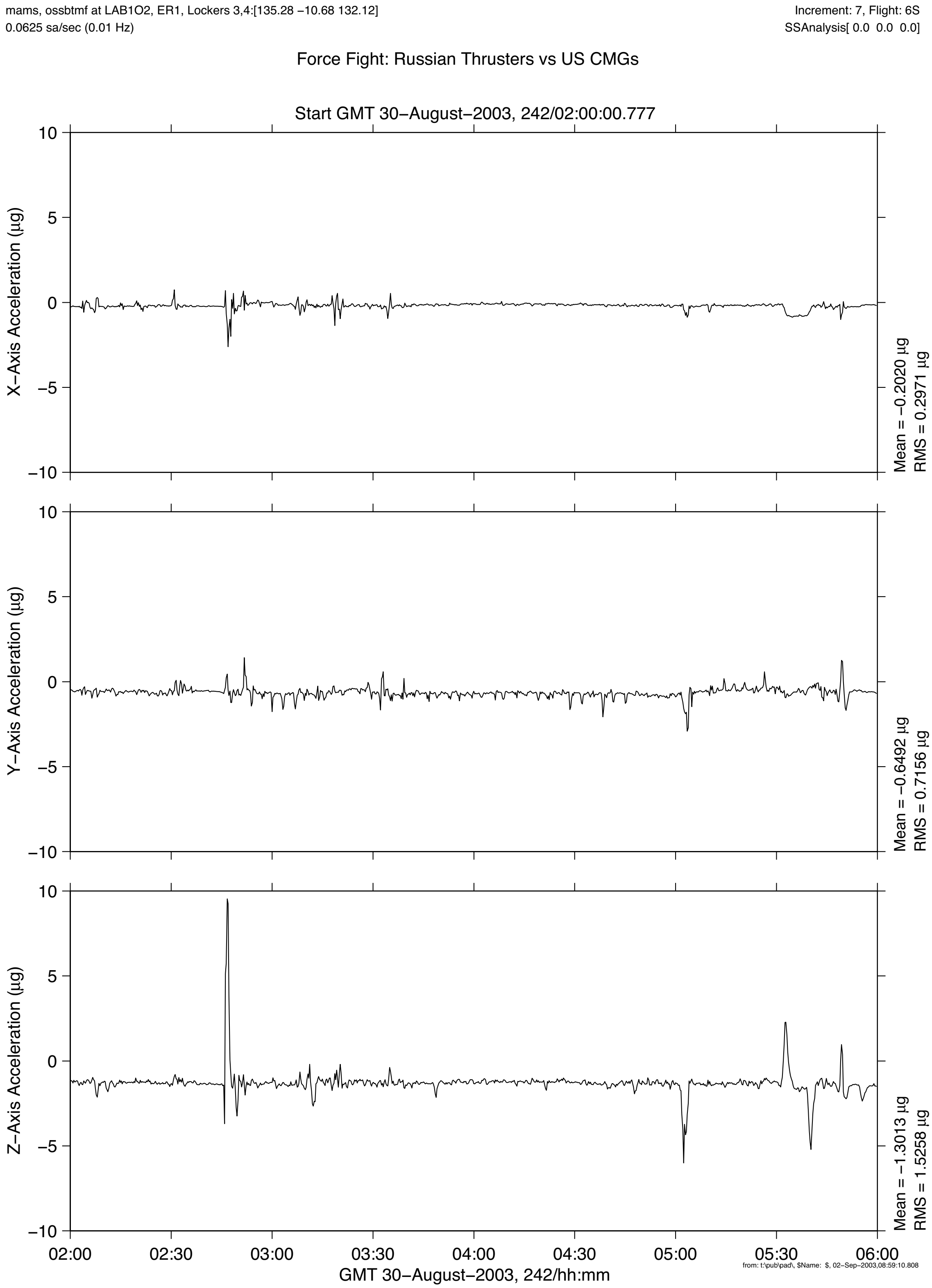

Figure 6-59 Time Series of Russian / US GNC Force Fight and Recovery (OSSBTMF)

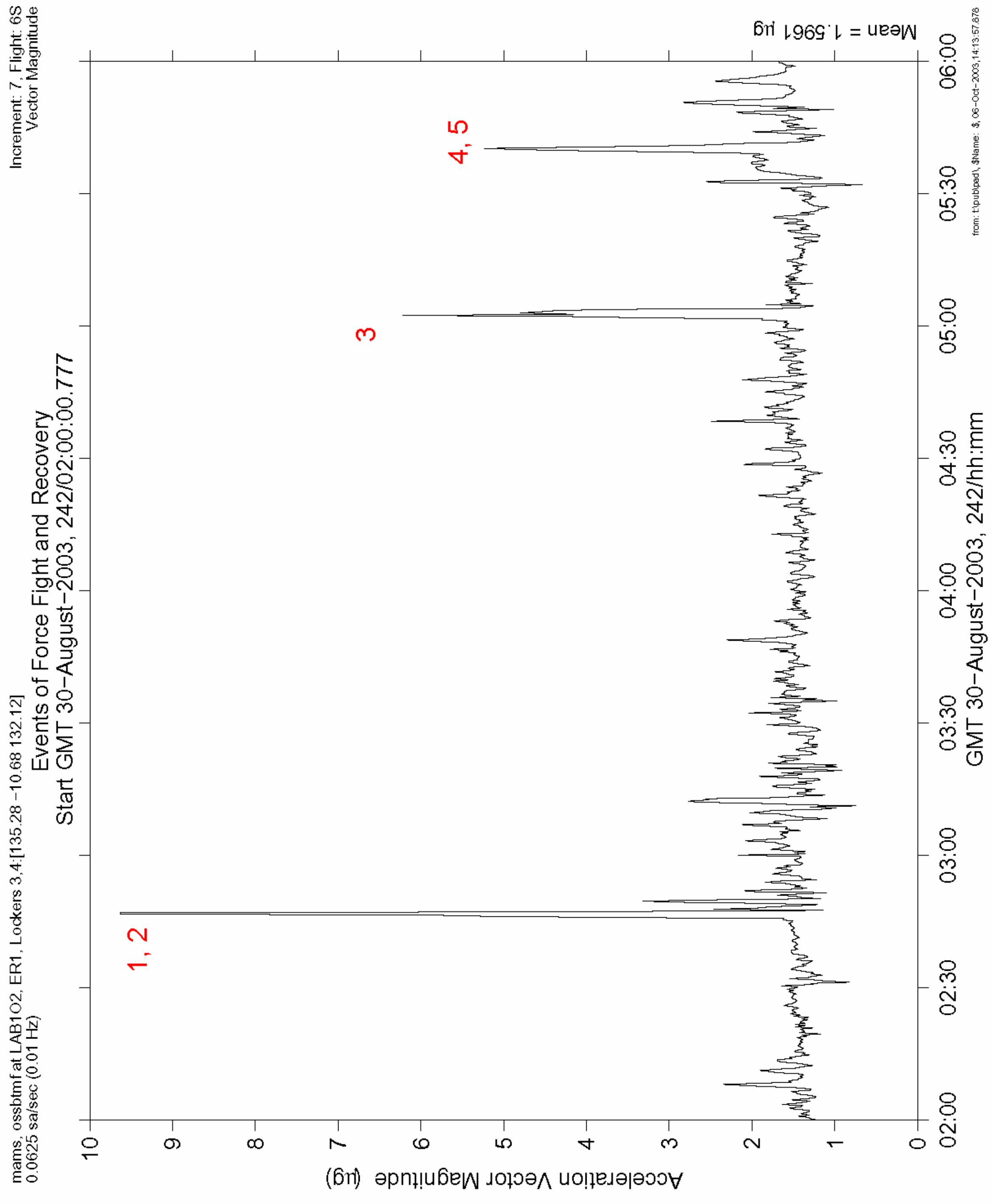

Figure 6-60 Vector Magnitude of Russian / US GNC Force Fight and Recovery (OSSBTMF)

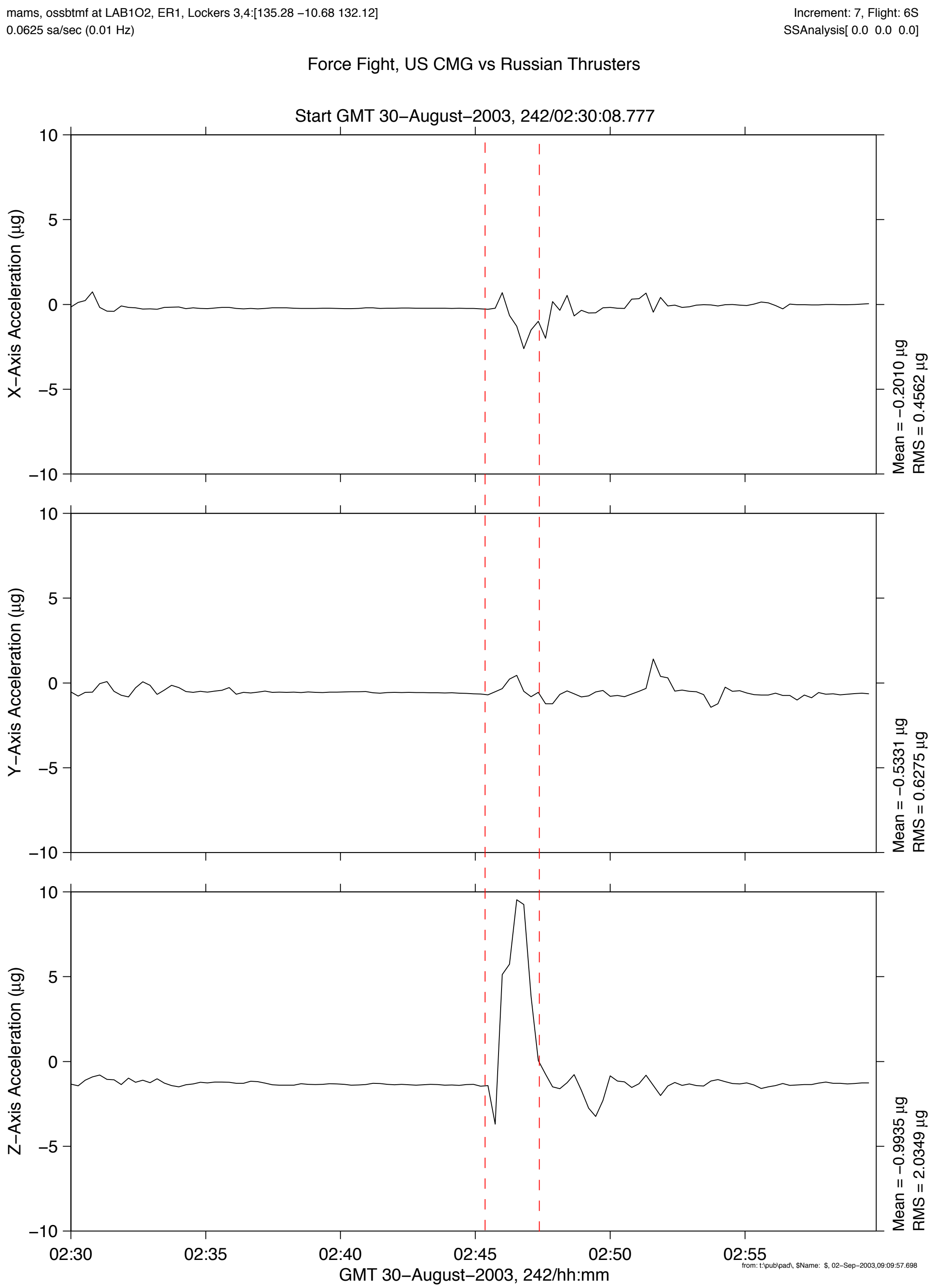

Figure 6-61 Russian / US GNC Force Fight - Zoom (OSSBTMF)

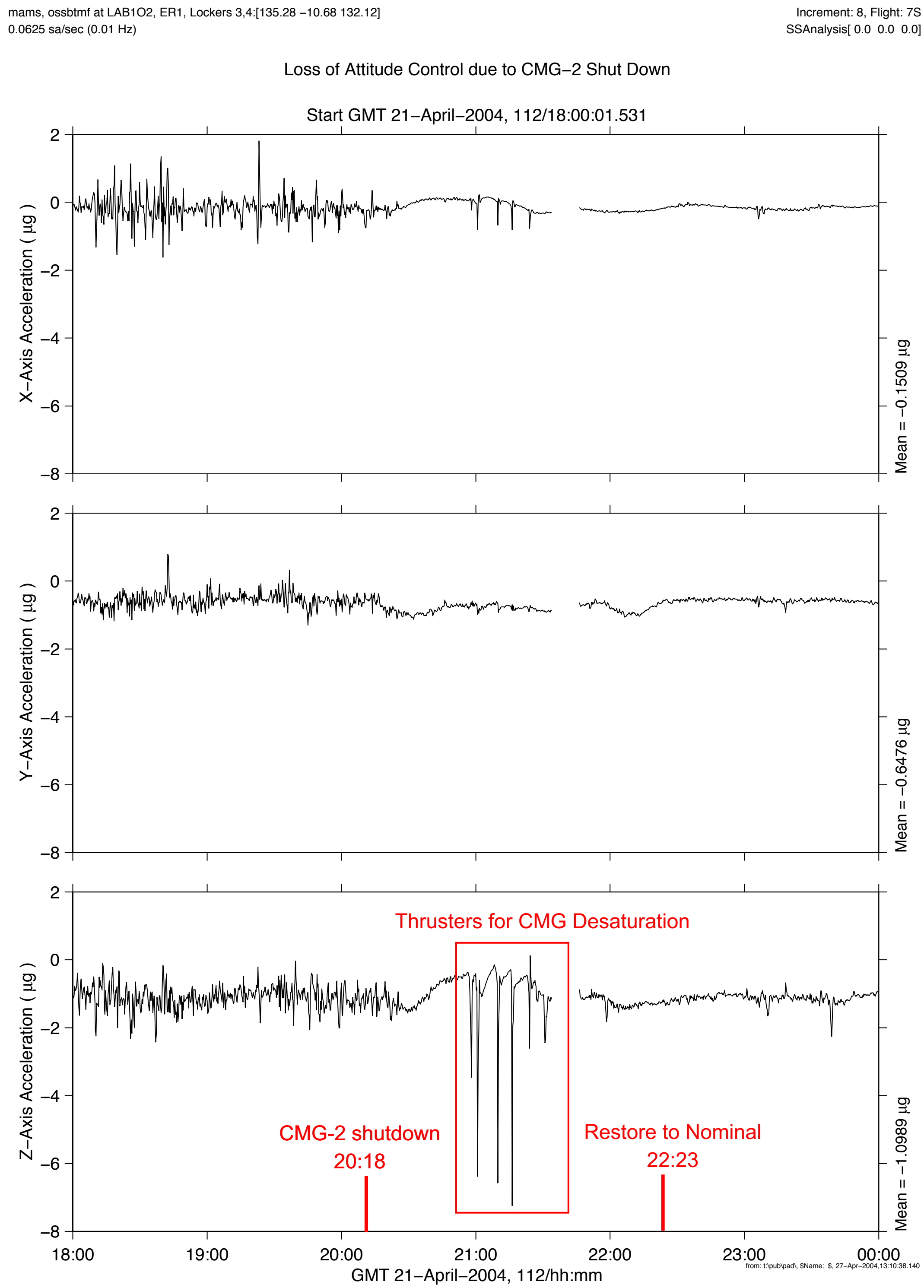

Figure 6-62 Time Series of CMG-2 Shutdown (OSSBTMF)

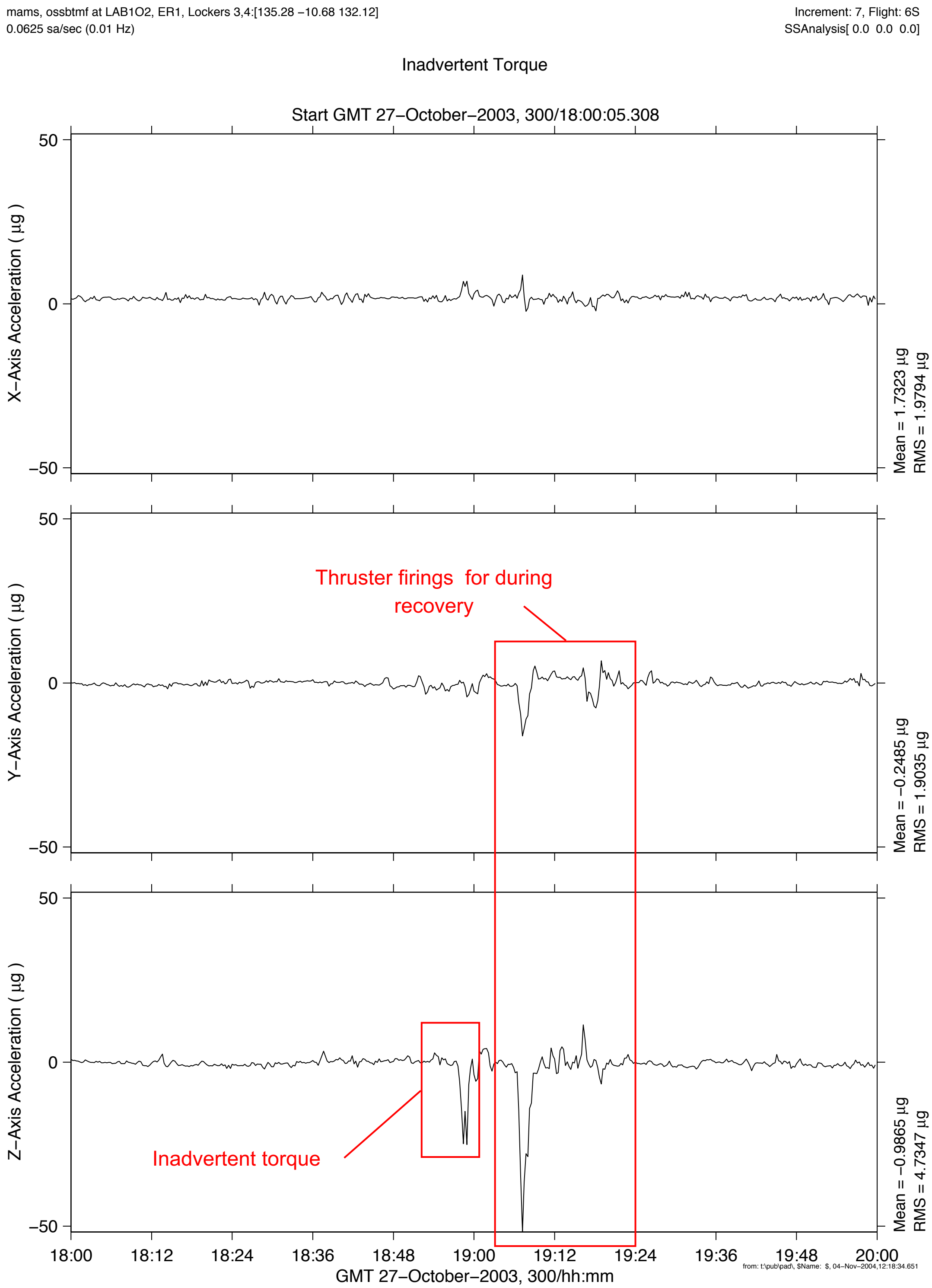

Figure 6-63 Time Series of Inadvertent Torque (OSSBTMF)

6.2 Vibratory Microgravity Environment

The vibratory acceleration regime consists of the acceleration spectrum from 0.01 to 400 Hz, with magnitudes expected to vary greatly depending on the nature of the disturbance and on the transmissibility from the source to locations of interest. The relatively high frequency accelerations that shape the vibratory environment of the ISS are usually associated with vehicle operations, vehicle systems, experiment-related equipment, and crew activity.

In this report, the vibratory acceleration environment consists of the acceleration spectrum from 0.01 to 200 Hz. In this region of the acceleration spectrum, magnitudes vary greatly depending on the disturbance source and on the transmissibility from the source to the measurement location. Typically, higher frequency (vibratory or so-called "g-jitter") accelerations are associated with vehicle operations, vehicle systems, experiment-related equipment, and crew activity. This section examines the effects of some of the vibratory disturbances aboard the ISS as measured by various SAMS sensor heads and the MAMS HiRAP sensor, all mounted toward the forward end of the US Lab.

In section 6.2.1, we examine vehicle subsystems including Ku-band antenna operations, control moment gyroscopes, the mobile transporter and the common cabin air assembly. Section 6.2.2 discusses the impact of vehicle operations such as vehicle traffic, both American and Russian. Activation of the ZCG experiment is the topic of section 6.2.3, while the last major category of vibratory disturbances considered for this section is crew activity. The impact of crew sleep versus wake and exercise are presented in section 6.2.4.

6.2.1 Vehicle Systems

Vehicle systems comprise the infrastructure needed for the health, maintenance and proper operation of the space station and its crew. Equipment for communication, attitude maintenance, life-support and such can produce accelerations that play a major role in shaping the vibratory regime. The vehicle systems considered in this section include: the Ku-band antenna system, control moment gyroscopes, the mobile transporter and the common cabin air assembly.

6.2.1.1 Ku-Band Antenna

Experiment and video activity on the ISS can generate large amounts of data. The Ku-band antenna system is located on the Z1 truss and serves as a primary link for transmission of these video and payload data from the space station to investigators and flight controllers on the ground. In addition to ordinary communications, this antenna interfaces with the GN&C system. The GN&C system provides data required for a method of open-loop antenna pointing, in addition to providing initial pointing vector information for closed-loop, auto-track antenna pointing. The Ku-band antenna system achieves the necessary pointing and tracking by means of a two-gimbal system – an elevation gimbal and a cross elevation gimbal. Numerous analyses over time have shown a high degree of correlation between the motion of these gimbals and a significant composite acceleration signature below about 30 Hz on the station.

The 24-hour spectrogram of Figure 6-64 shows the composite vibratory spectral signature of the Ku-band antenna between about 5 and 30 Hz. The interval RMS acceleration[3] for this same period is plotted with a black trace in the topmost of the 6 subplots in Figure 6-65. The 5 other subplots of this figure starting with the 2nd from the top show: (2) antenna mode information as red markers, (3) XEL gimbal angle, (4) EL gimbal angle, (5) XEL gimbal angular rate, and (6) EL gimbal angular rate. Careful examination of this figure shows that greater RMS acceleration levels in the 5 to 20 Hz frequency range come after the transition from XPOP to LVLH attitudes, which happened just before the midway time on these plots. An increase in acceleration levels consistently appears directly correlated with the increased gimbal motion required to track a particular geosynchronous TDRS while in an LVLH attitude.

Some plots and analysis not included in this report show correlation between familiar ascending and descending narrowband “swoosh” signatures with the ascending Ku-band antenna XEL gimbal angular rate and the descending EL gimbal angular rate, respectively. It may be of interest to some readers that in some Microgravity Measurements Group (MGMG) or Microgravity Environment Interpretation Tutorial (MEIT) meetings prior to this report, the Ku-band antenna disturbance was reported as the unknown “swoosh” or the unknown “picket fence” signature. The “swoosh” aspect is described above, while the following describes the “picket fence” trait.

Correlation with antenna mode information shows that “gimbal motion halted” results in the “picket fence” signature (not shown here), while auto-tracking in the LVLH attitude gives rise to the smooth “swoosh” signature. Figure 6-66 shows a substantial increase in RMS acceleration during Ku-band antenna gimbal motion. While standard operating procedure relies on this communication link, it may be beneficial for some researchers to become more knowledgeable on its vibratory impact. A comprehensive quantitative look at the vibratory environment below 25 Hz was undertaken to serve dual roles: (1) to assist researchers and others who might be interested in this particular aspect of ISS operations and (2) to summarize the station's vibratory environment for a long period of time.

Since the space station is still being assembled, there have not been any formal microgravity mode periods yet. However, there have been relatively quiescent time spans identified as microgravity periods in [24]. The median acceleration values cited in Table 6-10 were gleaned from more than 9,000 hours of vibratory data in those quiescent periods after having been low-pass filtered at 25 Hz.

[3] Correlation up to about 30 Hz is apparent in color spectrograms, but the confounding influence of the Russian air conditioner (SKV) signature at about 23.5 Hz was intentionally avoided in the RMS calculations to produce the RMS plots discussed here.

TABLE 6-10 ACCELERATION MAGNITUDE MEDIANS BELOW 25 HZ FOR LVLH VS. XPOP

Description	Crew State	Median Acceleration (μg)		
		121f02 (25 Hz)	121f03 (25 Hz)	121f04 (25 Hz)
Increment 7 LVLH	Combined*	163	124	147
Increment 7 XPOP	Combined	93	79	81
Increment 8 LVLH	Combined	141	118	131
Increment 8 XPOP	Combined	77	80	78

* Combined means the combination of sleep and wake periods

The choice of 25 Hz for the cutoff frequency serves a particular need to know more about this portion of the acceleration spectrum as solicited from and conveyed by microgravity investigators and in this double role to capture the impact of Ku-band antenna gimbal motion. While in the LVLH attitude, the station is effectively tumbling relative to the satellites it has to track in order to maintain communications with the ground. The station's Ku-band antenna rotates on a pair of gimbals in order to maintain line of sight with those satellites. As a result, Table 6-10 shows that increased gimbal action while in LVLH produces higher acceleration magnitudes compared to the relatively quiet XPOP attitude. It is not that there is no gimbal activity in the XPOP attitude, but rather the gimbal activity is such that there is less of a vibratory impact. It should also be noted that the Ku-band antenna gimbals are not always moving.

Since motion of the Ku-band antenna plays a major role in shaping the vibratory environment of the space station, we examine another aspect of its operation. That is, the antenna is parked when thermal conditions dictate the need. Some e-mail correspondence with the Data Manager Coordinator (DMC) gives these details:

1) The Ku-band is parked mostly in XPOP, but not strictly in XPOP. Anytime the sun starts to track to the starboard side of the station while in LVLH (+XVV) attitude, Ku-band spends a lot of time in the shadows, so the Space-to-Ground Antenna (SGANT) starts to get cool. You will find we do a lot of anti-sun pointing to warm sensors 1, 2, 4, 5, 6, and 8. Since sensors 3 and 7 are on the inside of the parabolic dish, we point near the sun to warm them, and away from it to cool them. This is more easily done and reasoned during XPOP because of how static the sun is, but during LVLH this is done by attempting to track a TDRS that is as close to synchronous to the sun as we can get for warming. At one time, we even attempted to get a solar tracking vector in TDRS slot 4 to permit solar tracking as needed, but the GNC could not handle the necessary parameters. LVLH attitude does not tend to cause Ku-band overheating, but certainly, XPOP can. You will see that the CATO's tend to point toward, or away from, the Sun as needed in XPOP, depending on which sensors need protection.

2) The definition of "park" for the Ku-antenna is just zero angular rate for both gimbals. There is no fixed guidance on where the Ku-band is to be parked. Each CATO parks

based on his/her experience. Philosophies vary regarding the best parking position and depend on the given situation.

3) Here are a few GMT spans when the Ku antenna was parked:
   a) GMT 13-Jun-2004, 165/17:55 - ~165/19:30
   b) GMT 15-Jun-2004, 167/17:17 - 167/19:00
   c) GMT 17-Jun-2004, 169/01:44 (duration unknown)
   d) GMT 17-Jun-2004, 169/18:34 (duration unknown)
   e) GMT 18-Jun-2004, 170/01:30 - ~170/07:00 (No Ku)

To conclude this topic, consider some logistics that may help investigators. First, at certain solar beta angles, the gimbals of the Ku-band antenna experience temperatures low enough that precautions need to be taken primarily during XPOP. To protect them, the antenna has to be parked periodically. Investigators may want to take an opportunity to do some experiment operations without the Ku-band antenna disturbance during these times. In this case, it would be advisable to forewarn the payload operations cadre at the MSFC to be on the lookout for such opportunities when the antenna may be parked and put this into the planning cycle for their particular experiment. Further, the capacity of the Ku-band antenna may be relatively large, but it is not without limit. At certain times, flight controllers must decide how best to reconcile the large amount of data generated among many experiments (video and recorded telemetry) to the capacity of the antenna transmission system. Typically, a communication outage recorder stores payload data during high-traffic conditions and during LOS for eventual playback to the ground. This presents the notion of perhaps a program-induced LOS. Since the largest impact from Ku antenna operations is during LVLH (when microgravity mode would be in effect) it is not without precedent that nominal vehicle subsystem operations would be inhibited in the interest of particular experiment objectives. For example, during some Shuttle microgravity missions, free drift was invoked whereby attitude maintenance (for communications and other reasons) was temporarily sacrificed so that investigators could get a quiescent acceleration environment for as long as practical. In effect, this happened recently too on the space station. Some ultrasound tests required that that the HRF consume all of the Ku bandwidth. As a result, an AOS period effectively became LOS for all but ultrasound customers. The other downlink customers had to wait and get their data after the fact from on-board recorder dumps. This shows at least one precedent where AOS was effectively sacrificed (in effect, the Ku antenna parked and not tracking) for the sake of science.

This section has presented the impact of Ku-band antenna activity on the vibratory acceleration regime. For further information from a quasi-steady perspective, see section 6.1.3. Also, future work at refining characterization of this impact would be to consider the spectrum up to 30 Hz or so while notching out the contribution from the narrowband Russian (SKV) air conditioner signature at about 23.5 Hz. Parseval's theorem can be used for that analysis.

6.2.1.2 Control Moment Gyroscope (CMG)

The primary vibratory effect from nominal operation of the CMGs is discussed in [25] along with some other details. Primarily, the tightly-controlled rotational rate of 6,600 revolutions per minute (RPM) for the CMG flywheel (located on the Z1 truss) gives rise to a distinct narrowband spectral peak at 110 Hz (measured at forward end of the US Lab). In this section, we examine unexpected events associated with CMG operation. Some significant vibration events (peaks) experienced by the CMG and resultant vibratory effects measured in the US Lab are listed in Table 6-11. Note that the acceleration peak values listed in the notes of the first column are from sensors independent of either SAMS or MAMS. There is a vehicle team at the JSC that monitors telemetry from sensors mounted right at the CMG location.

TABLE 6-11 CMG VIBRATION EVENTS

GN&C NOTES	OBSERVATIONS FROM ACCELERATION DATA
GMT 03-Nov-2003, 307/04:54:00 single peak of 0.066 g	MAMS HiRAP acceleration spectrogram in Figure 6-67 shows perturbation at 04:53:57 below about 10 Hz and possibly less severe precursor at about 04:47:18. A brief XYZ-axis acceleration history in Figure 6-68 shows the main event most clearly on the Y-axis.

At about GMT 21-Apr-2004, 112/20:18, CMG-2 went offline due to a faulty circuit breaker located on the S0 truss. By some accounts, the time cited was actually the beginning of a representative CMG spin-down sequence given that power was removed (unlike the "grinding metal noise" during the demise of CMG-1). The only aspect that did not seem to completely follow CMG design specifications was the time required to spin down as noted from some e-mail correspondence that suggests spin-down was expected to take about 11 hours instead of the observed duration of about 6.5 hours.

As mentioned above, it may be of interest to note that the vibration signature of a similar spin-down event was measured on the Russian Mir space station as described in [26]. However, that hardware was of different design as was the platform. Therefore, that event is not suitable for comparison here. However, when a CMG on the ISS is commanded to spin up, then we see similar effects to what was observed in the vibratory environment when a gyrodyne on Mir did likewise.

Vibratory measurements collected not long after GMT 01-Jul-2004, 183/13:00 by the MAMS HiRAP were used to derive the CMG-2 spin up rate. This came soon after an EVA by both crew members to repair a faulty circuit breaker. For the period from 13:58:01 to 15:09:35 in the 8-hour spectrogram of Figure 6-70, calculations based on HiRAP data shows a spin up rate of about 16.98 RPM/minute, which is in close agreement with the 17 RPM/minute expected by flight controllers. Furthermore, close examination of that spectrogram reveals that the acceleration power spectral density magnitude heightens at about 14:28:39 just below 46 Hz – near the expected "ball group" frequency (ball bearings in rotating assembly). This is seen more clearly when we rescale the PSD magnitude (color scale) as seen in the zoomed spectrogram of Figure 6-71.

Finally, only CMG-2, CMG-3 and CMG-4 are currently operational. An EVA to replace the failed circuit breaker for CMG-2 was successfully performed during Increment 9, and CMG-1 is scheduled for swap out on the next Shuttle flight to the ISS.

6.2.1.3 Common Cabin Air Assembly (CCAA)

The Common Cabin Air Assembly (CCAA) in the U.S. On-Orbit Segment modules of the ISS provides the capability to control the cabin air temperature, maintain the cabin air humidity level within desired limits, and generate ventilation air flow. During a normal shutdown operation of the CCAA, the inlet orbital replacement unit (ORU) fan speed is reduced from about 5700 RPM (~95 Hz) to about 3400 RPM (~57 Hz). At that point, the water separator ORU continues to operate at about 5900 RPM (~98 Hz) for approximately 200 minutes to accomplish dry-out prior to final shutdown. Both fans are then shutdown during the transition from port to starboard CCAA duty. It should be noted that the water separator operates at a fixed fan speed of 5900 ± 118 RPM (98 ± 2 Hz) and the inlet is a variable speed fan that operates between 3208 to 7668 RPM (53.5 to 127.8 Hz).

For a specific instance of the shutdown operation described above, the transition from port to starboard CCAA around GMT 13-Feb-03, 044/11:00:00 was studied. The background spectrogram of Figure 6-72 was computed to show the distinct transitions described above. From this spectrogram, notice that the inlet fan was stepped down from 95.4 Hz to 56.4 Hz at about GMT 13-Feb-03, 044/11:02:00 and kept at this rate until about GMT 13-Feb-03, 044/14:35:00 (~219 minutes) before shutdown. The water separator operated at 98.2 Hz until about GMT 13-Feb-03, 044/14:41:00. The inlay plot shows data queried from the Orbiter Data Reduction Complex (ODRC) database at the Johnson Space Center. The red trace shows a plot of Measurement/Stimuli IDentification (MSID) LAET06WS0002R (CCAA Speed Sensor Reading L1), and the green trace shows MSID LAET16FA0003R (CCAA Fan Speed Sensor Reading L1). While the transition times do match closely those gleaned from the acceleration measurements, they show slightly different rotational rates: the inlet fan stepping from 5681 RPM (~94.7 Hz) down to 3363 RPM (56.1 Hz) and the water separator operating at 5900 RPM (~98.3 Hz). These are independent measurements of the same acceleration source, and the fan speed sensor has a published "typical beginning of life offset" of up to 100 RPM (~1.7 Hz). This would account for the discrepancy.

In order to quantify this event, the interval RMS curves of Figure 6-73 were computed. These curves show that the higher frequency (red trace) water separator transitioned from nominal RMS values of about 268.3 μg_{RMS} to about 152 μg_{RMS} during dry-out before returning this narrow portion of the spectrum to a baseline of about 34 μg_{RMS}. The inlet fan operated between about 413 μgRMS during nominal operation up to550 μg_{RMS} before its step down to a lower frequency for dry-out. Note that the lower frequency operation of the inlet fan was not quantified due to its proximity to another strong, narrowband signal just above its operational rate. This is seen in spectrogram of Figure 6-72, just above 56.4 Hz.

6.2.1.4 Mobile Transporter (MT)

The MT is a rail line that runs along a truss outside of the ISS. The massive MT weighs approximately 30,000 pounds and is built from 5-inch thick aluminum and titanium. The MT train's top speed is about 1 inch per second and was designed to haul equipment. To ensure that the train stays on the track, a three-point suspension unit with wheels under and above the track holds it in place (like an amusement park suspension roller coaster ride). Despite its size and mass, the MT works with great precision and accuracy. Magnetic sensors and strips attached to the track help the vehicle stop exactly where it's supposed to (within a tenth of an inch), so that all power sources and openings can meet in exactly the right location [27]. The crew access the MT through space walks by using a special handcart and rail system called the Crew and Equipment Translation Aid (CETA). Furthermore, the crew can use the MT to move the space station's robotic arm.

Two periods known to span MT operations were analyzed. The first period contained 10 feet of translation within the span of GMT 30-Nov-2002, 334/16:20-16:31. None of the four SAMS sensors located in the forward end of the US Lab showed any remarkable transient or low-frequency effects. The second period analyzed was GMT 15-Jan-2003, 015/07:07-08:37. The effects noted in all four SAMS sensors for this period are represented by the spectrogram of Figure 6-74. Between GMT 15-Jan-2003, 015/08:10:06 and 08:18:15, a series of transients were recorded. From the available data, it is unclear whether we can attribute these impulsive acceleration events to the MT or to other, perhaps unrelated events. In any case, a quantitative look at those transients is shown in the interval min/max plot of Figure 6-75.

6.2.1.5 Attitude Control System - Global Positioning System (ACS-GPS)

A power cycle of both GPS R/Ps (ACS-GPS shutdown) occurred at GMT 14-Apr-2003, 104/14:54 [start at 15:40?]. Examination of roadmap spectrograms around this time frame shows an intensity dip of the narrowband peak at 110 Hz (the CMG spin rate), and a look at interval RMS plots as shown in Figure 6-76 shows this dip clearly in the rectangle annotation. However, a look at the big picture for that entire day shows other similar dips and therefore obscures this correlation. Also, here is an excerpt of a conversation with the responsible team at JSC:

> The GPS receiver (it's also called SIGI) is power cycled occasionally to clear its memory for reconfiguration (it doesn't have a reset button, so we just shut it off for a couple of minutes).
>
> The SIGI stands for "Space Integrated GPS/INS" - there's an INS portion in there that we don't use yet. In that INS portion, there are rate gyro assemblies (RGAs). RGAs have to be "shaken" slightly to eliminate a phenomenon called lock in when a rate of zero is sensed. I believe it is shaken by a piezoelectric dither motor that vibrates at a couple of thousand Hertz *[well above both SAMS and MAMS cutoff frequencies]* … we don't use the output in our software yet, but when the box is powered up the INS hardware is running, so the dither motors would be running.

The dither motors described in the correspondence above are far above the cutoff frequency of the SAMS and MAMS vibratory sensors.

6.2.1.6 P1 Truss Radiator Deployment

This entry from the Increment 6A As Flown ISS ATL: "P1 Rad Deployment, 015/14:28 - 015/15:07, P1 truss radiator deployment" states that the P1 radiator was deployed for heat rejection starting around GMT 15-Jan-2003, 015/14:28. The blue trace on the bottom of the 3 subplots in Figure 6-77 shows a brief history of "RAD_P1_1_INCREMENTAL_ACCELERATION" (MSID=P1TE65FC1610R) in RPM/s. Each subplot of that figure shows a black & green pair of traces corresponding to one-second interval min/max (envelope) statistics from SAMS 121f03 and 121f02 sensors, respectively. The incremental acceleration data of the blue trace were queried from the ODRC at the JSC and suggest motion primarily between about 14:50 and 15:01. However, the SAMS sensors did not register any significant impact above the background vibratory environment from this radiator deployment.

6.2.1.7 Pyro Valve Firing

The as-flown timeline provided this note: “Fire pyro valves, GMT 20-Jun-2003, 171/12:02, Firing of the ODY pyro valves”, however, none of the SAMS sensors active at that time was able to discern any obvious transients above the nominal vibratory background.

6.2.1.8 Propellant Transfer

Several ATL entries show "prop transfer", "fuel transferred", "tank compression", "repressurize tank", "fuel purge" or "oxidizer purge", however despite some definitive GMT start/stop times, there are no obvious traits that appear temporally aligned with those events.

6.2.2 Vehicle Operations

This section examines vibratory acceleration events related to vehicle operations such as docking and undocking events.

6.2.2.1 Dock and Undock

As discussed in previous reports, vehicle docking and undocking events happen on a regular basis for crew rotation, re-supply and construction. The events listed in Table 6-12 took place in the time span of interest for this report except for the last entry (Soyuz-9S docking) and Table 6-13 intends to put transient accelerations related to those events in a quantitative context.

TABLE 6-12 VEHICLE DOCK AND UNDOCK EVENTS

Event	ATL GMT	OOS GMT	Note
STS-113 Dock	25-Nov-2002, 329/22:58:00	22:59	acceleration data say softmate at 21:59, hardmate at 22:08
STS-113 Undock	02-Dec-2002, 336/20:05:00	20:05	acceleration data agree on undock time
Progress-9P Undock	01-Feb-2003, 032/15:57:00	none	undock from the aft of SM (indiscernible)
Progress-10P Dock	04-Feb-2003, 035/14:49:00	14:49	dock at aft of SM; acceleration data agree on dock time
Soyuz-6S Dock	28-Apr-2003, 118/05:57:00	05:56	dock at FGB nadir; no SAMS acceleration data
Progress-11P Dock	11-Jun-2003, 162/11:17:00	11:15	dock at DC-1 nadir; acceleration data say dock at 11:15
Progress-10P Undock	27-Aug-2003, 239/22:44:00	22:45	indiscernible
Progress-12P Dock	31-Aug-2003, 243/03:41:00	03:41	acceleration data agree on dock time
Progress-11P Undock	04-Sep-2003, 247/19:38:00	19:40	indiscernible
Soyuz-7S Dock	20-Oct-2003, 293/07:16:00	07:16	dock at DC-1 nadir; acceleration data agree on dock time
Soyuz-6S Undock	27-Oct-2003, 300/23:15:00	23:17	undock from FGB nadir; no SAMS acceleration data
Progress-12P Undock	28-Jan-2004, 028/08:33:00	08:36	indiscernible
Progress-13P Dock	31-Jan-2004, 031/13:14:29	13:13	acceleration data say dock at 13:13:26
Soyuz-8S Dock	21-Apr-2004, 112/05:03:00	05:01	dock at FGB nadir; acceleration data say dock at 05:01:19
Soyuz-7S Undock	29-Apr-2004, 120/20:52:00	20:52	undock from DC-1 nadir; indiscernible
Soyuz-9S Dock	16-Oct-2004, 290/04:15:00	04:16	manual dock at DC-1; accelerations show dock at 04:15:48

Note that entries in Table 6-12 which show "indiscernible" in the rightmost column indicate that no significant transient accelerations above ambient were observed around the undocking time. As a result, these were not included in Table 6-13. The note in Table 6-12 regarding the time of hardmate for the STS-113 Shuttle docking was derived from characteristics of the measured acceleration data as follows: (1) the spectrogram of Figure 6-79 shows that the Shuttle's 17 Hz Ku-band antenna dither signature started at that time and (2) the structural mode regime took on new "docked ops" traits at that time as seen at the 22:08 mark of Figure 6-80. At that time, a distinct "ISS alone" (nominal) structural mode at about 0.4 Hz vanishes and a new mode appears below it at about 0.144 Hz.

TABLE 6-13 VEHICLE UN/DOCK PEAK ACCELERATION EVENTS AT SAMS SENSOR LOCATIONS

	Peak Acceleration (mg)			
Event	**121f03 200 Hz**	**121f04 200 Hz**	**121f05 100 Hz**	**121f02 100 Hz**
Increment 7-8 95th Percentile	2.6	2.9	0.9	2.0
STS-113 Dock	47.4	61.4	19.3	19.9
STS-113 Undock	42.0	32.4	25.5	7.4
Progress-10P Dock	14.5	15.2	12.2	18.3
Progress-11P Dock	15.7	15.8	17.2	13.5
Progress-12P Dock	11.7	14.1	10.1	15.4
Soyuz-7S Dock	8.7	8.8	7.3	9.0
Progress-13P Dock	15.5	17.9	14.2	14.7
Soyuz-8S Dock	18.1	18.2	26.8	16.8
Soyuz-9S Dock	6.8	7.9	6.0	9.0

It should be noted that one-number or snapshot quantifications like those for the docking events in Table 6-13 can be misleading. For example, in some cases, crew movement for preparation before or clean-up after an event can produce transients at US Lab experiment locations that are comparable to the event itself. There might be a tendency by some to think that a docking with another massive vehicle might be the major concern for those susceptible to impulsive accelerations, while in fact, other concomitant events should be given equal (or perhaps more) weight in that consideration.

As a means of putting the impact of vehicle traffic into some quantitative context, the first row of Table 6-13 shows acceleration magnitude 95th percentile values taken from a large population of measurements from Increments 7 and 8. Using those values as a baseline, we observe from Table 6-13 that the STS-113 Shuttle docking and undocking events were somewhat more energetic than the Russian vehicle impacts. Furthermore, Table 6-13 demonstrates that the Russian Progress and Soyuz docking events are remarkably consistent in terms of peak transient acceleration magnitudes. One hypothesis might be that this consistency can be attributed to the Russian automatic docking system (whereas the Shuttle docking procedure has always had a human at the controls), but this would be dispelled by the fact that the Soyuz-9S docking was done under manual control. The Kurs-A autopilot of that Soyuz went into failure mode with an abort burn due to excessive closure speed at the range of less than 50 meters. The autopilot was aborted when the braking thrusters did not activate as expected. Ostensibly, the difference in mass accounts for the larger magnitude associated with the Shuttle docking.

6.2.2.2 Modes of Operation

The station is designed to operate according to a number of specific modes, each with distinct capabilities and conditions. Most modes support research payload operations to some degree, but others may inhibit payload operations altogether. Various modes of operation for the station are shown in Table 6-14 [28].

TABLE 6-14 ISS MODES OF OPERATION

Mode	Description
Microgravity	• Consists of capabilities required for microgravity research by user payloads in a habitable environment • Operated in a fashion that meets a strict set of microgravity environment requirements • Includes effects of crew equipment (e.g., exercise devices)
Standard	• Represents core operations when tended or preparing to support human presence • Provides "shirt sleeve" environment internal and external operations supported, monitored and controlled
Reboost	• Propulsively increase altitude • Maintain habitable environment and support internal and external user payload operations
Survival	• Initiated upon command or when a warning of imminent threat (e.g., loss of attitude control, loss of thermal conditioning, available power out-of-range) is not acknowledged by the crew or the ground • Autonomously attempts to correct the threatening condition • Provides keep-alive utilities to crew/core systems • Precludes support or commanding of external or internal operations
Proximity Operations	• Support safe operations with other vehicles while maintaining a habitable environment • Support internal and external user payload operations [before assembly complete?] • Vehicle is actively determining and controlling attitude non-propulsively
Assured Safe Crew Return	• Provides mitigation capability for life threatening illness, unrecoverable loss of Station habitability, or extended problem requiring resupply/servicing, which is prevented from occurring due to launch problems • Consists of actions, operations and functions necessary to safely populate a crew rescue vehicle, separate, return to Earth, and egress the crew rescue vehicle upon recovery on the ground
External Operations	• Utilizes functionality related to supporting station-based external operations while maintaining a habitable environment and supporting internal and external payload operations • Vehicle actively determining and controlling its attitude non-propulsively

Two modes are primarily intended for research: microgravity mode and standard mode. During microgravity mode, the station must be operated in a fashion that meets a strict set of microgravity environment requirements. Standard mode provides support for research payloads, but allows for activities that could result in violation of these microgravity environment requirements. An example of a standard mode activity that would not occur in the microgravity mode is propulsive control of the station's attitude as opposed to CMG control. Since the station is not at assembly complete, formal analysis based on acceleration measurements of the station in microgravity mode conditions cannot be presented. However, section 6.2.4 presents information for some quiescent periods that may prove helpful to some investigators.

Reboost is another mode that is necessary because of orbital (altitude) decay. Decay due to atmospheric drag occurs at an average rate of about 0.2 km/day [28]. As a result, periodic reboosts using thrusters must be performed.

6.2.2.2.1 Reboost

The primary intent of a reboost event is to increase the station's velocity in the direction of flight and thereby increase its altitude. This is inherently a quasi-steady event as discussed in section 6.1.5. However, along with the temporary DC shift that is manifested in the quasi-steady acceleration measurements, impulsive accelerations from the station's thrusters can be accounted for in the vibratory environment too. Table 6-15 lists several reboost events.

TABLE 6-15 REBOOST EVENTS

Event	GMT Start	Duration (minutes)
STS-113/ISS Reboost 1	27-Nov-2002, 331/17:11:00	45.0
STS-113/ISS Reboost 2	29-Nov-2002, 333/16:51:00	55.0
STS-113/ISS Reboost 3	01-Dec-2002, 335/16:38:47	45.0
Progress 10P Reboost	11-Feb-2003, 042/11:34:30	21.6
Progress Reboost	12-Mar-2003, 071/22:58:00	10.0
Progress Reboost	13-Mar-2003, 072/23:37:00	8.0
Progress 10P Reboost	04-Apr-2003, 094/12:59:18	20.0
Progress 10P Reboost	10-Apr-2003, 100/10:55:00	11.0
Reboost	30-May-2003, 150/16:50:00	7.5
Progress 12P Reboost	01-Oct-2003, 274/13:11:00	7.0
Progress 12P Reboost	08-Jan-2004, 008/19:59:00	6.4
Progress 13P Reboost	02-Mar-2004, 062/22:40:00	8.9

The SAMS 121f02 median interval RMS acceleration (calculated every 8.192 seconds) for the entire day of GMT 08-Jan-2004 was 365.7 μg_{RMS}, while during the reboost period, it was 482.5 μg_{RMS}. The reboost period is marked by the long, vertical ticks in the interval RMS plot shown in Figure 6-81.

6.2.3 Experiment Equipment

The Zeolite Crystal Growth (ZCG) experiment and the acceleration conditions surrounding its activation are the topic of this section.

6.2.3.1 ZCG Activation

There was a known desire for the ZCG team to have activation with thrusters inhibited from GMT 03-Jan-2003, 003/15:00 to 04-Jan-2003, 004/11:00. Therefore, a broad look at 6 Hz lowpass-filtered SAMS data serves to summarize the transient accelerations before, during and after activation. Ten-second interval min/max plots like the one in Figure 6-82 were used to gather the statistics in Table 6-16.

TABLE 6-16 ZCG INTERVAL MIN/MAX STATISTICS

SAMS Sensor	SSA Axis	Acceleration Min to Max (mg) Relative to ZCG Activation Period		
		Before	During	After
121f02	X	−5.32 to 5.20	−1.94 to 1.87	−3.66 to 3.45
	Y	−1.13 to 0.91	−1.42 to 1.66	−0.71 to 1.29
	Z	−2.75 to 2.22	−1.03 to 0.93	−1.39 to 1.58
121f03	X	−0.49 to 0.56	−0.44 to 0.56	−0.55 to 0.62
	Y	−1.45 to 1.14	−1.79 to 2.09	−1.01 to 1.02
	Z	−1.22 to 1.24	−1.25 to 1.20	−1.76 to 1.64
121f04	X	−0.50 to 0.54	−0.45 to 0.55	−0.55 to 0.63
	Y	−1.20 to 0.90	−1.45 to 1.69	−0.82 to 0.87
	Z	−1.08 to 1.12	−1.10 to 0.95	−1.51 to 1.38
121f05	X	−1.28 to 1.22	−0.90 to 1.02	−0.99 to 1.24
	Y	−1.45 to 1.22	−1.88 to 2.22	−1.01 to 1.20
	Z	−1.23 to 1.37	−1.38 to 1.24	−1.91 to 1.83

The topmost row of data in Table 6-16 shows that the X-axis of the SAMS sensor (121f02) in the RTS drawer of ER1 was consistently the most active, while the adjacent racks Z-panel SAMS sensor (121f03) consistently was the least active among the group. This difference stems primarily from the mounting location and arrangement for the different sensors.

6.2.4 Crew Activity

Crew activity is comprised mainly of equipment transfer or stowage, exercise, experimental setups, locomotive push offs and landings. All of these actions give rise to perturbations and reactive forces, which are manifested as vibratory and transient accelerations that are transferred through the vehicle’s structure. Analysis in this section includes crew sleep versus wake comparison based on a large volume of acceleration measurements and crew exercise. The wake designation represents an aggregate of crew activity.

6.2.4.1 Sleep Versus Wake

While the station is still under construction, there has not been an attempt to fully deliver a microgravity mode per the acceleration environment requirements. However, there have been relatively quiescent times identified as microgravity periods in [24]. The median acceleration values cited in Table 6-17 were gleaned from more than 9,000 hours of vibratory data in such quiescent periods after having been low-pass filtered at 6 Hz.

TABLE 6-17 ACCELERATION MAGNITUDE MEDIANS BELOW 6 HZ FOR SLEEP VS. WAKE

Description	Crew State	Median Acceleration (μg)		
		121f02 (6 Hz)	121f03 (6 Hz)	121f04 (6 Hz)
Increment 7 LVLH	Sleep	32.5	17.5	17.5
	Wake	55.0	37.5	35.0
Increment 7 XPOP	Sleep	20.0	15.0	12.5
	Wake	45.0	30.0	27.5
Increment 8 LVLH	Sleep	25.0	15.0	15.0
	Wake	52.5	35.0	32.5
Increment 8 XPOP	Sleep	15.0	15.0	10.0
	Wake	47.5	32.5	30.0

Table 6-17 shows that the median acceleration vector magnitude below 6 Hz during sleep periods is roughly half (or even less in some cases) than that of the corresponding wake periods. Regardless of increment or station attitude, the vibratory environment below 6 Hz was considerably better when the crew was sleeping. Ostensibly, this stems from a relative lack of structural mode excitation, which would otherwise come as a direct effect of crew activity during wake periods. Push offs, landings, stowing, unstowing, exercise and other crew activity provide the impetus to excite those structures.

6.2.4.2 Exercise

The impact of crew exercise on various devices such as the Treadmill Vibration Isolation System (TVIS), the Resistive Exercise Device (RED), Cycle Ergometer with Vibration Isolation System (CEVIS) and the Russian velosiped (velo) has been reported previously in [29]. Table 6-18 shows RMS acceleration levels below 6 Hz for a half-hour exercise period from GMT 12-Jan-2004, 012/17:31:15 to 18:01:48. The spectrogram of Figure 6-83 reinforces that the vibratory impact from this exercise was concentrated at the pedaling frequency (about 2 Hz), the shoulder sway frequency (about 1 Hz) and harmonics up to about 4.5 Hz. The plot of Figure 6-84 shows an interval RMS plateau during the exercise period at the 121f03 sensor location.

TABLE 6-18 ACCELERATION RMS MEDIANS BELOW 6 HZ FOR EXERCISE

GMT Span	Crew State	Median RMS Acceleration (μg)	
		121f03 (6 Hz)	121f04 (6 Hz)
12-Jan-2004, 012/16:00:00 - 19:00:00*	Not Exercising	69	66
12-Jan-2004, 012/17:31:15 - 18:01:48	Exercising	171	155

* this span excludes the exercise period shown below it

6.2.5 Principal Component Spectral Analysis (PCSA)

PCSA histogram plots are computed from a large number of constituent PSDs. The resultant three-dimensional plot serves to summarize magnitude and frequency variations of significant or persistent spectral contributors and envelops all of the computed spectra over the time frame of interest. The histogram is comprised of frequency-magnitude bins in units of Hz along the abscissa and units of $\log_{10}(g^2/Hz)$ along the ordinate. The third dimension, represented by a color scale, is the percentage of time that a spectral value was counted within a given frequency-magnitude bin.

As alluded to by the LVLH versus XPOP and sleep versus wake narrative of sections 6.2.1.1 and 6.2.4.1, respectively, the frequency domain gives keener insight than the amplitude domain when it comes to identifying and qualifying vibration sources. For example, comparing historical spectral records with the corresponding, more recent, PCSA figures in Table 6-19 leads to the discussion that follows.

TABLE 6-19 PRINCIPAL COMPONENT SPECTRAL ANALYSIS FIGURES

Description	121f03 200 Hz	121f04 200 Hz
Increment 7 & 8	Figure 6-85	Figure 6-86

The 50-60 Hz portion of the 121f03 acceleration spectrum is distinctly greater in the recent PCSA spectra of Figure 6-85 relative to the comparable corresponding figure in [30]. Similarly, the 50-60 Hz portion of the 121f04 acceleration spectrum is distinctly greater in the recent PCSA spectra of Figure 6-86 relative to comparable seen in [30].

6.2.6 Summary of Vibratory Analysis

A comprehensive analysis of ISS vibratory acceleration measurements and correspondence with those knowledgeable about various vehicle systems and operations has led to some important empirical results for investigators. For those phenomena sensitive up to 100 Hz or higher, there is no clear advantage to operate during crew sleep since higher frequency disturbances tend to dominate the acceleration spectrum irrespective of sleep or wake periods. However, for those sensitive between about 0.01 and 6 Hz, there is a definite advantage to operating during sleep periods, when or if possible, as demonstrated in section 6.2.4.1. There are also short public affairs events that mimic sleep and can also be exploited as accounted in previous increment reports. Finally, for experiments that are sensitive between about 0.01 and 25 Hz, there is a benefit to operating during the XPOP attitude. The vibratory environment below 25 Hz is quieter in XPOP than it is during the LVLH attitude. This stems from differences in how the Ku-band antenna gimbals are driven to deal with these different attitudes, not the total lack of gimbal activity in the XPOP attitude.

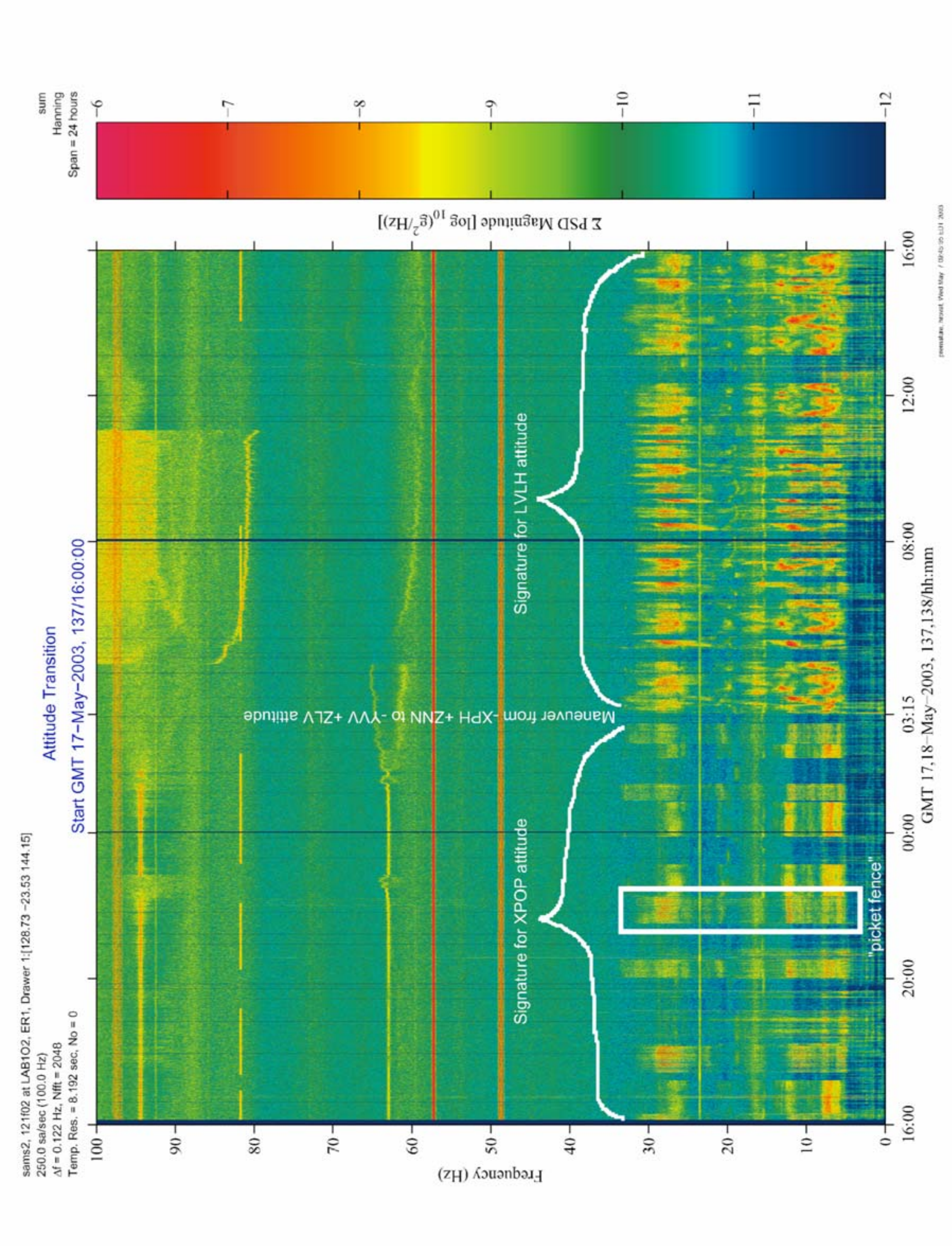

Figure 6-64 Spectrogram of Ku-Band Antenna Operations (121f02)

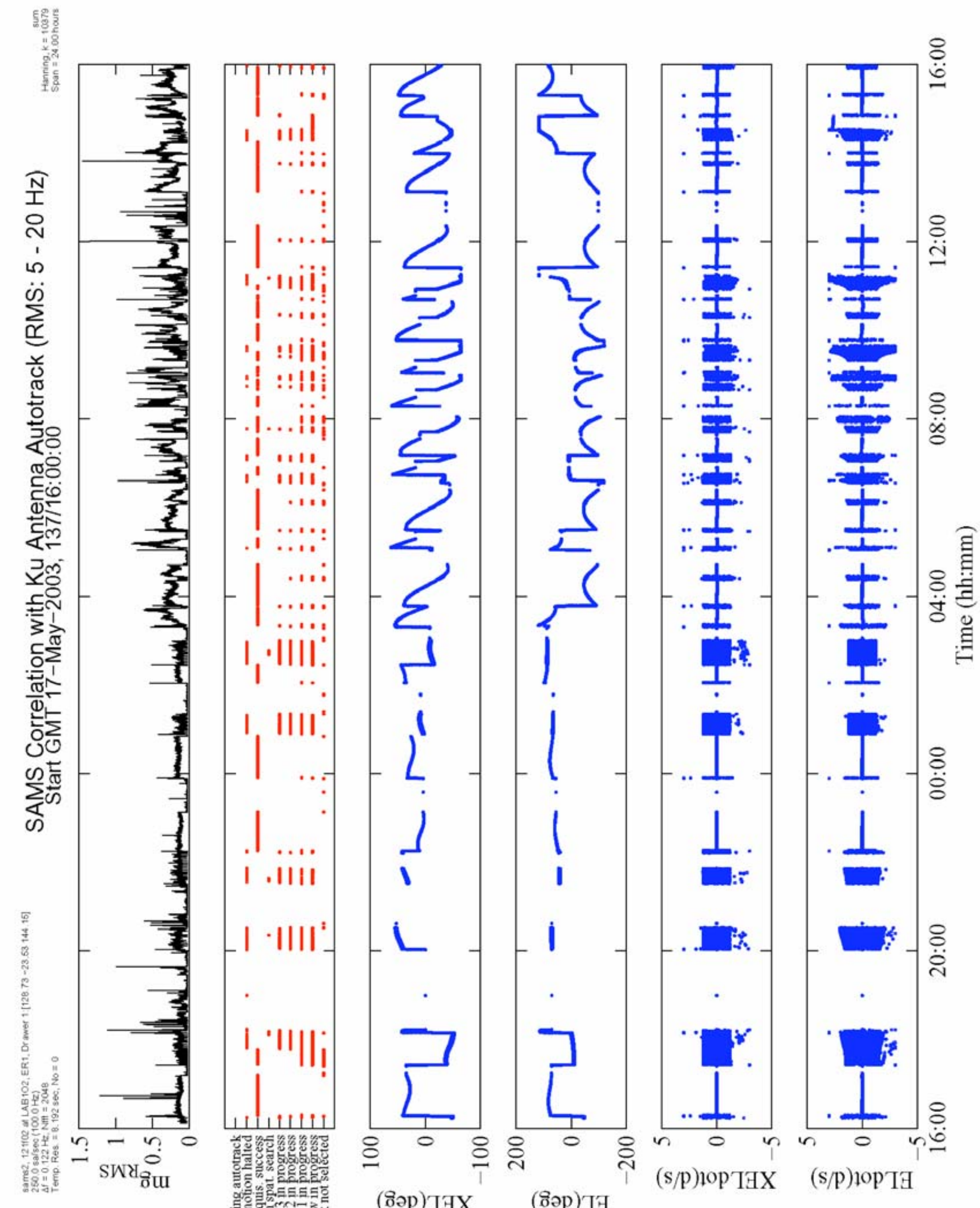

Figure 6-65 RMS Correlation Composite for Ku-Band Antenna Operations (121f02)

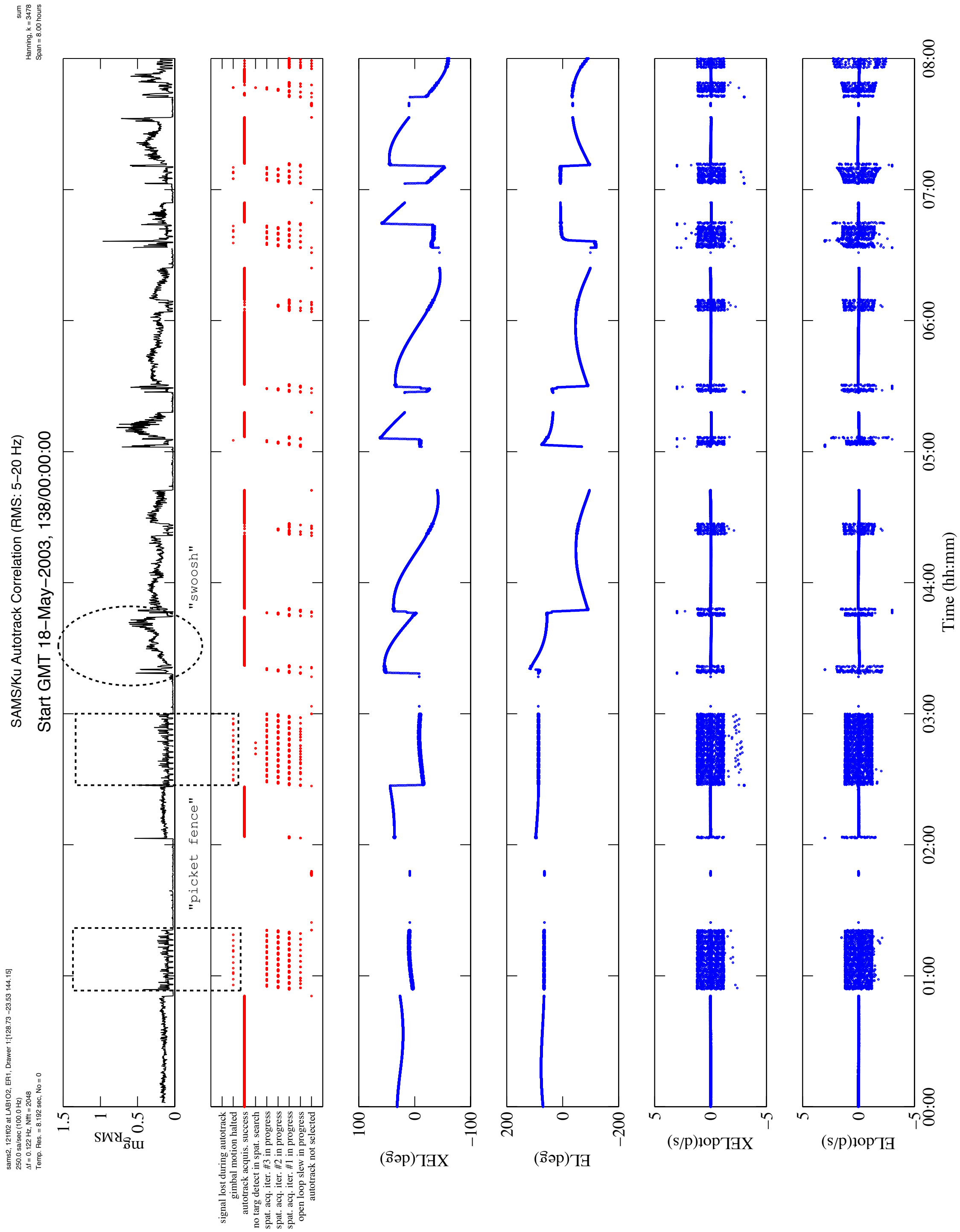

Figure 6-66 RMS Composite for Ku-Band Antenna Operations (121f02)

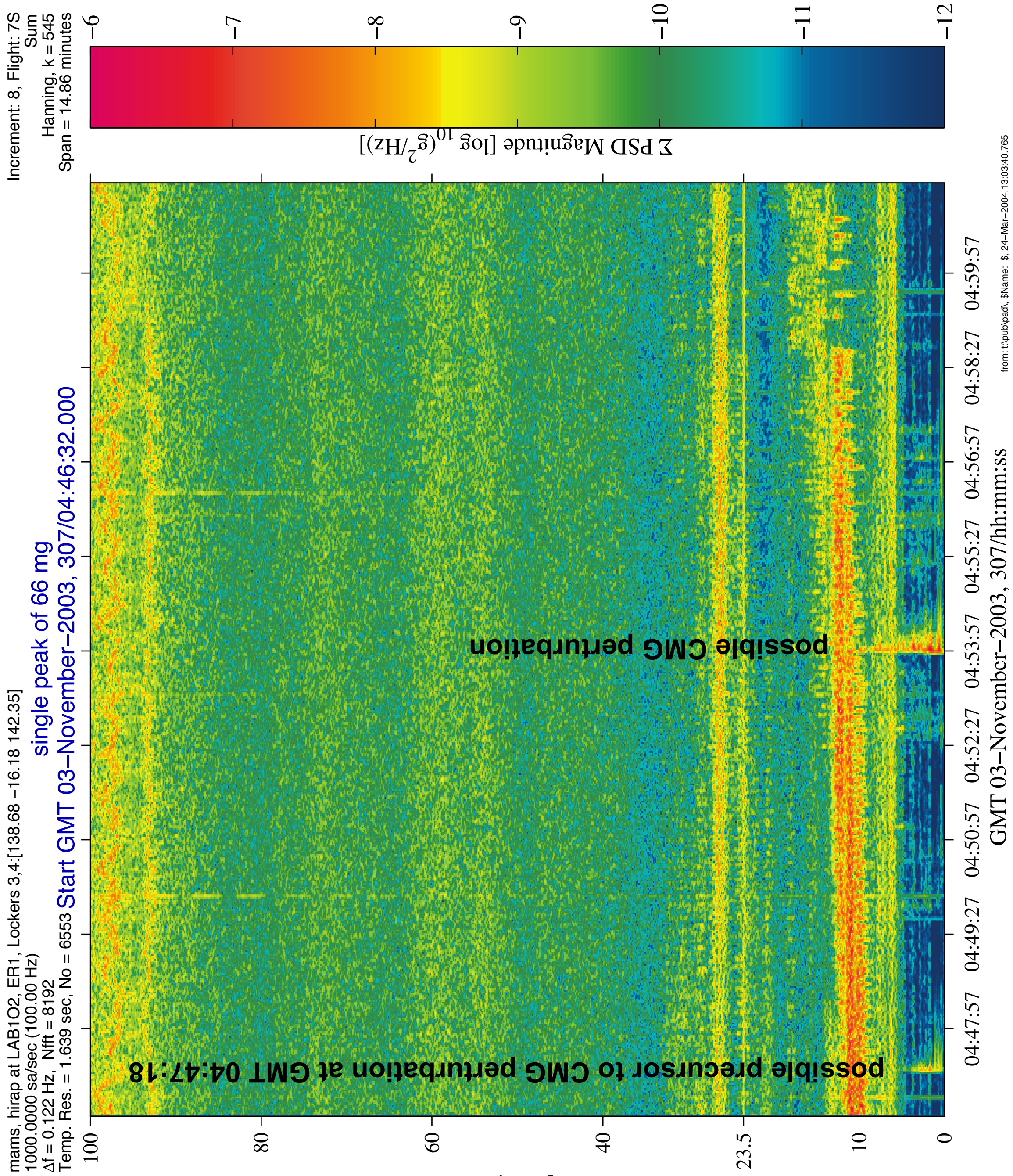

Figure 6-67 Spectrogram of CMG Single Peak Event (HiRAP)

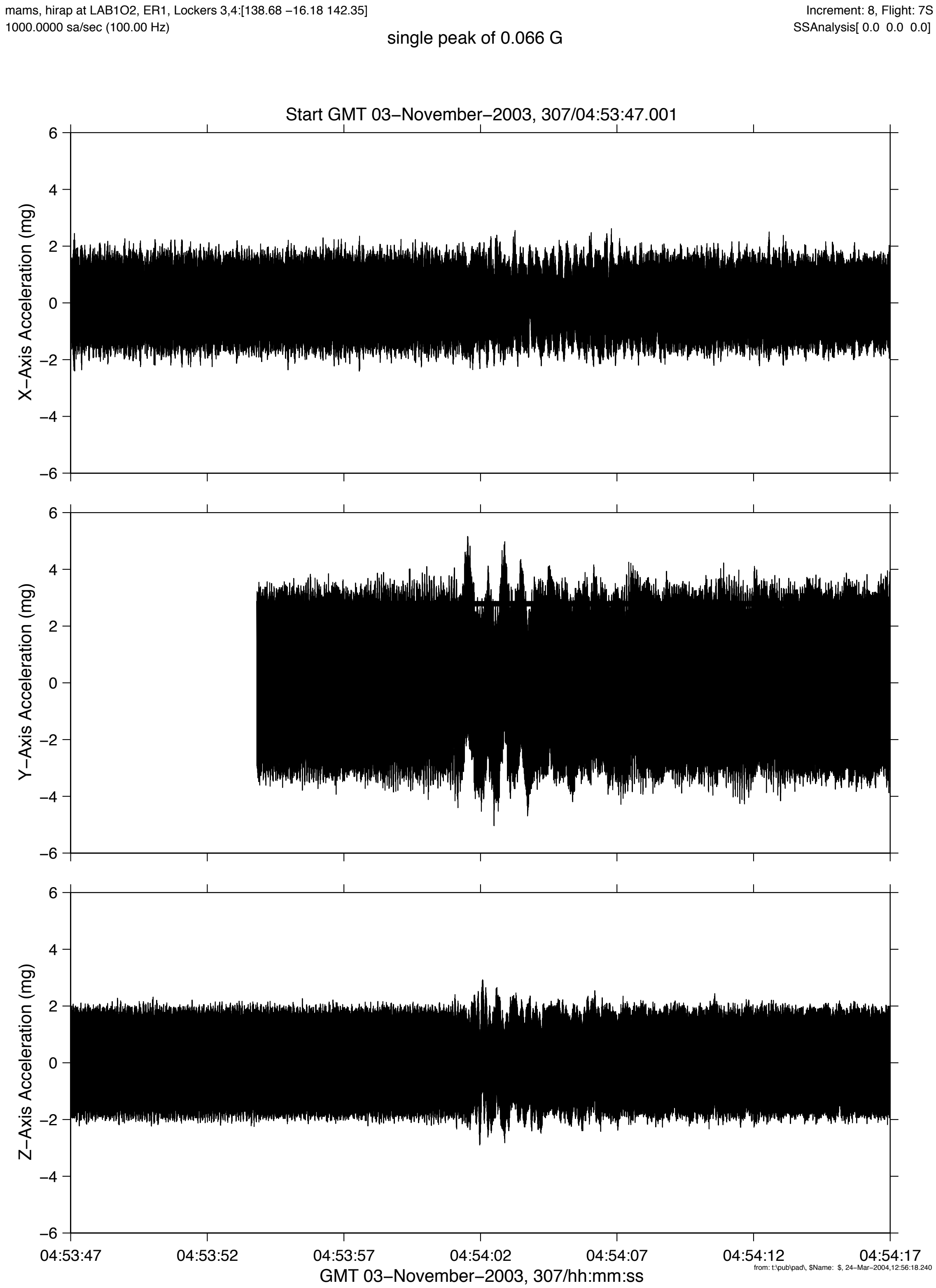

Figure 6-68 Time Series of CMG Single Peak Event (HiRAP)

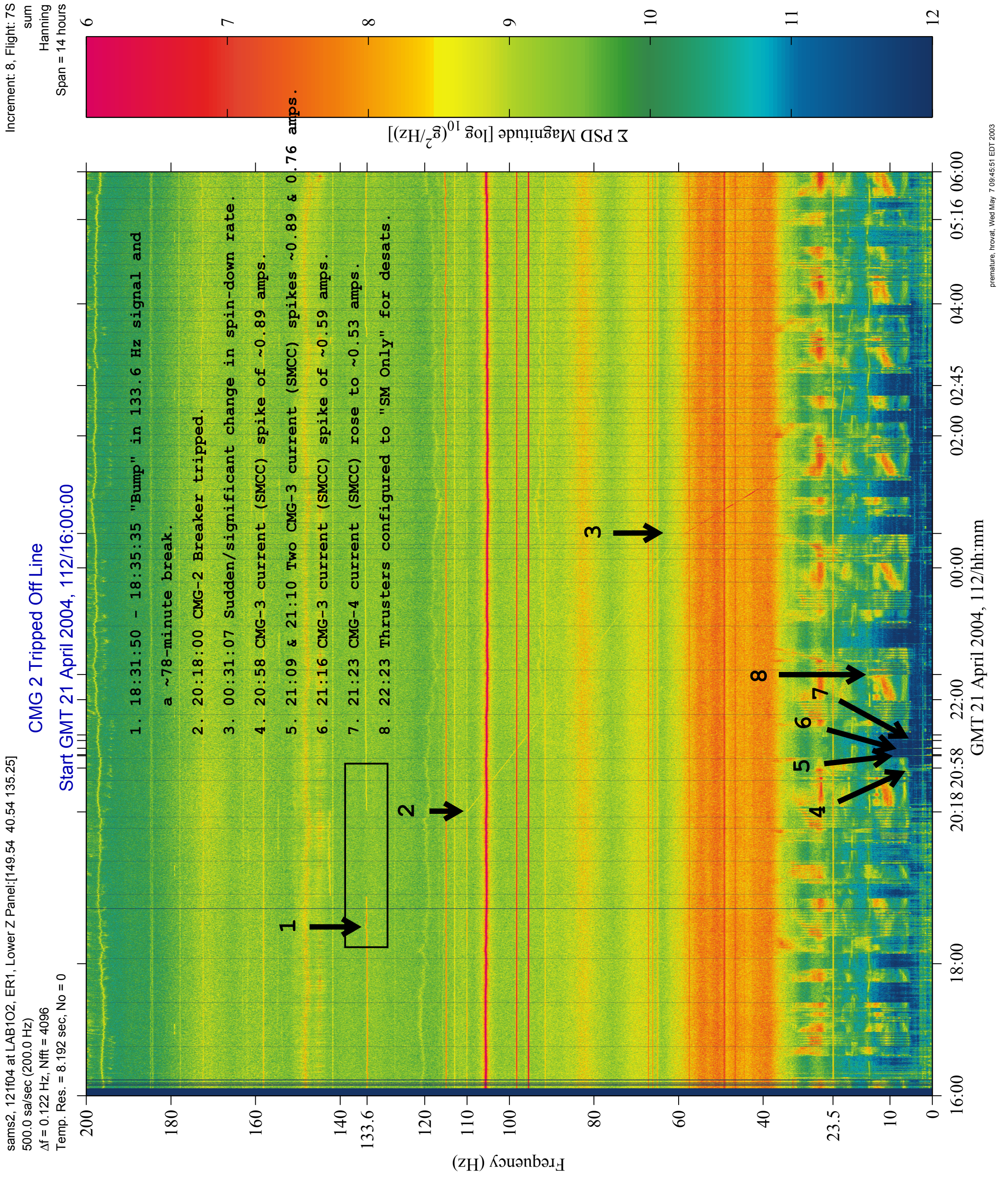

Figure 6-69 Spectrogram of CMG-2 Spin-Down (121f04)

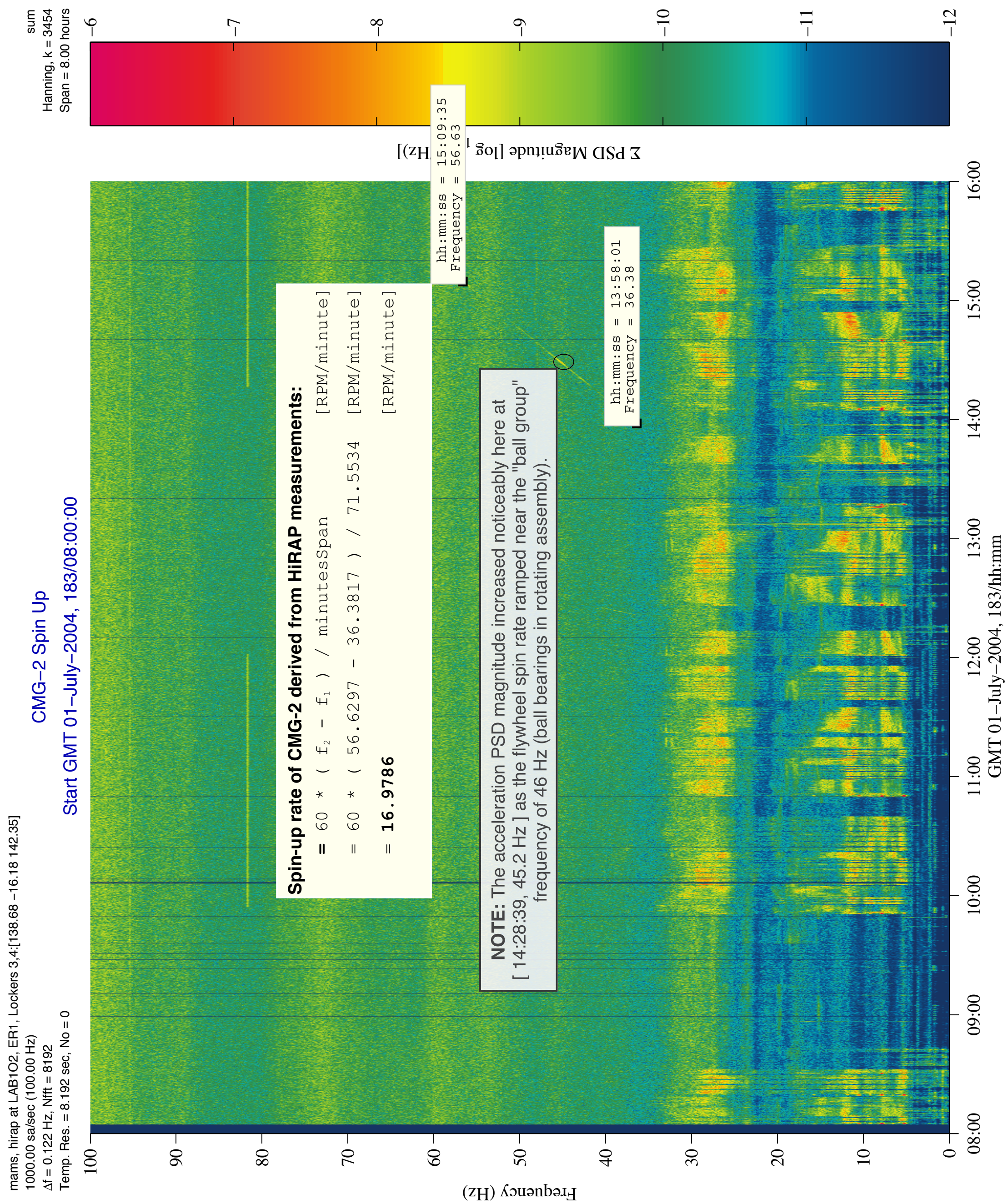

Figure 6-70 Spectrogram of CMG-2 Spin-Up (HiRAP)

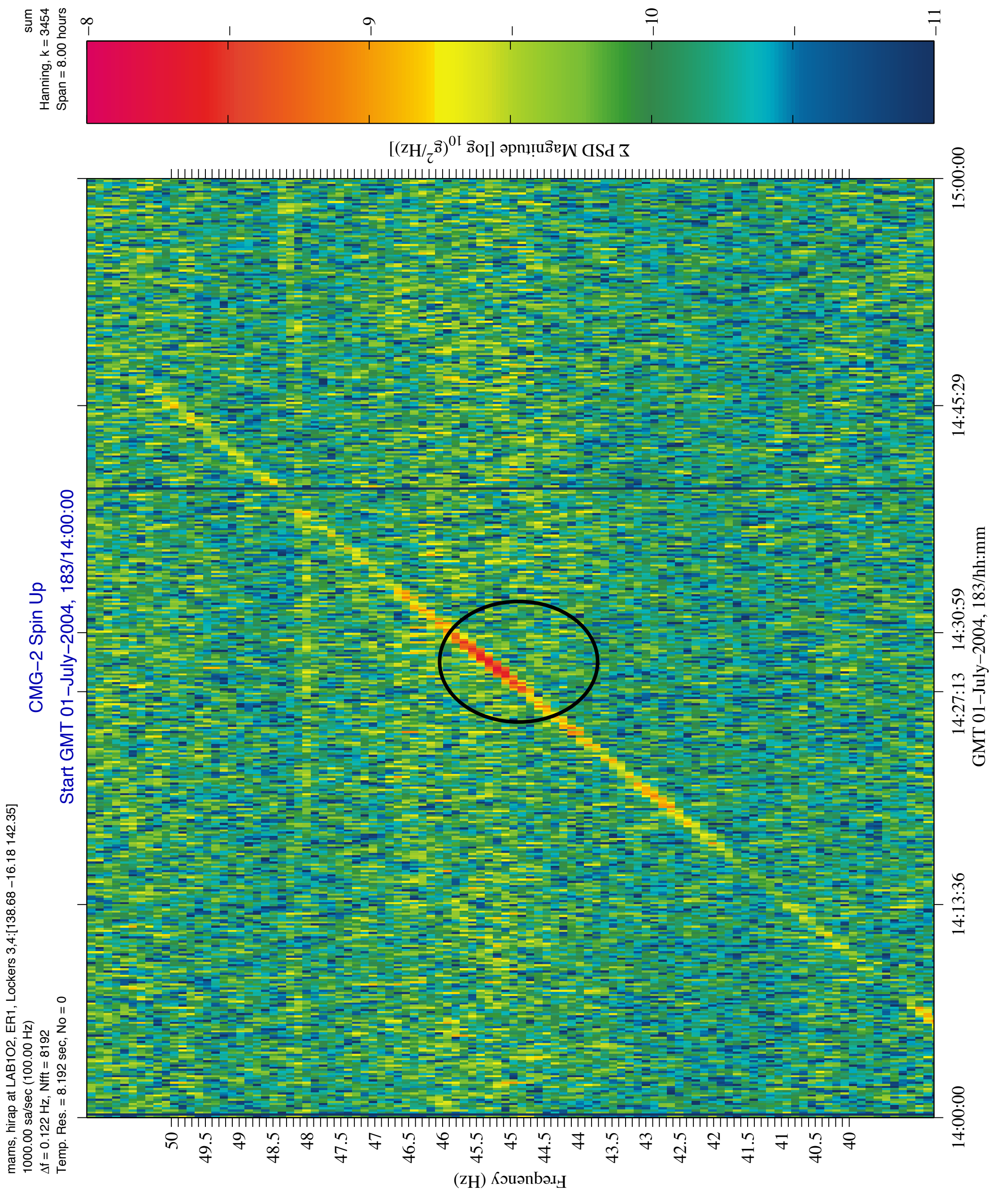

Figure 6-71 Spectrogram of CMG-2 Spin-Up Zoom (HiRAP)

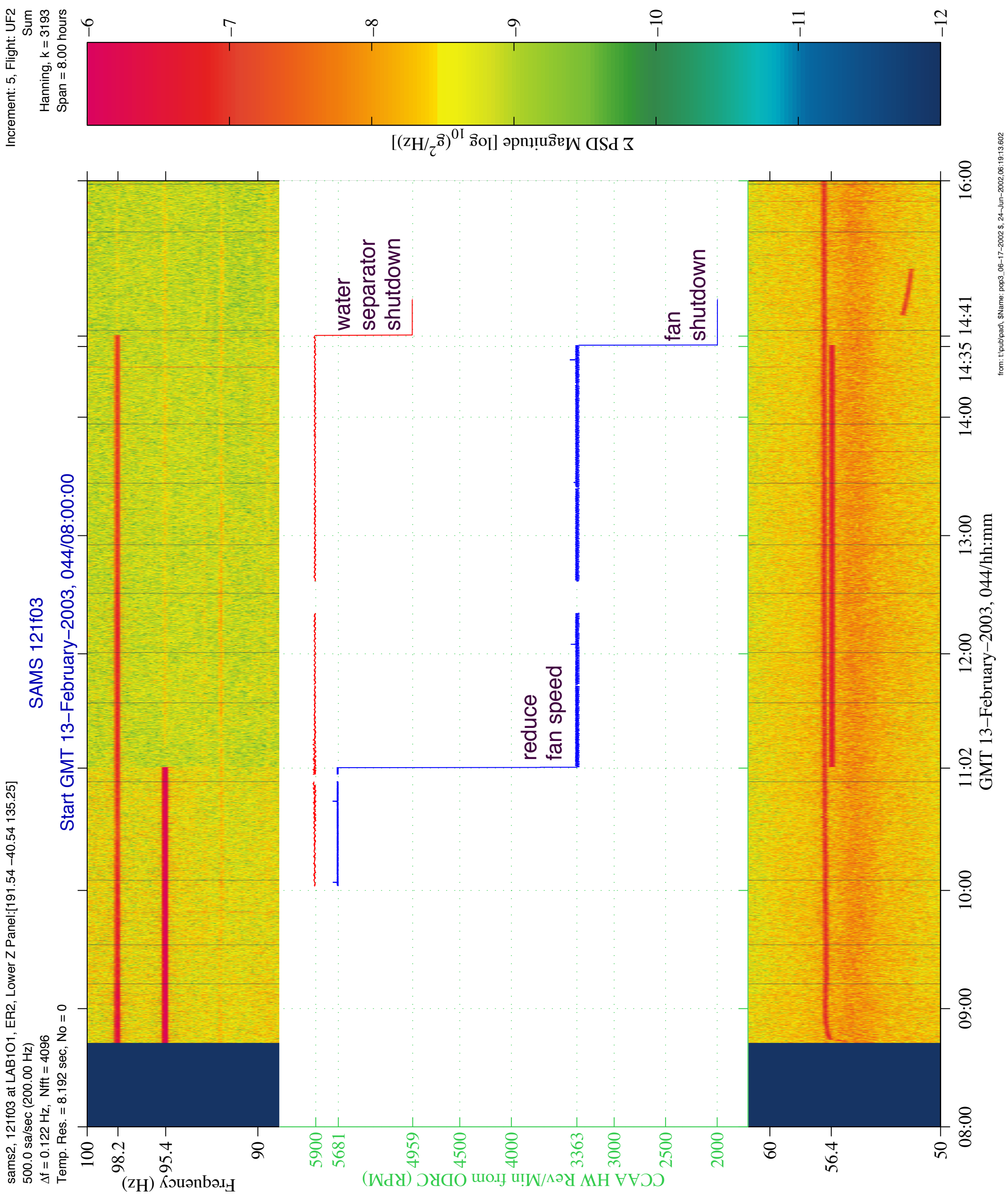

Figure 6-72 Spectrogram of Port CCAA Shutdown Operation (121f03)

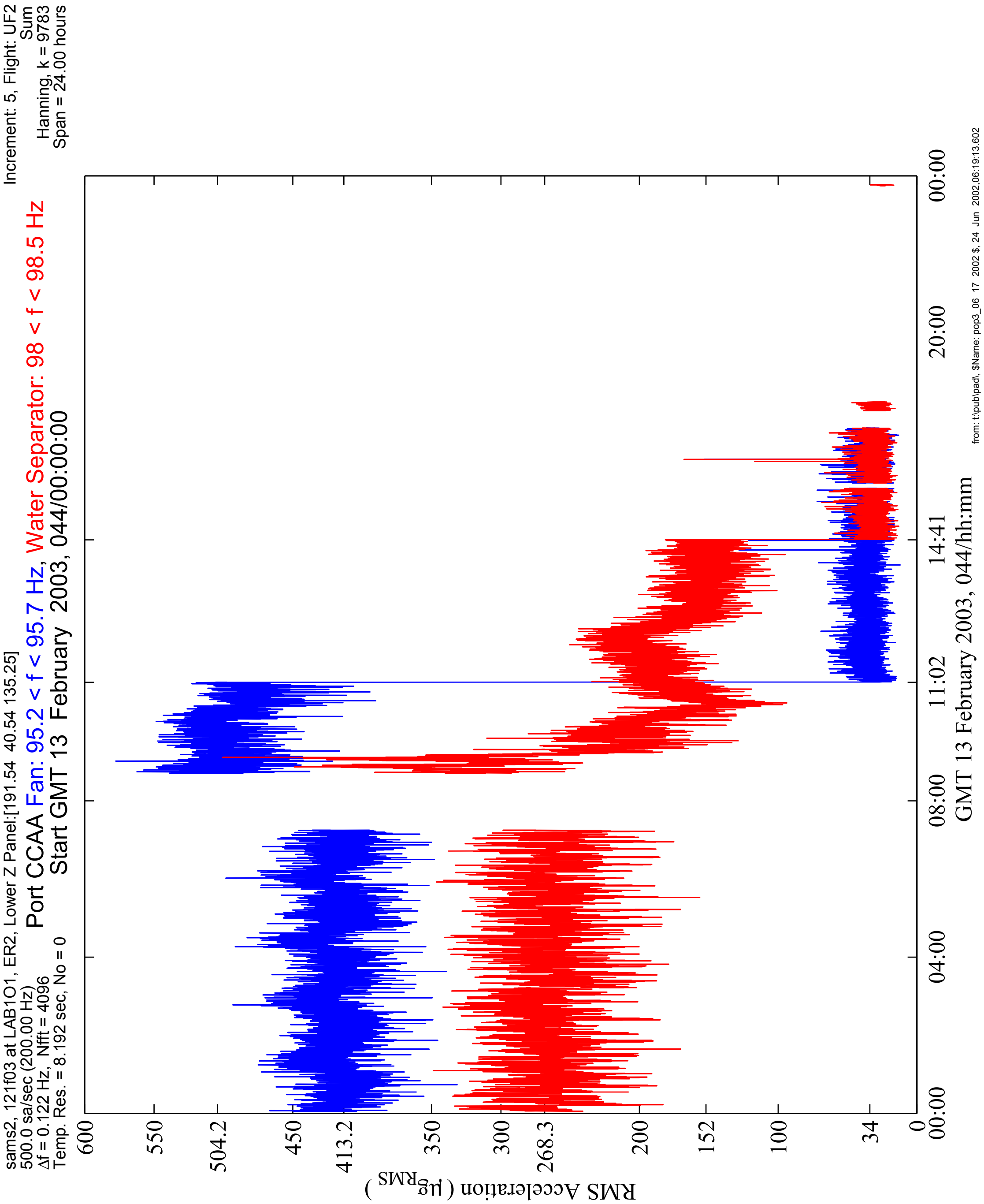

Figure 6-73 Interval RMS of Port CCAA Shutdown Operation (121f03)

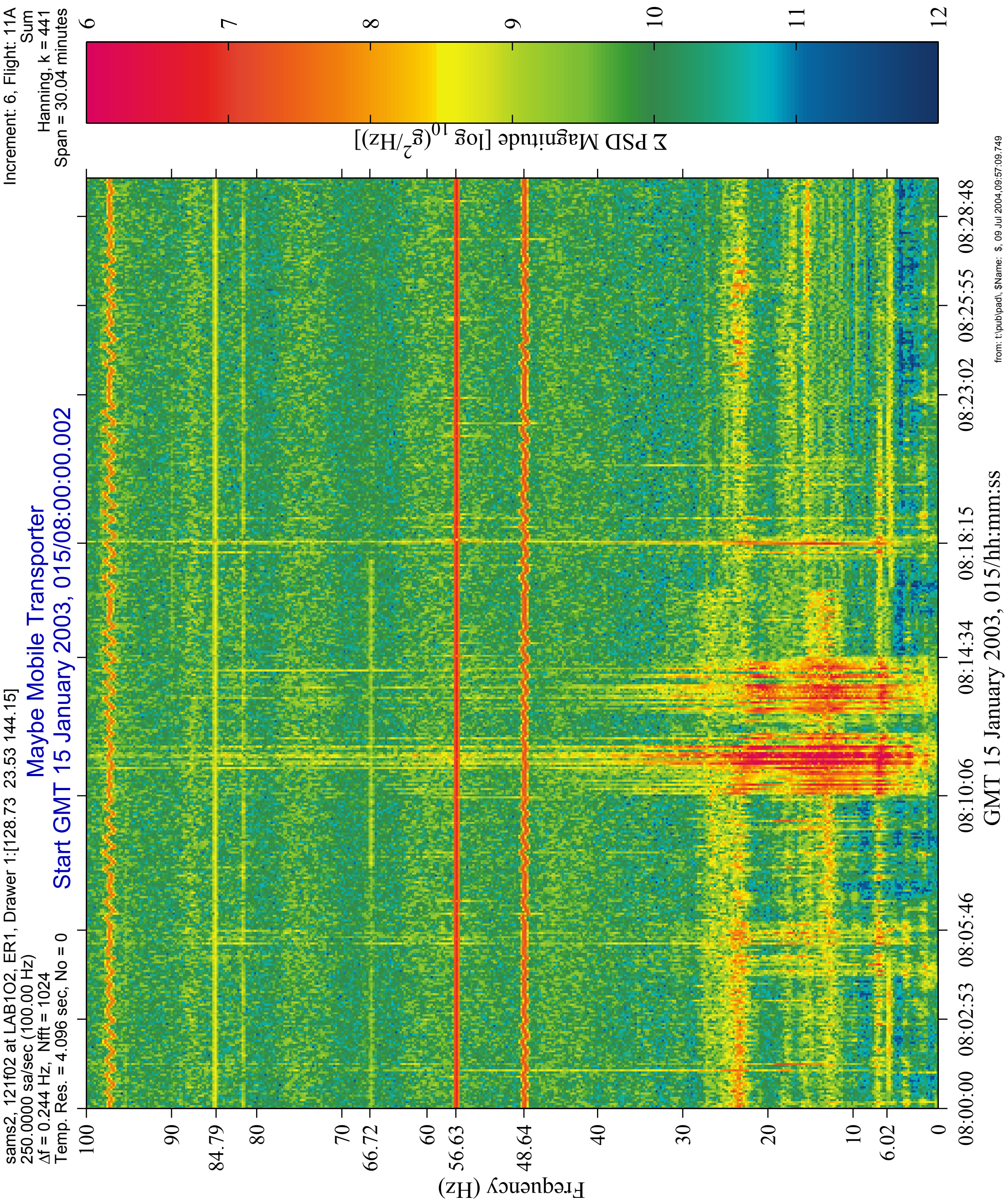

Figure 6-74 Spectrogram of Possible MT Operations (121f02)

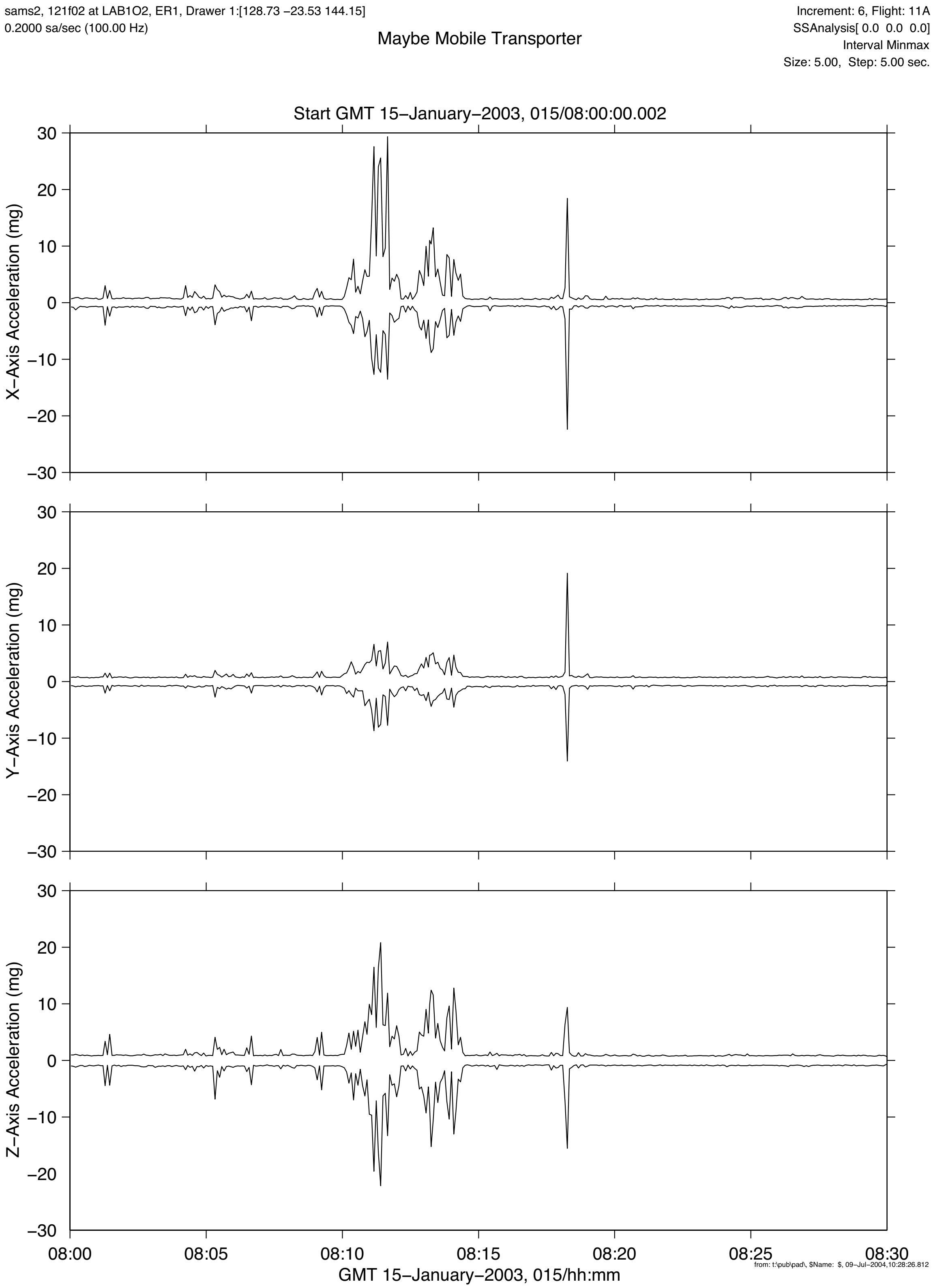

Figure 6-75 Interval Min/Max of Possible MT Operations (121f02)

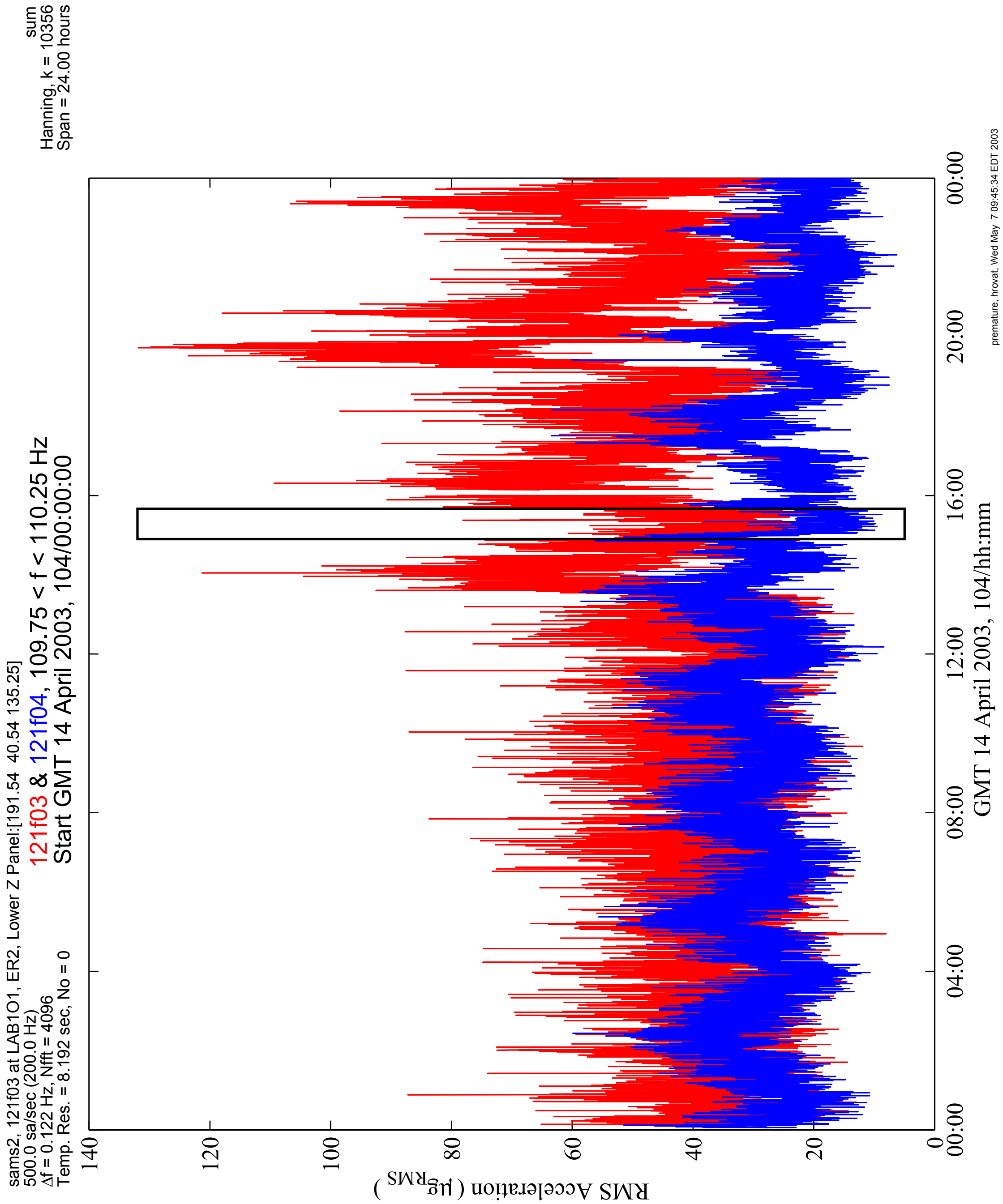

Figure 6-76 Interval RMS of ACS-GPS Shutdown/Start (121f03,121f04)

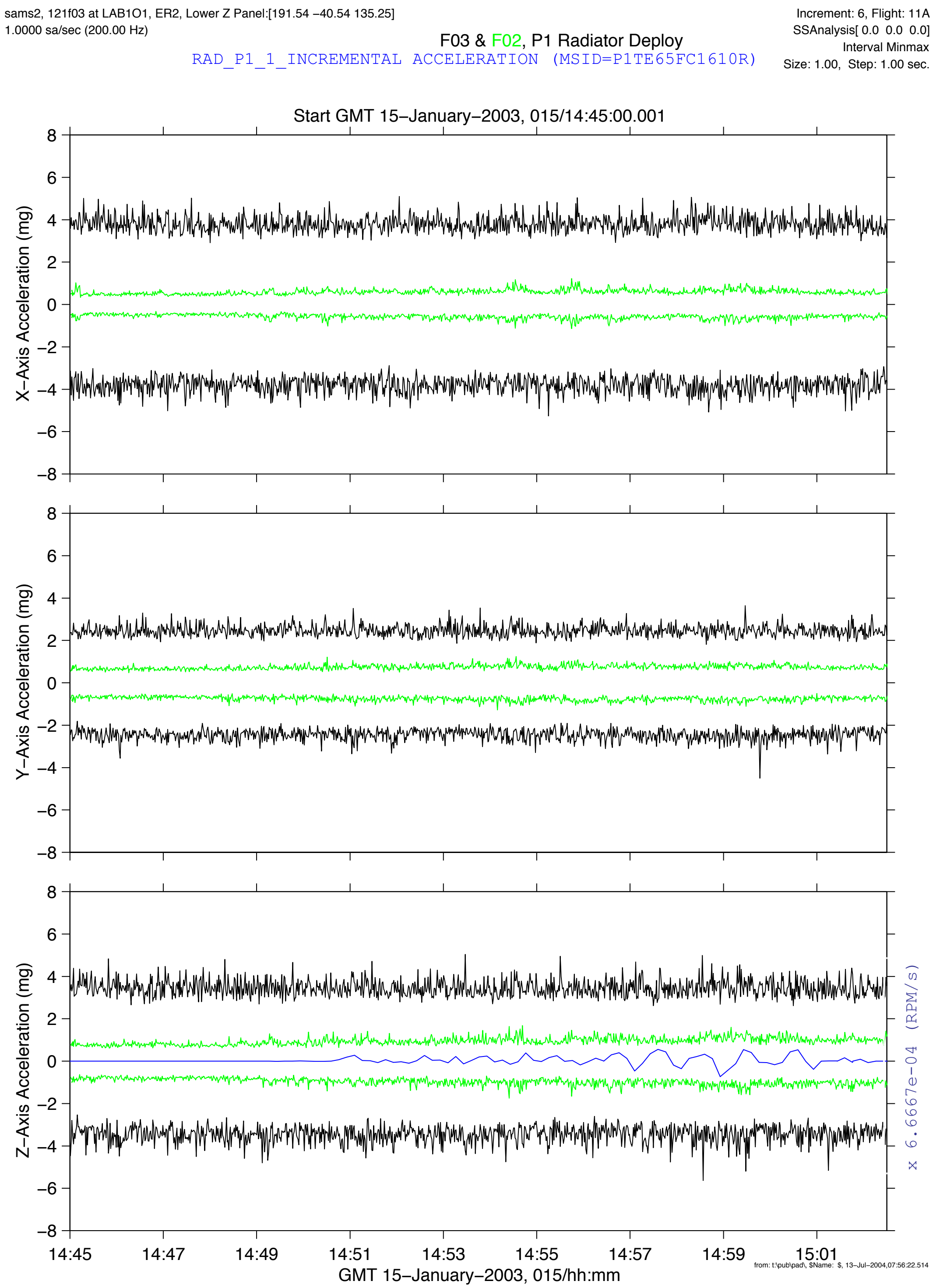

Figure 6-77 Interval Min/Max for Radiator Deployment (121f02, 121f03)

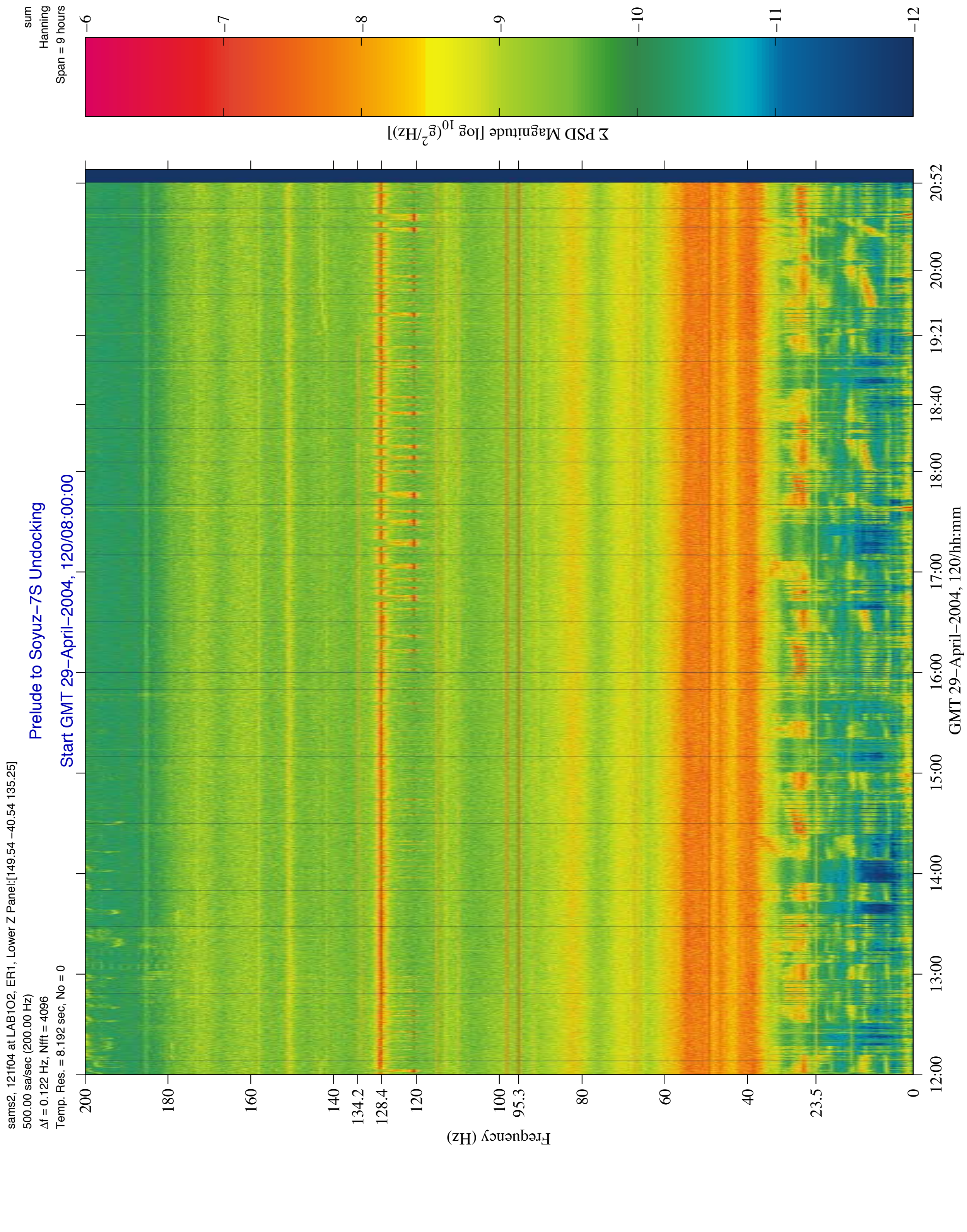

Figure 6-78 Spectrogram of Prelude to Soyuz-7S Undocking (121f04)

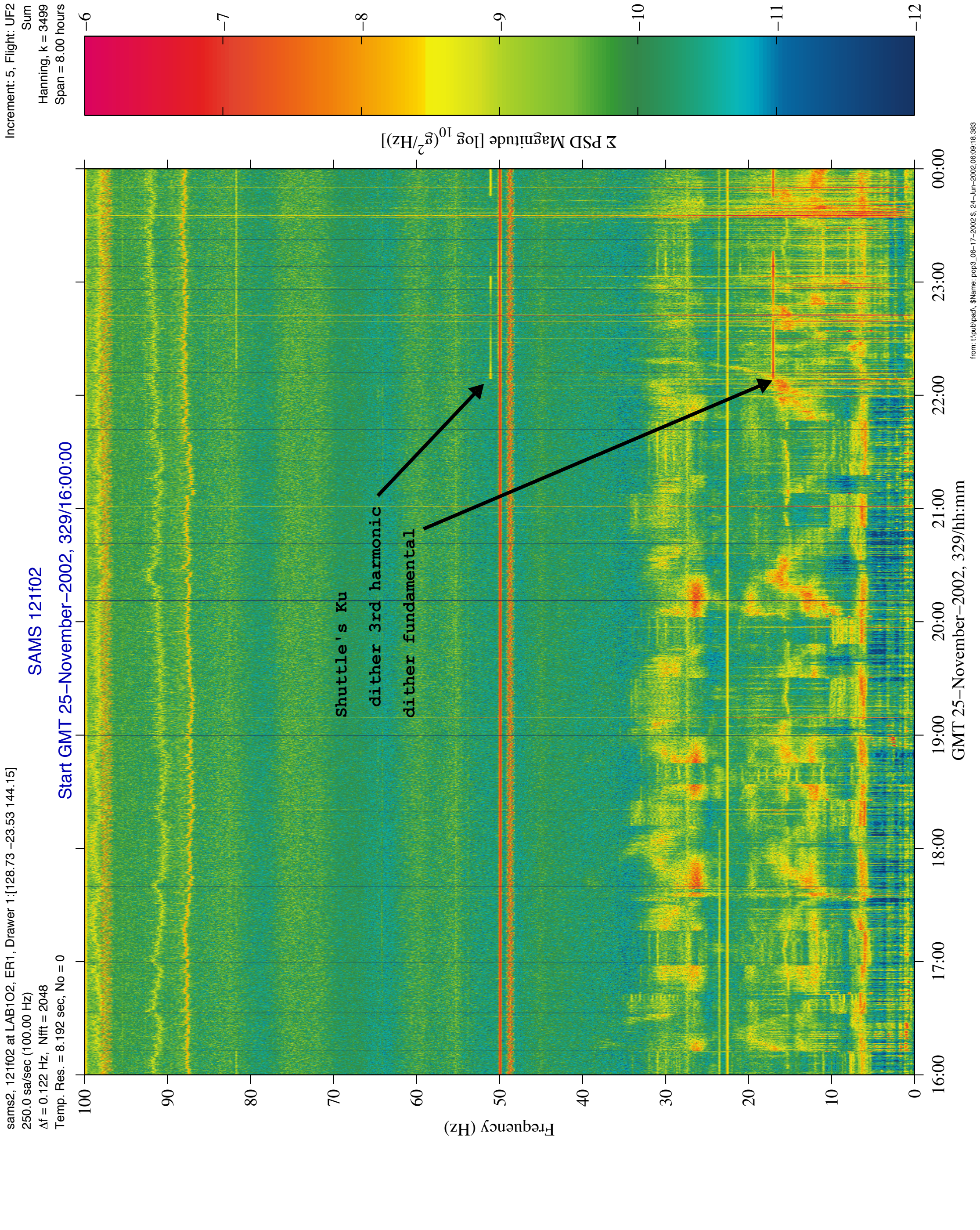

Figure 6-79 Spectrogram of STS-113 Docking (121f02)

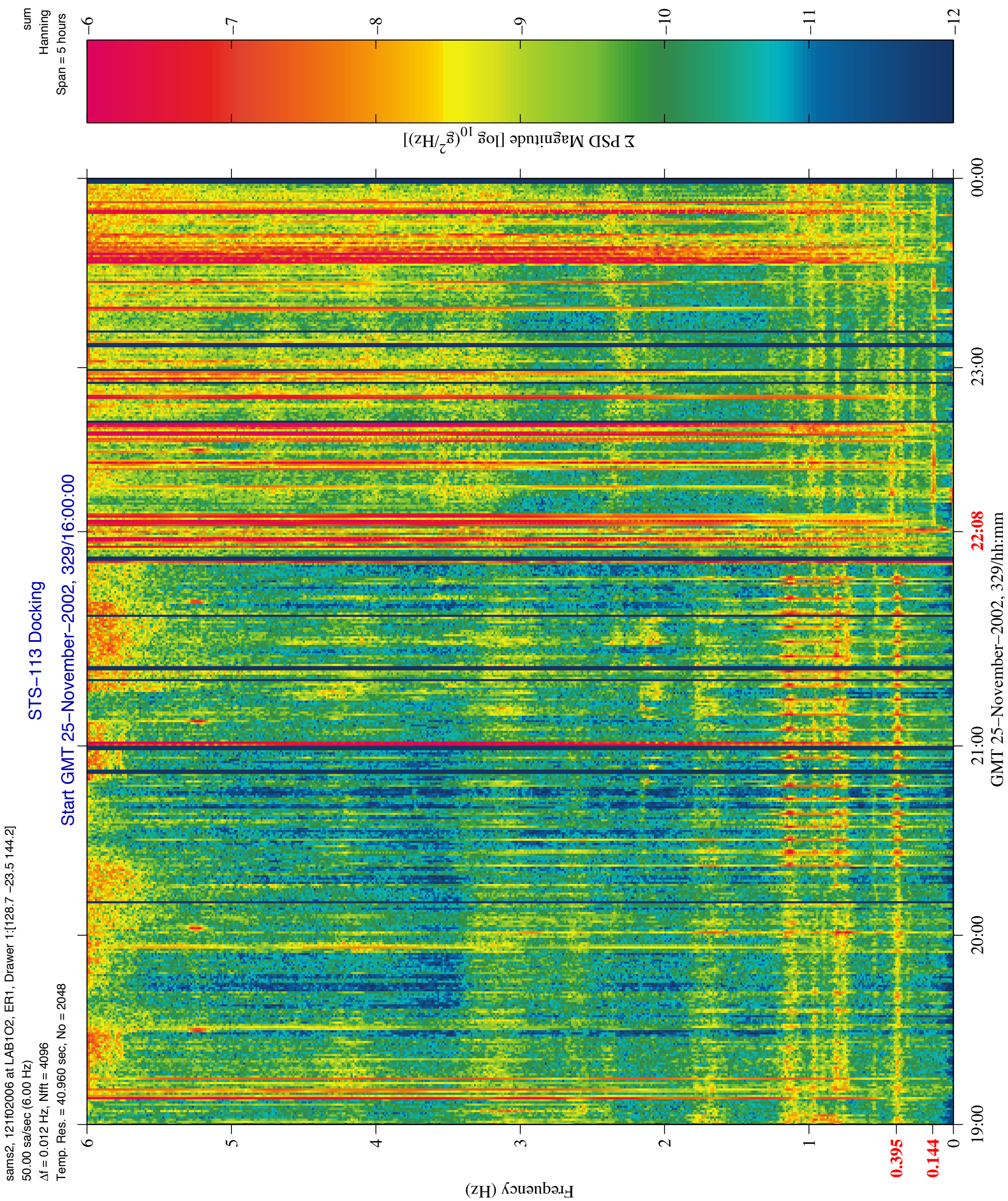

Figure 6-80 Spectrogram below 6 Hz of STS-113 Docking (121f02006)

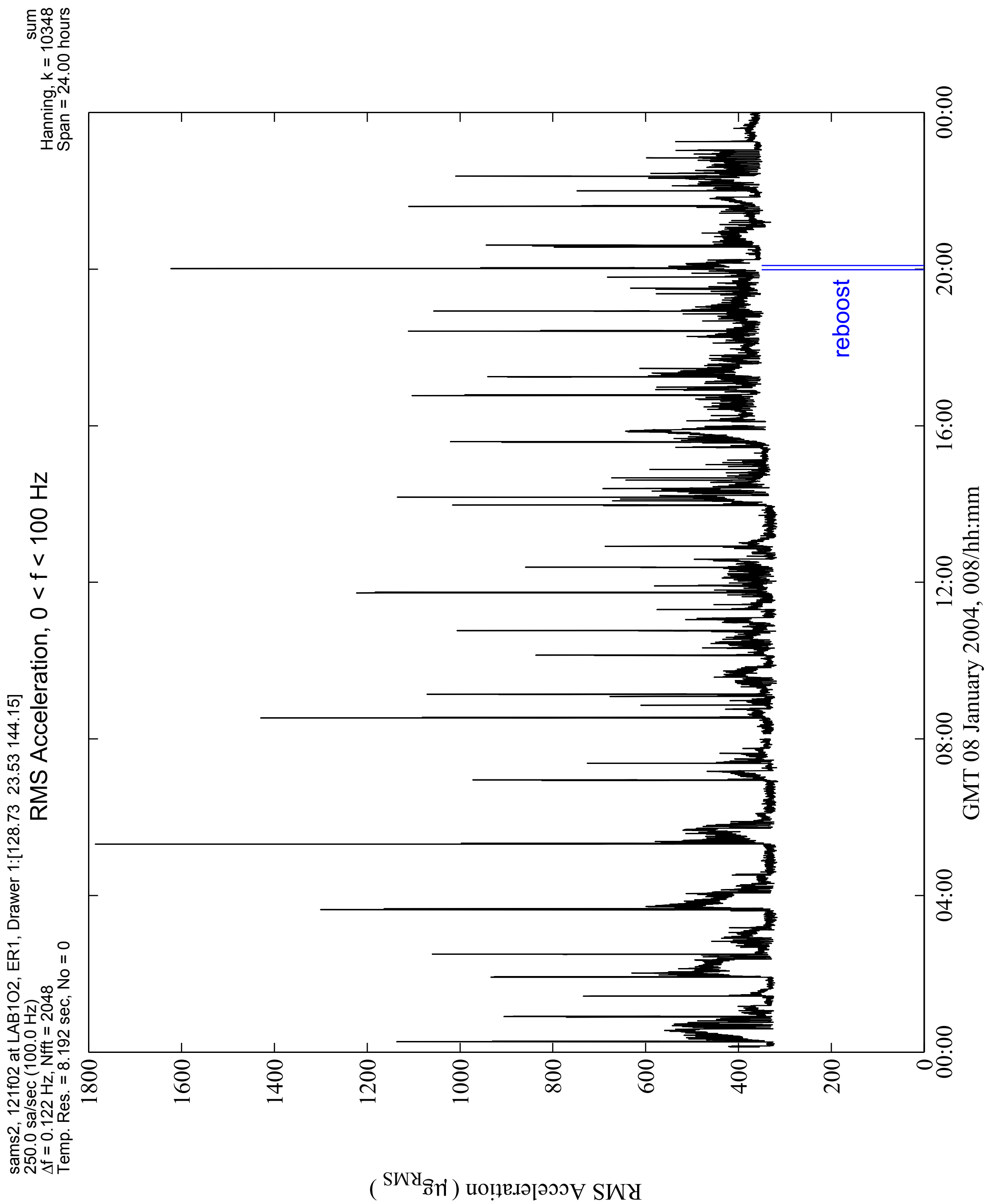

Figure 6-81 Interval RMS Including Reboost (121f02)

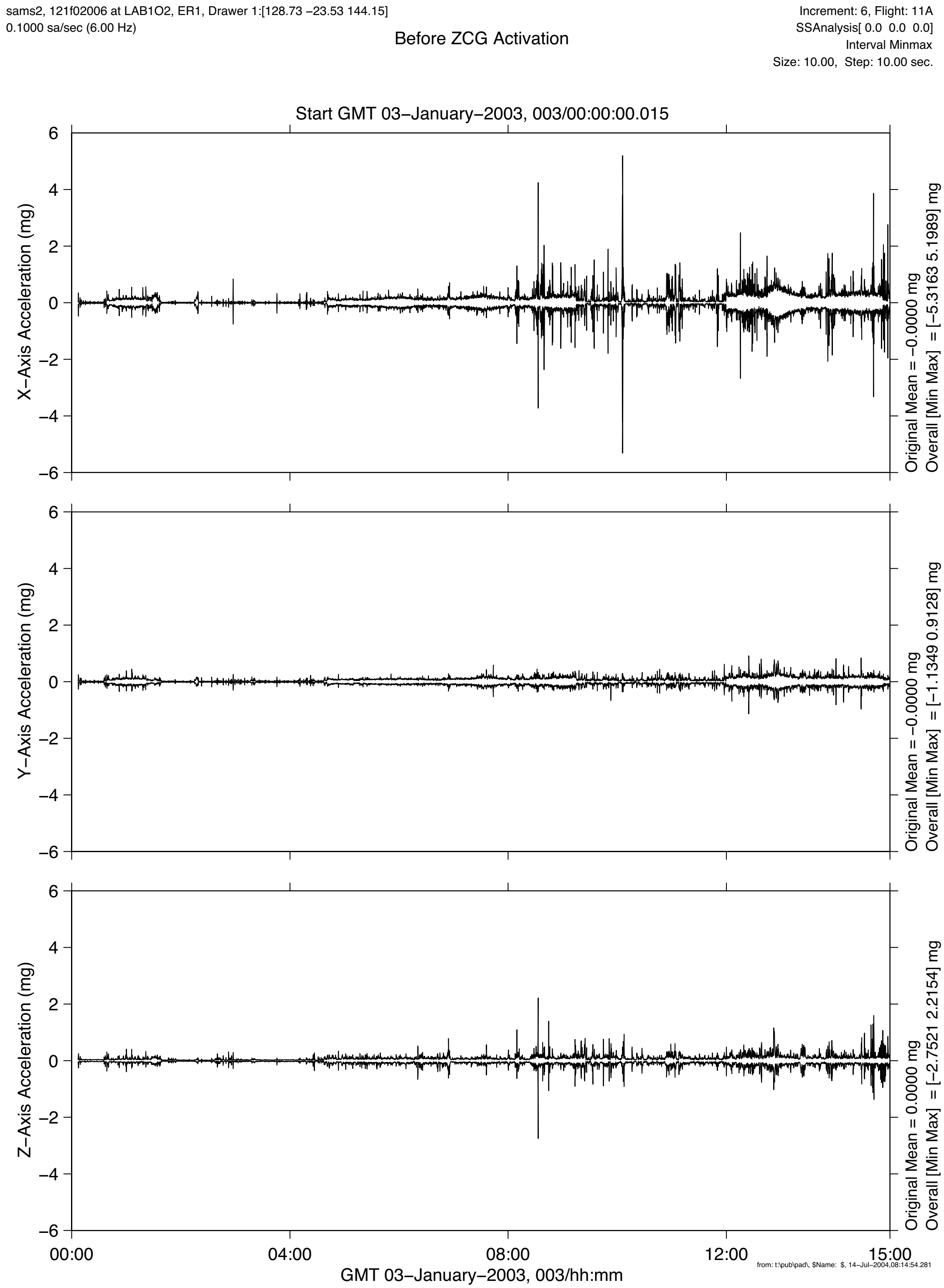

Figure 6-82 Interval Min/Max Before ZCG Activation (121f02)

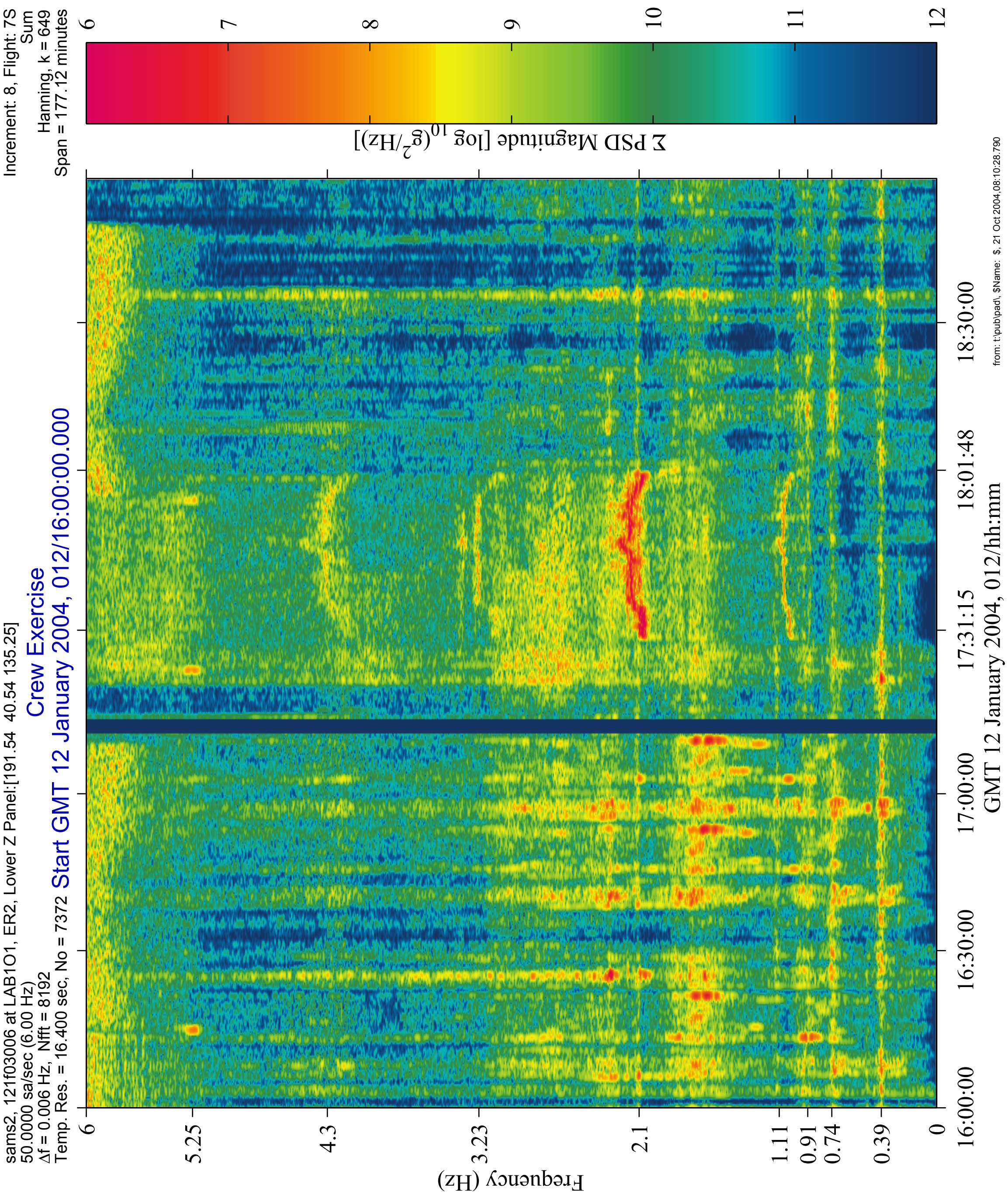

Figure 6-83 Spectrogram Below 6 Hz with Crew Exercise (121f03006)

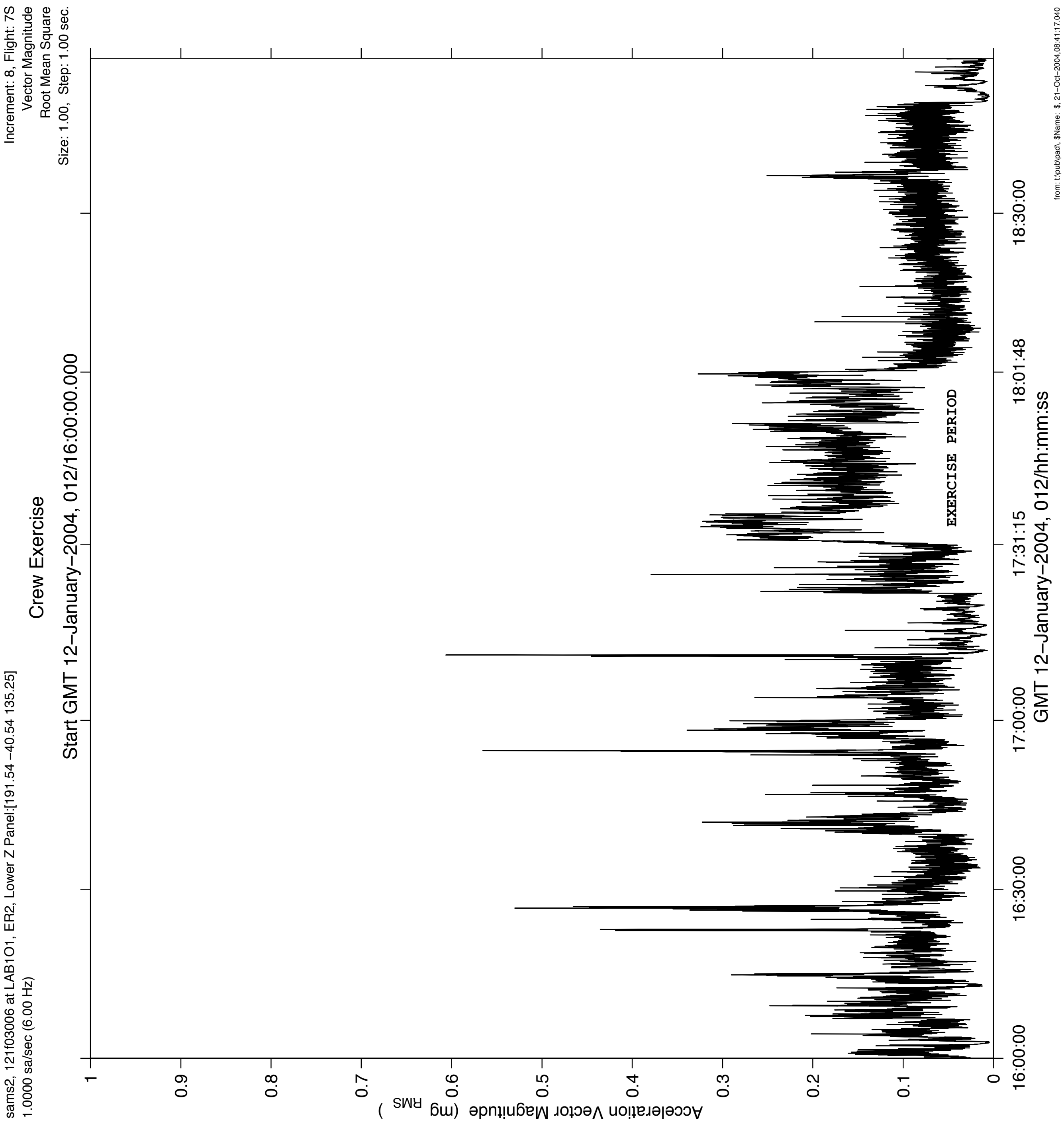

Figure 6-84 Interval RMS Below 6 Hz with Crew Exercise (121f03006)

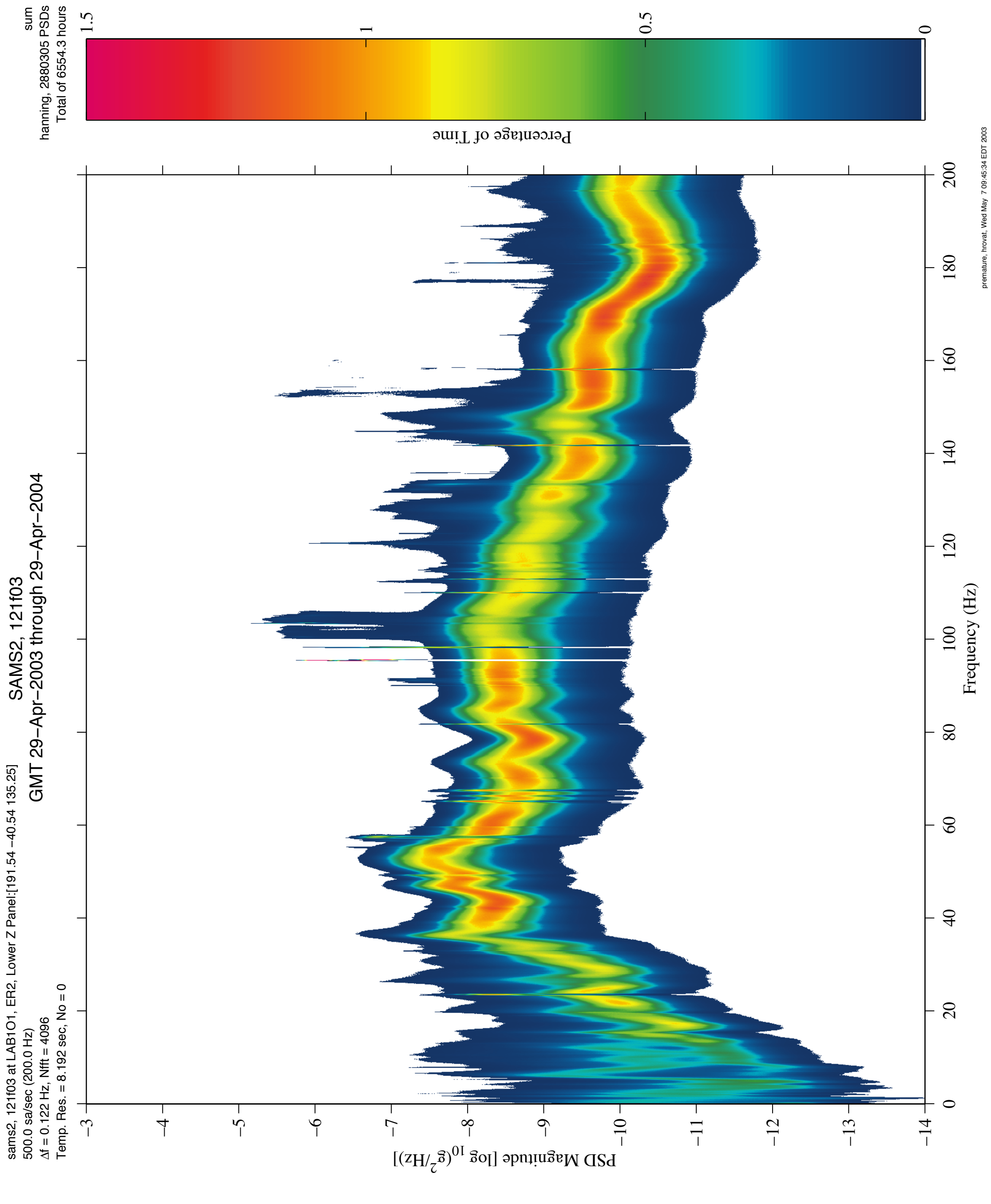

Figure 6-85 Principal Component Spectral Analysis for Increments 7 & 8 (121f03)

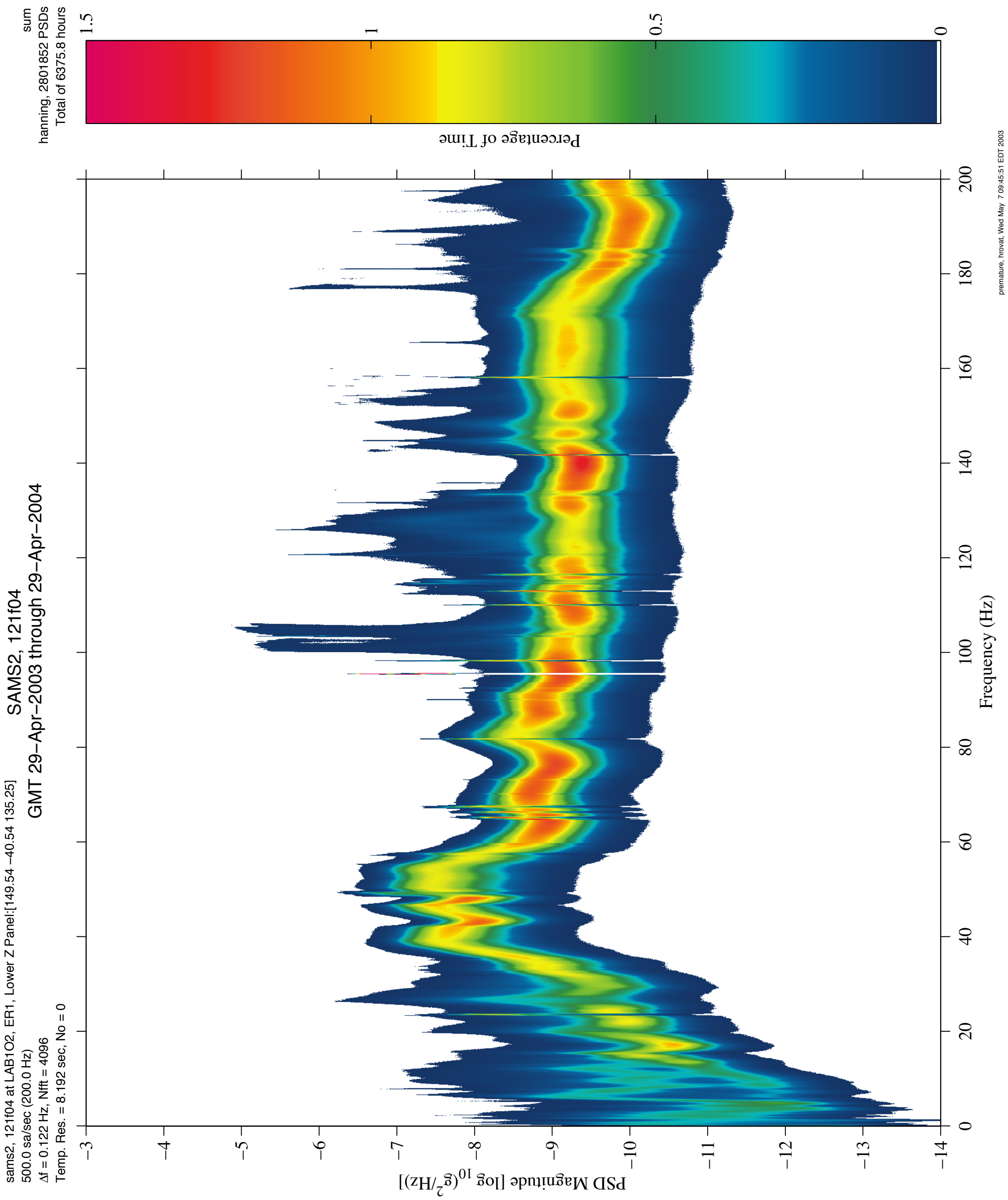

Figure 6-86 Principal Component Spectral Analysis for Increments 7 & 8 (121f04)

7 References

1. Hamacher, H., Fluid Sciences and Materials Science in Space, Springer-Verlag, 1987.

2. International Space Station User's Guide Release 2.0, NASA.

3. Expedition Three Press Kit: Expanding Space Station Scientific Research, Boeing/NASA/United Space Alliance, July 25, 2001

4. The International Space Station Fact Book, NASA, October 2000.

5. International Space Station Coordinate Systems, SSP-30219, Revision F.

6. International Space Station Flight Attitudes, D-684-10198-06 DCN-002, December 1, 1999.

7. Space Station Science Expedition Six Overview fact sheet, September 2002, NASA

8. Steelman, April., “Flight 6A Microgravity Analysis”, Microgravity AIT, August 1999.

9. Expedition Six Press Kit: Station Begins Third Year of Human Occupation, Boeing/NASA/United Space Alliance, October 25, 2002

10. Expedition Seven Press Kit: A Mission of Education and Science, Boeing/ NASA /United Space Alliance, April 17, 2003

11. Expedition Eight Mission Overview, NASA, September 2003

12. Expedition Eight Press Kit: Continuing To Carry the Torch, Boeing/NASA/United Space Alliance, September 26, 2003

13. On-Orbit Vehicle Configuration Data Book for Mission 6A, Shuttle-ISS NSTS-37324-6A, Rev. 001, NASA, March 01.

14. Microgravity Environment Interpretation Tutorial (MEIT), NASA Glenn Research Center, March 2001.

15. http://spaceresearch.nasa.gov/research_projects/ros/arctic.html

16. NASA Fact Sheets: FS-2002-03-59-MSFC- Release date April 2002

17. EXPRESS RACKS 1-2/4-5 Fact Sheet, NASA, February and July 2001

18. EXPRESS Rack, Flight 6A On-Orbit Configuration, Teledyne Brown Engineering DL-5221003, November 1999

19. Expedition Three Overview Fact Sheet, NASA, July 2001.

20. Continuing the Human Presence in Space, STS-111, Boeing/USA/NASA, May 16, 2001

21. NASA Fact Sheets: FS-2002-04-80-MSFC- Release date April 2002

22. Human Research Facility Rack 1 Fact Sheet, NASA, February 2001

23. Jules, K., Hrovat, K., Kelly, E., McPherson, K., and Reckart, T., “International Space Station Increment 4/5 Report”, NASA/TM—2003-212460, July 2003

24. Jules, K., Hrovat, K., and Kelly, E., "The Microgravity Environment Levels Of The International Space Station During The Buildup Period: Increments 2 To 8", International Astronautical Congress, IAC-04-J.6.01, October 2-8, 2004, Vancouver, Canada.

25. Jules, K., Hrovat, K., Kelly, E., McPherson, K., and Reckart, T., "International Space Station Increment-4/5 Microgravity Environment Summary Report, December 2001 to December 2002", NASA/TM-2003-212460, July 2003, Section 6.2.2.3.

26. Hrovat, K., Moskowitz, M., Truong, D., and Reckart, T., "SAMS Acceleration Measurements on Mir From March to September 1996", NASA Technical Memorandum 107524, August 1997, Section 8.2.

27. http://nasaexplores.nasa.gov/show2_articlea.php?id=02-046

28. http://stationpayloads.jsc.nasa.gov/D-aboutiss/D6.html

29. Jules, K., Hrovat, K., Kelly, E., McPherson, K., and Reckart, T., "International Space Station Increment-4/5 Microgravity Environment Summary Report, December 2001 to December 2002", NASA/TM-2003-212460, July 2003, Section 6.2.4.1

30. Jules, K., Hrovat, K., Kelly, E., McPherson, K., and Reckart, T., "A Status Report On The Characterization Of The Microgravity Environment Of The International Space Station", Acta Astronautica, Volume 55, Issues 3-9, August-November 2004, Pages 335-364

31. Canopus System, Inc., OARE Technical Report 149, STS-78 (LMS-1) Final Report, CSI-9604, September 1996

32. Canopus System, Inc., OARE Technical Report 151, STS-94 (MSL-1) Final Report, CSI-9704, August 1997

33. Hogg, Robert V., “Adaptive Robust Procedures: A partial Review and some Suggestions for Future Applications and Theory”, Journal of the American Statistical Association, Vol. 69, December 1974

34. Matisak, B.P., Rogers, M.J.B and Alexander J.I.D., “Analysis of the Passive Accelerometer System (PAS) Measurements During USML-1”, AIAA-94 0434, December 1994

35. Canopus System, Inc., Microgravity Environment Interpretation Tutorial 2001 Presentation, Section 5, James Fox, March 2001

36. Microgravity Analysis Integration Team, “Microgravity Control Plan (Revision B)”, Report No: SSP-50036 B, the Boeing Company, Houston, TX, NASA Contract No. NAS15-1000 (DRIVE-16), February 1999

37. Software Requirements for Processing Microgravity Acceleration Data from the International Space Station, PIMS-ISS-001, May 2000

Appendix A. Acronym List and Definition

Acronyms used in this Summary Report are listed below. A more extensive list of NASA ISS-related acronyms can be found through the Internet at:

http://spaceflight.nasa.gov/station/reference/index.html

ACRONYM	DEFINITION
AAA	Avionics Air Assembly
ADCO	Attitude Determination and Control Officer
AOS	Acquisition of Signal
APCF	Advanced Protein Crystalliz ation Facility
ARIS	Active Rack Isolation System
ARIS-ICE	ARIS ISS Characterization Experiment
ATL	Attitude Timeline
BCTA	Bias Calibration Table Assembly
CAM	Centrifuge Accommodation Module
CBM	Common Berthing Mechanism
CEVIS	Cycle Ergometer with Vibration Isolation System
CMG	Control Moment Gyro
DC	Direct Current (electrical acronym generalized for mean value)
DC-1	Russian Docking Compartment
DMC	Data Manager Coordinator
DTO	Detailed Test Objective
EE	Electronics Enclosure
ER 1/2	EXPRESS Rack 1 or 2
ESA	European Space Agency
ESMD	Exploration Systems Mission Directorate
EVA	Extravehicular Activity
EXPPCS	Experiment of Physics of Colloids in Space
EXPRESS	Expedite the Processing of Experiments to the Space Station
FGB	Functional Cargo Block (Russian translation: Functionalui Germatischeskii Block)
g	nominal gravitational acceleration at Earth's surface (9.81 m/s^2)
GMT	Greenwich Mean Time
GRC	NASA Glenn Research Center
GSE	Ground Support Equipment
HHPS	Human Health and Performance Systems
HiRAP	High Resolution Accelerometer Package
HOSC	Huntsville Operation Support Center
HSRT	Human System Research and Technology
Hz	Hertz
ICU	Interim Control Unit
ISPR	International Standard Payload Rack
ISS	International Space Station
JSC	NASA Johnson Space Center
kbps	kilobits per second
KSC	NASA Kennedy Space Center
LAB	U. S. Laboratory Module

LOS	Loss of Signal
LVLH	Local Vertical Local Horizontal
MAMS	Microgravity Acceleration Measurement System
MCC-H	Mission Control Center-Houston
MCOR	Medium-rate Communication Outage Recorder
MCS	Motion Control System
MEIT	Microgravity Environment Interpretation Tutorial
MEWS	Mission Evaluation Workstation System
MGMG	Microgravity Measurements Group
MPLM	Mini Pressurized Logistics Module or Multipurpose Logistics Module
MSFC	NASA Marshall Space Flight Center
MSID	Measurement/Stimuli IDentification
NASA	National Aeronautics and Space Administration
OARE	Orbital Acceleration Research Experiment
ODRC	Operational Data Request Center
OSS	OARE Sensor Subsystem
OTO	One-Third Octave
PAD	PIMS Acceleration Data
PAO	Public Affairs Office
PCSA	Principal Component Spectral Analysis
PDSS	Payload Data Services System
PI	Principal Investigator
PIMS	Principal Investigator Microgravity Services
PMA	Pressurized Mating Adapter
PRO	Payload Rack Officer
PSD	Power Spectral Density
QTH	Quasi-steady Three-dimensional Histogram
RED	Resistive Exercise Device
RMS	Root-Mean-Square
RPM	Revolutions Per Minute
RSS	Root-Sum-Square
SAMS	Space Acceleration Measurement System
SE	Sensor Enclosure
SGANT	Space-to-Ground Antenna
SO	Starboard Truss Segment 0
SSA	Space Station Analysis
SSPCM	Space Station Power Control Module
SSRMS	Space Station Remote Manipulator System
STS	Space Transportation System
TEA	Torque Equilibrium Attitude
THC	Temperature/Humidity Control System
TMF	Trimmed Mean Filtered
TSC	Telescience Support Center
TVIS	Treadmill Vibration Isolation System
μg	micro-g, 1 x 10^{-6}g
WWW	World Wide Web
XPOP	X Principal Axis Perpendicular to the Orbit Plane
XVV	X body axis toward the Velocity Vector

Appendix B. Data Analysis Techniques and Processing

This section briefly describes some assumptions, considerations, and procedures used to acquire and analyze the acceleration data measurements made by the two accelerometer systems: MAMS and SAMS.

B.1. Acceleration Data Coordinate Conversion

During the life of the Space Station, PIMS will frequently be asked to present acceleration data in a coordinate system other than that of the sensor. The purpose of this section is to provide the mathematical definitions and conventions PIMS will use when performing coordinate transformations.

PIMS maintains a coordinate system database for use in PIMS real-time and offline software that contains the information necessary to describe the location and orientation of various coordinate systems relative to the Space Station Analysis Coordinate System. Each entry for a coordinate system contains the location of the origin in SSA coordinates (x,y,z) and the Euler angles (Y, P, R) describing the orientation in a yaw-pitch-roll sequence of rotations with respect to the SSA frame. A positive rotation follows the right hand rule. So, an observer standing at positive infinity on the axis of rotation, looking towards the origin would see a counterclockwise rotation of the other two axes.

Transformation of acceleration data <u>from the SSA coordinate system to a NEW coordinate system</u> is accomplished by the formulation of a transformation matrix, M.

$$M_A^{NEW} = \begin{bmatrix} \cos P \cdot \cos Y & \cos P \cdot \sin Y & -\sin P \\ \sin R \cdot \sin P \cdot \cos Y - \cos R \cdot \sin Y & \sin R \cdot \sin P \cdot \sin Y + \cos R \cdot \cos Y & \sin R \cdot \cos P \\ \cos R \cdot \sin P \cdot \cos Y + \sin R \cdot \sin Y & \cos R \cdot \sin P \cdot \sin Y - \sin R \cdot \cos Y & \cos R \cdot \cos P \end{bmatrix}^{NEW}$$

Equation B.1-1

$$M_A^{NEW} = \begin{bmatrix} m_{11} & m_{12} & m_{13} \\ m_{21} & m_{22} & m_{23} \\ m_{31} & m_{32} & m_{33} \end{bmatrix}$$

Equation B.1-2

$$\begin{bmatrix} a_x \\ a_y \\ a_z \end{bmatrix}^{NEW} = M_A^{NEW} \cdot \begin{bmatrix} a_x \\ a_y \\ a_z \end{bmatrix}^{A}$$

Equation B.1-3

Transformation of acceleration data <u>from the NEW coordinate system to the SSA coordinate system</u> is accomplished by multiplying the vector by the transpose of matrix M**. The transpose of M, M^T, can be calculated by swapping the rows and columns as depicted in Equation B.1-4.

** For orthogonal matrices, $M^T = M^{-1}$.

$$M^T = M_{NEW}^{A} = \begin{bmatrix} m_{11} & m_{21} & m_{31} \\ m_{12} & m_{22} & m_{32} \\ m_{13} & m_{23} & m_{33} \end{bmatrix}$$

Equation B.1-4

$$\begin{bmatrix} a_x \\ a_y \\ a_z \end{bmatrix}^{A} = M^T \cdot \begin{bmatrix} a_x \\ a_y \\ a_z \end{bmatrix}^{NEW}$$

Equation B.1-5

In general, PIMS will transform data from SENSOR coordinate system to a NEW coordinate system. This is a four step process:

1. **The orientation of the SENSOR coordinate system is found $[YPR]_{SENSOR}$ from the coordinate system database and used to calculate the transformation matrix M,**

$$M_{A}^{SENSOR} = \begin{bmatrix} \cos P \cdot \cos Y & \cos P \cdot \sin Y & -\sin P \\ \sin R \cdot \sin P \cdot \cos Y - \cos R \cdot \sin Y & \sin R \cdot \sin P \cdot \sin Y + \cos R \cdot \cos Y & \sin R \cdot \cos P \\ \cos R \cdot \sin P \cdot \cos Y + \sin R \cdot \sin Y & \cos R \cdot \sin P \cdot \sin Y - \sin R \cdot \cos Y & \cos R \cdot \cos P \end{bmatrix}^{SENSOR}$$

Equation B.1-6

$$M_{A}^{SENSOR} = \begin{bmatrix} m_{11} & m_{12} & m_{13} \\ m_{21} & m_{22} & m_{23} \\ m_{31} & m_{32} & m_{33} \end{bmatrix}$$

Equation B.1-7

2. **Since the data is currently in SENSOR coordinates, the transpose of M is calculated.**

$$M_{SENSOR}^{A} = \begin{bmatrix} m_{11} & m_{21} & m_{31} \\ m_{12} & m_{22} & m_{32} \\ m_{13} & m_{23} & m_{33} \end{bmatrix}$$

Equation B.1-8

$$\begin{bmatrix} a_x \\ a_y \\ a_z \end{bmatrix}^{A} = M_{SENSOR}^{A} \cdot \begin{bmatrix} a_x \\ a_y \\ a_z \end{bmatrix}^{SENSOR}$$

Equation B.1-9

3. **The orientation of the NEW coordinate system is found $[YPR]_{NEW}$ from the coordinate system database and used to calculate the transformation matrix N,**

$$N_{A}^{NEW} = \begin{bmatrix} \cos P \cdot \cos Y & \cos P \cdot \sin Y & -\sin P \\ \sin R \cdot \sin P \cdot \cos Y - \cos R \cdot \sin Y & \sin R \cdot \sin P \cdot \sin Y + \cos R \cdot \cos Y & \sin R \cdot \cos P \\ \cos R \cdot \sin P \cdot \cos Y + \sin R \cdot \sin Y & \cos R \cdot \sin P \cdot \sin Y - \sin R \cdot \cos Y & \cos R \cdot \cos P \end{bmatrix}_{NEW}$$

Equation B.1-10

$$\begin{bmatrix} a_x \\ a_y \\ a_z \end{bmatrix}^{NEW} = N \cdot \begin{bmatrix} a_x \\ a_y \\ a_z \end{bmatrix}^{A}$$

Equation B.1-11

4. The equivalent transformation matrix T is calculated by substitution of Equation B.1-9 into Equation B.1-11

$$T_{SENSOR}^{NEW} = N_{A}^{NEW} \cdot M_{SENSOR}^{A}$$

Equation B.1-12

$$\begin{bmatrix} a_x \\ a_y \\ a_z \end{bmatrix}^{NEW} = T_{SENSOR}^{NEW} \cdot \begin{bmatrix} a_x \\ a_y \\ a_z \end{bmatrix}^{SENSOR}$$

Equation B.1-13

B.2. Quasi-steady Regime

MAMS OSS data is collected at 10 samples per second, low pass filtered with a cutoff frequency of 1 Hz and sent to GSE for further processing and storage. PIMS is currently storing the OSS data as raw acceleration files and also trimmed mean filtered data that are compensated for sensor bias. The trimmed mean filter algorithm used by the PIMS on the MAMS OSS acceleration data operates on a sliding window of 480 samples, resulting in a data point every 16 seconds. The trimmed mean filter algorithm is generically described below.

B.2.1. Trimmed Mean Filter

The OSS data is processed with an adaptive trimmed mean filter (TMF) to provide an estimate of the quasi-steady acceleration signal by rejecting higher magnitude transients such as thruster firings, crew activity, etc. The filtering procedure, depicted in Figure B - 2, sorts the data by magnitude and calculates the deviation from a normal distribution using the Q parameter according to the equation:

$$Q = \frac{[Upper(20\%) - Lower(20\%)]}{[Upper(50\%) - Lower(50\%)]}$$

Equation B.2-1

Where the upper and lower percentage is determined from the sorted data set. Q is used in the following equation to calculate α, an adaptively determined amount of data to trim from the tails.

$$\alpha(Q) = \begin{cases} 0.05 & Q <= 1.75 \\ 0.05 + 0.35 * \dfrac{(Q - 1.75)}{0.25} & 1.75 < Q < 2.0 \\ 0.4 & Q >= 2.0 \end{cases}$$

Equation B.2-2

The quasi-steady acceleration level is computed to be the arithmetic mean of the trimmed set. Trimmed mean filtered data is stored in the PAD archive under "ossbtmf". Further information concerning the trimmed mean filter can be found in [31-33].

B.2.2. Mapping of Quasi-Steady Data

During the life of the station, PIMS is required to "map" quasi-steady data to locations other than that of MAMS OSS. Mapping is a prediction of what the quasi-steady environment would be at an alternate location, knowing the acceleration levels at MAMS.

B.2.2.1 Background and Assumptions

The methods used by PIMS in offline and real-time algorithms make the assumption that the ISS vehicle can be considered a rigid body in regards to the quasi-steady regime. The three main contributions to the quasi-steady acceleration environment are aerodynamic drag, rotational and gravity gradient effects. Drag effect is the same for any point attached to the vehicle and is considered to act opposite to the direction of flight. Rotational effects are the tangential and radial acceleration contributions due to the rotation of the vehicle. It is assumed that the accelerations in the tangential direction are negligible.

The gravity gradient effect refers to accelerations acting on any point in a rigid body away from the center of mass. An independent particle will tend to gravitate towards the ISS center of mass (CM) if it is in front or behind the CM along the x-axis of LVLH. This is a positive acceleration in the vehicle frame of reference. The particle will also gravitate towards the CM if it is to the left or right of the CM (aligned with the y-axis of LVLH). The gravity gradient will tend to gravitate a particle away from the CM if it is above or below the CM (along the z-axis of LVLH). [34]

B.2.2.2 Mapping Algorithm

The following is a list of required parameters that are necessary to map data to any given location onboard the ISS.

- Location of MAMS sensor in Space Station Analysis (A) Coordinates
- Alternate locations to be mapped to in Space Station Analysis Coordinates
- Location of ISS center of mass in Space Station Analysis Coordinates
- Position of ISS in J2000 coordinate system.
- Quaternion representations for a yaw-pitch-roll sequence describing the orientation of the LVLH coordinate system relative to the Space Station Analysis coordinate system.

- ISS body angular rates about the X_A, Y_A and Z_A-axes.

These are the steps PIMS uses to map MAMS OSS acceleration data from the measurement location (MAMS) to any other location (NEW). All distances are in meters, angles in radians, angular rates in radians/s, radius of the earth, $r_e = 6.3781 \times 10^6$ (meters), and $g_e = 9.81\ m/s^2$. Definitions of the various coordinate systems can be found in [5].

1. **Calculate the position vectors of MAMS and NEW relative to the center of mass (CM).**

The distance from the center of mass to the MAMS location:

$$\vec{r}_{MAMS}^{\,SSA} = \begin{bmatrix} x \\ y \\ z \end{bmatrix}_{MAMS}^{A} - \begin{bmatrix} x \\ y \\ z \end{bmatrix}_{CM}^{A} = \begin{bmatrix} rx \\ ry \\ rz \end{bmatrix}_{MAMS}^{A}$$

Equation B.2-3

The distance from the center of mass to the NEW location:

$$\vec{r}_{NEW}^{\,SSA} = \begin{bmatrix} x \\ y \\ z \end{bmatrix}_{NEW}^{A} - \begin{bmatrix} x \\ y \\ z \end{bmatrix}_{CM}^{A} = \begin{bmatrix} rx \\ ry \\ rz \end{bmatrix}_{NEW}^{A}$$

Equation B.2-4

2. **Calculate transformation matrix from SSA to LVLH coordinate system using transformation matrix.**

$$T_{LVLH}^{A} = \begin{bmatrix} q_0^2 + q_1^2 - q_2^2 - q_3^2 & 2(q_1 \cdot q_2 + q_0 \cdot q_3) & 2(q_1 \cdot q_3 - q_0 \cdot q_2) \\ 2(q_1 \cdot q_2 - q_0 \cdot q_3) & q_0^2 - q_1^2 + q_2^2 - q_3^2 & 2(q_2 \cdot q_3 + q_0 \cdot q_1) \\ 2(q_1 \cdot q_3 + q_0 \cdot q_2) & 2(q_2 \cdot q_3 - q_0 \cdot q_1) & q_0^2 - q_1^2 - q_2^2 + q_3^2 \end{bmatrix} = \begin{bmatrix} m_{11} & m_{12} & m_{13} \\ m_{21} & m_{22} & m_{23} \\ m_{31} & m_{32} & m_{33} \end{bmatrix}$$

Equation B.2-5

ISS GN&C uses a yaw-pitch-roll sequence from LVLH to SSA coordinates. PIMS uses a yaw-pitch-roll sequence from SSA to LVLH. For this reason, when calculating acceleration transformations, we must use the transpose of the resultant of Equation B.2-5.

$$T_{A}^{LVLH} = \left[T_{LVLH}^{A}\right]^{T}$$

Equation B.2-6

$$T_{A}^{LVLH} = \begin{bmatrix} m_{11} & m_{21} & m_{31} \\ m_{12} & m_{22} & m_{32} \\ m_{13} & m_{23} & m_{33} \end{bmatrix}$$

Equation B.2-7

3. **Convert position vectors to LVLH coordinate system by matrix multiplication.**
Position vector of MAMS relative to center of mass in LVLH coordinate system:

$$\vec{r}_{MAMS}^{\,LVLH} = T_A^{LVLH} \cdot \vec{r}_{MAMS}^{\,A} = \begin{bmatrix} rx \\ ry \\ rz \end{bmatrix}_{MAMS}^{LVLH}$$

Equation B.2-8

Position vector of NEW relative to center of mass in LVLH coordinate system:

$$\vec{r}_{NEW}^{\,LVLH} = T_A^{LVLH} \cdot \vec{r}_{NEW}^{\,A} = \begin{bmatrix} rx \\ ry \\ rz \end{bmatrix}_{NEW}^{LVLH}$$

Equation B.2-9

4. Calculate the radius to the vehicle.

$$r_O = \sqrt{r_x^2 + r_y^2 + r_z^2}$$

Equation B.2-10

5. Calculate the gravity gradient components in LVLH coordinates (in micro-g)

Gravity gradient component at MAMS location:

$$gg_{MAMS}^{LVLH} = \left(\frac{g_e \cdot r_e^2}{r_O^2} \right) \begin{bmatrix} rx \\ ry \\ -2 \cdot rz \end{bmatrix}_{MAMS}^{LVLH} \cdot \left(\frac{1x10^6}{g_e} \right)$$

Equation B.2-11

Gravity gradient component at NEW location:

$$gg_{NEW}^{LVLH} = \left(\frac{g_e \cdot r_e^2}{r_O^2} \right) \begin{bmatrix} rx \\ ry \\ -2 \cdot rz \end{bmatrix}_{NEW}^{LVLH} \cdot \left(\frac{1x10^6}{g_e} \right)$$

Equation B.2-12

6. Convert the gravity gradient components to SSA coordinates by matrix multiplication

MAMS gravity gradient component in SSA coordinates:

$$gg_{MAMS}^{A} = T_{LVLH}^{A} \cdot gg_{MAMS}^{LVLH}$$

Equation B.2-13

NEW gravity gradient component in SSA coordinates:

$$gg_{NEW}^{A} = T_{LVLH}^{A} \cdot gg_{NEW}^{LVLH}$$

Equation B.2-14

7. Calculate rotational acceleration matrix

$$A = \begin{bmatrix} -(\omega_y^2+\omega_z^2) & \omega_x\omega_y & \omega_x\omega_z \\ \omega_x\omega_y & -(\omega_x^2+\omega_z^2) & \omega_y\omega_z \\ \omega_x\omega_z & \omega_y\omega_z & -(\omega_x^2+\omega_y^2) \end{bmatrix}$$

Equation B.2-15

8. **Calculate rotational components in SSA coordinates (in micro-g):**
   Rotational component at MAMS location:

$$rot^A_{MAMS} = A \cdot \vec{r}^{\,A}_{MAMS} \cdot \left(\frac{1x10^6}{g_e}\right)$$

Equation B.2-16

   Rotational component at NEW location:

$$rot^A_{NEW} = A \cdot \vec{r}^{\,A}_{NEW} \cdot \left(\frac{1x10^6}{g_e}\right)$$

Equation B.2-17

9. **Complete acceleration mapping by subtracting MAMS components and adding NEW components:**

$$A^A_{NEW} = A^A_{MAMS} - gg^A_{MAMS} - rot^A_{MAMS} + gg^A_{NEW} + rot^A_{NEW}$$

Equation B.2-18

B.2.3. OSS Bias Measurements

MAMS OSS triaxial sensor bias is measured by a sequence of Bias Calibration Table Assembly (BCTA) rotations. A complete bias measurement for a given axis consists of 50 seconds of data recorded in a normal orientation and 50 seconds of data recorded when the axis has been rotated 180 degrees to its opposite orientation. The 50 seconds of data are processed by the MAMS GSE with TMF algorithm applied to the resulting 500 points. Four measurements are made, corresponding with normal X_{oss} and Y_{oss}, opposite X_{oss} and Y_{oss}, opposite X_{oss} and normal Z_{oss}, and normal X_{oss} opposite Z_{oss}. The outputs for each axis and its opposite are summed and divided by two to obtain the bias value. The value is evaluated in relation to the collection of past bias measurements for a given power cycle and is included in the new mean bias calculation or ignored if determined to be out of range. A disturbance in the microgravity environment is sufficient to cause an up ranging in the OSS sensor, which, in turn, will automatically cause the bias to fail. Failed bias calibrations are not repeated. One of the initial goals during Increment-4/5 operations for MAMS was the characterization of the OSS sensor bias. To accomplish this, bias measurements were initially performed once per hour, but have since been set to one every six hours.

In the past, MAMS predecessor, the Orbital Acceleration Research Experiment (OARE), showed a significant initial transient in the bias measurements that would take one to two days to settle out. This phenomenon was not observed in the MAMS OSS data suggesting that the transient was an effect of launch. However, there is a bias temperature dependency. Ground testing indicates a temperature bias coefficient of 0.05 µg / °C [35]. At power up, the MAMS instrument takes roughly 4-6 hours to reach the nominal operating temperature of

40 °C, at which point, the bias values can be considered constant. We have not verified the bias coefficient on-orbit. For this reason, PIMS is recommending that users avoid OSS data within the first 6 hours after a MAMS power on event. When MAMS OSS support is requested, this 6-hour "settling" time must be taken into consideration.

B.2.4. Quasi-steady Plot Types

The two types of plots used in the analysis of quasi-steady data are acceleration versus time and the quasi-steady three-dimensional histogram (QTH). Unless otherwise noted, these plot types use trimmed mean filtered OSS data. Figure B - 1 shows a sample of the ancillary information associated with the quasi-steady plot types described below. Where defined and utilized for a given plot type, the definitions of the optional fields 1-4 are described in a table for that plot type.

B.2.4.1 OSS Trimmed Mean Acceleration versus Time

These are single (X, Y, Z, or vector magnitude) or three axes (X, Y, and Z) plots of acceleration in units of μg versus time. These plots give the best accounting of the quasi-steady acceleration vector as a function of time.

B.2.4.2 Quasi-steady Three-dimensional Histogram (QTH)

This type of analysis results in three orthogonal views of the quasi-steady vector. The time series is analyzed using a two-dimensional histogram method where the percentage of time the acceleration vector falls within a two-dimensional bin is plotted as a color. Areas showing colors toward the red end of the spectrum indicate a higher number of occurrences. Conversely, areas showing colors towards the blue end are indicative of a lower percentage, with no occurrences being shown as white. This plot provides a summary of the quasi-steady vector during the total time period considered. Exact timing of an acceleration event is lost in this type of plot.

TABLE B - 1 ANCILLARY PLOT INFORMATION FOR QTH PLOT TYPE

Ancillary Information Field	Generic Description	Specific Example
Optional Field 1	Timespan	Time Span = 162.8 hours
Optional Field 2		
Optional Field 3	Resolution	Resolution = 0.04 μg
Optional Field 4		

B.3. Vibratory Regime

The frequency response of the accelerometer systems used to collect vibratory data may extend below 0.01 Hz down to DC, but those instruments are not optimized for making quasi-steady or DC measurements. The MAMS OSS instrument is specialized for this purpose. Therefore, unless otherwise noted, it is assumed that the vibratory data have been demeaned for plots and analyses of vibratory data. Access to data availability plots for a given calendar month can be obtained via ftp at:

http://pims.grc.nasa.gov/ftp/pad/yearXXXX/monthYY/XXXX_YY_padprofile.pdf

where XXXX=the year of interest and YY=the month of interest. For example,

http://pims.grc.nasa.gov/ftp/pad/year2001/month10/2001_10_padprofile.pdf

provides access to data availability for October, 2001 for the five SAMS SEs and the MAMS sensors. Availability for a given month is listed across the x-axis and cutoff frequencies for the sensor heads are listed at the top. Notice that the figures are color-coded. Each color is associated with a cutoff frequency. The white vertical lines in-between the color bars are the gaps in the acceleration data collected by that specific sensor. This means that data is not available for that time span. These figures should be used as a starting point to determine whether certain sets of data are available before filling out and submitting a data request form at:

http://pims.grc.nasa.gov/html/RequestDataPlots.html.

B.3.1. Demeaned Vibratory Acceleration Data

In the analysis of the vibratory regime, it is understood that a certain amount of bias intrinsic to the measurement process does exist. This bias is manifest as a DC shift of the acceleration measurements away from the true mean value. Similar bias considerations also exist for measurements collected with the intent of analyzing the quasi-steady regime. However, much effort is expended to account for and remove bias from quasi-steady acceleration measurements, whereas in the vibratory regime, the mean value is effectively ignored in the process of demeaning. That is, for vibratory acceleration data, the mean value of the acceleration (on a per-axis basis) is subtracted over the time frame under consideration leaving effectively zero mean acceleration.

B.3.2. Vibratory Plot Types

The two types of plots used in the analysis of quasi-steady data are acceleration versus time and the quasi-steady three-dimensional histogram (QTH). Unless otherwise noted, these plot types use trimmed mean filtered OSS data. Figure B - 1 shows a sample of the ancillary information associated with the vibratory plot types described below. Where defined and utilized for a given plot type, the definitions of the optional fields 1-4 are described in a table for that plot type.

A plot of acceleration interval statistics in units of g versus time gives some measure of acceleration fluctuations as a function of time. This display type allows relatively long periods to be displayed on a single plot. There are three such interval statistic plots that are employed for this and other reasons as described below: (1) interval average, (2) interval root-mean-square and (3) interval minimum/maximum.

B.3.2.1 Interval Average

Interval average plots show net accelerations, which last for a number of seconds equal to or greater than the interval parameter, used. Short duration, high amplitude accelerations can also be detected with this type of plot; however, the exact timing and magnitude of specific acceleration events cannot be extracted. This type of display is useful for identifying overall effects of extended thruster firings and other activities that tend to cause the mean acceleration levels to shift. This display type is rarely used for vibratory data.

TABLE B - 2 ANCILLARY PLOT INFORMATION FOR INTERVAL AVERAGE PLOT TYPE

Ancillary Information Field	Generic Description	Specific Example
Optional Field 1		
Optional Field 2		
Optional Field 3	Interval Statistic Plot Type	Interval Average
Optional Field 4	Size: X, Step: Y	Size: 0.25, Step: 0.25 sec.

B.3.2.2 Interval Root-Mean-Square

Interval root-mean-square (RMS) plots show oscillatory content in the acceleration data. For the period of time considered, this quantity gives a measure of the variance of the acceleration signal. This data representation is useful for identifying gross changes in acceleration levels usually caused by the initiation or cessation of activities such as crew exercise or equipment operations.

TABLE B - 3 ANCILLARY PLOT INFORMATION FOR INTERVAL ROOT-MEAN-SQUARE PLOT TYPE

Ancillary Information Field	Generic Description	Specific Example
Optional Field 1		
Optional Field 2		
Optional Field 3	Interval Statistic Plot Type	Interval Root Mean Square
Optional Field 4	Size: X, Step: Y	Size: 0.25, Step: 0.25 sec.

B.3.2.3 Interval Minimum/Maximum

An interval minimum/maximum plot shows the peak-to-peak variations of the acceleration data. For each interval, this plot type shows both the minimum and maximum values, and thereby shows the acceleration data envelope. This type of display is another way to track gross changes in acceleration.

TABLE B - 4 ANCILLARY PLOT INFORMATION FOR INTERVAL MINIMUM/MAXIMUM PLOT TYPE

Ancillary Information Field	Generic Description	Specific Example
Optional Field 1		
Optional Field 2		
Optional Field 3	Interval Statistic Plot Type	Interval Minmax
Optional Field 4	Size: X, Step: Y	Size: 0.25, Step: 0.25 sec.

B.3.2.4 Power Spectral Density

The power spectral density (PSD) is computed from the Fourier transform of an acceleration time series and gives an estimate of the distribution of power with respect to frequency in the acceleration signal. It is expressed in units of g^2/Hz. The method used for computation of the PSD is consistent with Parseval's theorem, which states that the RMS value of a time series signal is equal to the square root of the integral of the PSD across the frequency band represented by the original signal.

TABLE B - 5 ANCILLARY PLOT INFORMATION FOR PSD PLOT TYPE

Ancillary Information Field	Generic Description	Specific Example
Optional Field 1	Frequency Resolution, NFFT	Δf=0.031 Hz, Nfft=8192
Optional Field 2	Overlap %, Number of Overlap Points	P=0.0%, No = 0
Optional Field 3	Window Type, # PSD's Averaged	Hanning, k=3
Optional Field 4	Span	Span = 120.00 secs

B.3.2.5 Power Spectral Density Versus Time (Spectrogram)

Spectrograms provide a road map of how acceleration signals vary with respect to both time and frequency. To produce a spectrogram, PSDs are computed for successive intervals of time. The PSDs are oriented vertically on a page such that frequency increases from bottom to top. PSDs from successive time slices are aligned horizontally across the page such that time increases from left to right. Each time-frequency bin is imaged as a color corresponding to the base 10 logarithm of the PSD magnitude at that time and frequency. Spectrograms are particularly useful for identifying structure and boundaries in time and frequency over relatively long periods of time.

TABLE B - 6 ANCILLARY PLOT INFORMATION FOR SPECTROGRAM PLOT TYPE

Ancillary Information Field	Generic Description	Specific Example
Optional Field 1	Frequency Resolution, NFFT	Δf=0.122 Hz, Nfft=8192
Optional Field 2	Temporal Resolution, Number of Overlap Points	Temp. Res. = 4.096 sec, No = 4096
Optional Field 3	Window Type, # PSD’s Considered	Hanning, k=2389
Optional Field 4	Timespan	Span = 180.19 minutes

B.3.2.6 RMS Acceleration Versus Time

This type of plot quantifies the measured acceleration in a fixed frequency band of interest. Nominally, this band extends from above DC to the cutoff frequency, but can be any arbitrary band that is at least as wide as the frequency resolution and wholly contained below the cutoff frequency. These plots are especially useful for tracking a portion of the acceleration spectrum of interest. For example, tracking the RMS level for a narrowband disturbance can isolate activation or deactivation events.

TABLE B - 7 ANCILLARY PLOT INFORMATION FOR RMS ACCELERATION VERSUS TIME PLOT TYPE

Ancillary Information Field	Generic Description	Specific Example
Optional Field 1	Frequency Resolution, Frequency Range	Δf=0.061 Hz, Range: 0-5 Hz
Optional Field 2	Temporal Resolution	Temp. Resolution: 16.384 sec.
Optional Field 3	Window Type, #PSDs	Hanning, k=1
Optional Field 4		

B.3.2.7 RMS Acceleration Versus One-Third Octave Frequency Bands

This type of plot quantifies the spectral content in proportional bandwidth frequency bands for a given time interval of interest (nominally 100 seconds). The (nearly) one-third octave bands are those defined by the ISS microgravity requirements; see Table 4 [36]. The results of this analysis are typically plotted along with a bold stair step curve representing the ISS combined vibratory limits in order to compare the acceleration environment to these prescribed limits. These plots are not particularly useful for identifying the source of a disturbance for a band that exceeds the desired limits.

TABLE B - 8 ANCILLARY PLOT INFORMATION FOR ONE-THIRD OCTAVE BANDS PLOT TYPE

Ancillary Information Field	Generic Description	Specific Example
Optional Field 1	Frequency Resolution, NFFT	Δf=0.010 Hz, Nfft=50568
Optional Field 2	Mode	Mode: 100 sec
Optional Field 3	Window Type, # PSD's Averaged	Hanning, k=1
Optional Field 4	Timespan	Span = 101.00 secs

B.3.2.8 Cumulative RMS Acceleration Versus Frequency

A plot of cumulative RMS acceleration versus frequency quantifies, in cumulative fashion, the contributions of spectral components to the overall measured RMS acceleration level for the time frame of interest. This plot is also derived from the PSD using Parseval's theorem. It quantitatively highlights key spectral regions - steep slopes indicate strong narrowband disturbances that contribute significantly to the acceleration environment, while shallow slopes indicate relatively quiet portions of the spectrum.

TABLE B-9 ANCILLARY PLOT INFORMATION FOR CUMULATIVE RMS ACCELERATION VS FREQUENCY PLOT TYPE

Ancillary Information Field	Generic Description	Specific Example
Optional Field 1	Frequency Resolution, NFFT	Δf=0.061 Hz, Nfft=8192
Optional Field 2		
Optional Field 3	Window Type, # PSD's Averaged	Hanning, k=2
Optional Field 4	Timespan	Span = 25.00 sec.

B.3.2.9 Principal Component Spectral Analysis (PCSA)

The PCSA histogram is computed from a large number of constituent PSDs. The resultant three-dimensional plot serves to summarize magnitude and frequency variations of significant or persistent spectral contributors and envelops all of the computed spectra over the time frame of interest. The two-dimensional histogram is comprised of frequency bins in units of Hz and PSD magnitude bins in units of $\log_{10}(g^2/Hz)$. The third dimension, represented by a color scale, is the percentage of time that a spectral value was counted within a given frequency-magnitude bin.

TABLE B - 10 ANCILLARY PLOT INFORMATION FOR PCSA PLOT TYPE

Ancillary Information Field	Generic Description	Specific Example
Optional Field 1	Frequency Resolution, NFFT	Δf=0.122 Hz, Nfft=8192
Optional Field 2	Temporal Resolution, Number of Overlap Points	Temp. Res. = 8.192 sec, No = 0
Optional Field 3	Window Type, # PSD's	Hanning, 102694 PSDs
Optional Field 4	Timespan	Total of 233.7 hours

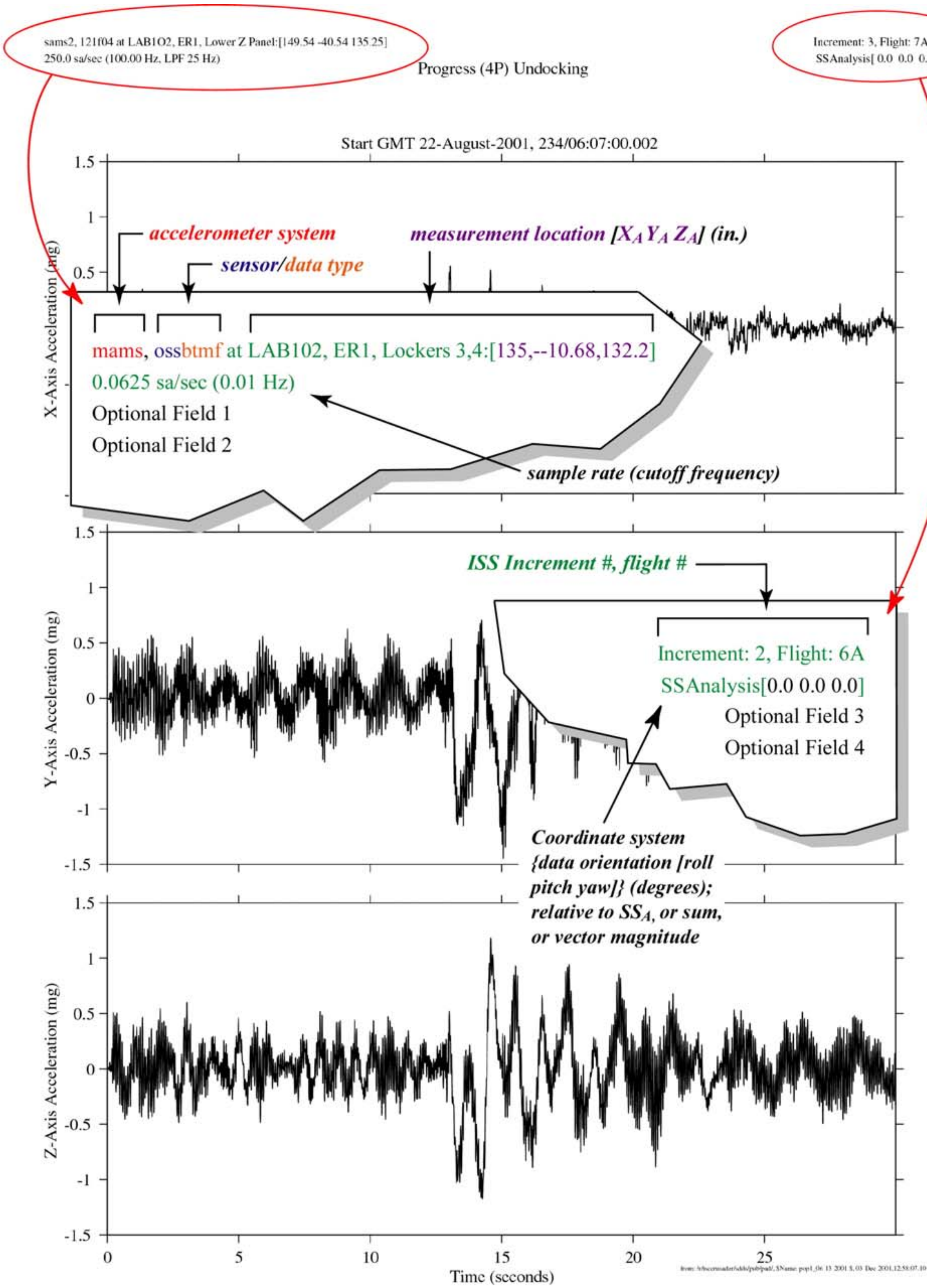

Figure B - 1 Ancillary Plot Information Description

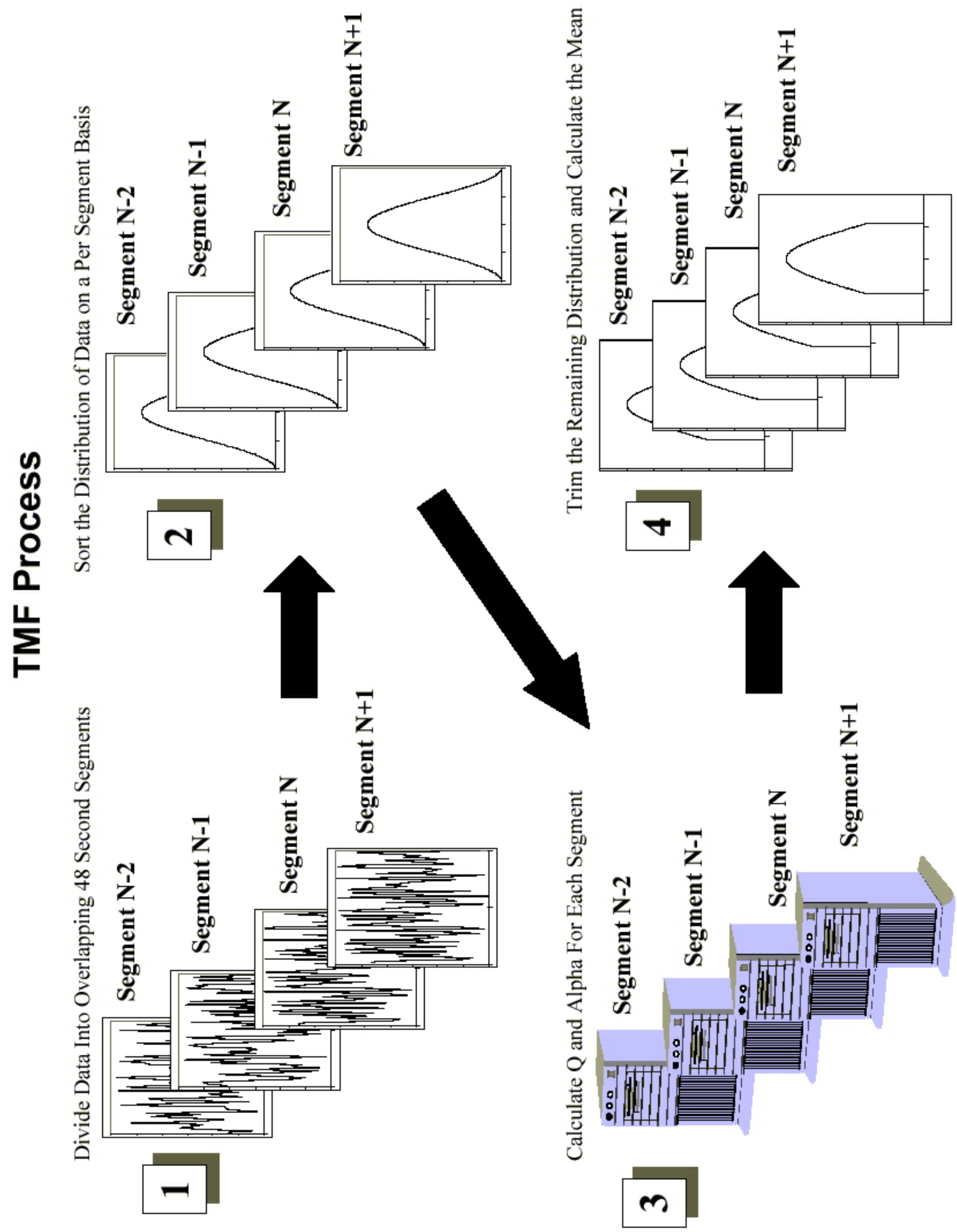

Figure E-2 Trimmed Mean Filter Process

Appendix C. SAMS and MAMS Data Flow Descriptions

The MAMS hardware contains two acceleration measurement systems called MAMS OSS and MAMS HiRAP, each with a distinct measurement objective. The purpose of the MAMS OSS data is to measure the quasi-steady accelerations on the ISS. MAMS OSS data are obtained at a rate of 10 samples per second and are low-pass filtered with a cutoff frequency of 1 Hz. Each MAMS OSS data packet contains 16 seconds of MAMS OSS acceleration data and is transmitted in real-time at a rate of one data packet every 16 seconds. MAMS has the capability to store 25.6 hours of MAMS OSS data on board. Activated at MAMS power up or via ground command, this on board storage capability allows capturing of critical quasi-steady acceleration events for later downlink. These stored acceleration data can be transmitted to ground at a ground commanded rate between 20 and 200 kbps.

The MAMS HiRAP data are obtained at a fixed rate of 1000 samples per second and low pass filtered with a cutoff frequency of 100 Hz. The purpose of the MAMS HiRAP data is to measure the vibratory and transient accelerations on the ISS. Each MAMS HiRAP data packet contains 192 acceleration readings and is transmitted at a rate of one data packet every 0.192 seconds. MAMS does not have any capability to store MAMS HiRAP data on board.

Like MAMS HiRAP, the SAMS sensor heads are designed to measure the vibratory and transient accelerations on the ISS. Each SAMS sensor can be commanded to measure and downlink acceleration data at one of five sampling rates, with five corresponding cutoff frequencies. Since the SAMS sampling rate can be varied, the number of readings per packet and the number of packets per second varies as a function of the user selected sampling rate. Table C - 1 illustrates the relationship amongst sampling rate, cutoff frequency, acceleration readings per packet, and acceleration data packets per second for the SAMS sensors.

TABLE C - 1 SAMS DATA FLOW RATES

Sampling Rate (samples/sec)	Cutoff Frequency (Hz)	Readings Per Packet	Packets Per Second
62.5	25	31 or 32	2
125	50	62or 63	2
250	100	74 or 51	4
500	200	74 or 28	8
1000	400	74 or 56	14

Telemetry from the ISS is not continuous. A time interval where real time data downlink is available is referred to as an Acquisition of Signal (AOS) interval. Similarly, the lack of real time data downlink availability is referred to as a Loss of Signal (LOS) interval. Both SAMS and MAMS acceleration data must rely on ISS on board storage capabilities to eventually obtain acceleration data collected during LOS intervals. The Medium-rate Communication Outage Recorder (MCOR) provides this ISS on board storage capability. Consequently, real time acceleration data are available on the ground during AOS periods and acceleration data are stored on the MCOR during LOS periods for eventual downlink. Under normal circumstances, both SAMS and MAMS will measure and transmit acceleration data continuously throughout a given increment.

When acceleration data are transmitted to the ground, either real time data downlink or data transmitted from a dump of the MCOR memory, the resultant acceleration data packets are routed through the White Sands Facility, through Johnson Space Center (JSC), through the Marshall Space Flight Center (MSFC), Huntsville Operation Support Center (HOSC), and ultimately to PIMS Ground Support Equipment (GSE) located at the TSC. The PIMS GSE writes each received packet into a database table dedicated to each accelerometer supported by PIMS. Therefore, a separate database table exists for MAMS OSS, MAMS HiRAP, and for each of the five SAMS sensor heads.

The primary function of the database tables is to automatically merge AOS and LOS data packets for each accelerometer. As there exists overlap between the AOS and LOS acceleration data packets received, each sensor's dedicated database table discards any redundant data packets, resulting in a table containing a contiguous set of acceleration data packets.

Data are accessed from the database table to serve two separate purposes. The first purpose involves obtaining the most recent acceleration data from the table to generate real time plots of the acceleration data in a variety of plot formats supported by PIMS [37]. These real time plots are updated during AOS intervals and electronic snapshots of the data are routed to the PIMS ISS web page (http://pims.grc.nasa.gov).

The second purpose involves obtaining the oldest acceleration data from the "bottom" of the table. These acceleration data are used to generate the PIMS acceleration data archives used by the PIMS data analysts to generate the plots described in this report. Since the data are processed from the "bottom" of the table, MCOR dumps will have had time to be downlinked, received, and merged by the database table. PIMS currently waits 24 hours before generating any acceleration data archives. Like the electronic snapshots of the real time acceleration data plots, the acceleration data archives are available for download via the PIMS ISS web page.

Appendix D. On-line Access to PIMS Acceleration Data Archive

Acceleration data measured by the MAMS and the SAMS on the ISS are available over the Internet via FTP from a NASA GRC file server. The flow chart shown in Figure D - 1 diagrams a procedure that can be used to download data files of interest:

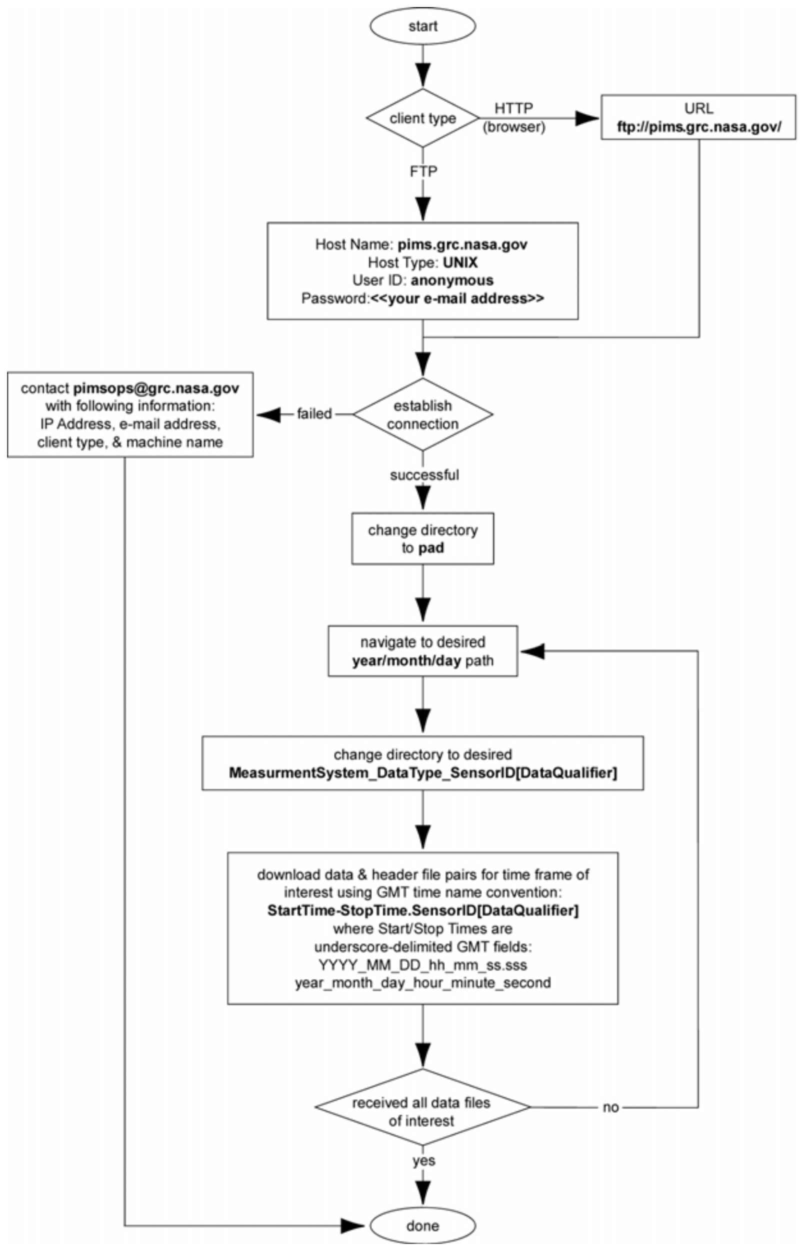

Figure D - 1 On-Line Data Access Flow Chart

A fictitious file listing is shown in Figure D - 2 depicting the PIMS Acceleration Data (PAD) file system hierarchy.

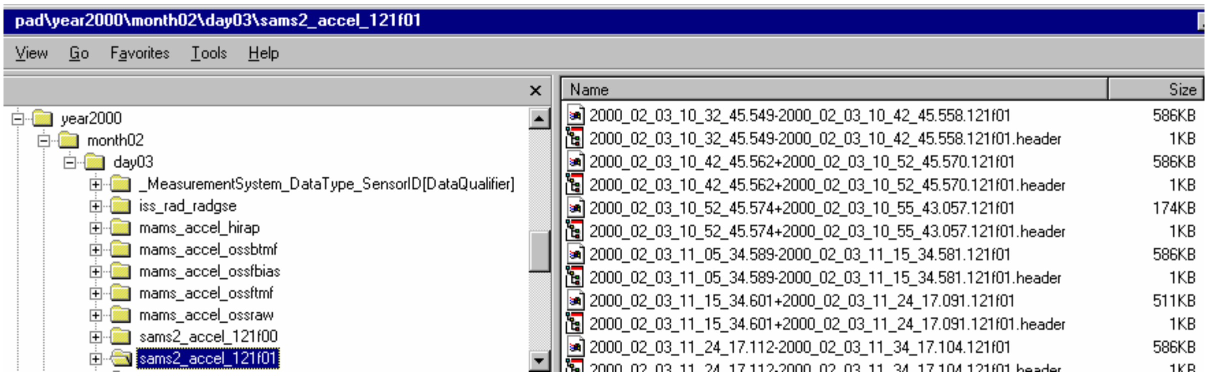

Figure D - 2 Screenshot of Sample PAD File Listing

For the directory highlighted on the left of this sample listing, the measurement system is "sams2" and the sensor identifier is "121f01". On the right, there is a partial listing of the acceleration header and data files available for this sensor collected on the day indicated (day 3). These files are named according to the PIMS-ISS-001 document [37].

If you encounter difficulty in accessing the data using this procedure, then send an electronic mail message to pimsops@grc.nasa.gov. Please describe the nature of the difficulty, and give a description of the hardware and software you are using to access the file server, including the domain name and/or IP address from which you are connecting.

Appendix E. Some Useful Acceleration Data and Microgravity Related URLs

Below is a list of some URLs that the microgravity scientific community might find very useful. They are all microgravity related. NASA does not endorse or cannot be held liable for the information contained on any site, which is not NASA's. The PIMS Project provides this listing only as a service to the microgravity community.

1. For more information on EXPRESS RACK go to: http://liftoff.msfc.nasa.gov/Shuttle/msl/science/express.html

2. For more information on Microgravity Acceleration Measurement go to: http://exploration.grc.nasa.gov/MSD/MSD_htmls/mmap.html

3. For more information on MAMS OSS, MAMS HiRAP and SAMS go to: http://pims.grc.nasa.gov

4. For information on MAMS, SAMS data request go to: http://pims.grc.nasa.gov/html/RequestDataPlots.html

5. For information on upcoming Microgravity Environment Interpretation Tutorial (MEIT) go to: http://www.grc.nasa.gov/WWW/MMAP/PIMS/MEIT/meitmain.html

6. For information on upcoming Microgravity Meeting Group (MGMG) go to: http://www.grc.nasa.gov/WWW/MMAP/PIMS/MGMG/MGMG_main.html

7. For information on SAMS go to: http://exploration.grc.nasa.gov/MSD/MSD_htmls/sams.html

8. For information on MAMS/HiRAP go to: http://exploration.grc.nasa.gov/MSD/MSD_htmls/mams.html